MODELING FULLY PLASTIC, PLANE STRAIN CRACK GROWTH

by

Yun-Jae Kim

B. S., Mechanical Engineering
Korea University (1985)

M. S., Mechanical Engineering
Michigan State University (1989)

Submitted to the Department of Mechanical Engineering
in partial fulfillment of the requirements for the degree of

Doctor of Philosophy in Mechanical Engineering

at the

MASSACHUSETTS INSTITUTE OF TECHNOLOGY

May, 1993

Author _____
Department of Mechanical Engineering
May 14, 1993

Certified by _____
Professor Emeritus Frank A. McClintock
Thesis Supervisor

Accepted by _____
Chairman
Departmental Committee on Graduate Studies

MODELING FULLY PLASTIC, PLANE STRAIN CRACK GROWTH

by

YUN-JAE KIM

Submitted to the Department of Mechanical Engineering on May 12, 1993,
in partial fulfillment of the requirements for
the degree of Doctor of Philosophy in Mechanical Engineering.

ABSTRACT

Under monotonic loading, structures should ideally be ductile, in order to provide both a warning before crack growth and continued resistance during crack growth. Such fully plastic behavior is of interest in design against collisions, tank car accidents, earthquakes, and ship groundings. For fully plastic crack growth in low strength alloys, existing asymptotic solutions for elastic-plastic growing cracks are shown to dominate only within sub-atomic size, and thus to be inapplicable.

The thesis presents a theoretical framework for modeling of fully plastic, plane strain crack growth in the limiting case of non-hardening materials. For non-hardening, fully-plastic plane strain crack growth in a number of geometries and loadings, near tip fields are characterized by three parameters: the slip line angle θ_s and the normal stress σ_s and shear displacement δu_s across the slip line. (This three-parameter characterization of near tip fields in fully plastic fracture crack growth mechanics presents a contrast to the one-parameter (K) in elastic fracture mechanics or the two-parameter (K or J and T or Q) characterization in linear or non-linear elastic fracture mechanics.) These parameters are found in terms of the far-field geometries and loadings through slip line fields or least upper bound analyses based on circular arcs. Then a crack growth criterion in terms of the crack tip opening angle ($CTOA$) is proposed as a function of the near-tip parameters θ_s, σ_s and δu_s, and material properties. The dependence of $CTOA$ on those variables is found from a proposed sliding off and shear-cracking model for a growing crack together with micromechanisms of crack growth. In case of negligible nucleation strain, the estimated $CTOA$ has inverse exponential dependence on σ_s/k and higher order parabolic dependence on θ_s. A set of experiments is also suggested to determine the dependence of $CTOA$ on θ_s and σ_s for a given material.

Based on the above results, a line-spring model is developed for fully plastic, plane strain crack growth in plates and shells. An incremental compliance of the line-spring is developed based on rigid-plastic, non-hardening plasticity, and is embedded in elastic plates and shells to predict fully plastic crack growth of a part-through crack in a plate subject to either a pinned or a fixed grip boundary condition, and of a complete circumferential crack in a sufficiently long shell subject to tension.

Thesis Supervisor: Dr. Frank A. McClintock
Title: Professor Emeritus of Mechanical Engineering

ACKNOWLEDEGEMENT

I wish to express my sincere gratitude to Professors Frank A. McClintock and David M. Parks for their encouragement, patience, and above all, their insightful advice and guidance. I also wish to thank Professors Leung, Argon and Anand for providing many physical insights which I would otherwise overlooked.

I am deeply indebted to my father and mother. Without their emotional and financial support, I would never dream whatever I have achieved now.

I appreciate the friendship and support of many Korean students at MIT, especially, Dae-Eun Kim, Hyungyil Lee, Hyun-Jun Yim, Hyun-Seok Yang, Sang-Joo Kim, Jaebog Song, Sungdo Ha and many others.

I also wish to thank my former and present officemates, specially to Drs. Sarah Wineman and Esteban Busso.

Table of Content

CRITERIA FOR PLANE STRAIN, FULLY PLASTIC QUASI-STEADY CRACK GROWTH

CHAPTER 1

INTRODUCTION

1. BACKGROUND

1.1. Review of Fracture Mechanics for Crack Initiation

For brittle structures in tensile (Mode I) loading across a crack, only a criterion for initial growth is needed, because the crack is immediately unstable. The criterion is based on the discovery in the 1950's that there can be a region around the crack tip, large compared to either a plastic zone or to the microstructural fracture process zone, and small compared to the distance to the next nearest boundary, in which the stress and strain are uniquely defined in terms of a single parameter, the stress intensity factor K_I (see Irwin, 1957; Kanninen and Popelar, 1985). At a critical value for a given material, K_{IC}, the crack begins to grow unstably. (At lower values of K_I, the growth is negligible unless loading is repeated thousands of times as in fatigue.) The value of the applied K_I is determined from the far-field geometry and loading (Tada, et al., 1985; Murakami, et al., 1987). Thus for a brittle structure (one with a crack tip plastic zone small compared to any characteristic dimension of the part and to a crack in it), unstable crack growth occurs under the local condition

$$K_I(\text{geometry and loading}) \geq K_{IC}(\text{material}). \tag{1.1}$$

For elastic-plastic materials, the above concept (1.1) can still be applied as long as the plastic zone at the crack tip is sufficiently small compared to the crack length and other relevant geometric length quantities. The condition is referred to as small scale yielding (SSY).

For more extensive plastic flow around a stationary crack in power-law strain hardening materials, Hutchinson (1968) and Rice and Rosengren (1968) (termed HRR) found the asymptotic singular non-linear elastic crack tip fields, and Rice (1968) introduced the J-integral as a basis for generalizing the concept of a dominant crack tip parameter such as K_I. Therefore, the initiation criterion (1.1) is extended to

$$J_I(\text{geometry, loading, strain hardening}) \geq J_{IC}(\text{material}). \tag{1.2}$$

A simple experimental procedure to measure J_{IC} was proposed by Landes and Begley (1974).

The HRR fields exhibit high near-tip stress triaxialities (defined by the ratio of the mean normal stress to the equivalent stress ahead of the crack) which are associated with small-scale yielding or with deeply cracked bending. McClintock (1965, 1971) pointed out that, at large-scale yielding, there is a wide range of plane strain crack-tip stress and deformation fields which depend critically on specimen geometry and type of loading. A similar trend has been found numerically by McMeeking and Parks (1979) and Shih and German (1981). This issue has been recently addressed by introducing an additional parameter based either on a second term in Williams' expansion (T-stress) (Betagón and Hancock, 1986; Parks, 1991) or on approximate descriptions of large geometry change finite element solutions (Q-stress) (O'Dowd

and Shih, 1992). In any event, both T and Q stress are parameters which affect the crack tip stress triaxiality (within the plastic zone). Negative T-stress (a radius-independent compressive stress parallel to the crack tip) lowers the near-tip stress triaxiality but raises the plastic strain directly ahead of a crack tip. On the other hand, a positive T-stress increases slightly the near-tip stress triaxiality but decreases the plastic strain level. The effect of the crack-tip stress triaxiality (due to T-stress) on crack initiation and early growth has been experimentally investigated by Hancock, et al. (1993).

1.2. Review of Fracture Mechanics for Crack Growth

For transient crack growth (i.e., crack growth inside the annular region in which a J-field dominates), the J-concept is applicable. The crack resistance curve is called the J resistance or J_R curve. The criterion for crack growth is

$$J \geq J_R. \tag{1.3}$$

Paris, et al. (1979) have introduced a dimensionless form of J resistance, a tearing modulus of the material T_{mat}:

$$T_{mat} = \frac{E}{\sigma_y^2}\frac{dJ}{da}, \tag{1.4}$$

where E and σ_y are the Young's modulus and yield strength, respectively. However, since the J-concept is based on nonlinear elastic material responses, it is no longer valid for continued crack growth: it would have to be based on the current crack tip, and would not include the prior history which has left residual stresses and strain-hardening, and thus it becomes questionable whether J controls crack growth. Hutchinson and Paris (1979) showed that J-controlled crack growth occurs only if (a)

the J curve rises very steeply with crack growth and (b) the amount of crack growth is limited to the radius of an annular J-dominant region.

Asymptotic solutions have been found for an elastic-plastic growing crack. For plane strain Mode I, near-tip solutions for a crack growing in an elastic, perfectly-plastic solid have been constructed by Rice and Sorensen (1978) and by Drugan, et al. (1982) for small-scale yielding conditions, and by Drugan and Chen (1989) and Chen and Drugan (1991) for large-scale and general yielding conditions. Corresponding work for linearly-hardening, elastic-plastic solids has been done by Ponte Castañeda (1987), and for power-law hardening solids by Gao and Hwang (1981). The effect of specimen geometry and loading condition on the growing crack has been studied by Varias and Shih (1993) from a numerical study within the framework of a "boundary layer formulation" whereby the remote loading is fully specified by the first two terms in Williams' expansion, characterized by K_I and T. The above asymptotic solutions can be applied to crack growth in high strength steels under high crack tip triaxialities, as supported by experiments by Hermann and Rice (1980). In their experiments, crack growth occurred in high strength steels (AISI 4140 steel with nominal yield strength of $\sigma_y = 1173MPa$ and tensile strength of $\sigma_u = 1327MPa$) under high stress triaxiality (deeply cracked bend specimens). However, the region of the dominance of the above solutions suggests that they can hardly be applied to ductile alloys or growing cracks under low crack tip triaxialities. For example, for a steadily growing crack in Mode I, the equivalent plastic strain ϵ^p at distance r from the crack tip in the centered fan field can be approximated in terms of the tensile yield strain ϵ_y and the plastic zone size r_p (Drugan, et al. 1982):

$$\epsilon^p \approx \epsilon_y \ln(\frac{0.2r_p}{r}). \tag{1.1}$$

Rearranging (1.1) with ϵ^p replaced by the fracture strain ϵ_f at a radius of dominance r_d that must be large enough to include the fracture mechanism or process zone size:

$$r_d \approx 0.2 r_p \exp(-\epsilon_f/\epsilon_y). \tag{1.2}$$

For low strength steel with possible high crack tip triaxialities, typical material properties (ϵ_y=0.002 and even taking ϵ_f as low as 0.05) give

$$r_d \approx 1.44\, 10^{-10} r_p. \tag{1.3}$$

(With lower crack tip triaxialities, r_d becomes even smaller than that.) Simulating fully plastic flow by an elastic-plastic zone of size $r_p = 100mm = 10^5 \mu m$ shows that the asymptotic solutions dominate only within $r_d \approx 1.44\, 10^{-5} \mu m$ even for high crack tip triaxialities, far smaller than typical hole spacing of 1-10μm. Therefore the asymptotic solutions can hardly be applied to a growing crack in low strength alloys. This limitation of existing asymptotic solutions is explained more in the Introduction to Chapter 3 in this thesis.

1.3. Need for Fully Plastic Fracture Mechanics

Under monotonic loading, structures should ideally be ductile, in order to provide both a warning before initial crack growth and continued resistance during crack growth. Such fully plastic behavior is of interest in design against collisions, tank car accidents, earthquakes, and ship groundings.

As argued in the last section, the problem of crack growth of low strength alloys is far from being solved. *Specifically, a fracture criterion with a physical basis and*

with engineering applicability is lacking. The present work discusses such a fracture criterion for Mode I, plane strain crack growth in low strength alloys.

2. PRESENT WORK

The thesis presents a theoretical framework for modeling Mode I crack growth under fully plastic, plane strain conditions in the limiting case of non-hardening materials. The model discussed in the thesis is restricted to crack tip fields approximated by a pair of slip lines surrounded by rigid regions. For plane strain crack growth, crack tip fields typically consist of symmetric shear bands where strains are concentrated, and the strain ahead of the crack tip is a few times the yield strain. For elastic-plastic crack growth, the strain ahead of the crack tip would be important and thus should be taken into account. However, for fully plastic crack growth, the crack tip region is typically subject to a fracture strain a hundred times higher than the elastic strain, and thus the strain ahead of the crack tip is negligible. Therefore, the model discussed in the thesis is valid for fully plastic, plane strain crack growth such as surface crack growth in low strength alloys. In contrast, in Mode III crack growth and in plane stress crack growth, the strain accumulation ahead of the crack tip is important.

The thesis is divided into two parts. The first part (Chapter 2 and 3) discusses the fully plastic fracture mechanics of plane strain crack growth for near crack tip fields approximated by a pair of slip lines surrounded by rigid regions. A fully plastic crack growth criterion in a low strength alloy, expressed in terms of a crack tip opening angle ($CTOA$), is proposed through micromechanisms of cracks growing in a zig-zagging fashion (Chapter 3). The second part (Chapter 4 and 5) develops a line-spring model for a growing crack based on the above methodology. The developed line-spring

is embedded in shell-like structures (Chapter 5). The details of each chapter are explained below.

Chapter 2 discusses cases where useful information concerning local stress is obtained from the least upper bound (LUB) of a particular class of plane strain fields, namely relative sliding along a circular arc. It is proven that, for the particular arc giving the LUB, a one-parameter description of traction across the arc which is consistent with the appropriate Hencky equilibrium equation can be chosen such that the traction distribution satisfies all three global equilibrium conditions. This gives a rationale for using the LUB arc and tractions across it at the crack tip in a criterion for fully plastic crack growth, as will be discussed in Chapter 3. The accuracy of the method is tested from three examples for which slip line fields are known: singly grooved plates in pure shear, punch indentation, and three-point bend specimens with variable crack depths. Then the method is applied to three problems for which slip line fields are not available: deep, single-face-cracked plates under combined bending and tension and under shear in addition, and unequally grooved plates under pure bending. In particular for deep, single-face-cracked specimens under combined bending and tension, the slip line angle and the crack tip normal stress, estimated from the present analysis, are compared with the finite element results (Lee and Parks, 1994). At the end, we discuss application of the present analysis to predict fully plastic crack growth.

In Chapter 3, for fields approximated by a pair of slip lines, a decohering zone which models the three-dimensional aspect of crack growth is shown to have rigid flanks, and the near tip fields are characterized by three parameters from either

slip line field (SLF) analysis or the least upper bound (LUB) analysis based on a circular arc, discussed in Chapter 2. Those SLF or LUB analyses relate far-field geometry, loadings, and their increments to three parameters characterizing near tip fields: the slip line angle θ_s and the normal stress σ_s and displacement increment δu_s across the slip line. Then a fracture criterion is developed from micromechanisms of crack growth such as hole nucleation, hole growth, linkage, and decohering, which are related to near tip fields through a proposed meso-mechanical model of sliding off and shear-cracking for a growing crack. The model, together with the micromechanisms, provides an estimate of the macroscopic $CTOA$ in terms of σ_s, θ_s, and material properties. Combining the above two analyses at different scales, crack growth in fully-plastic, plane strain conditions is predicted. Note that, in plane stress, the crack tip triaxialities do not vary much for different geometry and loadings, as can be seen from slip line fields (McClintock, 1965, 1971).

Chapter 4 provides a complete analytical formulation of the least upper bound based on circular arcs for a deep, single-face-cracked plate under combined bending with large tension. Then we propose an improved approximate elliptical yield locus and compare it with finite element limit analyses of Lee and Parks (1994). The proposed yield locus is then used to construct a plastic line-spring element to simulate fully plastic crack growth in shell-like structures, which is dicussed in the next chapter.

Chapter 5 develops a line-spring model for fully plastic, plane strain crack growth in plates and shells. Based on rigid-plastic, non-hardening plasticity, an incremental compliance of the line-spring is developed from a single-face-cracked specimen under combined bending and tension. This line-spring is first embedded in elastic plates

to study fully plastic crack growth of part-through cracks in plates subject to either a pinned or a fixed grip boundary condition. Effects of parameters such as plate length, plate ductility, and initial crack depth are studied. Then the line-spring is embedded in shells to study the curvature effect on fully plastic crack growth of complete circumferential cracks in sufficiently long shells subject to axial tension.

REFERENCES

Betegón, C. and Hancock, J.W., 1991, "Two Parameter Characterization of Elastic-Plastic Crack Tip Fields", *Journal of Applied Mechanics*, **58**, pp. 104-110.

Chen, X.Y., and Drugan, W.J., 1991, "Plane-Strain, Elastic-Ideally Plastic Crack Fields For Mode I Quasistatic Crack Growth at Large-Scale Yielding - II. Global Analytical Solutions for Finite Geometries", *Journal of the Mechanics and Physics of Solids*, **39**, pp. 895-925.

Drugan, W.J., and Chen, X.Y., 1989, "Plane Strain Elastic-Ideally Plastic Crack Fields For Mode I Quasistatic Growth at Large-Scale Yielding - I. A New Family of Analytical Solutions", *Journal of the Mechanics and Physics of Solids*, **37**, pp. 1-26.

Drugan, W.J., Rice, J.R. and Sham, T.L., 1982, "Asymptotic Analysis of Growing Plane Strain Tensile Cracks in Elastic-Ideally Plastic Solids", *Journal of the Mechanics and Physics of Solids*, **30**, pp. 447-473.

Gao, Y.C., and Hwang, K.C., 1981, "Elastic-Plastic Fields in Steady Crack Growth",

in *Three-Dimensional Constitutive Relations and Ductile Fracture*, S. Nemat-Nasser (ed.), North-Holland Publishing Company, Amsterdam, pp. 417-434.

Hancock, J.W., Reuter, W.G., and Parks, D.M., 1993, "Constraint and Toughness Parameterized by T", *Constraint Effects in Fracture*, ASTM STP 1171, E.M. Hackett, K.-H. Schwalbe and R.H. Dodds, Jr. (eds.), American Society of Testing Materials, Philadelphia, pp. 21-40.

Hermann, L., and Rice, J.R., 1980, "Comparison of the Theory and Experiment for Elastic-Plastic Plane-Strain Crack Growth", *Metal Science*, August-September, pp. 285-291.

Hutchinson, J.W., 1968, "Singular Behavior at the End of a Tensile Crack in Hardening Material", *Journal of the Mechanics and Physics of Solids*, Vol.16, pp. 13-31.

Hutchinson, J.W., and Paris, P.C., 1979, "Stability Analysis of J-controlled Crack Growth", ASTM STP 668, American Society of Testing Materials, Philadelphia, pp. 37-64.

Irwin, G., 1957, "Analysis of Stresses and Strains Near the End of a Crack Transversing a Plate", *Journal of Applied Mechanics*, **24**, pp. 361-364.

Kanninen, M.F., and Popelar, C.H., 1985, *Advanced Fracture Mechanics*, Oxford University Press, New York.

Landes, J.D., and Begley, J.A., 1974, "Test Results from J integral Studies: An Attempt to Establish a J_{IC} Testing Procedure", ASTM STP 560, American Society of Testing Materials, Philadelphia, pp. 170-186.

Lee, H., and Parks, D.M., 1994, "Fully Plastic Analyses of Plane Strain Single Edge Cracked Specimens Subject to Combined Tension and Bending", *International Journal of Fracture* (in press).

McClintock, F.A., 1971, "Plasticity Aspects of Fracture", in *Fracture Vol. 3*, Academic Press, New York, pp. 47-225.

McClintock, F.A., 1965, "Effects of Root Radius, Stress, Crack Growth and Rate on Fracture Instability", *Proceedings of the Royal Society*, A, Vol. 285, pp. 58-72.

McClintock, F.A. and Argon, A.S., 1966, *Mechanical Behavior of Materials*, Addison Wesley. Reprinted 1993 by Tech Books, Fairfax, VA.

McMeeking, R.M., and Parks, D.M., 1979, "On criteria for J-Dominance of Crack Tip Fields in Large-Scale Yielding", *Elastic-Plastic Fracture*, ASTM STP 668, American Society for Testing and Materials, Philadelphia, pp. 175-194.

Murakami, Y., et al., eds., 1987, *Stress Intensity Factors Handbook*, Pergamon Press, Oxford.

O'Dowd, N.P., and Shih, S.F., 1992, "Family of Crack-Tip Fields Characterized by a

Triaxiality Parameter: Part II-Fracture Applications, *Journal of the Mechanics and Physics of Solids*, **40**, pp. 939-963

Paris, P.C., Tada, H., Zahoor, H, and Ernst, H., 1979, "Instability of the Tearing Model of Elastic-Plastic Crack Growth", ASTM STP 668, American Society of Testing Materials, Philadelphia, pp. 5-36.

Parks, D.M., 1991, "Advances in Characterization of Elastic-Plastic Crack-Tip Fields", in *Topics in Fracture and Fatigue*, A.S. Argon (ed), Springer-Verlag, 58-98.

Ponte Castañeda, P., 1987, "Asymptotic Fields in Steady Crack Growth with Linear Strain-Hardening", *Journal of the Mechanics and Physics of Solids*, **35**, pp. 227-268.

Rice, J.R., 1968, "A Path Independent Integral and Approximate Analysis of Strain Concentration by Notches and Cracks", *Journal of Applied Mechanics*, **35**, pp. 379-386.

Rice, J.R., and Sorensen, E.P., 1978, "Continuing Crack-Tip Deformation and Fracture for Plane-Strain Crack Growth in Elastic-Plastic Solids", *Journal of the Mechanics and Physics of Solids*, **26**, pp. 163-186.

Rice, J.R., and Rosengren, G.F., 1968, "Plane Strain Deformation Near a Crack Tip in a Power Law Hardening Material", *Journal of the Mechanics and Physics of Solids*, Vol. 16, pp. 1-12.

Shih, C.F. and German, M.D., 1981, "Requirement for a One Parameter Characterization of Crack-Tip Fields by the *HRR* Singularity", *International Journal of Fracture Mechanics*, **17**, pp. 27-43.

Tada, H., Paris, P.C., and Irwin, G.R., 1985, *The Stress Analysis of Cracks Handbook*, Paris Productions, Saint Louis, MO.

Tvergaard, V., and Hutchinson, J.W., 1992, "On the Relation between Crack Growth Resistance and Fracture Process Parameters in Elastic-Plastic Solids", *Journal of the Mechanics and Physics of Solids*, **40**, pp. 1377-1397.

Varias, A.G., and Shih, C.F., 1993, "Quasi-Static Crack Advance Under a Range of Constraint - Steady-State Fields Based on a Characteristic Length", *Journal of the Mechanics and Physics of Solids*, **41**, pp. 835-862.

Williams, M.L., 1957, "On the Stress Distribution at the Base of a Stationary Crack", *Journal of Applied Mechanics*, **24**, pp. 111-114.

CHAPTER 2

GLOBAL EQUILIBRIUM OF THE LEAST UPPER BOUND CIRCULAR ARCS AND ITS APPLICATION TO FRACTURE MECHANICS

ABSTRACT

Fully plastic crack tip stresses are estimated from the least upper bounds (LUB's) to plane strain limit loads based on circular arcs. Suppose that two of the three in-plane components of loading are given, and the arc giving the LUB to the third has been found. Then, it is proven that the one-parameter description of traction across the arc which is consistent with the Hencky equilibrium equation can be chosen such that the tractions on the LUB arc satisfy all three in-plane components of global equilibrium. Therefore, the LUB arc and the approximate stress from it provide useful estimates of stress as well as deformation fields at the crack tip. The theorem is supported with three examples with known slip line fields: singly grooved plates in shear, punch indentation, and three-point bending of plates with variable crack depths.

The theorem is then applied to three problems where slip line solutions are not available. For deep, single-face-cracked plates under combined bending with large tension, the resulting limit loads from arcs are within 3% of finite element (FE) results. For various tension-to-bending ratios, the slip line angles, the crack tip normal stresses

and the crack tip opening displacement per unit far field generalized displacement agree with FE results within 6%, 8%, and 10% respectively. The above procedures are generalized to deep, single-face-cracked plates under combined shear, tension, and bending. Lastly, the theorem is applied to unequally grooved plates under pure bending. Application of the present method to predict fully plastic crack growth is discussed, along with the approximation of the crack tip deformation field by LUB arcs.

1. INTRODUCTION

Constructing complete slip line fields for plane strain, non-hardening plasticity involves discovering a field that satisfies *i*) the Hencky equations for equilibrium and yield condition in the deforming region; *ii*) the Geiringer equations for incompressibility there, and *iii*) equilibrium and the yield inequality in the rigid region. It is therefore desirable to obtain estimates which bound the limit load by satisfying only some of the fundamental equations for a complete solution. Useful upper bounds to the limit load can be constructed from kinematically admissible deformation fields (which satisfy incompressibility and any displacement boundary conditions). However, these upper bounds do not directly provide information on the local stress distribution within the body. In principle, such information can be gleaned from stress fields satisfying equilibrium, the yield condition, and traction boundary conditions, which provide lower bounds to the limit load. However, the construction of useful lower bound fields is often a very difficult task.

This chapter discusses cases where useful information concerning local stress is

obtained from the least upper bound (LUB) of a particular class of plane strain fields, namely relative sliding along a circular arc. In Section 2, it is proven that, for the particular arc giving the LUB, the one-parameter description of traction across the arc which is consistent with the Hencky equilibrium equation can be chosen such that the traction distribution satisfies all three global equilibrium conditions. This gives some rationale for using the LUB arc and tractions across it at the crack tip in a criterion for fully plastic crack growth. In Section 3, the theorem is supported with three examples for which slip line fields are known: singly grooved plates in pure shear (McCLINTOCK and CLERICO, 1980), punch indentation (HILL, 1950; NEIMARK, 1968), and three-point bend specimens with variable crack depths (WU *et al.*, 1987). In Sec. 4, the theorem is applied to three problems for which slip line fields are not available: deep, single-face-cracked plates under combined bending and tension and under combined shear, tension, and bending, and unequally grooved plates under pure bending. In each case, the LUB arc and the corresponding bound are found, and the theorem is applied to estimate the stresses across the slip line at the crack tip. In particular for deep, single-face-cracked specimens under combined bending and tension, the slip line angle and the crack tip normal stress, estimated from the present analysis, are compared with the finite element results (LEE and PARKS, 1993). Section 5 discusses application of the present analysis to predict fully plastic crack growth, and accuracy of this approximate analysis.

2. LEMMA AND THEOREM

2.1. Global equilibrium of upper bound fields with a circular arc

Consider a kinematically admissible plane strain deformation field consisting of rigid-body rotation across a circular arc extending from a crack tip across a ligament of constant width b in a plate with shear strength k. The three loading components, transmitted across the ligament, are a shear force V, a normal force N, and a bending moment M, as shown schematically in Fig. 2.1. Suppose that two loading components are specified, that a circular arc of radius R and angular extent 2ω has been chosen, and that the corresponding upper bound to the unspecified loading component has been found. Along the velocity discontinuity of the arc, the shear component of traction is k. Take the 1-direction in the 1-2 coordinate system centered at the origin of the arc to be in the chordal direction (Fig. 2.1). The angular coordinate ψ is measured counter-clockwise from the center of the arc. For the rotation shown, the arc is analogous to an α-line, with the maximum principal stress 45^o clockwise from it. Further, $\delta\psi$ increases with increasing counter-clockwise rotation of the α-line from the x-axis. Thus the first Hencky equation of equilibrium applies.

Lemma

Assume the normal component of traction across the arc, σ, satisfies the Hencky equation of equilibrium with one unknown (the reference stress σ_r) evaluated at $\psi = 0$:

$$d\sigma = 2kd\psi \quad or \quad \sigma = \sigma_r + 2k\psi. \tag{2.1}$$

Then, if a) the arc parameters are chosen to satisfy equilibrium in the chordal direction, and b) the single unknown constant in the Hencky equation is chosen to satisfy

equilibrium in any other than the chordal direction, the tractions on the arc satisfy global equilibrium.

The proof of this lemma is given in the Appendix. Consider this lemma in a specific analytical form:

If a) the arc is chosen to satisfy equilibrium in the chordal direction,

$$2kR(2\omega\cos\omega - \sin\omega) - (V\cos\xi + N\sin\xi) = 0, \tag{2.2}$$

where $\xi = \widehat{\xi}(R/b, \omega)$ is the angle from the x-axis to the chord (Fig. 2.1), and

if b) the single unknown constant σ_r in (2.1) is chosen to satisfy equilibrium normal to the chord:

$$\sigma_r = \frac{-V\sin\xi + N\cos\xi}{2R\sin\omega}, \tag{2.3}$$

then moment equilibrium about the center of the arc is automatically satisfied by the principle of virtual work that gives the bound. Thus the traction distribution on the arc satisfies all three global equilibrium conditions.

Note that (2.2) can be viewed as a restriction on the arc parameters. There exist infinitely many arcs which satisfy (2.2), which is only one equation with two unknowns, R and ω. In general, however, the least upper bound (LUB) is of most interest. The question is, "Do the LUB arc parameters satisfy equilibrium parallel to the chord, namely, (2.2)?". Yes, indeed, as will be stated in the next section and proved in the Appendix.

2.2. Global equilibrium of the LUB arc

Consider the conditions of the lemma, with the further condition that the LUB arc and the corresponding upper bound to the limit load of the unspecified loading component have been found, for example as discussed in Secs. 3 and 4.

Theorem

Assume that the normal component of traction, σ, on the LUB arc satisfies the Hencky equation of equilibrium with one unknown, σ_r in (2.1). Then if σ_r is chosen to satisfy force equilibrium in any other than the chordal direction, the tractions on the LUB arc satisfy global equilibrium.

The proof of this theorem is also given in the Appendix. The essential part of the theorem is that the LUB arc parameters always satisfy equilibrium in the chordal direction. Then the theorem follows from the lemma.

In specific analytical form, define ψ and σ_r as before. When two force components, V^* and N^*, are specified, equilibrium normal to the chord leads to

$$\sigma_r = \frac{-V^* \sin \xi_o + N^* \cos \xi_o}{2R_o \sin \omega_o}, \tag{2.4}$$

where the subscript o denotes the value for the LUB. In other cases, for convenience, the unknown σ_r can be chosen to equilibrate any one of the prescribed loading components. The normal stress across the LUB arc at the crack tip, σ_s, can then be approximated from the Hencky equation (2.1) with the determined reference stress σ_r. Thus stress fields which can be locally associated with the LUB arc satisfy global equilibrium. The arcs therefore provide an approximation to the stress and deforma-

tion fields at a crack tip under loadings for which a complete slip line field solution and lower bound rigid-region stress fields are not available. Such results are very useful in characterizing fully plastic crack growth in structures (McCLINTOCK *et al.*, 1993).

3. EXAMPLES

In this section, we support the theorem and test the crack tip stress results with three examples for which slip line fields are known: singly grooved plates in pure shear, punch indentation, and three-point bend test specimens with variable crack depths.

3.1. Singly grooved plates in pure shear

Premise: the LUB arc (and its corresponding bound)

A kinematically admissible displacement field with a flow discontinuity across a curved arc is shown in Fig. 2.2a. For the given normal force $N(=0)$ and moment $M(=Vh)$ to offset the effect of V at the net section, V^{LUB} is sought. From relative sliding along the circular arc, the principle of virtual work gives

$$M + VL = kR^2(\beta - \alpha) \quad \text{or} \quad V = \frac{kR^2(\beta - \alpha)}{(L + h)}. \tag{3.1}$$

Geometry gives two constraints:

$$L + h = R\cos\alpha \quad \text{and} \quad R = \frac{b}{\sin\beta - \sin\alpha}. \tag{3.2}$$

Introducing (3.2) gives (3.1) in terms of only α and β:

$$V = kb\frac{(\beta - \alpha)}{\cos\alpha(\sin\beta - \sin\alpha)}. \tag{3.3}$$

Minimization of the RHS of (3.3) with respect to α and β gives, for $\alpha \neq \pi/2$,

$$(\beta - \alpha)(\sin\alpha \sin\beta + \cos 2\alpha) = \cos\alpha(\sin\beta - \sin\alpha), \quad \text{and} \tag{3.4}$$

$$(\beta - \alpha)\cos\beta = \sin\beta - \sin\alpha. \tag{3.5}$$

Replacing $(\beta - \alpha)/(\sin\beta - \sin\alpha)$ in (3.3) by using (3.5) gives

$$V = \frac{kb}{\cos\alpha \cos\beta}. \tag{3.6}$$

By inspection, V is a minimum when $\alpha = \beta = 0$, which satisfy both (3.4) and (3.5). Therefore, the LUB arc is the straight line shown in Fig. 2.2b.

$$\alpha_o = \beta_o = 0; \quad V^{LUB} = kb. \tag{3.7}$$

Note that the $V^{LUB} = kb$ is only 2.2% higher than the slip line field (SLF) solution $V^{SLF} = 0.978kb$ (McClintock and Clerico, 1980).

Premise: the reference stress σ_r

As in the theorem, assume that the normal traction on the LUB arc, σ, satisfies the Hencky equation of equilibrium (2.1), which gives the normal stress as constant along the straight line:

$$\sigma(\psi) = \sigma_r. \tag{3.8}$$

The reference stress σ_r is chosen to satisfy equilibrium normal to the chord (in the 2-direction of Fig. 2.2b, with $N = 0$):

$$0 = \Sigma F_2 = \sigma(\psi)b = \sigma_r b; \quad \sigma_r = 0 = \sigma. \tag{3.9}$$

Conclusion: global equilibrium

Since σ_r was chosen to equilibrate $N(= 0)$, it is sufficient to show the validity of the conclusion that the traction on the LUB arc is in equilibrium with the loading

components, $V^{l\,\prime\prime B}(= kb)$ and $M(= V^{LUB}h)$. For the *1-2* coordinate system of Fig. 2.2b, equilibrium in the *1*-direction is

$$\Sigma F_1 = V^{LUB} - kb = 0.$$

Moment equilibrium about the point O is

$$\Sigma M_C = M(h) - kbh = V^{LUB}h - kbh = 0.$$

Thus the assumed traction on the LUB arc is in global equilibrium with the loadings, as predicted by the theorem.

Estimated vs. slip line crack tip stress

Geometry gives the slip angle at the crack tip, θ_s:

$$\theta_s = \alpha_o = 0. \tag{3.10}$$

The assumed normal traction distribution (3.9) gives σ_s at $\theta_s = 0$ (trivially):

$$\left(\frac{\sigma_s}{2k}\right)_{\theta=0} = 0. \tag{3.11}$$

The slip line solution for this asymmetric problem (McCLINTOCK and CLERICO, 1980) gives the crack tip stress varying linearly with θ. The maximum (minimum) stress occurs at $\theta = 8.1761^o(-8.1761^o)$:

$$\left(\frac{\sigma_s}{2k}\right)^{SLF}_{\theta_s=\pm 8.1761^o} = \pm 0.1427. \tag{3.12}$$

The slip line field has displacement discontinuities of $\delta u_s/\delta(2u_V)$=0.1541 at $\theta =$

$\pm 8.1761^o$, either side of a fan with shear strain singularity $\gamma/(2u_V) = 2.4441/r$.

3.2. Punch indentation

The punch indentation problem can also be thought of as a doubly, deep-grooved specimen in tension. Slip line displacement fields are non-unique: three were proposed by PRANDTL, HILL, and NEIMARK, respectively (HILL, 1950; NEIMARK, 1968).

Premise: the LUB arc (and its corresponding bound)

Figure 2.3a shows a kinematically admissible displacement field with a flow discontinuity across a curved arc with its radius R and half-angle ω. For the given $M_C(=0)$ and $V(=0)$, we seek the LUB arc parameters, R_o and ω_o, and the corresponding bound N^{LUB}. From relative sliding along the circular arc, the principle of virtual work gives

$$N\delta u_N = k(2R\omega)R\delta\phi. \tag{3.13}$$

Geometry gives the relation between δu_N and $\delta\phi$:

$$\delta u_N = (R\sin\omega - \frac{b}{2})\delta\phi. \tag{3.14}$$

Eliminating δu_N in (3.13) using (3.14) gives

$$N = 2k\frac{\omega R^2}{(R\sin\omega - b/2)}. \tag{3.15}$$

Minimization of the RHS of (3.15) with respect to R and ω gives two conditions for the LUB arc:

$$R\sin\omega = b. \tag{3.16}$$

$$2R(\sin\omega - \omega\cos\omega) = b. \tag{3.17}$$

The LUB arc parameters, ω_o and R_o, can be determined by solving (3.16) and (3.17), and N^{LUB} can be determined from (3.15):

$$\omega_o = 66.78^o; \quad R_o = 1.0881b; \quad N^{LUB} = 4k\omega_o R_o^2/b = 2.7601(2kb). \tag{3.18}$$

The LUB arc is shown in Fig. 2.3b. Note that $N^{LUB}/(2kb) = 2.7601$ is only 7.4% higher than the SLF solution $N^{SLF}/(2kb) = (2+\pi)/2 = 2.5708$ (HILL, 1950).

Premise: the reference stress σ_r

For the theorem, choose the reference stress to satisfy equilibrium normal to the chord (in the 2-direction). Then with $\sigma(\psi) < 0$ for indentation,

$$0 = \Sigma F_2 = \int_{-\omega_o}^{\omega_o} (k\sin\psi - \sigma(\psi)\cos\psi)R_o d\psi - N^{LUB}. \tag{3.19}$$

For the incremental rotation shown, the slip line is analogous to an α-line and its increment counter-clockwise from the x-axis is $-\delta\psi$. Then the first Hencky equation is $\sigma(\psi) = \sigma_r - 2k\psi$, and (3.19) gives, with N^{LUB} from (3.18),

$$\sigma_r = -2k\frac{\omega_o R_o}{b\sin\omega_o} = -1.3801(2k). \tag{3.20}$$

Thus the normal traction distribution on the LUB arc is

$$\sigma(\psi) = \sigma_r - 2k\psi = -2k(1.3801 + \psi). \tag{3.21}$$

Conclusion: global equilibrium

Since σ_r was chosen for equilibrium normal to the chord, to validate the theorem for plane equilibrium, it is sufficient to show that the traction on the LUB arc is in equilibrium with the loading component parallel to the chord, and with the moment about any convenient point.

For the *1*-direction of Fig. 2.3b, with $\sigma(\psi)$ from (3.21),

$$\begin{aligned}\Sigma F_1 &= \int_{-\omega_o}^{\omega_o} [k\cos\psi + (\sigma_r - 2k\psi)\sin\psi] R_o d\psi, \\ &= 2kR_o(\sin\omega_o - 2\omega_o\cos\omega_o),\end{aligned}$$

which is zero from (3.16) and (3.17).

Moment equilibrium, taken about the center of the arc (the point O) for convenience, with N^{LUB} from (3.18) is

$$\Sigma M_O = N^{LUB}\left(\frac{b}{2}\right) - 2kR_o^2\omega_o = 0.$$

Thus the assumed traction on the LUB arc is in global equilibrium with the loadings, as assured by the theorem.

Estimated vs. slip line edge (crack tip) stress

Geometry gives the slip line angle at the edge, θ_s:

$$\theta_s = \omega_o (= 66.8^o). \tag{3.22}$$

The assumed normal traction (3.21) with $\psi = \omega_o$ gives the estimated normal stress on the LUB arc at the edge, σ_s :

$$\left(\frac{\sigma_s}{2k}\right)^{LUB}_{\theta_s = 66.8^o} = \frac{\sigma_r}{2k} - \omega_o = -2.5459. \tag{3.23}$$

For crack growth in tension, the sign in (3.23) would be reversed. For a fully-plastic crack growth criterion based on alternating sliding off and cracking on a symmetrical pair of slip planes (McClintock *et al.*, 1993), the fan of the Prandtl field would be

replaced by a concentrated slip plane within it. For slip planes at $\theta = 45^o$ to 90^o, for example, the Prandtl solution gives $\sigma_s/2k$=2.0708 to 1.2854, respectively. Thus the estimate is high by a factor of 1.2 to 2. If cleavage cracking is of concern, one can estimate σ_{max} directly ahead of the crack by assuming that σ varies linearly with θ from $\theta = \theta_s$ to $\theta = 45^o$, and remains constant from $\theta = 45^o$ to $\theta = 0^o$, as in the Prandtl field. Then

$$\left(\frac{\sigma_{max}}{2k}\right)^{LUB}_{0^o \le \theta \le 45^o} = \left(\frac{\sigma_s}{2k}\right)^{LUB}_{\theta=66.8^o} + \frac{1}{2} + \left(\theta_s - \frac{\pi}{4}\right) = 3.4264 \qquad (3.24)$$

which is 33.3% higher than $(\sigma_{max}/2k)^{SLF}_{0^o \le \theta \le 45^o} = (2 + \pi)/2 = 2.5708$ in the Prandtl field solution.

3.3. Three-point bending plates with deep cracks and various length-to-ligament ratios

Wu *et al.* (1987) studied slip line fields for three-point bend test specimens (Fig. 2.4a) with various a/t and a fixed $L/t(= 8)$. For deep cracks ($a/t \ge 0.2$), the remaining ligament b rather than the specimen thickness t is important, so this problem is analogous to plates with various L/b.

Premise: the LUB arcs (and their corresponding bounds)

Consider three-point bending of single-face-cracked plates with cracks deep enough to prevent shoulder deformation and sharp enough to prevent flank deformation. For such plates, the net section is subject to combined bending and shear. (The effect of concentrated load is ignored.) The principle of virtual work relates the work by the applied moment and force to that due to relative sliding along the circular arc (Fig.

2.4b),

$$\frac{P}{2}\left(\frac{L}{2}-h\right)+\frac{P}{2}(H+h)=kR^2(\alpha-\beta). \tag{3.25}$$

The parameters H and R are related to α and β through geometry:

$$H=R\cos\alpha;\quad R=\frac{b}{\sin\alpha-\sin\beta}. \tag{3.26}$$

Eliminating H and R in (3.25) using (3.26) gives

$$P=2kb\frac{(\alpha-\beta)}{(\sin\alpha-\sin\beta)[(\sin\alpha-\sin\beta)(L/2b)+\cos\alpha]}. \tag{3.27}$$

Minimization of the RHS of (3.27) with respect to α and β gives two equations with two unknowns, α and β:

$$\begin{aligned}&(\sin\alpha-\sin\beta)[\frac{L}{2b}(\sin\alpha-\sin\beta)+\cos\alpha]\\&-(\alpha-\beta)[\cos 2\alpha+\sin\alpha\sin\beta+2\left(\frac{L}{2b}\right)\cos\alpha(\sin\alpha-\sin\beta)]=0.\end{aligned} \tag{3.28}$$

$$\begin{aligned}&(\sin\alpha-\sin\beta)[\frac{L}{2b}(\sin\alpha-\sin\beta)+\cos\alpha]\\&-(\alpha-\beta)[\cos\alpha\cos\beta+2\left(\frac{L}{2b}\right)\cos\beta(\sin\alpha-\sin\beta)]=0.\end{aligned} \tag{3.29}$$

Note that in the limit when $(L/2)/b\to 0$, (3.28) and (3.29) become (3.15) and (3.16) for pure shear. For a given specimen half-length $(L/2)/b$, the LUB arc parameters α_o and β_o can be found by solving (3.28) and (3.29). The resulting values are shown in Fig. 2.5 for $0<(L/2)/b\leq 25$. The LUB analysis gives $\alpha_o=\beta_o=0$ for pure shear, and $\alpha_o=-\beta_o=66.8^o$ for pure bending, as approached in Fig. 2.5. Note that, from geometry, the slip line angle θ_s is

$$\theta_s=\alpha_o. \tag{3.30}$$

Figure 2.5 also includes the slip line angles[1] θ_s from the SLF analysis, drawn with circles. Note that θ_s from Wu *et al.* (1980) approaches to 76^o, not to 72^o, as $L/(2b)\to$

[1]The slip line angle θ_s can be deduced from Fig. 2.2 and Table 1 of Wu *et al.* (1987): $\theta_s=\gamma+2\lambda-\pi/4$.

∞. It is because, as $a/t \to 1$ (or as $L/(2b) \to \infty$), the (slip line) field proposed by WU *et al.* (1987) can not recover Green and Hundy slip line field for pure bending, and therefore their fields give only upper bounds to the limit loads. The values of slip angles from the LUB analysis underestimate those from the SLF analysis by 17.2–14.0% for $(L/2)/b = 2.5 - 20$. Note that in the limit of pure bending, $\theta_s^{LUB} = 66.8^o$ is 7.2% lower than $\theta_s^{SLF} = 72.0^o$ (GREEN and HUNDY, 1956).

Once α_o and β_o are determined, P^{LUB} can be determined from (3.27). Figure 2.6 shows resulting values together with the slip line solutions. The LUB analysis overestimates the limit loads by 2.2–6.6% for $L/2b = 2.5 - 20$.

Premise: the reference stress σ_r

As in the theorem, assume the normal component of traction σ along the LUB arcs satisfies the Hencky equilibrium equation (2.1). The unknown constant σ_r is chosen to equilibrate the given zero normal force, $N_n = 0$. Normal force equilibrium gives

$$\Sigma F_y = 0 = \int_{\beta_o}^{\alpha_o} [\sigma(\psi) \cos\psi + k \sin\psi] R d\psi. \tag{3.31}$$

Equation (3.31) with the Hencky equation, $\sigma(\psi) = \sigma_r + 2k\psi$, gives

$$\frac{\sigma_r}{2k} = -\frac{2(\alpha_o \sin\alpha_o - \beta_o \sin\beta_o) + (\cos\alpha_o - \cos\beta_o)}{2(\sin\alpha_o - \sin\beta_o)}. \tag{3.32}$$

For brevity, and since the previous two examples should be sufficient to support the theorem, we do not show here that the resulting assumed tractions are indeed in

global equilibrium with the loading.

Estimated vs. slip line crack tip stresses

The crack tip normal stress on the LUB arc, σ_s, can be found from the Hencky equation with $\psi = \alpha_o$:

$$\left(\frac{\sigma_s}{2k}\right)^{LUB}_{\theta=\alpha_o} = \left(\frac{\sigma_r}{2k}\right) + \alpha_o, \tag{3.33}$$

where $\sigma_r/(2k)$ is given by (3.32). Figure 2.7 shows resulting values of $(\sigma_s/2k)^{LUB}_{\theta=\alpha_o}$ from the LUB analysis. Note that the stresses are evaluated at $\theta = \theta_s^{LUB}(= \alpha_o) < \theta_s^{SLF}$. For comparison, correct $\sigma_s/(2k)$ as in Sec. 3.2:

$$\left(\frac{\sigma_s}{2k}\right)^{LUB}_{\theta=\theta_s^{SLF}} = \left(\frac{\sigma_s}{2k}\right)^{LUB}_{\theta=\alpha_o} + (\theta_s^{SLF} - \alpha_o). \tag{3.34}$$

The resulting corrected values of $\sigma_s/2k$ at $\theta = \theta_s^{SLF}$ are shown in Fig. 2.7 together with the SLF solutions. The corrected values of $(\sigma_s/2k)_{\theta=\theta_s^{SLF}}$ from the LUB analysis differ from the SLF solutions only by 6%. (Note that in the limit of pure bending, $(\sigma_s/2k)_{\theta=66.8^o} = 1.162$ and $(\sigma_s/2k)_{\theta=72^o} = 1.542$).

4. APPLICATIONS OF THE THEOREM TO PROBLEMS WITHOUT SLIP LINE FIELDS

In this section, we apply the theorem to three problems for which slip line fields are not available: deep, single-face-cracked plates under both combined bending and tension and under combined bending, tension, and shear, and unequally grooved plates under pure bending. For compact notation throughout the section, length variables are normalized with respect to the remaining ligament b:

$$\hat{R} = R/b; \quad \hat{L} = L/b; \quad \hat{H} = H/b; \quad \hat{h} = h/b. \tag{4.1}$$

Loading variables based on the net section are normalized with respect to unnotched plane strain limit loads using b and the shear strength k:

$$\hat{V}_n = V_n/(kb); \qquad \hat{N}_n = N_n/(2kb); \qquad \hat{M}_n = M_n/(2kb^2/4). \tag{4.2}$$

4.1. Deep, single-face-cracked plates under combined bending and tension

Consider combined bending and tension of single-face-cracked plates with cracks deep enough to prevent shoulder deformation, and sharp enough to prevent flank deformation. For such plates under pure extension, the slip line field (McCLINTOCK, 1971) gives the slip line angle θ_s and the crack tip triaxiality on that line $\sigma_s/2k$:

$$\theta_s = 45.0^o; \quad \left(\frac{\sigma_s}{2k}\right)_{\theta=\theta_s} = 0.500. \tag{4.3}$$

Under opening bending with compression or small tension ($-1 \leq \hat{N}_n < 0.5512$), the modified Green and Hundy slip line fields (SHIRATORI and MIYOSHI, 1980; SHIRATORI and DODD, 1980) give $\sigma_s/2k$ and θ_s as constants:

$$\theta_s \doteq 72.0^o; \quad \left(\frac{\sigma_s}{2k}\right)_{\theta=\theta_s} \doteq 1.542. \tag{4.4}$$

The fields also give a yield locus:

$$\Phi = \hat{M}_n + 0.7394\hat{N}_n^2 - 0.5212\hat{N}_n - 1.2606 = 0 \text{ for } -1 \leq \hat{N}_n < 0.5512. \tag{4.5}$$

Under large tension ($0.5512 \leq \hat{N}_n < 1$), slip line fields are not known but RICE (1972) proposed kinematically admissible flow fields, each consisting of a curved arc

(Fig. 2.8a).

The LUB arcs and their corresponding bounds

For given $\hat{V}_n(=0)$ and $\hat{N}_n$, the LUB to $\hat{M}_n$ is sought (Fig. 2.8a). From relative sliding along the circular arc, the principle of virtual work gives

$$\hat{M}_n = 2\hat{R}^2(\alpha - \beta) - 4\hat{N}_n(\hat{L} + \frac{1}{2}). \tag{4.6}$$

If α and β are chosen as two independent arc parameters, then two additional parameters $\hat{R}$ and $\hat{L}$ can be found in terms of α and β from the geometry in Fig. 2.8a:

$$\hat{L} = \hat{R}\sin\beta, \qquad \hat{L} + 1 = \hat{R}\sin\alpha. \tag{4.7}$$

Minimization of $\hat{M}_n$ with respect to α and β, subject to the two constraints (4.7), gives two equations for the two unknowns α and β:

$$(\alpha - \beta)\cos\alpha - (\sin\alpha - \sin\beta)(\frac{1}{2} + \hat{N}_n\cos\alpha\sin\beta) = 0. \tag{4.8}$$

$$(\alpha - \beta)\cos\beta - (\sin\alpha - \sin\beta)(\frac{1}{2} + \hat{N}_n\sin\alpha\cos\beta) = 0. \tag{4.9}$$

Resulting values of α_o and β_o are shown in terms of $\hat{N}_n$ ($0.5512 \leq \hat{N}_n < 1$) in Fig. 2.9. The values of α_o and β_o from the LUB analysis are consistent with the slip line solutions at both ends; $\alpha_o = 72.0^o$; $\beta_o = -45.0^o$ at $\hat{N}_n = 0.5512$, and $\alpha_o = \beta_o = 45^o$ at $\hat{N}_n = 0$. (The strange minimum of curvature for β_o has been verified numerically.)

Once α_o and β_o are determined, $\hat{M}_n^{LUB}$ can be determined from (4.6) with (4.7):

$$\hat{M}_n^{LUB} = 2\frac{\alpha_o - \beta_o}{(\sin\alpha_o - \sin\beta_o)^2} - 2\hat{N}_n\frac{(\sin\alpha_o + \sin\beta_o)}{(\sin\alpha_o - \sin\beta_o)}. \tag{4.10}$$

Figure 2.10 shows the resulting yield locus, including that from the SLF analysis (4.5).

LEE and PARKS (1993) studied yield loci for various crack depths via finite elements. By comparing yield loci for various crack depths, they suggest that relative crack depths of a/t to prevent shoulder deformation range from 0 for pure tension through 0.35 for combined tension and bending to 0.3 for pure bending. Their results for relative crack depths of $a/t = 0.5$ and 0.6 are shown with circles in Fig. 2.10. For predominant bending ($0 \leq \hat{N}_n < 0.5512$), their results are consistent with the slip line solutions. For combined bending with large tension ($0.5512 \leq \hat{N}_n \leq 1.0$), the locus from the LUB analysis overestimates the FEM results by up to 3%.

Reference stress σ_r

As in the theorem, assume the normal component of traction, σ, along the LUB arcs satisfies the Hencky equilibrium equation (2.1). The reference stress σ_r is chosen to equilibrate the given zero shear force, $V_n = 0$. Shear force equilibrium gives

$$0 = \frac{\Sigma F_x}{2kb} = \int_{\beta_o}^{\alpha_o} \left(\frac{\cos\psi}{2} - \frac{\sigma(\psi)}{2k}\sin\psi\right)\hat{R}_o d\psi. \tag{4.11}$$

Equation (4.11) with the Hencky equation, $\sigma(\psi) = \sigma_r + 2k\psi$, gives $\sigma_r/2k$ in terms of α_o and β_o:

$$\frac{\sigma_r}{2k} = \frac{(\sin\alpha_o - \sin\beta_o) - 2(\alpha_o\cos\alpha_o - \beta_o\cos\beta_o)}{2(\cos\alpha_o - \cos\beta_o)}. \tag{4.12}$$

Estimated crack tip stress

The slip line angle (θ_s) can be found from geometry:

$$\theta_s = \alpha_o. \tag{4.13}$$

The normal stress across the LUB arc at the crack tip, σ_s, is found from the Hencky

equilibrium equation (2.1) with the constant σ_r determined from (4.12):

$$\left(\frac{\sigma_s}{2k}\right)_{\theta_s} = \frac{\sigma_r}{2k} + \alpha_o. \tag{4.14}$$

Resulting values of $\sigma_s/2k$ and θ_s are shown in Fig. 2.11 in terms of a "net section bending ratio", μ_n:

$$\mu_n \equiv \frac{M_n}{bN_n} = \frac{\hat{M}_n}{4\hat{N}_n}. \tag{4.15}$$

The net section bending ratio varies from 0 for pure extension to ∞ for pure bending. Modified Green and Hundy slip line fields (SLF) can be applied for $\hat{N}_n \leq 0.5512$, or $\mu_n \leq 0.6001$. The estimated values of $(\sigma_s/2k)_{\theta_s}$ and θ_s agree with SLF solutions at μ_n=0 ($\hat{N}_n = 1$) and μ_n=0.6001 ($\hat{N}_n = 0.5512$). For predominant bending, θ_s from FE analysis (LEE and PARKS, 1993) is consistent with the slip line solution, but the FE estimate of $(\sigma_s/2k)_{\theta_s}$ at $\mu_n = 0.64$ underestimates the slip line solution by 4.5%. For bending with large tension, the LUB approximation agrees with the FE results within 6% in θ_s and within 8% in $(\sigma_s/2k)_{\theta_s}$.

4.2. Deep, single-face-cracked plates under combined shear, tension, and bending

Consider a deep, single-face-cracked plate of length h, subject to combined shear $V_n(\geq 0)$, tension $N_n(\geq 0)$, and opening bending $M_n(h) = M_n(0) - V_n h$, as shown in Fig. 2.12.

The LUB arcs and their corresponding bounds

For given V_n and N_n, M_n^{LUB}, is sought. From relative sliding along the circular arc, the principle of virtual work gives, in terms of normalized variables,

$$\hat{M}_n(\hat{h}) = 2\hat{R}^2(\alpha - \beta) - 4\hat{N}_n\left(\hat{L} + \frac{1}{2}\right) - 2\hat{V}_n(\hat{H} + \hat{h}). \tag{4.16}$$

Replacing $\hat{M}_n(\hat{h})$ in (4.16) by using $\hat{M}_n(0) - 2\hat{V}_n\hat{h}$ gives

$$\hat{M}_n(0) = 2\hat{R}^2(\alpha - \beta) - 4\hat{N}_n\left(\hat{L} + \frac{1}{2}\right) - 2\hat{V}_n\hat{H}. \tag{4.17}$$

With two independent arc parameters as α and β, define additional parameters $\hat{R}$, $\hat{L}$, and $\hat{H}$ in terms of α and β from geometry in Fig. 2.12:

$$\hat{R} = \frac{1}{\sin\alpha - \sin\beta}; \quad \hat{L} = \hat{R}\sin\alpha - 1; \quad \hat{H} = \hat{R}\cos\alpha. \tag{4.18}$$

Minimization of $\hat{M}_n(0)$ with respect to α and β, subject to the three constraints (4.18), gives two equations for the two unknowns α and β:

$$(\alpha - \beta)\cos\alpha - (\sin\alpha - \sin\beta)\left[\frac{1}{2} + \hat{N}_n\sin\beta\cos\alpha + \frac{1}{2}\hat{V}_n(1 - \sin\alpha\sin\beta)\right] = 0. \tag{4.19}$$

$$(\alpha - \beta)\cos\beta - (\sin\alpha - \sin\beta)\left[\frac{1}{2} + \hat{N}_n\sin\alpha\cos\beta + \frac{1}{2}\hat{V}_n\cos\alpha\cos\beta\right] = 0. \tag{4.20}$$

Note that in the limiting case of $\hat{V}_n = 0$, (4.19) and (4.20) recover (4.8) and (4.9). For given $\hat{V}_n$ $(0 \le \hat{V}_n \le 1)$ and $\hat{N}_n$ $(0 \le \hat{N}_n \le 1)$, the LUB arc parameters, α_o and β_o, can be determined by solving (4.19) and (4.20). The resulting values are shown in Fig. 2.13.

The corresponding $M_n^{LUB}(0)$ can be determined from (4.17) with (4.18):

$$\hat{M}_n^{LUB}(0) = 2\frac{\alpha_o - \beta_o}{(\sin\alpha_o - \sin\beta_o)^2} - 2\hat{N}_n\frac{(\sin\alpha_o + \sin\beta_o)}{(\sin\alpha_o - \sin\beta_o)} - 2\hat{V}_n\frac{\cos\alpha_o}{(\sin\alpha_o - \sin\beta_o)}. \tag{4.21}$$

The resulting yield locus is shown in Fig. 2.14. Figure 2.15 shows the locus for $M_n^{LUB}(0) = 0$, which is the yield locus for deep, single-face-cracked plates under combined shear and tension.

Traction distribution and crack tip stresses on the LUB arcs

Choose the midpoint of the LUB arc as the reference point, $\psi = 0$ (Fig. 2.12).

Then the reference stress σ_r can be determined from (2.4), with $\omega_o = (\alpha_o - \beta_o)/2$ and $\xi_o = (\alpha_o + \beta_o)/2$:

$$\sigma_r = \left[-V_n^* \sin\left(\frac{\alpha_o + \beta_o}{2}\right) + \hat{N}_n^* \cos\left(\frac{\alpha_o + \beta_o}{2}\right)\right] \frac{(\sin\alpha_o - \sin\beta_o)}{2\sin[(\alpha_o - \beta_o)/2]}. \tag{4.22}$$

The normal stress on the LUB arc at the crack tip can be found from the Hencky equation with $\psi = (\alpha_o - \beta_o)/2$:

$$\left(\frac{\sigma_s}{2k}\right)_{\theta_s} = \frac{\sigma_r}{2k} + \frac{(\alpha_o - \beta_o)}{2}. \tag{4.23}$$

General results for $(\sigma_s/2k)_{\theta_s}$ are shown in Fig. 2.16, and those under only shear and tension (with $M_n^{LUB}(0) = 0$) are shown in Fig. 2.17.

4.3. Unequally grooved plates under pure bending

Consider an unequally grooved plate in pure bending (Fig. 2.18a). Suppose that an arbitrary circular arc is chosen, and assume that the normal component of traction on the arc, σ, satisfies the Hencky equation (2.1), $\sigma(\psi) = \sigma_r + 2k\psi$. In the *1-2* coordinates parallel and normal to the chord of the arc, denote the resultant generalized forces due to the assumed traction distribution as $P_{iH}(i = 1, 2, 3)$ (Fig. 2.18a). Then

$$P_{1H}(R, \omega) = -\int_{-\omega}^{\omega} [k\sin\psi + (\sigma_r + 2k\psi)\cos\psi] R d\psi = -2kR(2\omega\cos\omega - \sin\omega). \tag{4.24}$$

$$P_{2H}(\sigma_r; R, \omega) = -\int_{-\omega}^{\omega} [k\cos\psi - (\sigma_r + 2k\psi)\sin\psi] R d\psi = -2R\sigma_r \sin\omega. \tag{4.25}$$

Since no force components are applied, $N = V = 0$, force equilibrium requires

$$P_{1H} = P_{2H} = 0. \tag{4.26}$$

For $P_{1H} = 0$, from (4.24),

$$2\omega = \tan\omega \quad \text{or} \quad 2\omega = 133.6^o. \tag{4.27}$$

This implies that under pure bending the included angle of the arc 2ω is independent of back angle. For $P_{2H} = 0$, from (4.25),

$$\sigma_r = 0. \tag{4.28}$$

This implies similarly that under pure bending, from the Hencky equation (2.1), the normal stress on the arc at the crack tip, σ_s, should be constant under pure bending condition:

$$\left(\frac{\sigma_s}{2k}\right) = \omega = 1.166. \tag{4.29}$$

Also from relative sliding along the circular arc, the principle of virtual work gives

$$M = 2kR^2\omega. \tag{4.30}$$

To minimize M for the LUB, since ω=constant R should be minimized. This leads to the field of Fig. 2.18b, with $R_o \sin\omega_o = b/2$ and $\omega_o = 66.8^o$. In summary, the LUB arc for unequally grooved plates is independent of back angle ϕ, as shown in Fig. 2.18b:

$$\frac{M^{LUB}}{0.5kb^2} = 1.380; \quad \theta_s = 66.8^o; \quad \left(\frac{\sigma_s}{2k}\right)_{\theta_s} = 1.166. \tag{4.31}$$

It is indeed the same as the SLF solution for symmetric doubly-face-grooved plates in pure bending (e.g. GREEN and HUNDY, 1956; MCCLINTOCK, 1972). Note that for a single-face-cracked plate, the Green and Hundy slip line field gives

$$\frac{M^{LUB}}{0.5kb^2} = 1.261; \quad \theta_s = 72.0^o; \quad \left(\frac{\sigma_s}{2k}\right)_{\theta_s} = 1.542. \tag{4.32}$$

Thus back angles do affect the slip line field, in contrast to the present LUB approach.

5. DISCUSSION

5.1. Predicting fully plastic crack growth from the LUB fields

For a given far field (generalized) displacement increment δq^{∞} in a fully plastic structure, predicting fully plastic crack growth requires finding the crack growth increment δa. From crack growth kinematics, the crack tip opening displacement $CTOD$ per unit crack growth is related to the crack tip opening angle $CTOA$:

$$\frac{\delta CTOD/2}{\delta a} = \tan\left(\frac{CTOA}{2}\right). \tag{5.1}$$

If the CTOD per unit far field displacement, $\delta CTOD/\delta q^{\infty}$, can be found, then from (5.1),

$$\frac{\delta a}{\delta q^{\infty}} = \left[\frac{1}{\tan(CTOA/2)}\right]\left[\frac{\delta CTOD/2}{\delta q^{\infty}}\right]. \tag{5.2}$$

Therefore, prediction of fully plastic crack growth requires estimates of $CTOA$ and $\delta CTOD/\delta q^{\infty}$.

For crack tip fields approximated by a pair of slip lines, McCLINTOCK *et al.* (1993) proposed modeling crack growth as a zig-zagging process, sliding off and cracking along a slip plane before changing direction . Using this model together with equations from micromechanisms of crack growth, they gave equations for the $CTOA$ in terms of θ_s, σ_s, and material parameters. For instance, with negligible void nucleation strain in a non-hardening material, the estimated $CTOA$ exhibits an inverse exponential dependence on σ_s and a higher order parabolic dependence on θ_s:

$$\tan\left(\frac{CTOA}{2}\right) = \left[\frac{A\sin 2\theta_s}{2\sinh(\sigma_s/k) - A\sin 2\theta_s}\right]\tan\theta_s, \tag{5.3}$$

where the parameter A in (5.3) reflect material properties and must be determined

from fully plastic crack growth tests. As shown in Secs. 3 and 4, the present analysis provides estimates of θ_s and σ_s.

The LUB arc also provides $\delta CTOD/\delta q^\infty$ through its assumed deformation (rotation across the arc). In three-point bending plates of a length L and a remaining ligament b for $(L/2)/b = 2.5 - 25$, the $CTOD$ per unit load-point displacement u_P, $\delta CTOD/\delta u_P$, is

$$\left(\frac{\delta CTOD}{\delta u_P}\right)^{SLF} = \frac{R^{SLF}\sin\theta_s}{(L/2)} \; ; \; \left(\frac{\delta CTOD}{\delta u_P}\right)^{LUB} = \frac{R^{LUB}\sin\theta_s}{(L/2)}, \qquad (5.4)$$

where R is the radius of the circular arc. Note that due to the constant stress sector in the slip line fields, R^{SLF} is smaller than R^{LUB}, and thus $(\delta CTOD/\delta u_P)^{SLF}$ is smaller than $(\delta CTOD/\delta u_P)^{LUB}$. As shown in Fig. 2.19, the LUB arc overestimates $(\delta CTOD/\delta u_P)$ by a factor of 2.1 to 2.31. In pure bending of deep, single-face-cracked plates, for a given rotation increment $\delta\phi$, the LUB arc overestimates $(\delta CTOD/b\delta\phi)$ by a factor of 1.35 $((\delta CTOD/b\delta\phi)^{LUB} = 0.5$; $(\delta CTOD/b\delta\phi)^{SLF} = 0.37)$. In punch indentation, the $CTOD$ per unit far-field end-to-end displacement $2\delta u_N$, $\delta CTOD/2\delta u_N$, varies from 1.5 to 2 for various assumed slip line fields, but is 1 for the arcs.

For deep, single-face-cracked plates under combined bending and tension, LEE and PARKS (1993) also found the $\delta CTOD$ in terms of far-field generalized displacement increments, δu^∞ and $\delta\theta^\infty$ via finite elements:

$$\delta CTOD = \delta u^\infty + \left(\frac{t}{2} - a\right)\delta\theta^\infty, \qquad (5.5)$$

where a is the crack depth. In terms of the net-section variables $\delta u_n^\infty (= \delta u^\infty - a\delta\theta^\infty/2)$

and $\delta\theta_n^\infty (= \delta\theta^\infty)$,

$$\delta CTOD = \delta u_n^\infty + \frac{b}{2}\delta\theta_n^\infty, \tag{5.6}$$

where $b(= t - a)$ is the remaining ligament. From (5.6),

$$\left(\frac{\delta CTOD}{\delta u_n^\infty}\right) = 1 + \frac{b}{2}\frac{\delta\theta_n^\infty}{\delta u_n^\infty} \; ; \; \left(\frac{\delta CTOD}{b\delta\theta_n^\infty}\right) = \frac{1}{2} + \frac{\delta u_n^\infty}{b\delta\theta_n^\infty}. \tag{5.7}$$

Therefore, the accuracy of $\delta CTOD/\delta q_n^\infty$ depends on how well the LUB analysis predicts the normal to the (real) yield surface. Judging from Fig. 2.10, the LUB analysis predicts normal to the yield surface within at most 20% (at around $\hat{N}_n = N_n/(2kb) \approx 0.6 - 0.7$ where $\delta u_n^\infty/(b\delta\theta_n^\infty)$, and thus predicts $\delta CTOD/\delta q^\infty$ within 10%.

The above results, with the results for σ_s discussed in Sec. 3, indicate that while the arcs are useful for estimating the limit load, they may not be of much help in predicting fully plastic crack growth for some cases. The next section discusses this issue.

5.2. Accuracy of the present analysis

When we apply the present method to problems for which slip line fields are not available, can we say something about the accuracy of the results from the present analysis? In general the accuracy of the present method should depend on the difference between the LUB field and the corresponding slip line field.

For the limit load, the LUB arc provides a close upper bound, even when the LUB field is quite different from the slip line field. For example, in punch indentation and deep, single-face-cracked plates in pure bending, the LUB arc overestimates the limit loads only by 7.3% and 9.5%, respectively.

For the slip plane angle θ_s, the LUB arc also provides a close estimate. For example, in deep, single-face-cracked plates in pure bending, the LUB arc underestimates θ_s only by 7% ($\theta_s^{LUB} = 66.8^o$ and $\theta_s^{SLF} = 72.0^o$). In punch indentation, the LUB arc gives $\theta_s^{LUB} = 66.8^o$, whereas slip line fields give $\theta_s^{SLF} = 45^o$ to 90^o due to the central fan. The θ_s^{LUB} would be close to the average θ_s^{SLF}.

However, the accuracy of the estimated crack tip stress σ_s and the $CTOD$ per unit far-field generalized displacement, $\delta CTOD/\delta q^\infty$ seem to depend much more strongly on the difference between the LUB arc and the SLF, especially when constant stress regions are present. For example, the Prandtl field consists of two constant stress regions and a fan between them. As shown in Sec. 3, the present method overestimates the normal crack tip stress by 33%. It also underestimates $\delta CTOD/\delta u^\infty$ by 33% to 50%. Another example is the Green and Hundy field for pure bending (Fig. 2.20a), where there is a constant compressive region in free surface to cancel out tensile force resulting from the circular arc. In this case, the present analysis underestimates the crack tip normal stress by 30%, and overestimates $\delta CTOD/(b\delta\theta^\infty)$ by 35%. The examples where the LUB arc resembles the slip line field are deep, single-face-cracked plates under pure shear (Sec. 3.1) and under combined bending with large tension (Sec. 4.1)(judging from a possible slip line field of Fig. 2.20b.) As shown in Fig. 2.11, the present analysis predicts $\sigma_s/2k$ within 8%, compared with the FE results, and $\delta CTOD/\delta q^\infty$ within 10% with the FE results.

6. CONCLUSION

Fully plastic crack tip stresses are estimated from the least upper bounds (LUB's) for plane strain fields based on circular arcs. Suppose that two of the three in-plane components of loading are given, and the arc giving the LUB to the third has been found. Then, it is proven that the one-parameter description of traction across the arc which is consistent with the Hencky equilibrium equation can be chosen such that the tractions on the LUB arc satisfy all three in-plane components of global equilibrium. Therefore, the LUB arc and the approximate stress from it provide useful estimates of stress as well as deformation fields at the crack tip. Together with the fully plastic crack growth criterion proposed by McCLINTOCK*et al.* (1993), the present analysis can be used to predict fully plastic crack growth, as discussed in Sec. 5.1. The theorem is supported with three examples with known slip line fields: singly grooved plates in pure shear (McCLINTOCK and CLERICO, 1980), punch indentation (HILL, 1950; NEIMARK, 1968), and three-point bend test specimens with variable crack depths (WU*et al.*, 1987), and is applied to deep, single-face cracked specimens under combined bending with large tension where the FE limit load analysis (LEE and PARKS, 1993) is available.

Comparing the present analysis with known slip line fields and finite element results gives a number of points about the accuracy of the present analysis:

1. The accuracy of the present method depends on the difference between the LUB field and the corresponding SLF, especially due to the presence of constant stress regions. The examples where the LUB arc differs significantly from

the SLF are punch indentation (Sec. 3.2) and deep, single-face cracked plates in pure bending (Sec. 4.3). The examples where the LUB arc resembles the SLF are deep, single-face-cracked plates under pure shear (Sec. 3.1), and under combined bending with large tension (Sec. 4.1).

2. For limit loads, the LUB arc provides a close upper bound, even when the LUB field is quite different from the SLF. For example, in punch indentation and deep, single-face-cracked plates in pure bending, the LUB arc overestimates the limit load only by 7.3 and 9.5%, respectively.

3. For slip plane angles θ_s, the LUB arc also provides a close estimate. For example, in deep, single-face-cracked plates in pure bending, the LUB arc underestimates θ_s only by 7%. In punch indentation, the LUB arc gives a reasonable θ_s as discussed in Sec. 5.2.

4. For σ_s and $\delta CTOD/\delta q^\infty$, the accuracy depends strongly on the difference between the LUB arc and the SLF. In punch indentation, the present method overestimates σ_s by 33%, and underestimates $\delta CTOD/\delta q^\infty$ by 33% to 50%. In deep, single-face cracked plates in pure bending, the present analysis underestimates σ_s by 30%, and overestimates $\delta CTOD/\delta q^\infty$ by 35%. In contrast, in deep, single-face-cracked plates under combined bending with large tension, as shown in Fig. 2.11, the present analysis predicts $\sigma_s/2k$ within 8% and $\delta CTOD/\delta q^\infty$ within 10%, compared with the FE results as discussed in Sec. 5.1.

REFERENCES

EWING, D.J.F., (1968), "Calculations on the bending of rigid/plastic notched bars", *Journal of the Mechanics and Physics of Solids*, **16**, 205-213.

GREEN, A.P. and HUNDY, B.B., (1956), "Initial plastic yielding in notched bend Tests", *Journal of the Mechanics and Physics of Solids*, **4**, 128-144.

HILL, R., (1950), *The Mathematical Theory of Plasticity*, Oxford University Press, New York.

KIM, Y.J., MCCLINTOCK, F.A. and PARKS, D.M., (1993), "Yield locus in deep, single-face-cracked specimens under combined bending and tension", submitted as Brief Note to *Journal of Applied Mechanics.*

LEE, H. and PARKS, D.M., (1993), "Fully plastic analyses of plane strain single edge cracked specimens subject to combined tension and bending", submitted to *International Journal of Fracture.*

NEIMARK, J.E., (1968), "The fully plastic, plane strain tension of a notched bar", *Journal of Applied Mechanics*, **35**, 111-116.

MCCLINTOCK, F.A., (1971), "Plasticity aspects of fracture", *Fracture Vol. 3* (ed. H. LIEBOWITZ), pp. 47-225. Academic Press, New York.

McCLINTOCK, F.A. and CLERICO, M., (1980), "The transverse shearing of singly-grooved specimens", *Journal of the Mechanics and Physics of Solids*, **28**, pp. 1-16.

McCLINTOCK, F.A., KIM, Y.J. and PARKS, D.M., (1993), "Criteria for plane strain, fully plastic quasi-steady crack growth", submitted to *International Journal of Fracture.* See also Chapter 3 in this volume.

RICE, J.R., (1972), "The line spring model for surface flaws", *The Surface Crack: Physical Problems and Computational Solutions*, pp. 171-185. American Society of Mechanical Engineers, New York.

SHIRATORI, M. and DODD, B, (1980), "Effect of deep wedge-shaped notches of small flank angle on plastic failure", *International Journal of Mechanical Science*, **22**, pp. 127-131.

SHIRATORI, M. and MIYOSHI, T, (1980), 'Evaluation of constraint factor and *J*-integral for single-edge notched specimen", *Proceedings: Third International Conference on Materials Vol. 3*, pp. 425-434. Cambridge, U.K.

WU, S.X., MAI, Y.W. and COTTRELL, B, (1987), "Slip line field solutions of three-point bend specimens with deep notches", *International Journal of Mechanical Science*, **29**, pp. 557-564.

APPENDIX

Proof of the lemma

Characterize a circular arc passing from the crack tip to a free surface by two parameters R and ω, shown in Fig. 2.1. Denote the resultant generalized forces of the assumed traction distribution of Fig. 2.1 as $P_i(i = 1, 2)$. With these conventions and the Hencky equation (2.1), $\sigma(\psi) = \sigma_r + 2k\psi$, the resultants used in the premises of the lemma are

$$P_1(R, \omega) = -\int_{-\omega}^{\omega} (k \sin\psi + \sigma(\psi)\cos\psi) R d\psi = -2kR(2\omega\cos\omega - \sin\omega). \qquad (A.1)$$

$$P_2(\sigma_r; R, \omega) = -\int_{-\omega}^{\omega} (k\cos\psi - \sigma(\psi)\sin\psi) R d\psi = -2R\sigma_r \sin\omega. \qquad (A.2)$$

Denote forces statically equivalent to the applied loadings, V and N, in the *1-2* frame centered at O_A as $P_{iQ}(i = 1, 2)$;

$$P_{1Q} = V\cos\xi + N\sin\xi. \qquad (A.3)$$

$$P_{2Q} = -V\sin\xi + N\cos\xi. \qquad (A.4)$$

For the assumed traction distribution (resultants P_i) to equilibrate the applied forces on the body above the arc, the following two force equilibrium conditions should be satisfied.

$$0 = P_1 + P_{1Q} = -2kR(2\omega\cos\omega - \sin\omega) + (V\cos\xi + N\sin\xi). \qquad (A.5)$$

$$0 = P_2 + P_{2Q} = -2R\sigma_r \sin\omega + (-V^*\sin\xi + N^*\cos\xi). \qquad (A.6)$$

Assume R and ω have been chosen to satisfy equilibrium in the chordal direction, (A.5).

$$2kR(2\omega\cos\omega - \sin\omega) = V\cos\xi + N\sin\xi. \tag{A.7}$$

Equilibrium normal to the chord (A.6) can be satisfied if we choose σ_r as

$$\sigma_r = \frac{-V^*\sin\xi + N^*\cos\xi}{2R\sin\omega}. \tag{A.8}$$

Note that (A.5) and (A.6) are force equilibrium conditions in the orthogonal (*1-2*) coordinates. Since force equilibrium conditions in oblique coordinates gives equilibrium in orthogonal coordinates, the reference stress σ_r can be chosen for equilibrium condition in any other than the chordal direction of (A.5).

With the premises of two force equilibrium conditions satisfied, global equilibrium for the lemma requires only moment equilibrium. This is shown by applying a virtual rotation $\delta\phi$ across the arc and the principle of virtual work with two force equilibrium conditions satisfied. Therefore, if two force equilibrium conditions are satisfied, global equilibrium is always satisfied and thus the lemma is proven.

Proof of the theorem

Conditions for the least upper bound

We seek a convex yield surface corresponding to three independent loading parameters. In this context, minimizing one variable while other two variables are fixed is equivalent to minimizing one of the latter variables with two remaining variables fixed. Therefore it suffices to prove the theorem for the least upper bound to M

when two force components, V and N, are specified. To prove the theorem, we have to show that, for given $V = V^*$ and $N = N^*$, the LUB arc parameters R_o and ω_o providing M^{LUB} satisfy equilibrium in the chordal direction:

$$2kR_o(2\omega_o \cos\omega_o - \sin\omega_o) = V^* \cos\xi_o + N^* \sin\xi_o, \qquad (A.9)$$

where $\xi_o = \hat{\xi}_o(R_o/b, \omega_o)$. With (A.9), the theorem follows from the lemma. The proof will be carried out by showing that an expression for the LHS of (A.9), derived from one LUB condition, is identical to an expression for the RHS of (A.9) derived from the other LUB condition.

For convenience, in addition to the arc parameters R and ω, introduce three additional geometrical parameters, L, H, and ξ (Fig. 2.1):

$$L = R\sin(\xi - \omega), \qquad (A.10)$$

$$L + b = R\sin(\xi + \omega), \qquad (A.11)$$

$$H = R\cos(\xi + \omega). \qquad (A.12)$$

From the principle of virtual work, the work done by external forces is equal to the internal work in the admissible deformation field of rotation by sliding along the arc:

$$M^{UB}\delta q_3 + V^*\delta q_1 + N^*\delta q_2 = 2kR^2\omega\delta\phi. \qquad (A.13)$$

From the conventions in Fig. 2.1,

$$\delta q_3 = \delta\phi, \;\; \delta q_1 = [L + b - x_P]\delta\phi, \text{ and } \delta q_2 = [H + y_P]\delta\phi, \qquad (A.14)$$

where the fixed lengths x_P and y_P are the coordinates of the point at which loads Q_i are applied (Fig. 2.1). From (A.13) and (A.14),

$$M^{UB} = \widehat{M}(V^*, N^*; R, \omega) = 2kR^2\omega - V^*(H + y_P) - N^*(L + b - x_P). \qquad (A.15)$$

The LUB conditions on the arc parameters R_o and ω_o are obtained by minimizing M with respect to R and ω:

$$\frac{\partial \widehat{M}}{\partial R} = 4kR\omega - V^*\frac{\partial H}{\partial R} - N^*\frac{\partial L}{\partial R} = 0; \qquad (A.16)$$

$$\frac{\partial \widehat{M}}{\partial \omega} = 2kR^2 - V^*\frac{\partial H}{\partial \omega} - N^*\frac{\partial L}{\partial \omega} = 0. \qquad (A.17)$$

The solutions to (A.16) and (A.17) give the LUB arc parameters, R_o and ω_o, and

$$M^{LUB} = \widehat{M}(V^*, N^*; R_o, \omega_o). \qquad (A.18)$$

For more compact notation, the arc parameters, R, ω, H, L, and ξ, are from here on understood as LUB parameters, and the partial derivatives of H and L are understood as those evaluated at the LUB points.

First eliminate the partial derivatives of H in the LUB conditions. By geometry, from Fig. 2.1,

$$H^2 + (L + b)^2 = R^2. \qquad (A.19)$$

Differentiating (A.19) with respect to R and ω gives

$$\frac{\partial H}{\partial R} = \frac{R}{H} - \frac{(L + b)}{H}\frac{\partial L}{\partial R}, \qquad (A.20)$$

$$\frac{\partial H}{\partial \omega} = -\frac{(L + b)}{H}\frac{\partial L}{\partial \omega}. \qquad (A.21)$$

Eliminating $\partial H/\partial\omega$ and $\partial H/\partial R$ in (A.16) and (A.17) with (A.20) and (A.21) gives

$$\left[N^* - V^*\frac{(L + b)}{H}\right]\frac{\partial L}{\partial R} = 4kR\omega - V^*\frac{R}{H}. \qquad (A.22)$$

$$\left[N^* - V^*\frac{(L+b)}{H}\right]\frac{\partial L}{\partial \omega} = 2kR^2. \tag{A.23}$$

Eliminating the common factor $[N^* - V^*(L+b)/H]$ in (A.22) and (A.23) gives an alternative LUB condition that will be used with (A.22):

$$\frac{\partial L}{\partial \omega} = \left(\frac{2kR^2}{4kR\omega - V^*R/H}\right)\frac{\partial L}{\partial R}. \tag{A.24}$$

Note that $(4kR\omega - V^*R/H) \neq 0$ for the following reasons: If $(4kR\omega - V^*R/H) = 0$, then from (A.22), either $(N^* - V^*L/H) = 0$ or $\partial L/\partial R = 0$. From (A.23), since $R \neq 0$, $(N^* - V^*L/H) \neq 0$. Also, we will see that $\partial L/\partial R = R\cos^2\omega/(L + b/2)$ cannot vanish for $\omega \neq \pi/2$ (see (A.29)).

An explicit expression for $\partial L/\partial R$ can be obtained from geometric relations as follows. Eliminating L from geometric constraints (A.10) and (A.11) gives

$$\cos\xi = \frac{b}{2R\sin\omega}. \tag{A.25}$$

Again from (A.10),

$$L = R\sin(\xi - \omega) = R[\sin\xi\cos\omega - \cos\xi\sin\omega]. \tag{A.26}$$

Introducing (A.26) into (A.25) gives

$$\sin\xi = \frac{(L + b/2)}{R\cos\omega}. \tag{A.27}$$

Using the identity $\sin^2\xi + \cos^2\xi = 1$ along with (A.25) and (A.27) gives

$$4(L + \frac{b}{2})^2\sin^2\omega + b^2\cos^2\omega = 4R^2\sin^2\omega\cos^2\omega. \tag{A.28}$$

Differentiation of (A.28) with respect to R gives the explicit expression for $\partial L/\partial R$:

$$\frac{\partial L}{\partial R} = \frac{R\cos^2\omega}{L + b/2}. \tag{A.29}$$

Inserting (A.29) into (A.22) and (A.24) gives two LUB conditions:

$$N^* = V^* \frac{1}{H}\left[(L+b) - \frac{(L+b/2)}{\cos^2\omega}\right] + \frac{4k\omega(L+b/2)}{\cos^2\omega}. \tag{A.30}$$

$$\frac{\partial L}{\partial \omega} = \frac{2kR^3\cos^2\omega}{(4kR\omega - V^*R/H)(L+b/2)}. \tag{A.31}$$

Equality of the chordal equilibrium equation (A.9)

We will show using the LUB conditions, (A.30) and (A.31), that the LHS and RHS of the chordal equilibrium equation (A.9) are equal. First, evaluate the RHS of (A.9), $V^*\cos\xi + N^*\sin\xi$, using N^* from (A.30) and replacing $\sin\xi$ and $\cos\xi$ from the geometrical conditions (A.27) and (A.25),

$$V^*\cos\xi + N^*\sin\xi = V^*\frac{1}{H}\left[\frac{(L+b)(L+b/2)}{R\cos\omega} + \frac{Hb}{2R\sin\omega}\right] + \left(4k\omega - V^*\frac{1}{H}\right)\frac{(L+b/2)^2}{R\cos^3\omega}. \tag{A.32}$$

Consider the first term on the RHS in (A.32). Re-introducing $\sin\xi$ and $\cos\xi$ back by using (A.27) and (A.25) gives

$$V^*\frac{1}{H}\left[\frac{(L+b)(L+b/2)}{R\cos\omega} + \frac{Hb}{2R\sin\omega}\right] = V^*\frac{[(L+b)\sin\xi + H\cos\xi]}{H}. \tag{A.33}$$

From (A.10) and (A.12) along with the trigometric relation, $\sin(\xi+\omega)\sin\xi + \cos(\xi+\omega)\cos\xi = \cos\omega$,

$$V^*\frac{[(L+b)\sin\xi + H\cos\xi]}{H} = V^*\frac{R}{H}\cos\omega. \tag{A.34}$$

Therefore the RHS of (A.9) is

$$V^*\cos\xi + N^*\sin\xi = V^*\frac{R}{H}\cos\omega + \left(4k\omega - V^*\frac{1}{H}\right)\frac{(L+b/2)^2}{R\cos^3\omega}. \tag{A.35}$$

To evaluate the LHS of (A.9), namely, $2kR(2\omega\cos\omega - \sin\omega)$, we use the LUB condition (A.31). First, differentiating the geometrical relation (A.28) with respect

to ω gives

$$4(L+\frac{b}{2})(\frac{\partial L}{\partial \omega})\sin\omega + 4(L+\frac{b}{2})^2\cos\omega - b^2\cos\omega = 4R^2\cos\omega(\cos^2\omega - \sin^2\omega). \quad (A.36)$$

Replacing $\partial L/\partial\omega$ in (A.36) by using the condition (A.31) and dividing by $4\cos\omega$ gives

$$\frac{2kR^3\cos\omega\sin\omega}{(4kR\omega - V^*R/H)} + L(L+b) = R^2(\cos^2\omega - \sin^2\omega). \quad (A.37)$$

Also from the geometrical relations (A.10) and (A.11),

$$L(L+b) = R^2\sin(\xi-\omega)\sin(\xi+\omega) = R^2(\sin^2\xi - \sin^2\omega). \quad (A.38)$$

Introducing (A.38) into (A.37), eliminating $\sin\xi$ by using the geometrial relation (A.27), and multiplying both sides by $(4kR\omega - V^*R/H)(\neq 0)$ gives

$$\left(4k\omega - V^*\frac{1}{H}\right)\frac{(L+b/2)^2}{R\cos^3\omega} + V^*\frac{R}{H}\cos\omega = 2kR(2\omega\cos\omega - \sin\omega). \quad (A.39)$$

Comparing (A.39) and (A.35) provides chordal equilibrium (A.9) for the LUB arc. Therefore, from the lemma, if the unknown σ_r is chosen to satisfy equilibrium in any direction other than the chordal direction, the tractions on the LUB arc satisfy global equilibrium, and the theorem is proven.

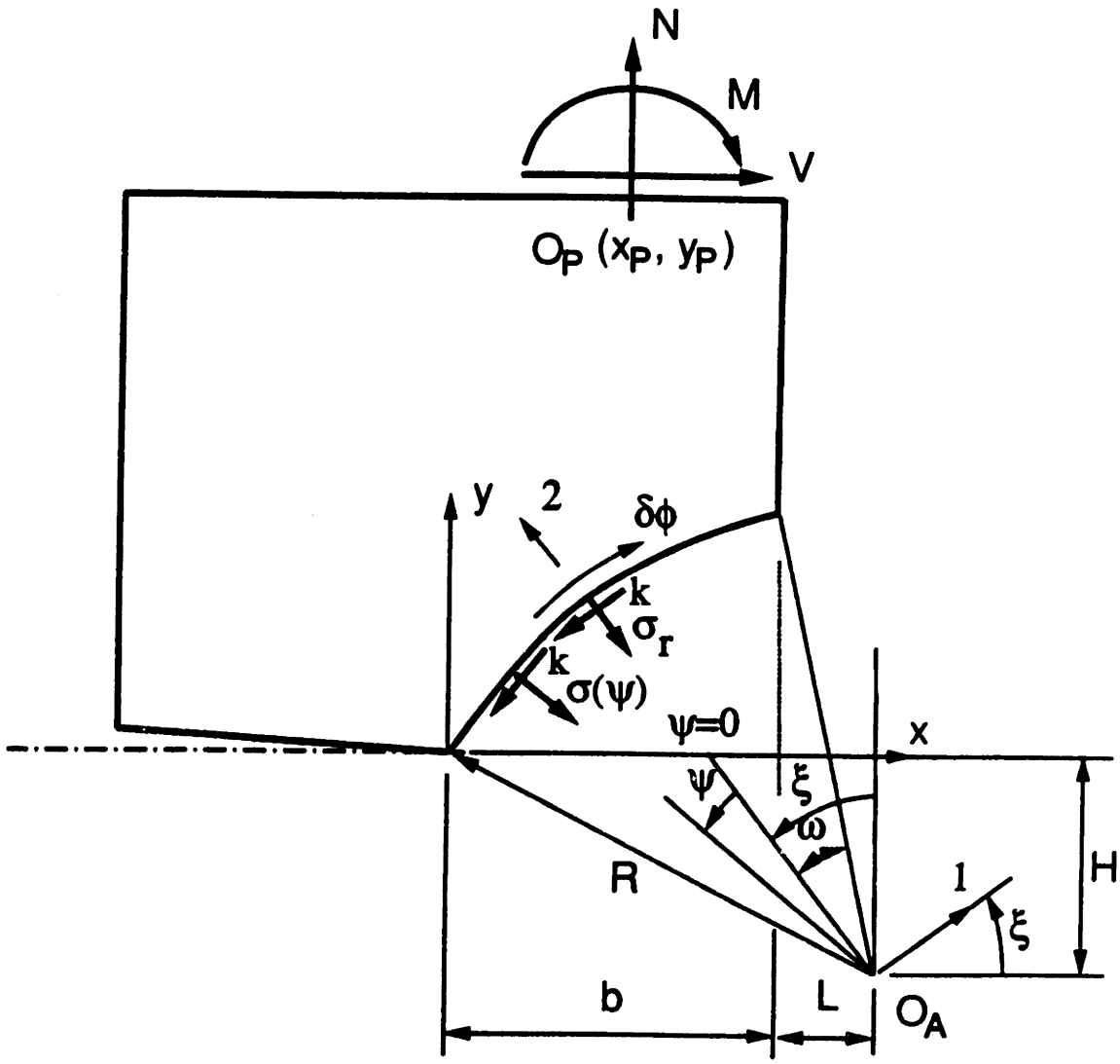

Fig. 2.1. Kinematically admissible plane strain deformation field consisting of rigid-body rotation across a circular arc in a cracked plate.

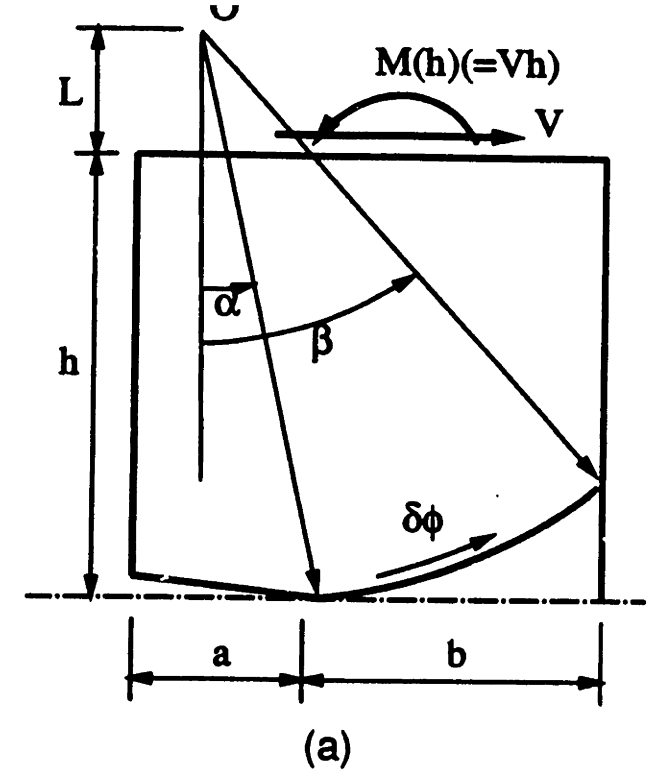

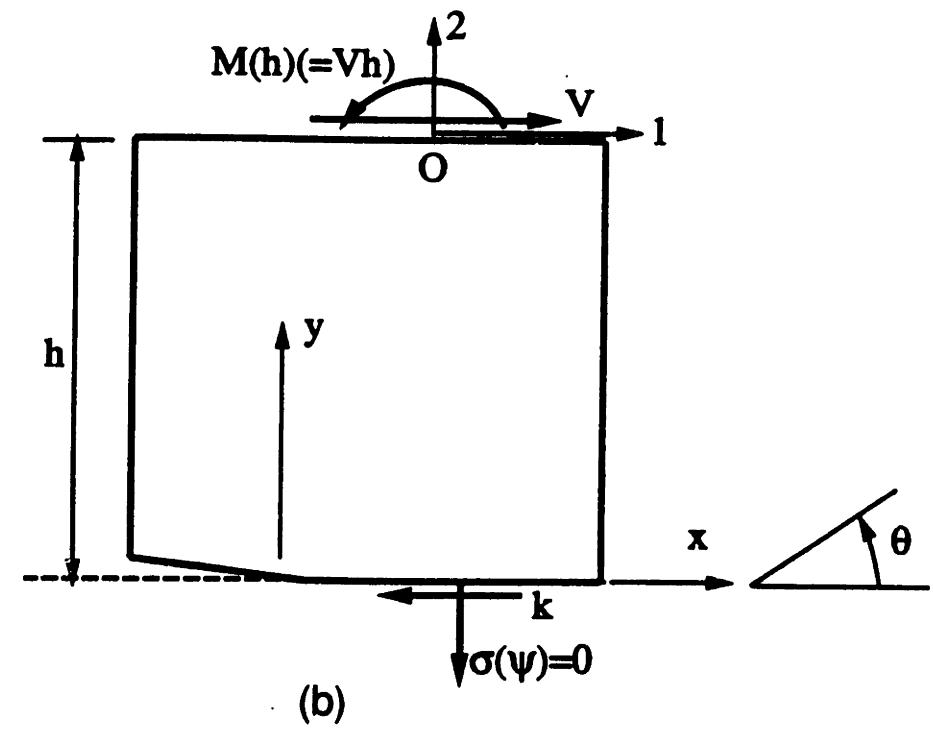

Fig. 2.2. Singly grooved plate in pure shear
(a) kinematically admissible field for an upper bound (arc sliding by $\delta\phi$)
(b) the assumed traction distribution on the LUB arc.

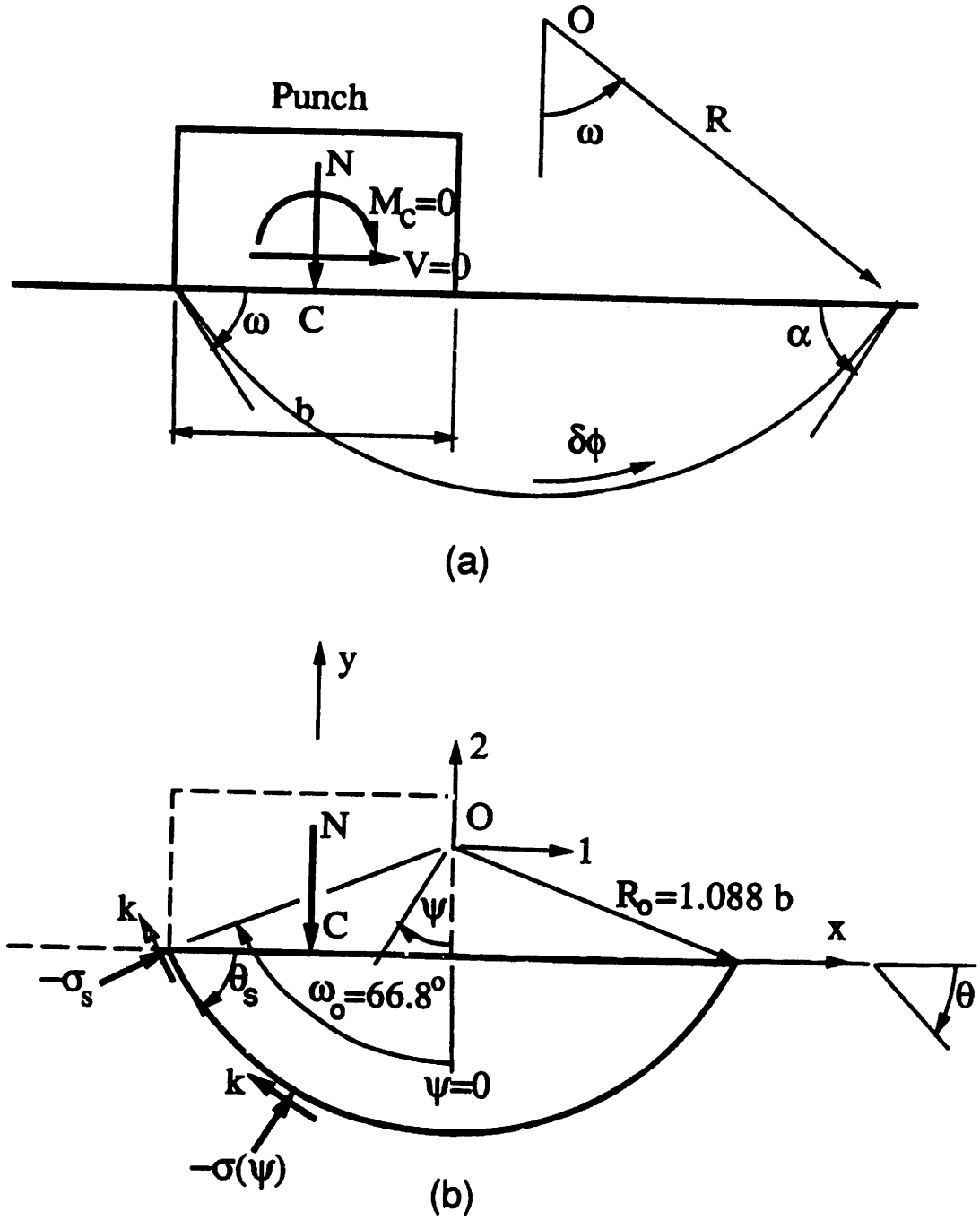

Fig. 2.3. Punch indentation problem
(a) kinematically admissible field for an upper bound (arc sliding by $\delta\phi$)
(b) the assumed traction distribution on the LUB arc.

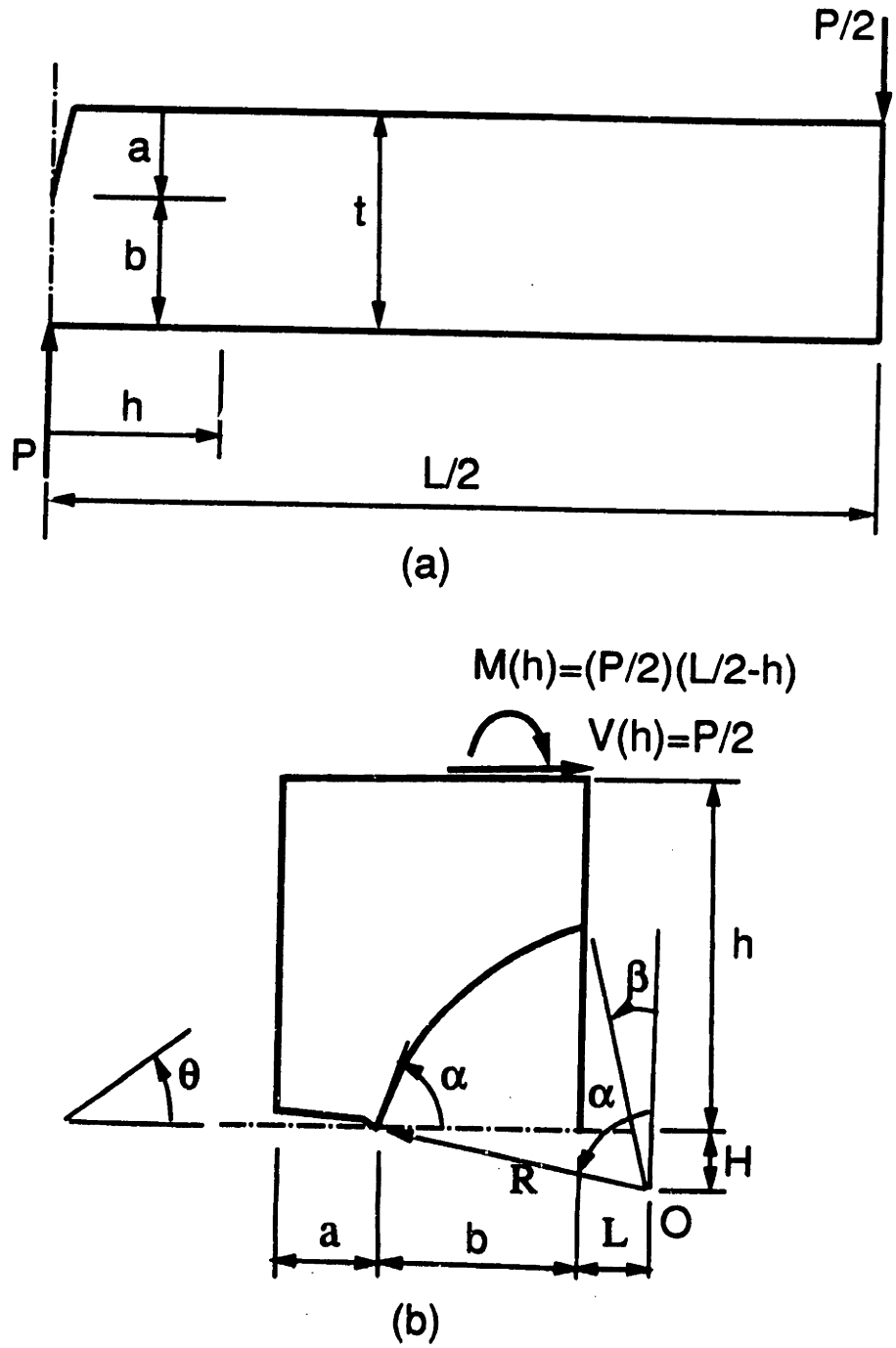

Fig. 2.4. (a) Three-point bending plate, (b) deep, single-face-cracked plate under combined shear and bending.

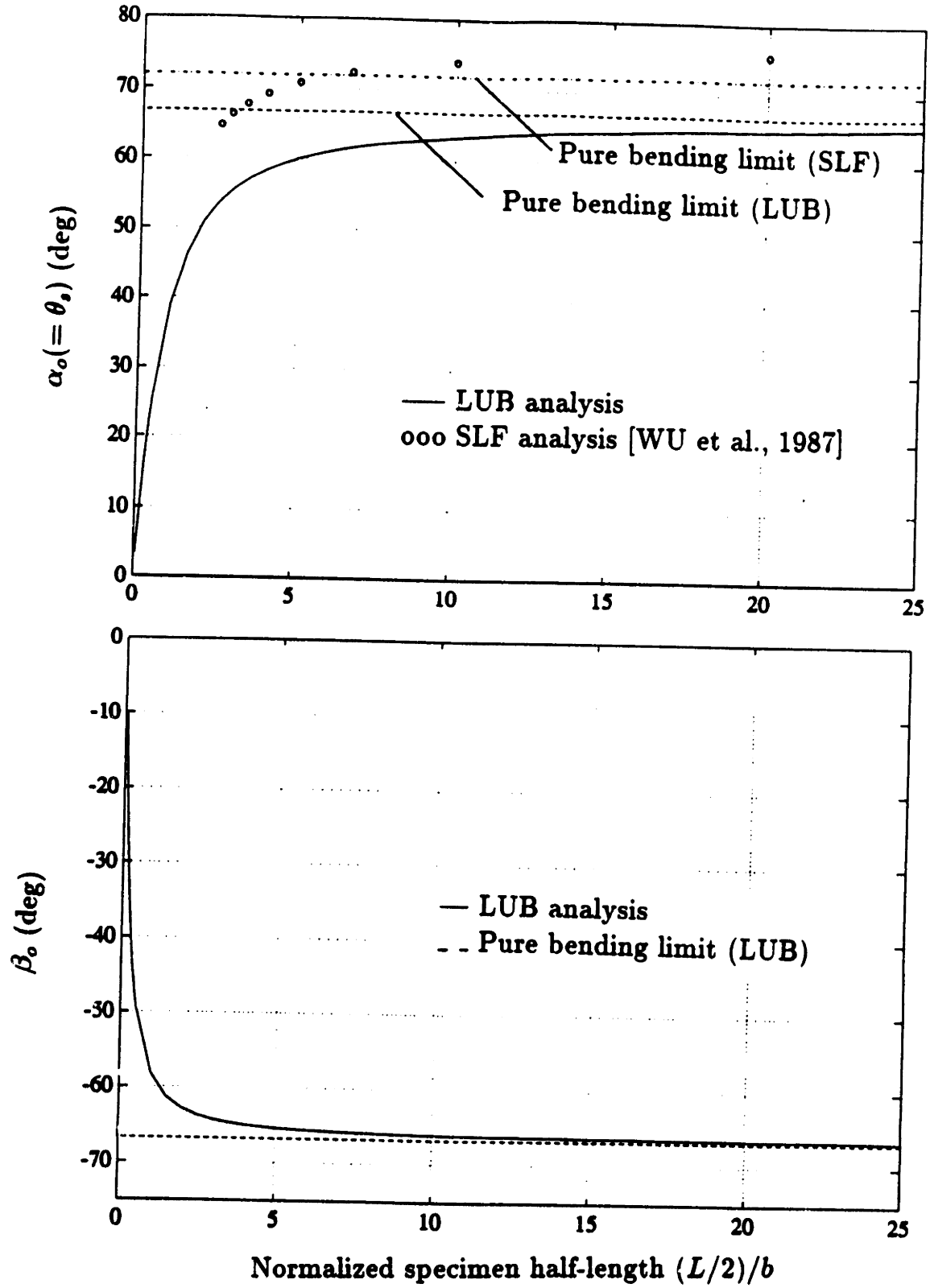

Fig. 2.5. The LUB arc angles for three-point bending plates with a varying length.

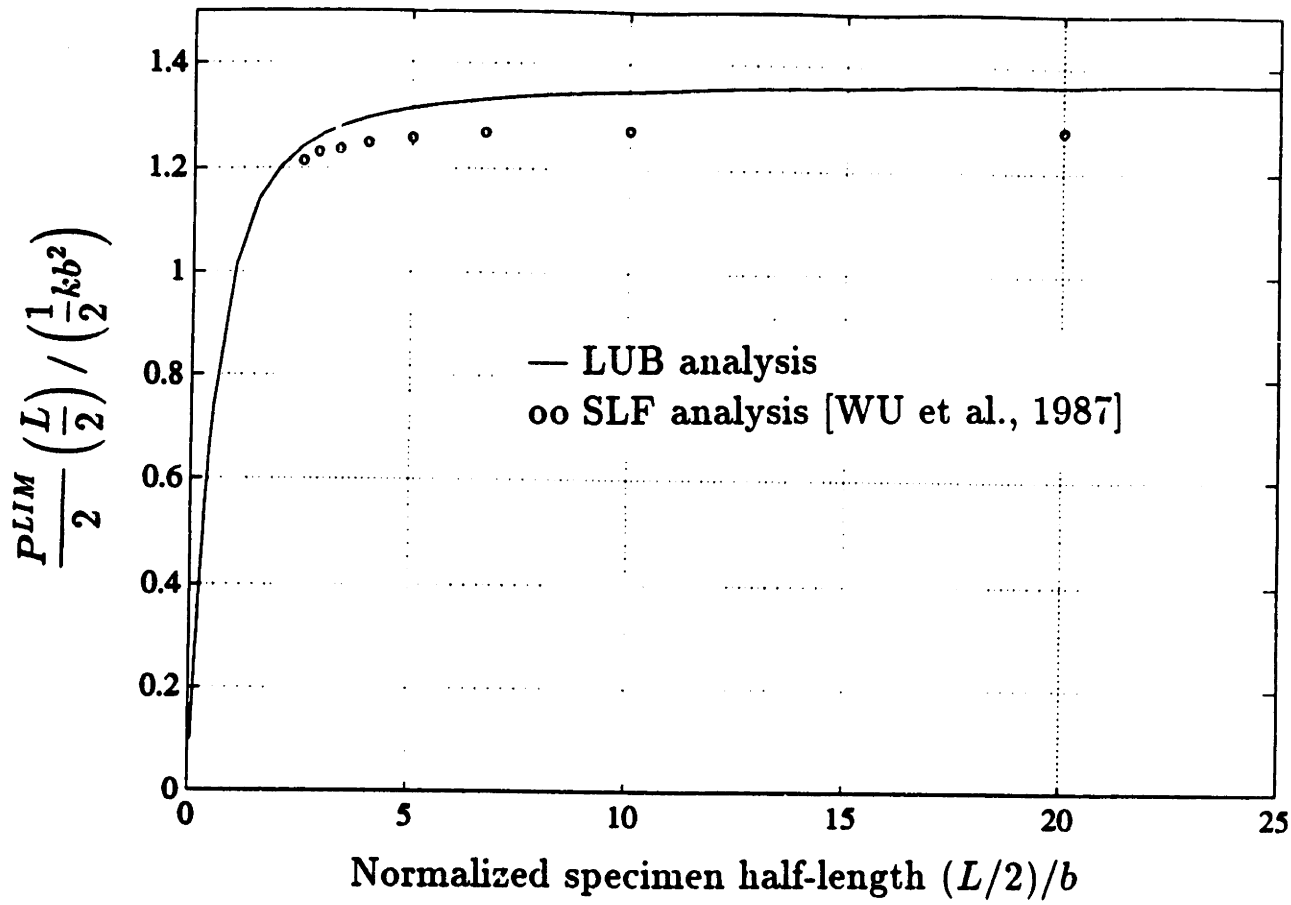

Fig. 2.6. Limit loads for three-point bending plates with varying length.

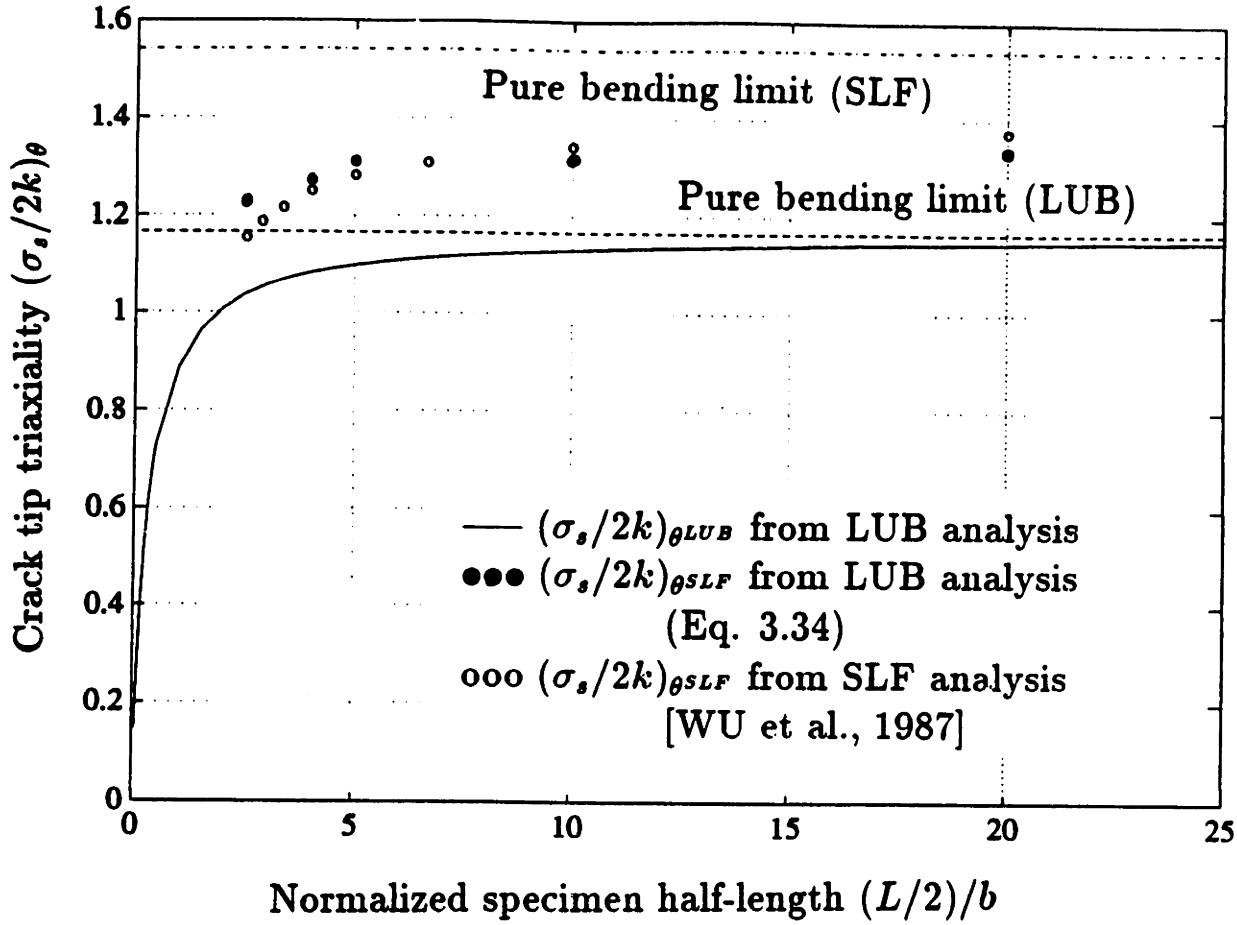

Fig. 2.7. The crack tip normal stress on the LUB arc for three-point bending plates with varying length.

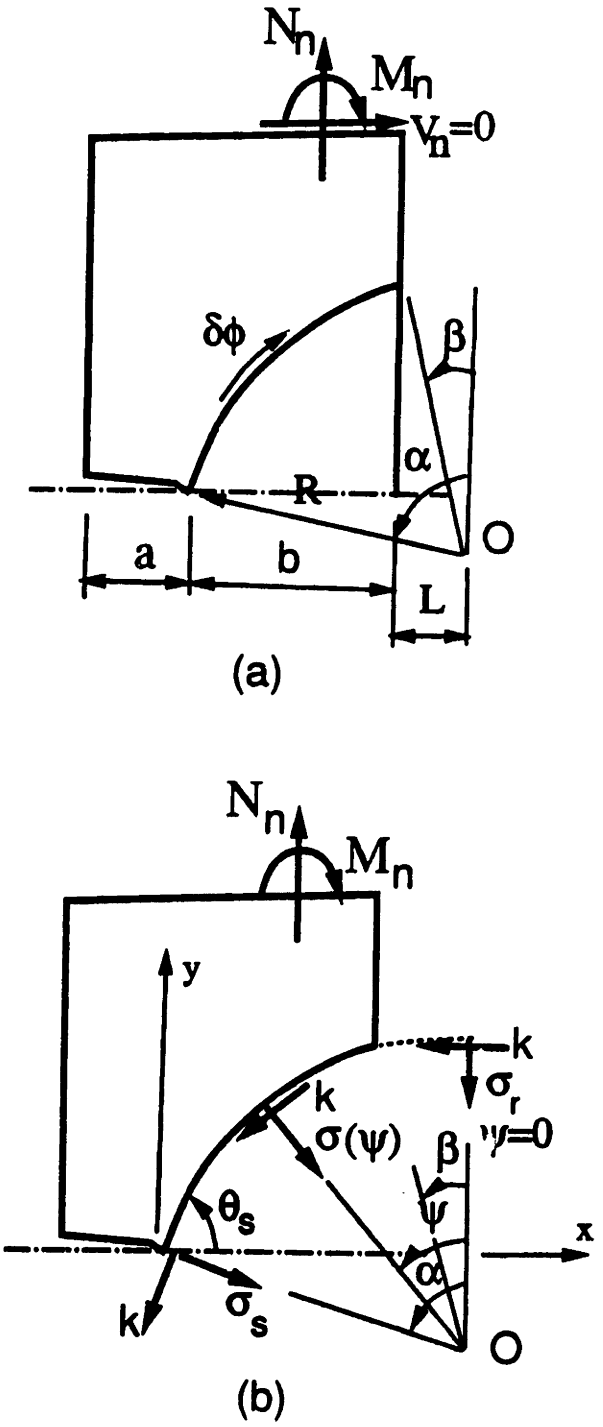

Fig. 2.8. Deep, single-face-cracked plate under opening bending with large tension
(a) kinematically admissible field for an upper bound
(arc sliding by $\delta\phi$)
(b) the assumed traction distribution on the LUB arc.

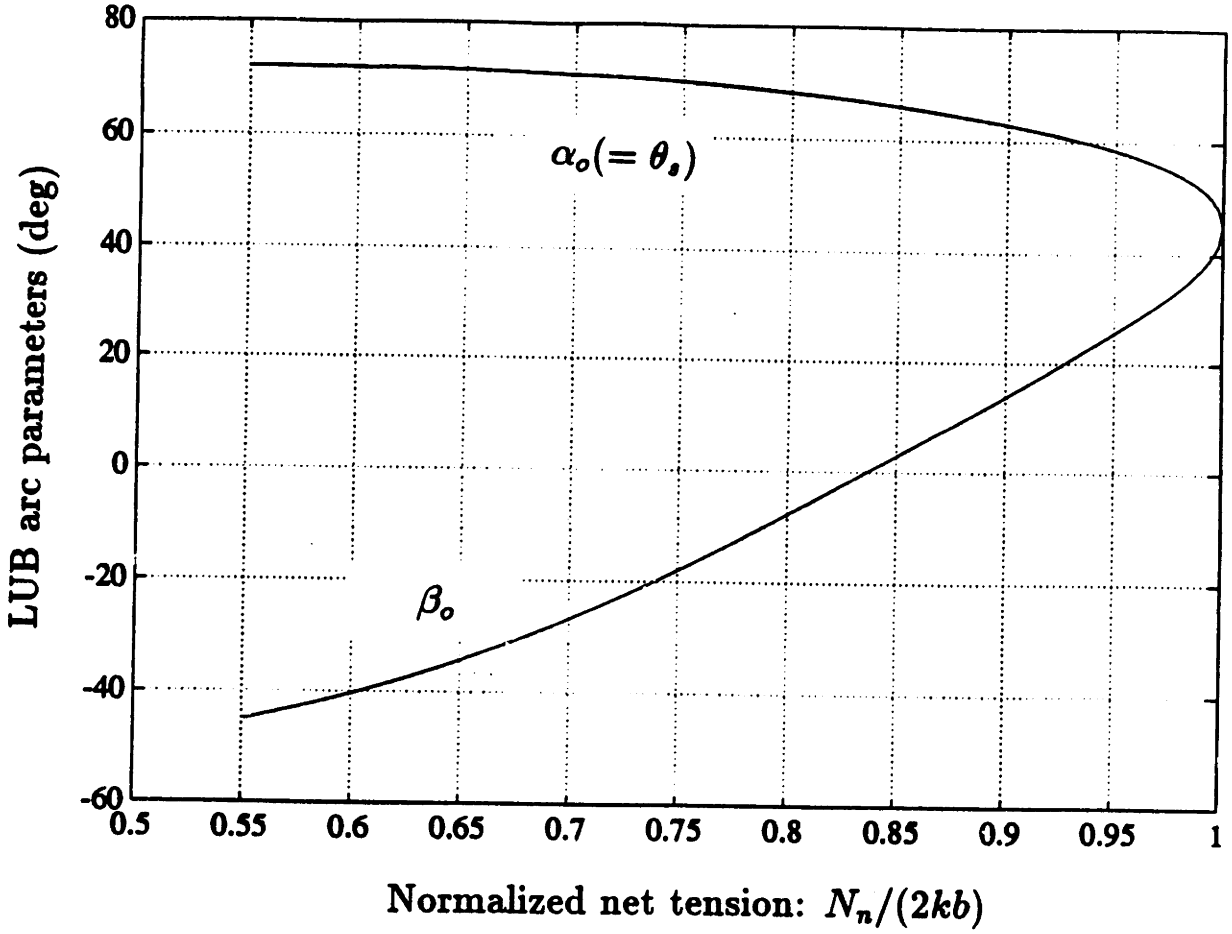

Fig. 2.9. The LUB arc angles for deep, single-face-cracked plates under opening bending with large tension.

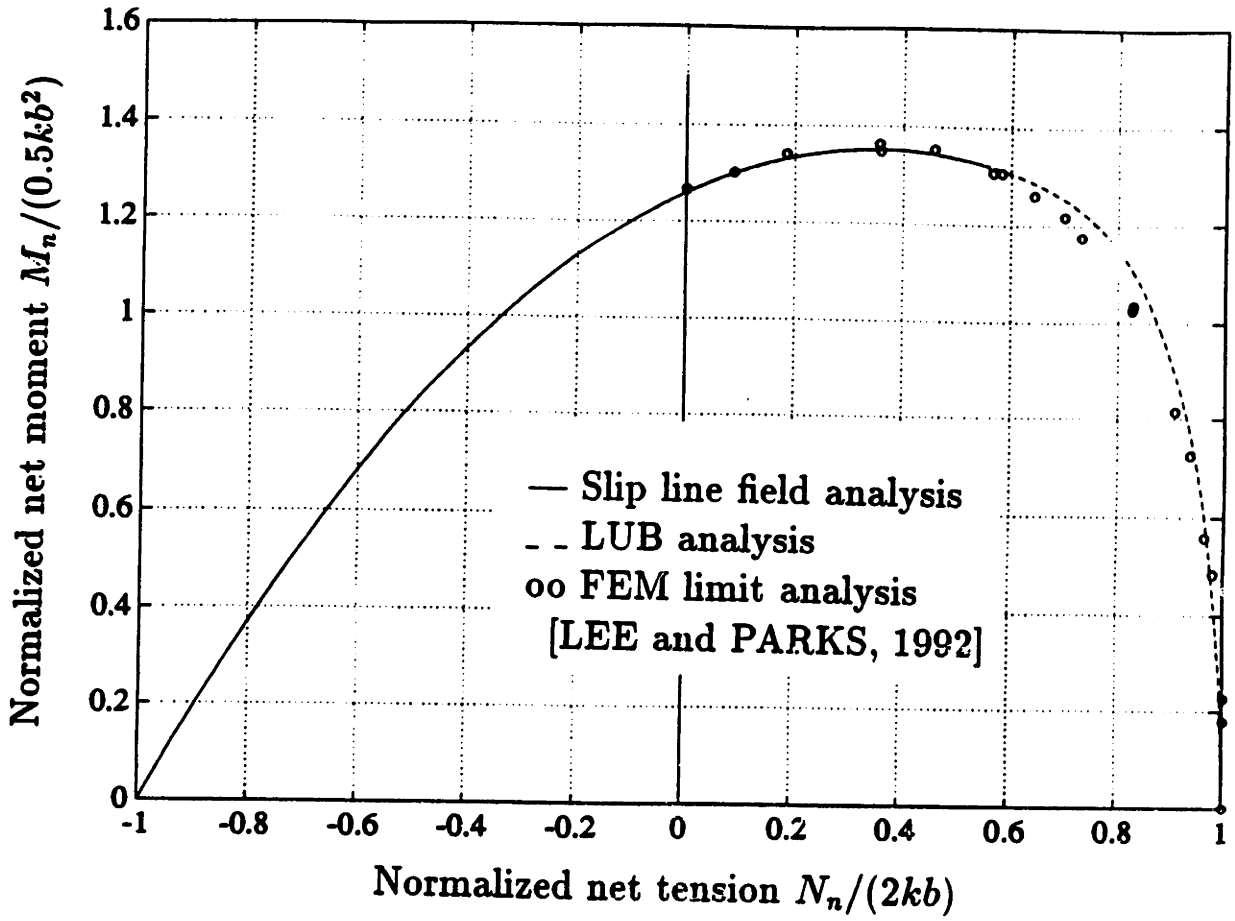

Fig. 2.10. Yield locus for deep, single-face-cracked plates under combined bending and tension.

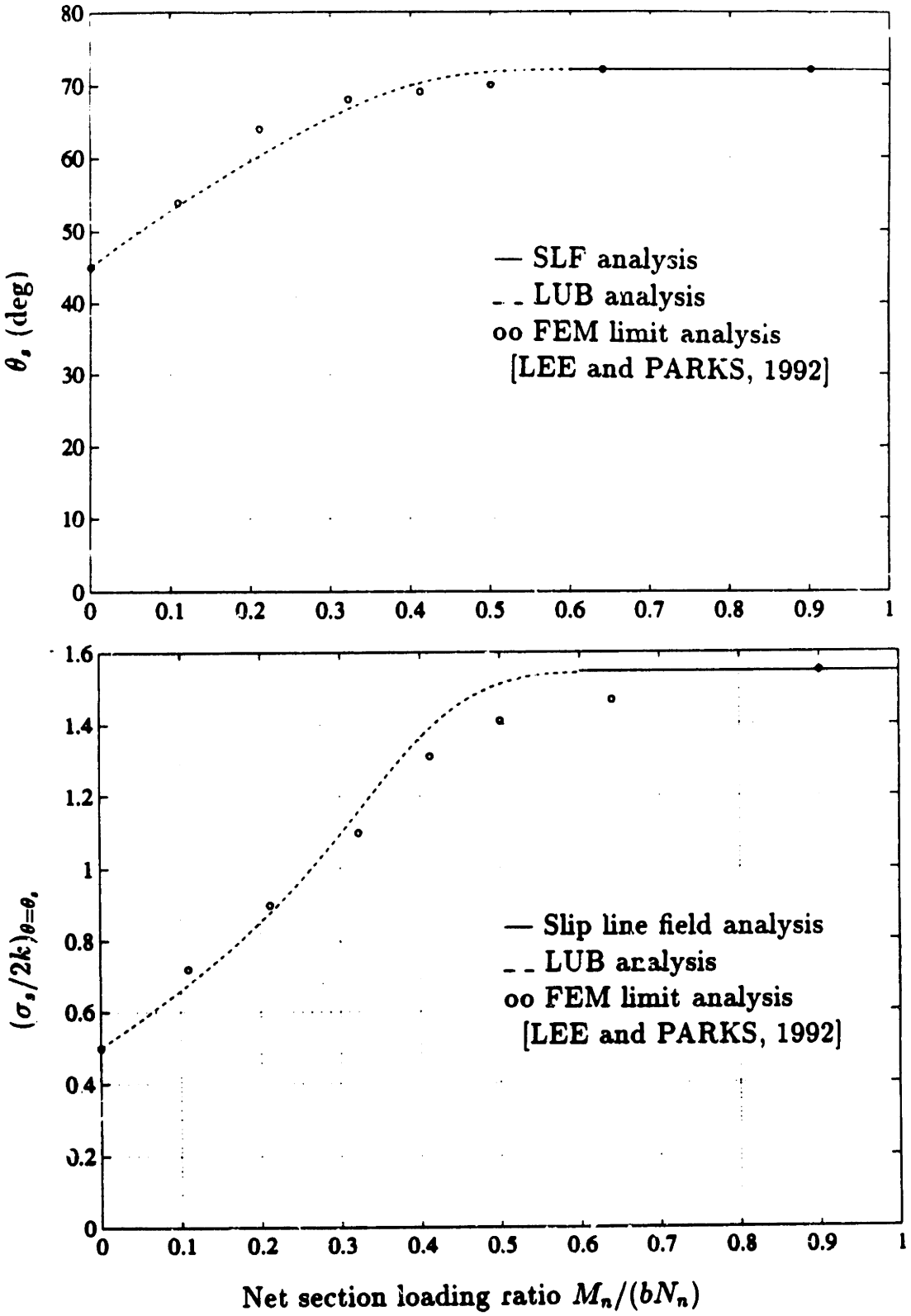

Fig. 2.11. Near tip slip angle and normal stress for deep, single-face-cracked plates under combined bending and tension.

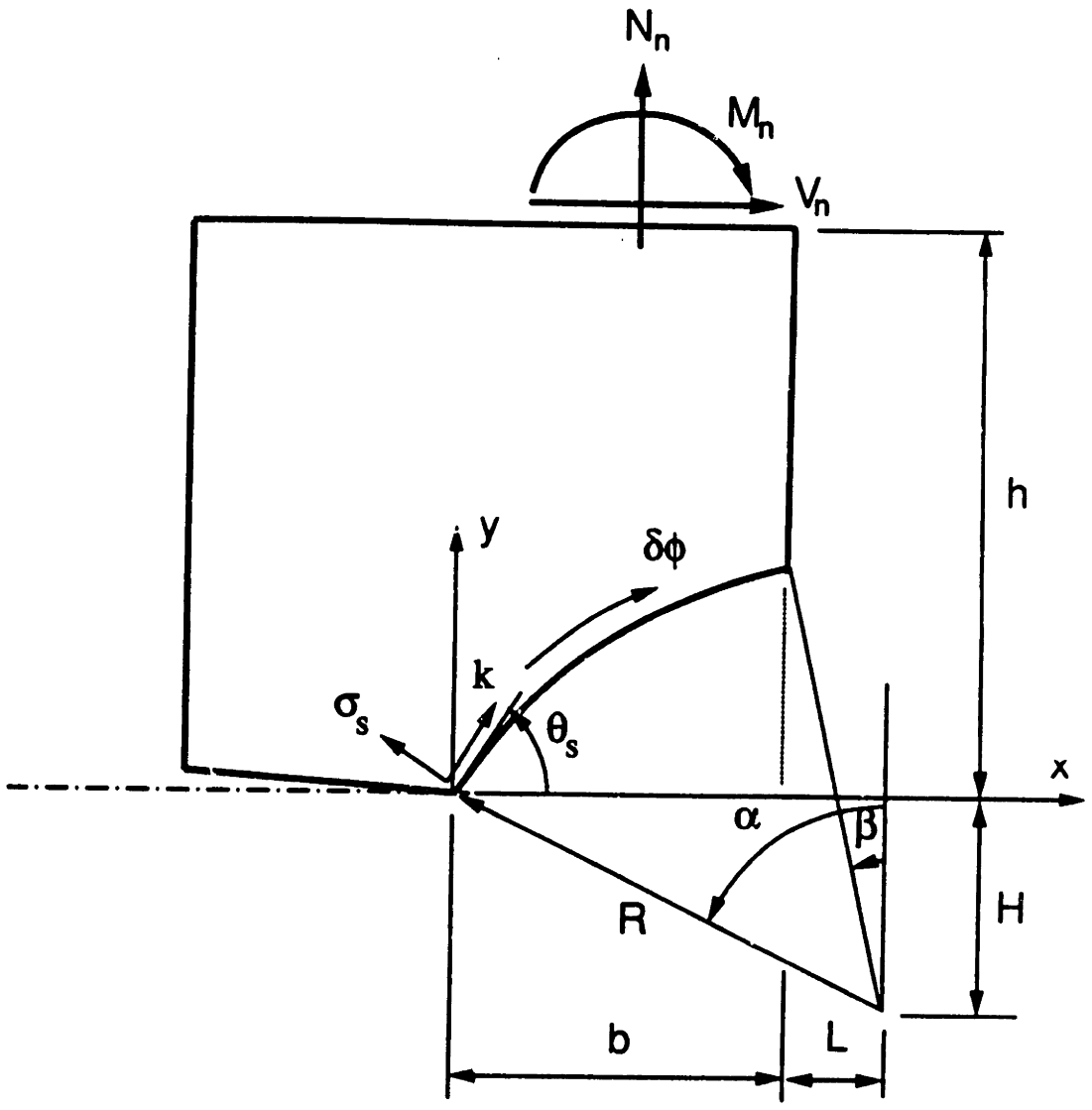

Fig. 2.12. Deep, single-face-cracked plate under combined shear, tension, and bending.

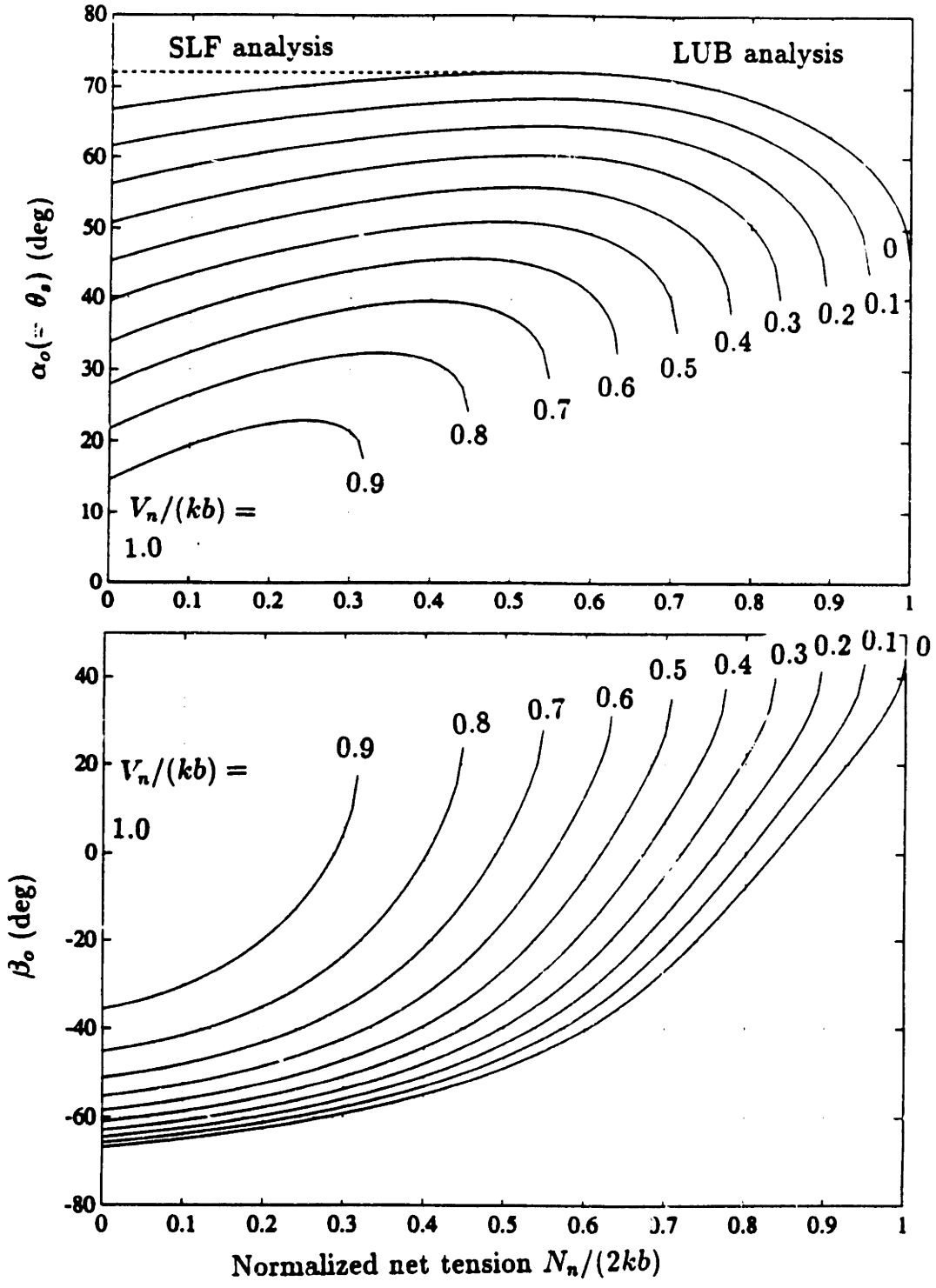

Fig. 2.13. The LUB arc angles for deep, single-face-cracked plates under combined shear, tension, and bending.

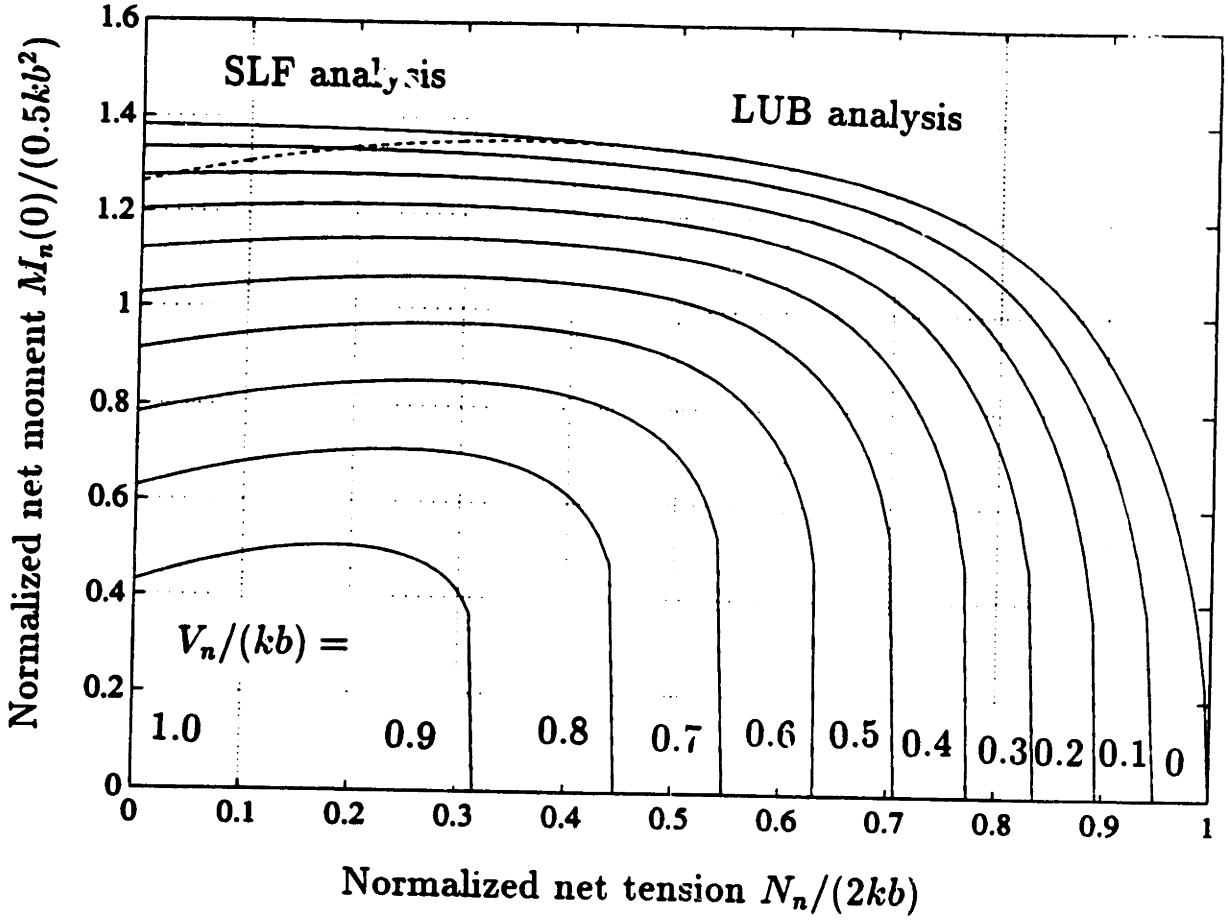

Fig. 2.14. Yield locus for deep, single-face-cracked plates under combined shear, tension, and bending.

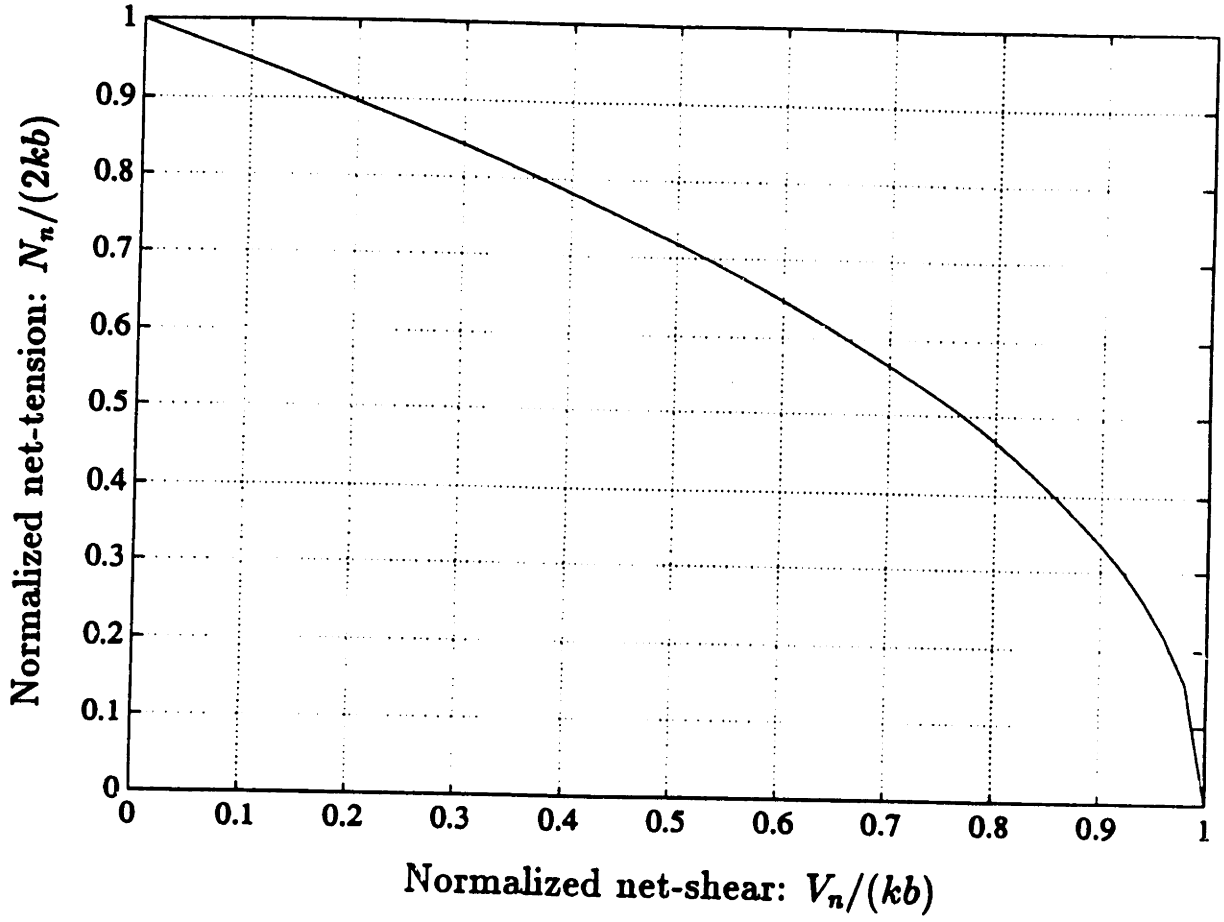

Fig. 2.15. Yield locus for deep, single-face-cracked plates under combined shear and tension ($M_n(0) = 0$).

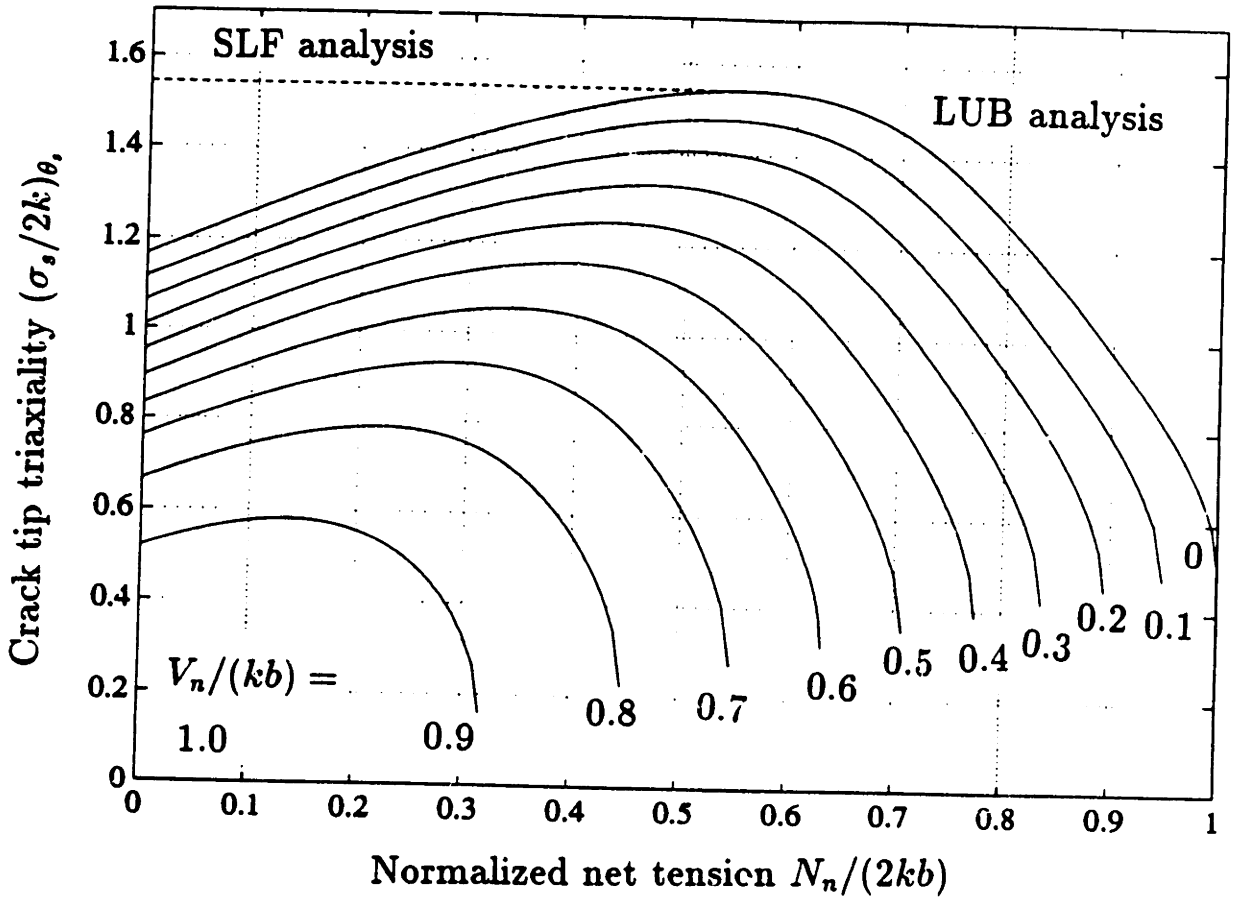

Fig. 2.16. Crack tip normal stress on the LUB arc for deep, single-face-cracked plates under combined shear, tension, and bending. It is understood that, for the indicated values of $N_n/(2kb)$ and $V_n/(kb)$, $M_n(0)/(0.2kb^2)$ assumes the value shown in Fig. 2.14.

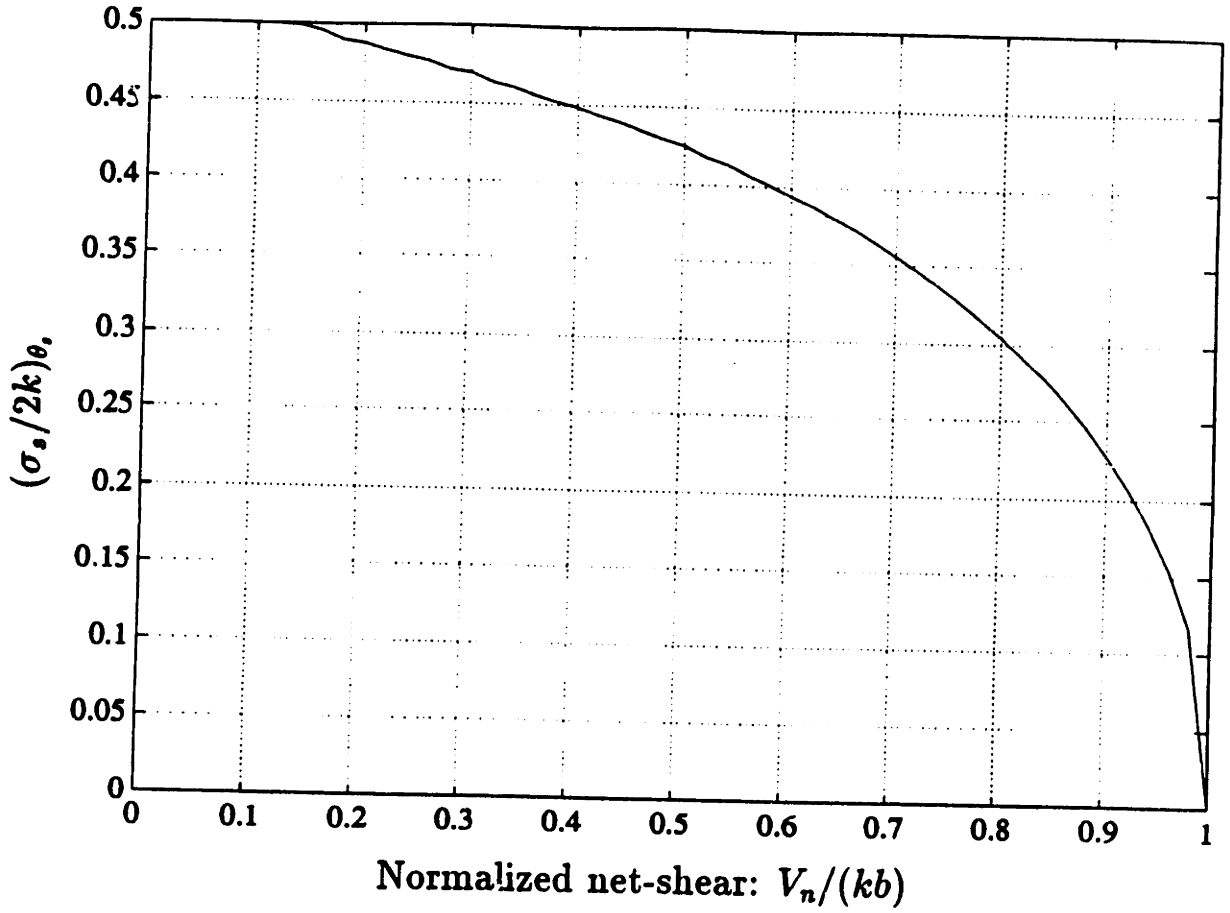

Fig. 2.17. Crack tip normal stress on the LUB arc for deep, single-face-cracked plates under combined shear and tension ($M_n(0) = 0$). It is understood that, for each value of $V_n/(kb)$, $N_n/(2kb)$ assumes the value shown in Fig. 2.15.

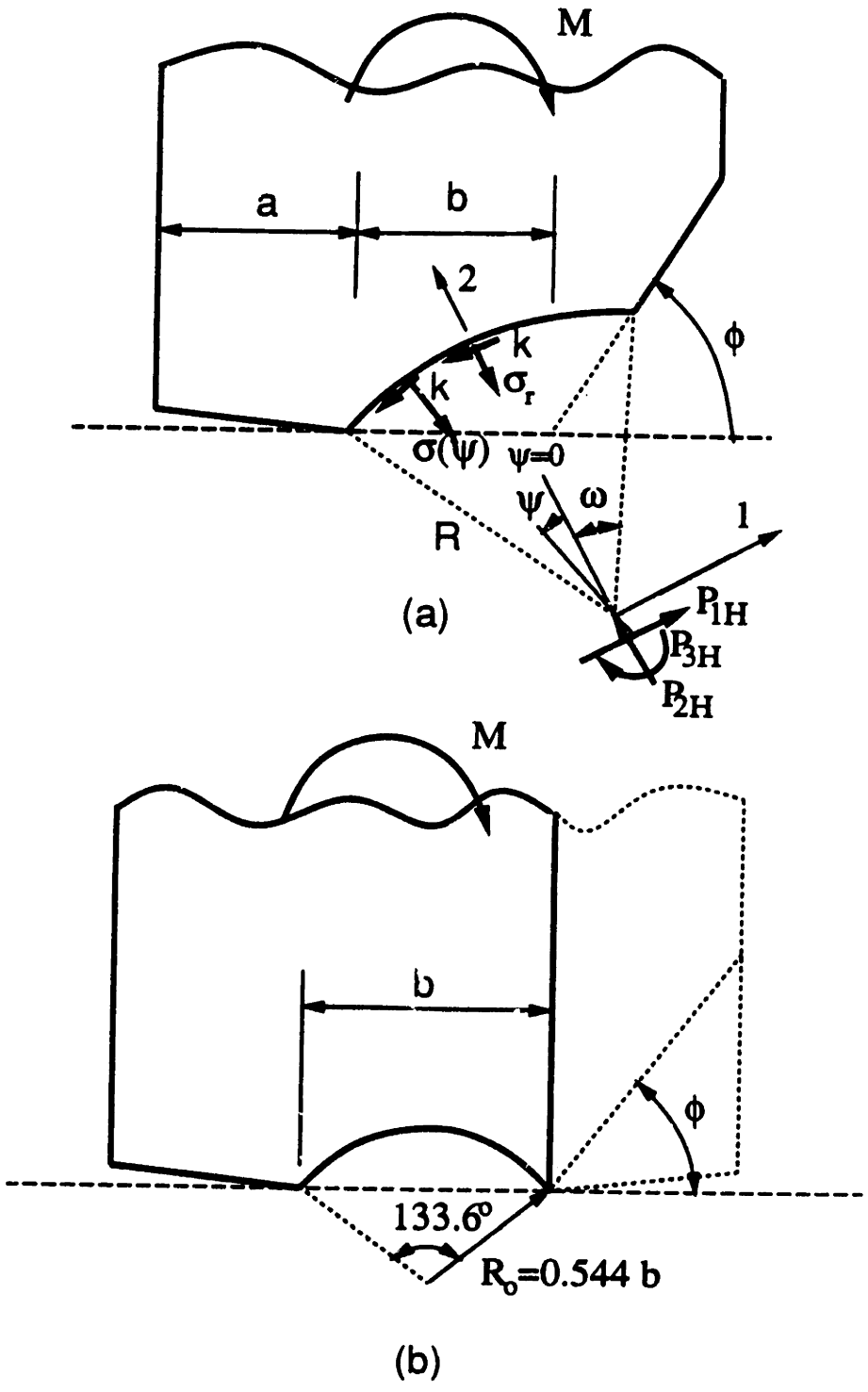

Fig. 2.18. (a) Unequally grooved plate in pure bending, (b) LUB arc in a deep, single-face-cracked plate in pure bending.

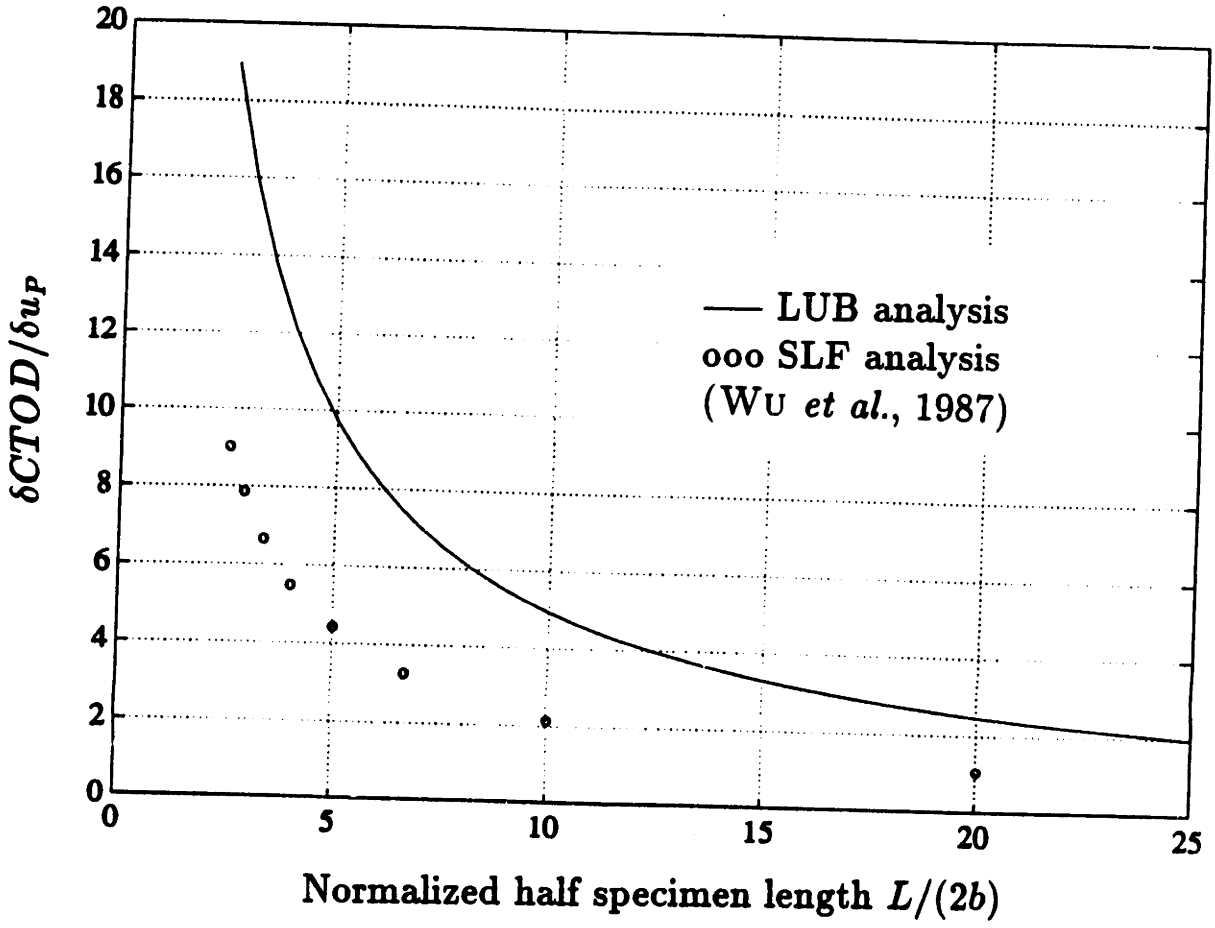

Fig. 2.19. The crack tip opening displacement per unit load-point displacement, $\delta CTOD/\delta u_P$, in three-point bending plates.

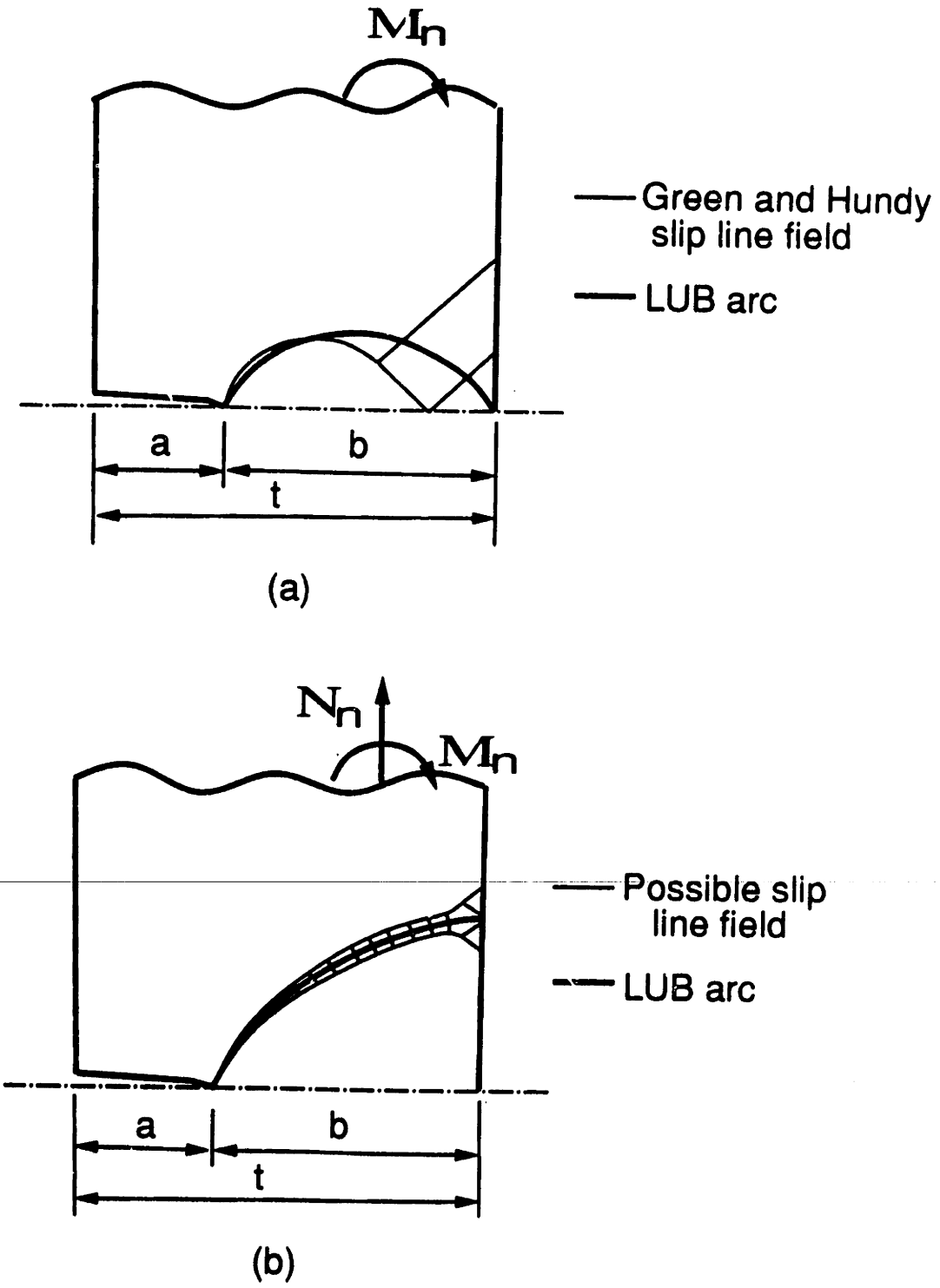

Fig. 2.20. (a) The Green and Hundy slip line field and the LUB arc for deep, single-face-cracked plates under pure bending, (b) possible slip line field and the LUB arc for deep, single-face-cracked plates under combined bending with large tension.

CHAPTER 3

CRITERIA FOR PLANE STRAIN, FULLY PLASTIC QUASI-STEADY CRACK GROWTH

ABSTRACT

Plane strain fracture by hole growth in ordinary-sized parts of low-to-medium strength steels is essentially rigid-plastic, and may be approximated as non-hardening. Quasi-steady crack growth for such materials is predicted for crack tip fields approximated by a pair of slip lines, such as unequally grooved specimens in tension and deeply single-face-cracked specimens under combined bending and tension. The crack growth increment δa is given in terms of material parameters, far-field geometry, and loadings and their increments.

For the rigid-plastic, non-hardening approximation, stress and strain increment fields for growing cracks are identical to those for stationary cracks. For fields with a pair of symmetric slip-lines, the flanks of the decohering zone turn out to be rigid, and the decohering zone does not affect the crack tip opening angle ($CTOA$), which then depends only on the micromechanisms of hole nucleation, growth, and linkage by flow localization or fine cracking. These mechanisms are in turn approximately controlled by the near-field plasticity parameters: the angle of the slip plane θ_s, and the normal stress and displacement increment across the slip plane, σ_s and δu_s. Note the three-parameter characterization of the near tip fields, in contrast to the one- or two-parameter characterization in elastic or non-linear elastic fracture mechanics.

A sliding off and shear-cracking model for a growing crack, based on a hole growth

equation, gives an approximate $CTOA$ in terms of σ_s, θ_s, and material parameters. When void nucleation strain is negligible, the estimated $CTOA$ exhibits an inverse exponential dependence on σ_s and a higher order parabolic dependence on θ_s. For a given material, a series of fully plastic crack growth experiments is suggested to determine the approximate material parameters needed to characterize the dependence of $CTOA$ on σ_s and θ_s.

1. INTRODUCTION

Under monotonic loading, structures should ideally be ductile, in order to provide a warning before crack growth and a continued resistance during crack growth. Such fully plastic behavior is of interest in metal working and in design against earthquakes, collisions, and ship groundings, for example. Here we focus on relatively deep surface cracks under combined bending and tension in plane strain, away from any support.

Microscopically ductile fracture in pre-cracked specimens consists of initial, transient, and continued growth. Initial and transient growth are very difficult to predict from fundamental mechanisms, because of crack tip blunting and initially steep strain gradients. They have been extensively studied experimentally and correlated in terms of the Hutchinson-Rice-Rosengren (HRR) singular stress and strain fields. As the limiting case after the initiation and transient stages, we concentrate here on continuing, quasi-steady crack growth.

1.1. Limitations of asymptotic fields around growing cracks in elastic-plastic materials

For plane strain Mode I, near-tip solutions for a crack growing in an elastic, perfectly-plastic solid have been constructed by Rice and Sorensen (1978) and by Drugan, et al. (1982). The solutions exhibit high stress triaxiality fields and thus are believed to apply under small-scale yielding conditions, but are not unique for large scale yielding. Drugan and Chen (1989) proposed a family of near-tip asymptotic fields, which can be applied under large-scale and general yielding conditions. They have obtained an m-family of analytical solutions which can describe a wide range of high- and low triaxiality stress fields which have been related to different fully yielded crack geometries (Chen and Drugan, 1991). The similar result has been found by Varias and Shih (1993). They performed a numerical study of a crack growing under steady-state, quasi-static conditions within the framework of a boundary layer formulation whereby the remote loading is fully specified by the first two terms in William's expansion, characterized by K_I and T (Parks, 1991). They found that the near tip field can be described by one parameter field and eventually exhibits high stress triaxiality regardless of the sign of T-stress. For $T > 0$, the crack starts to grow under high stress triaxiality which remains high throughout the growth history. Whereas, for $T < 0$, crack growth begin under low stress triaxiality, but the stress triaxiality increases steadily and eventually reaches levels similar to those prevailing under positive T.

However, the region of the dominance of the above solutions suggests that they can hardly be applied to ductile alloys or growing cracks under low crack tip triaxialities (defined by the ratio of the mean normal stress to the equivalent stress). For example,

for a steadily growing crack in Mode I, the equivalent plastic strain ϵ^p at distance r from the crack tip in the centered fan field can be approximated in terms of the tensile yield strain ϵ_y and the plastic zone size r_p (Drugan, et al. 1982):

$$\epsilon^p \approx \epsilon_y \ln(\frac{0.2r_p}{r}). \tag{1.1}$$

Rearranging (1.1) with ϵ^p replaced by the fracture strain ϵ_f provides a radius of dominance r_d:

$$r_d \approx 0.2r_p \exp(-\epsilon_f/\epsilon_y). \tag{1.2}$$

Note the inverse exponential dependence of r_d on the ratio of the fracture strain to the yield strain, ϵ_f/ϵ_y. For the above asymptotic solutions to be applicable, their dominance regions should exceed the process zone size, including macroscopic roughness. Applicability of these solutions to fully plastic crack growth is discussed here in four extreme cases: crack growth in a high strength steel with a high and a low crack tip triaxiality, and in a low strength steel with a high and a low crack tip triaixiality.

Typical material properties for high strength steels with high and low crack tip triaxialities, (ϵ_y=0.01, $\epsilon_f = 0.02 - 0.03$), give

$$r_d \approx (0.03 \ - \ 0.01)r_p. \tag{1.3}$$

For example, for a plastic zone size of $r_p = 10mm = 10^4\mu m$, the asymptotic solutions dominate within $r_d \approx (300 - 100)\ \mu m$ for high and low crack tip triaxialities, respectively. The fracture process zone size, including macroscopic roughness, is typically the order of $100\mu m$. Therefore, (1.2) and the examples shown above are consistent with the fact that elastic-plastic asymptotic solutions (linear elastic fracture mechanics) can be applied to crack growth in high strength steels under the high crack tip triaxialities. This fact was directly supported by experiments by Hermann and Rice

(1980), where crack growth occured in high strength steels (AISI 4140 steel with nominal yield strength of $\sigma_y = 1173MPc$ and ultimate strength of $\sigma_u = 1327MPa$) under high stress triaxiality (deeply cracked bend specimens).

For low strength steel with possible high crack tip triaxialities, typical material properties (ϵ_y=0.002 and even taking ϵ_f as low as 0.05) give

$$r_d \approx 1.44\,10^{-10} r_p. \tag{1.4}$$

(With lower crack tip triaxialities, r_d becomes even smaller than that.) For fully plastic flow across a ligament, now of $L(\approx r_p) = 100mm = 10^5 \mu m$, the asymptotic solutions dominate only within $r_d \approx 1.44\,10^{-5}\mu m$ even for high crack tip triaxialities. Therefore, according to (1.2) the asymptotic solutions can hardly be applied to a growing crack in low strength steels, which are of interest here.

Corresponding work for linearly-hardening, elastic-plastic solids has been done by Ponte Castañeda (1987), and for power-law hardening solids by Gao and Hwang (1981). The estimated size of the zone in which these asymptotic solutions dominate has been studied by Gudmundson (1989), and Nilsson and Stahle (1988). Gudmundson (1989) expressed the radius of dominance, r_d, (normalized by a characteristic length L) as that in which the effective stress at fracture, σ_f, for small hardening is greater than that for non-hardening σ_y by $\delta\sigma \equiv \sigma_f - \sigma_y$. For linear hardening with slope H and typical Poisson's ratios, his result is nearly

$$\frac{r_d}{L} \approx 0\,2 \exp(-\frac{E}{H}\frac{\delta\sigma}{\sigma_y}). \tag{1.5}$$

Substitution of

$$\frac{E}{H}\frac{\delta\sigma}{\sigma_y} = \frac{(\sigma_f - \sigma_y)/H}{\sigma_y/E} \approx \frac{\epsilon_f}{\epsilon_y} \tag{1.6}$$

and taking L as the plastic zone size reduces (1.5) to (1.2). Likewise for power law hardening, characterized by $\sigma[(\sigma/\sigma_y)^{(n-1)} - 1] = E\epsilon^p$, Gudmundson found

$$\frac{r_d}{L} \approx 0.2 \exp[-(\exp(n\frac{\delta\sigma}{\sigma_y}) - 1)]. \tag{1.7}$$

Again, (1.7) is essentially identical to (1.2) in the linearly-hardening case. Therefore, for the dominance regions of asymptotic solutions for hardening, elastic-plastic solids, we can draw the same conclusion as in non-hardening cases, namely, for the fully plastic crack growth in low strength steels of interest here, the regions of dominance for elastic-plastic asymptotic solutions around growing crack tips are far smaller than the fracture process zone. Thus, the fields for cracks growing in rigid-plastic materials are needed.

1.2. Fields around growing cracks in rigid-plastic materials

In non-hardening, rigid-plastic materials, elastic effects are negligible, and thus fields of strain increments and stress for growing cracks are the same as those for stationary cracks. The strain fields are found by superposition of the strain increments for successive crack tip positions. Thus known slip line fields for stationary cracks (e.g. McClintock, 1971; McClintock, 1990) are applicable to growing cracks.

For linearly-hardening, rigid-plastic materials, strength is spatially nonuniform due to non-uniform strain fields and work-hardening. Therefore, kinematic superposition is inapplicable and "history dependent" rigid/plastic analysis is required. For a growing crack, Kardomateas (1985) has found a strain singularity with a narrow deforming fan extending from the lower (entering) boundary at $\theta = \theta_l$ to the upper boundary at $\theta = \theta_u (> \theta_l)$. It has an undetermined, and in fact logarithmically

unbounded, mean normal stress. (The infinity presumably could be eliminated by elastic-plastic strains that are negligible in rigid-plastic materials.) His analysis gives the $CTOA$ in terms of three parameters: θ_l, θ_u, and the shear strain reached at the upper boundary, γ_u:

$$\tan(CTOA + \theta_u) = \frac{P - \tan\alpha\theta_l}{\alpha(1 + P\tan\alpha\theta_l)}, \tag{1.8}$$

$$\text{where} \qquad P = \frac{\alpha\tan\theta_l + \tan\alpha\theta_u}{1 - \alpha\tan\theta_l\tan\alpha\theta_u} \qquad \text{and} \qquad \alpha^2 = 1 + \frac{\gamma_u}{(\theta_l - \theta_u)}.$$

If complete fields for growing cracks in linearly hardening materials are found, they should satisfy (1.8). Kardomateas' tensile experiments on single-face-cracked, fully plastic specimens made from six structural alloys with different hardening coefficients showed that γ_u ranges from 0.37 to 0.60. The fan was so narrow that he assumed that replacing it by a single slip line was a good approximation.

1.3. Macroscopic fracture criteria

The J-integral can be used for the analysis of quasi-statically growing cracks when the conditions of J-dominance are satisfied; i.e., when there is an annular J-dominant region where HRR fields are undistorted by effects of free boundaries on the outside or by crack growth on the inside. The required distances from the outer radius to a free boundary and from the inner radius to the crack tip are larger for lower strain hardening and for greater differences between HRR and the nonhardening field. With insufficient inner distances, the strain hardening and the residual stresses left in the wake distort the HRR singularity implied by J, and make it no longer a descriptor of local stress and strain fields. Moreover, J (or HRR) is itself unable to deal with the different crack tip triaxialities of nonhardening fields (McClintock, 1971). The concept of the R-curve as a fundamental material property for monotonic loading is

no. valid in general, as shown by the fact that a final elastic-plastic instability occurs at nearly the same K under two different paths, monotonic loading and crack growth at constant applied load (as in stress corrosion cracking) (McClintock, 1958).

A promising fracture descriptor for a growing fully plastic crack seems to be the crack tip opening angle ($CTOA$). A varying $CTOA$ was observed in analysis and experiments on fully plastic crack growth in doubly grooved specimens in tension (McClintock, 1969). The varying $CTOA$ is apparently due to varying crack tip triaxialities and/or damage accumulation ahead of the growing crack. The $CTOA$ results from near-field plasticity parameters acting on the local fracture micromechanisms such as hole nucleation, hole growth, linking by localization or fine cracks, and decohering, whose continuum modeling is briefly summarized next.

1.4. Modeling the micromechanisms of crack growth

Hole nucleation

Continuum modeling of hole nucleation is very complicated due to many microstructural and macroscopic variables. Hole nucleation can occur at particles either by particle fracture or by decohesion of the particle-matrix interface. With particle-matrix decohesion, the nucleation strain decreases as the stress triaxiality decreases, as the particle size increases, as the particle volume fraction increases, as the strength of the particle-matrix bond decreases, and as the flow strength of the matrix increases. Note the dependence of the nucleation strain on the stress triaxiality. For a recent

summary, see Dodd and Bai (1987) for example.

Hole growth

The growth of a single hole in an infinite block of plastic material has been analyzed with several models: cylindrical holes in hardening materials in generalized plane strain (McClintock, 1968b) as well as in a shear band (McClintock, et al., 1966), initial growth of spherical holes in rigid, non-hardening materials (Rice and Tracey, 1969), and a spherical hole in power-law, viscous materials (Budiansky, et al. 1982). All of the above studies indicate the strong exponential effect of triaxiality. A recent study by Huang, et al. (1991) shows that the dilatational rate suggested in Rice and Tracey (1969) and duplicated in Budiansky, et al. (1982) is underestimated by a factor of nearly 1.5. Moreover, all of the above studies neglect the hole-hole interaction, which is considered next.

Hole linkage

Continuum modeling of the experimentally-observed hole-linkage by localization, with criteria for the localization of plastic flow in terms of the shape, size, and spacing of holes in a non-hardening matrix, has been explored approximately by a number of workers (McClintock, 1968b; Nagpal, et al. 1972; Cox and Low, 1974; Thomason, 1990). Finite element simulations of growing fine-scale holes have been developed based on the Gurson constitutive equation (Koplik and Needleman, 1988; Tvergaard, 1982; Tvergaard, 1988). The model has been applied to shear band localization between large-scale holes. While such planar localization has been observed, the formation of irregular fine cracks as in Fig. 3.1 appears to be due to some other

mechanism.

Decohering zone

A decohering zone can model three-dimensional aspects of crack growth, where crack surfaces are typically rough at the scale of fractions of a millimeter or more. The physical mechanisms in the decohering zone include zig-zagging, 3-D meandering, and tearing. As confirmed in experiments (McClintock, 1969; Miyamoto, et al., 1990), in slip line field studies (Carson, 1970), and in finite element simulations (Tvergaard and Needleman, 1992), crack growth on a macroscopic scale appears to be the result of microscopic zig-zagging. An example of the roughness of a crack surface is shown by the cross-section of a crack growing in 2024-T4 aluminum alloy in Fig. 3.1. Although holes are growing over a wide area ahead of the crack tip, the *CTOA* is only a few degrees, and much of the work of fracture is spent not in hole growth, but in tearing between the irregular crack paths running up or down on successive sections parallel to the plane of the figure, due to planar localization or to fine cracks. Figure 3.2a shows an idealization of Fig. 3.1 with two zig-zagging fracture surface profiles: one, drawn with a solid line, is a "front zig-zag", and the other, drawn with a dashed line, is a "back zig-zag", with a phase lag. Due to the phase lag, there are bridges between these zig-zag surfaces. To take an extreme example, assume that the two zig-zags meet on a common plane, perpendicular to the leading edge of the macro-crack, and that the intact material on that plane (dark areas in Fig. 3.2a) shears off as the profiles open with crack advance. This bridged region, constituting what will be termed a "decohering zone", can be modelled by postulating an appropriate traction-displacement law. Behind the decohering zone, the surface becomes completely fractured and traction-free. Ahead of the decohering

zone, damage is accumulating due to hole nucleation, hole growth, and void sheet localization or fine cracking.

To relate local fracture micromechanisms to near field plasticity parameters, the fracture criterion *CTOA* resulting from near tip plasticity should account for these local micromechanisms of crack growth, hole nucleation, hole growth, localization and decohering, as shown schematically in Fig. 3.2b.

1.5. Present work

This chapter presents an analysis for fully plastic, plane strain, quasi-steady crack growth for macroscopic flow fields approximated by a pair of slip lines. This approximation applies to crack growth in singly and unequally grooved specimens in tension, and deep, single-face-cracked specimens under combined bending and tension.

Section 2 discusses macro-mechanics. For crack tip fields with a pair of symmetric slip lines, slip line fields for a growing crack are constructed from fields for stationary cracks, with an emphasis on the decohering zone. Those slip line fields relate far-field geometry, loadings, and their increments to near tip fields characterized by the slip line angle θ_s and the normal stress and displacement increment across it, σ_s and δu_s:

$$\left\{ \begin{array}{c} \theta_s \\ \sigma_s \\ \delta u_s \end{array} \right\} = \left\{ f \right\} \text{(far-field geometry, loadings and their increments).} \qquad (1.9)$$

The crack flank opening displacement increment at the crack tip, δu_t, is related to δu_s and θ_s through

$$\delta u_t = \delta u_s \sin\theta_s. \qquad (1.10)$$

Also from geometry, the crack growth per unit flank-to-flank crack tip displacement, $\delta a/\delta u_t$, is related to the $CTOA$ through the tangent of its half angle:

$$\delta a/\delta u_t = 1/(2\tan(CTOA/2)). \tag{1.11}$$

In Sec. 3, micromechanisms of crack growth such as hole nucleation, hole growth, linkage, and decohering are related to near tip fields through a proposed meso-mechanical model of sliding off and shear-cracking for a growing crack. The model, together with the micromechanisms, provides an estimate of the macroscopic $CTOA$ in terms of σ_s, θ_s, and material properties:

$$CTOA = \widehat{CTOA}(\sigma_s, \theta_s, \text{material parameters}). \tag{1.12}$$

Successively substituting (1.12), (1.10) and (1.9) into (1.11) provides a prediction of the crack growth increment δa in structures:

$$\delta a = \widehat{\delta a}(\text{ far field geometry, loadings and their increments, material parameters}). \tag{1.13}$$

2. MACRO-MECHANICS FOR FIELDS WITH A PAIR OF SLIP LINES

In non-hardening, rigid-plastic materials, there is no elastic redistribution of strain during crack growth, no strain-hardened material left behind, and no change in deformation resistance, so fields of strain increments and stress are the same as for a stationary crack. Superposition of the strain increments for successive crack tip positions provides the strain field. Therefore, if a slip line field can be found for a stationary crack, including a decohering zone, it will be valid for a growing crack.

2.1. Fields for decohering zones with rigid flanks

Single-face-cracked specimens in tension

Consider single-face-cracked specimens in tension (Fig. 3.3) of width h normal to the paper, with $h \gg b$ for plane strain. (Refer to McClintock (1971) for the required shoulder thickness for rigid flanks without a decohering zone.) We show here that the flanks of the decohering zone remain rigid.

An upper bound to the limit load can be found from a simple kinematically admissible field of displacement increments consisting of sliding along a 45^o plane from the crack tip at the leading edge of the decohering zone through to the back surface (Fig. 3.3a). Note that the virtual displacement increment on the decohering zone is assumed to be constant. For a traction in the decohering zone $T(x)$ and the length of the zone d, with a shear strength k, the work in the decohering zone is

$$\delta W_d = h\delta u \int_0^d T(x)dx. \tag{2.1}$$

The work on the slip plane is

$$\delta W_s = 2kbh\delta u. \tag{2.2}$$

The corresponding upper bound to the limit load per unit width, P_{UB}, is found from the total work:

$$P_{UB} = \frac{(\delta W_d + \delta W_s)}{h\delta u} = 2kb + \int_0^d T(x)dx. \tag{2.3}$$

For a lower bound, assume that the only nonvanishing stress component is σ_{yy}, with spatial distribution $\sigma_{yy} = 2k$ in the ligament, $\sigma_{yy} = T(x)$ in the decohering zone, and $\sigma_{y_1} = 0$ on the fully decohered crack flank, not only in the crack plane, but also all along the length of the specimen (Fig. 3.3b). This stress distribution satisfies equilibrium, the yield criterion, and lateral traction(-free) boundary conditions. The resulting lower bound to the limit load, P_{LB}, is

$$P_{LB} = 2kb + \int_0^d T(x)dx. \tag{2.4}$$

Since these upper and lower bounds coincide, their fields provide a complete solution. Any region necessarily rigid in one complete solution is rigid in all (Drucker, 1960). The low stress shoulders will remain rigid and confine deformation to the region between two slip lines emanating from the tip of the decohering zone. Thus the flanks of the decohering zone are rigid. *Note that the consequence of rigid flanks of the decohering zone is that for a steady crack growth rate, the increment of the separation along the decohering zone per unit crack advance is constant and the separation itself is proportional to the distance from the tip.* From Fig. 3.2a, the linear displacement (separation) across the decohering zone suggests the linearly decreasing dimension of the partially sheared idealized interface between the out-of-plane zig-zags. Since in

the extreme model of Fig. 3.2, the traction in the decohering zone is proportional to the area of the partially sheared interface, the traction decreases quadratically with distance from the tip. For instance, as in Fig. 3.3 with the size of the decohering zone taken as d and the coordinate x measured from the tip of completely fractured surface,

$$T(x) = T_C(\frac{x}{d})^2, \tag{2.5}$$

where T_C is crack plane traction at the tip of the decohering zone. The size of the decohering zone d depends on the $CTOA$ and on the length scales of roughness of microscopic zig-zagging:

$$d \propto \text{roughness} \cdot f(CTOA). \tag{2.6}$$

The size d will increase as $CTOA$ decreases and as the amplitude of zig-zagging increases.

Unequally grooved specimens in tension

Consider unequally grooved specimens in tension (Fig. 3.4). For the corresponding doubly grooved specimens of angle 2ϕ, Ewing and Hill (1967) have found the minimum shoulder width for which the slip line field shown provides a complete solution. Without the decohering zone, adding stress-free shoulders on one side to form the crack ($2\phi = 0$) does not affect the complete solution. With a decohering zone, it appears likely from the three stress states shown in Fig. 3.4 that the flanks of the decohering zone, under opening traction intermediate between those of rigid regions on either side, will remain rigid. The decohering zone is thus not likely to cause yielding in shoulders large enough to be rigid with a crack. The resulting opening

displacement $u_t(x)$ and traction $T(x)$ are shown schematically in Fig. 3.4.

Deep, single-face-cracked specimens under combined bending and tension

We have proven rigidity of flanks of the decohering zone for crack tip fields with a pair of $\pm 45^o$ slip lines, such as singly-face-cracked and unequally grooved specimens in tension. Presumably the similar conclusions hold for other fields with a pair of $\pm 72^o$ slip lines, such as single-face-cracked specimens under predominant bending (modified Green and Hundy fields). Assume also that the rigid flanks of the decohering zone hold not only for fields with a pair of slip lines, but also for upper bound fields with a pair of curved arcs which will be discussed below. Note that these assumptions are highly likely to be true, although rigorous proof would not be easy

Consider deep, single-face-cracked specimens under combined bending and tension (Fig. 3.5). These are of interest in surface-cracked plates (Rice, 1972; White, et al., 1983). Figures 3.6 show a series of fields for cracks deep enough to prevent shoulder deformation, and sharp enough to prevent flank deformation, with varying net-section moments M_n and tensions N_n. Note that if the half flank angle is greater than 3.2^o in predominant bending, the flanks can no longer be rigid, but give fans and a constant stress triangle at the flank (McClintock, 1971). Although the flanks of the decohering zone cannot remain rigid in this case, the displacement fields nearly coincide with those for slip on a single pair of arcs (Huff, et al., 1969). A pair of arcs is still a useful approximation, although at the crack tip their angles will decrease, as will the mean normal stress across them.

For compact notation, the net-section tension N_n and moment M_n are normalized

with respect to unnotched plane strain limit loads using the shear strength k and remaining ligament b:

$$\hat{N}_n \equiv N_n/(2kb) \qquad \text{and} \qquad \hat{M}_n \equiv M_n/(0.5kb^2). \tag{2.7}$$

Define a "net-section loading ratio" μ_n:

$$\mu_n \equiv \frac{M_n}{bN_n} = \frac{\hat{M}_n}{4\hat{N}_n}. \tag{2.8}$$

The net section loading ratio μ_n varies from 0 for pure tension ($\hat{N}_n = 1$) to ∞ for pure bending ($\hat{N}_n = 0$). Note that the modified Green and Hundy slip line fields for predominant bending may apply up to $\hat{N}_n = 0.5512$ or $\mu_n = 0.6001$ (Kim, et al., 1993a; Shiratori and Dodd, 1980). For pure extension ($\hat{N}_n = 1$; $\mu_n = 0$) and both predominant and pure bending ($0 \leq \hat{N}_n < 0.5512$; $0.6001 < \mu_n \leq \infty$), slip line fields are known (Kim, et al., 1993a; Shiratori and Dodd, 1980). For combined bending with large tension ($0.5512 \leq \hat{N}_n < 1$; $0 < \mu_n \leq 0.6001$), Rice (1972) proposed kinematically admissible fields for upper bounds consisting of pairs of symmetric, circular arcs characterized by two variables. To find the least upper bound (LUB), he minimized the bound with respect to one variable with the other fixed, and then performed a graphical minimization. A complete analytical formulation of the LUB for this field has been presented in Kim, et al. (1993a) and is summarized here. The minimization of the bound gives two nonlinear equations in the two angular unknowns for an arc, α and β, shown in Fig. 3.6b:

$$(\alpha - \beta)\cos\alpha - (\sin\alpha - \sin\beta)(\frac{1}{2} + \hat{N}_n \sin\beta\cos\alpha) = 0. \tag{2.9}$$

$$(\alpha - \beta)\cos\beta - (\sin\alpha - \sin\beta)(\frac{1}{2} + \hat{N}_n \sin\alpha\cos\beta) = 0. \tag{2.10}$$

For $0.5512 \leq \hat{N}_n \leq 1$, the LUB arc parameters α_o and β_o are found numerically and plotted in Fig. 3.7. The values of α_o and β_o at both ends of this range match

the corresponding slip line solution values, namely, $\alpha_o = 72^o$ and $\beta_o = -45^o$ at $\hat{N}_n = 0.5512$, and $\alpha_o = \beta_o = 45^o$ at $\hat{N}_n = 1$. The corresponding LUB for $\hat{M}_n$ can be determined from the principle of virtual work by relative sliding along the circular arc:

$$\hat{M}_n = 2\frac{(\alpha_o - \beta_o)}{(\sin\alpha_o - \sin\beta_o)^2} - 2\hat{N}_n\frac{(\sin\alpha_o + \sin\beta_o)}{(\sin\alpha_o - \sin\beta_o)}. \tag{2.11}$$

The yield locus from the LUB analysis is shown in Fig. 3.8, including that from slip line field analysis (Kim, et al., 1993a; Shiratori and Dodd, 1980):

$$\Phi_{SLF} = \hat{M}_n + 0.7394\hat{N}_n^2 - 0.5212\hat{N}_n - 1.2606 = 0 \quad \text{for } -1 \le \hat{N}_n \le 0.5512. \tag{2.12}$$

Lee and Parks (1993) used finite elements to study yield loci for various crack depths. For a given crack depth and bending-to-tension ratio, they found the limit tension and the limit moment. By comparing yield loci for various crack depths, they suggest that, for all bending-to-tension ratios, relative crack depths of a/t greater than about 0.35 would be "deep enough" to prevent shoulder deformation. (For pure extension, any crack depth is sufficient.) Their results for deep cracks ($a/t = 0.5$ and 0.6) are shown with circles in Fig. 3.8. For predominant bending ($0 \le \hat{N}_n < 0.5512$), their results are consistent with the slip line solutions. For combined bending with large tension ($0.5512 \le \hat{N}_n \le 1.0$), their results suggest that the LUB analysis overestimates the limit load by no more than 3%.

2.2. Three-parameter characterization of near tip fields

For families of slip line fields with a pair of symmetric crack tip slip lines, discussed above, the near tip fields are characterized by three parameters: the slip line angle θ_s and the normal stress and shear displacement increment across it, σ_s and

δu_s. This three-parameter characterization of near tip fields in fully plastic fracture mechanics presents a contrast to one-parameter (K) in elastic fracture mechanics or two-parameter (K or J and T or Q) characterization in linear or non-linear elastic fracture mechanics (Betegón and Hancock, 1991; O'Dowd and Shih, 1992).

In pure extension of unequally grooved specimens with back angle 2ϕ (Fig. 3.4), the slip line fields give (McClintock, 1971)

$$\theta_s = 45^o; \qquad \left(\frac{\sigma_s}{2k}\right)_{\theta=\theta_s} = \frac{1}{2} + (\frac{\pi}{2} - \phi). \tag{2.13}$$

For these geometries the slip line fields also provide the third local parameter, either the shear displacement increment across the slip line δu_s, or the normal displacement increment at the crack tip δu_t, in terms of the far field displacement increment δu:

$$\delta u_s (= \sqrt{2}\delta u_t) = \sqrt{2}\delta u. \tag{2.14}$$

For combined bending and tension of single-face-cracked specimens with the half flank angle less than 3.2^o (to assure rigid flanks), θ_s and $(\sigma_s/2k)_{\theta_s}$ are related to the normalized net tension $\hat{N}_n$ (or equivalently the net-section tension-to-bending ratio $\mu_n \equiv M_n/(bN_n) = 4\hat{M}_n/\hat{N}_n$). For predominant bending ($0 \leq \hat{N}_n < 0.5512$, Fig. 3.6c and 6d), the modified Green and Hundy slip line fields give θ_s and $(\sigma_s/2k)_{\theta_s}$ as constants:

$$\theta_s \doteq 72^o; \qquad \left(\frac{\sigma_s}{2k}\right)_{\theta=\theta_s} \doteq 1.54. \tag{2.15}$$

The slip line fields provide the displacement parameters in terms of far field increments of displacement δu and rotation $\delta\theta$ (Fig. 3.5a):

$$\delta u_s \left(= \frac{1}{\sin\theta_s}\delta u_t\right) = \frac{1}{\sin\theta_s}\left[\delta u + (\frac{t}{2} - a)\delta\theta\right]. \tag{2.16}$$

For intermediate tension and bending ($0.5512 \leq \hat{N}_n < 1$, Fig. 3.6b), only upper bound fields are known (Rice, 1972). In general, stresses cannot be determined from upper bound analyses. However, an assumed traction distribution on the arc which gives the LUB does satisfy some aspects of equilibrium (Kim, et al., 1993b). If the traction transmitted across the LUB arc satisfies the first Hencky equation of local equilibrium, and the one free parameter of the Hencky normal stress distribution along the arc is chosen to satisfy zero shear force, the resulting tractions on the LUB arc satisfy global equilibrium. Thus the normal stress on the arc and in particular that at the crack tip can be approximated. The LUB arc and the above equilibrium analysis give θ_s and $(\sigma_s/2k)_{\theta_s}$ in terms of the LUB arc parameters α_o and β_o as (Kim, et al., 1993b)

$$\theta_s = \alpha_o. \tag{2.17}$$

$$\left(\frac{\sigma_s}{2k}\right)_{\theta=\theta_s} = \alpha_o + \frac{\sin\alpha_o - \sin\beta_o - 2(\alpha_o\cos\alpha_o - \beta_o\cos\beta_o)}{2(\cos\alpha_o - \cos\beta_o)}. \tag{2.18}$$

Figure 3.9 shows the variations of θ_s and $(\sigma_s/2k)_{\theta_s}$ according to (2.17) and (2.18) for varying $\hat{N}_n$. It also includes the variations as determined from finite element (FE) limit load analysis (Lee and Parks, 1993), drawn with circles. For predominant bending, θ_s-value from FE analysis are consistent with the slip line solution, but $(\sigma_s/2k)_{\theta_s}$ at $\mu_n = 0.64$ is low by 4.5%. For bending with large tension, the approximation from the LUB arc agrees with the finite element results within 6% in θ_s and within 8% in $(\sigma_s/2k)_{\theta_s}$. For the displacement parameters, the (least) upper bound fields give the same relation (2.16) as in predominant bending.

2.3. Effects of the decohering zone

Recently, Tvergaard and Hutchinson (1992) studied the effect of the decohering zone in small scale yielding. They considered Mode I crack growth in plane strain

without zig-zagging. By postulating various traction-displacement laws on the crack plane, they found a strong effect of the decohering zone on the crack growth resistance K_{IC}. In contrast, in fully plastic crack growth, we showed above that the flanks of the decohering zone remain rigid, which implies no direct effect on the crack tip opening angle ($CTOA$). Therefore, in fully plastic crack growth, the only controlling mechanisms are hole nucleation, growth, and coalescence by localization or by fine cracking. However, there are some indirect effects due to the decohering zone. Define the crack tip as the tip of the decohering zone, and measure the remaining ligament b from the tip of the decohering zone to the free surface, as shown in Fig. 3.3. Then, for the given remaining ligament b and the net-section loadings M_n and N_n, the work-conjugate net-section displacement and rotation increments, δu_n and $\delta\theta_n$, are affected by the presence of the traction in the decohering zone. Hence crack tip parameters such as σ_s, θ_s and δu_s, which determine the $CTOA$, are affected. When δu_n and $\delta\theta_n$ are given, however, M_n and N_n will be affected but the $CTOA$ will not. As an example, we next study the effect of the decohering zone on the yield locus in deep, single-face-cracked specimens under combined bending and tension.

Yield locus for growing cracks in deep, single-face-cracked specimens under combined bending and tension

The traction $T(x)$ in the decohering zone increases the net-section loadings N_n and M_n and thus changes the yield surface. The decohering zone is characterized by its length d and a specified traction-displacement law $T(x)$. Note that the traction law is quadratic as discussed before (see (2.5)):

$$T(x) = T_C(\frac{x}{d})^2, \tag{2.19}$$

where T_C is crack plane traction at the tip of the decohering zone. Note that T_C is not available from either a slip line field (when available) or the equilibrium stress field associated with the LUB arc because the latter provide the stresses only on the slip line or on the arc. Further, T_C can be discontinuous along the crack plane. As an extreme case, take T_C by assuming that the mean normal stress σ varies linearly with θ from $\theta = \theta_s$ to $\theta = 45^o$, and remains constant from $\theta = 45^o$ to $\theta = 0^o$, as in the Prandtl field. Then

$$T_C = [\sigma_s + 2k(\theta_s - \frac{\pi}{4})] + k. \tag{2.20}$$

For example, in predominant bending ($\sigma_s \doteq 3.08k$, $\theta_s \doteq 72^o$), $T_C = 5.02k$, and, in predominant tension (σ_s=k, θ_s=45^o), $T_C = 2k$. Define the centroid of the traction distribution d_c:

$$d_c = \frac{\int_0^d T(x)xdx}{\int_0^d T(x)dx} = \frac{3}{4}d. \tag{2.21}$$

Normalize the variables with respect to a shear strength k and the remaining ligament b as in (2.7) and also

$$\hat{T}_d = \frac{T_C}{2kb}\int_0^d \left(\frac{x}{d}\right)^2 dx = \left(\frac{T_C}{2kb}\right)\left(\frac{d}{3}\right) \qquad \hat{d}_c = \frac{d_c}{b} = \frac{3}{4}\left(\frac{d}{b}\right). \tag{2.22}$$

For both predominant bending and bending with large tension, the effect of the decohering zone on the yield locus can be found by adding the forces and moments transmitted across the decohering zone. It turns out that in both cases, the effect is to increase $\hat{N}_n$ and $\hat{M}_n$ by the amounts $\hat{T}_d$ and $2\hat{T}_d(1 + 2\hat{d}_c)$, respectively. This effect of the decohering zone on the yield surface is shown in Fig. 3.10 for d/b= 0.0 and 0.1. However, since in most cases the decohering zone size d would be much smaller than the remaining ligament b, the effect of the decohering zone on the yield locus would be negligible.

3. MESO-MECHANICS

3.1. Meso-mechanical determination of CTOA in terms of crack tip parameters

Sliding off and shear-cracking model for a growing crack

As shown in Fig. 3.1, crack growth results from hole nucleation, hole growth, and linkage by localization or fine cracking between the crack tip and a large hole or between large holes which are randomly distributed. The resulting crack path is irregular, running up and down. Thus macroscopically straight crack growth is the result of microscopic zig-zagging (McClintock, 1969; Carson, 1970; Tvergaard and Needleman, 1992). In a sliding off and shear-cracking model, a crack grows in a zig-zagging fashion, sliding off by s and cracking by c along a shear band before changing direction (Fig. 3.11). The geometry gives the form of $CTOA$ in terms of θ_s and s/c:

$$\tan(\frac{CTOA}{2}) = \frac{s\sin\theta_s}{(c+s+s)\cos\theta_s} = \frac{1}{2(c/s)+1}\tan\theta_s. \tag{3.1}$$

The proposed sliding off and shear-cracking model is physically sound in the sense that the microscopic zig-zagging and the resulting crack roughness are taken into account. It does not apply to cracks which advance macroscopically along a slip line, as in torsion or in asymmetrical (e.g. mixed-mode) configurations.

The model of the slip line field surrounding the crack tip requires a ratio of cracking to sliding off, c/s, in each step of the zig-zag. Take $(s+c)$ to be the distance between steps. If this is one side of a square element straddling the slip line, some of the shear strain of the element can be thought of as being that required to grow the holes, and some as that to link holes to form macro-cracks, for example by micro-shear-band

localization or by fine cracks. There is also some strain to initiate the holes. The total fracture shear strain in the band $\gamma_f (= \gamma_b)$ will depend on the mean normal stress in the shear band, σ_s, and on material properties such as hardening and an initial volume fraction of holes:

$$\gamma_f = \widehat{\gamma_f}(\sigma_s, \text{material properties}). \tag{3.2}$$

The sliding off and shear cracking model also gives the relation between $\gamma_f (= \gamma_b)$ and the alternating incremental cracking and sliding. From the slip geometry (Fig. 3.11),

$$\gamma_f = \gamma_b = \frac{s}{(s+c)\sin 2\theta_s}. \tag{3.3}$$

Eliminating (c/s) in (3.1) with (3.3) gives

$$\tan(\frac{CTOA}{2}) = \frac{1}{[2/(\gamma_f \sin 2\theta_s) - 1]} \tan\theta_s. \tag{3.4}$$

Equation (3.4) gives the $CTOA$ in terms of θ_s and γ_f. The desired relation (1.12) can be achieved if γ_f can be determined in terms of σ_s and material properties, as follows.

Critical hole growth strain in shear band

McClintock, et al., (1966) analyzed hole growth in shear bands. The growth of mean radius (R) of a cylindrical void in a shear band per unit strain γ was found in terms of the shear strength k and normal stress σ_s in the shear band and the strain hardening exponent n in $k = k_o \gamma^n$ with k_o=constant:

$$\frac{1}{R}\frac{dR}{d\gamma} = \frac{1}{2(1-n)} \sinh[(1-n)\frac{\sigma_s}{k}]. \tag{3.5}$$

For a constant σ_s/k, integration of (3.5) up to the point at which linkage between large holes takes over leads to the fracture shear strain γ_f in terms of σ_s/k and a

critical hole growth ratio for linkage, (R_l/R_o), which is the ratio of the hole size at linkage, R_l, to the initial hole size, R_o:

$$\gamma_f = \frac{2(1-n)\ln(R_l/R_o)}{\sinh[(1-n)\sigma_s/k]}. \tag{3.6}$$

From Fig. 3.1, the strain for linkage itself is negligible (adds little $CTOA$). To account for hole nucleation strain roughly, extend (3.6) to

$$\gamma_f = \frac{(1-n)A}{\sinh[(1-n)\sigma_s/k]} + B(\sigma_s). \tag{3.7}$$

The parameters A and B in (3.7) reflect material properties and must be determined from experiments. The first term on the RHS of (3.7) can be viewed as a strain for hole growth to linkage by localization or by fine cracking. For example, unnotched tensile tests on crack initiation in axi-symmetric, round-grooved steel specimens (McClintock, 1968a) give A=0.2 – 1.2 (corresponding to (R_l/R_o) of 1.1 – 1.8). The second term, $B(\sigma_s)$, can be viewed as a strain for hole nucleation, which is generally a function of mean normal stress (Argon, et al., 1975). When the hole growth mechanism is dominant, the hole nucleation strain is negligible ($A \gg\sim B\sinh(\sigma_s/k)$), and γ_f has an inverse exponential dependence on triaxiality σ_s/k. When hole nucleation mechanism is dominant, the triaxiality dependence in (3.7) will be determined by the triaxiality dependence of B. For preliminary insight, assume no nucleation strain, $B(\sigma_s)$=0. Placing (3.7) into (3.4) gives the $CTOA$ in terms of σ_s, θ_s, and the material properties:

$$\tan(\frac{CTOA}{2}) = \frac{(1-n)A\sin 2\theta_s}{2\sinh[(1-n)\sigma_s/k)] - (1-n)A\sin 2\theta_s}\tan\theta_s. \tag{3.8}$$

Figure 3.12 shows an inverse exponential dependence on σ_s/k for non-hardening (n = 0) flow and for typical values of A, ranging from 0.2 to 1.2, along with limited available

experimental data on $CTOA$ from the literature (Kardomateas and McClintock, 1989; McClintock and Wineman, 1987). Even though there exist other sets of fully plastic crack growth test data, they do not meet plane strain conditions. For instance, Hancock, et al. (1992) performed fully plastic (crack initiation and growth) tests providing a wide range of crack tip triaxiality: three point bending, compact tension, and center cracked panel (CCP) test. However, their CCP test specimens did not meet plane strain requirements, so the resulting crack tip triaxiality would be lower than that for single-face-cracked specimens in tension. In any event they also showed a dramatic decrease in $CTOA$ with increasing crack tip triaxiality as in Fig. 3.12. Figure 3.13 shows a higher order parabolic dependence on θ_s ($45^o \leq \theta_s \leq 72^o$) for non-hardening ($n = 0$) and for two values of $A = 1.0, 0.5$. Therefore, to a first order for small n, (3.8) suggests that the $CTOA$ has inverse exponential dependence on σ_s/k and higher order parabolic dependence on θ_s for $45^o \leq \theta_s \leq 72^o$. For fully plastic crack growth in a surface-cracked plate, the resulting dependence of the estimated $CTOA$ on various net-section loading ratios $\mu_n (= M_n/(bN_n))$ is shown in Fig. 3.14.

Improved data for the parameters A and $B(\sigma_s)$ should be obtained from crack growth experiments, which will be discussed next.

3.2. Experimental determination of $CTOA$ from fully plastic tests

For example, assume

$$B(\sigma_s) = B_1 \frac{\sigma_s}{k} + B_2. \tag{3.9}$$

Then the resulting form of $CTOA$ is, from (3.4) and (3.7),

$$\tan(\frac{CTOA}{2}) = \frac{1}{[2/(\gamma_f \sin 2\theta_s) - 1]} \tan\theta_s,$$

$$\text{with } \gamma_f = \frac{(1-n)A}{\sinh[(1-n)\sigma_s/k]} + B_1\frac{\sigma_s}{k} + B_2. \tag{3.10}$$

At least three different fully plastic tests are needed to determine the three unknown constants A, B_1, and B_2. For instance,

i) extension of single-face-cracked specimens (Fig. 3.5)

(from (2.13), $\theta_s = 45^o$; $\sigma_s/k = 1$),

ii) extension of unequally grooved specimens with back angle $2\phi = 120^o$ (Fig. 3.4)

(from (2.13), $\theta_s = 45^o$; $\sigma_s/k \doteq 2.05$),

iii) extension of unequally grooved specimens with back angle $2\phi = 60^o$ (Fig. 3.4)

(from (2.13), $\theta_s = 45^o$; $\sigma_s/k \doteq 3.09$),

iv) bending of single-face-cracked specimens (Fig. 3.5)

(from (2.15), $\theta_s \doteq 72^o$; $\sigma_s/k \doteq 3.08$).

More tests can be generated from tensile tests of unequally grooved specimens by varying back angles. Refer to McClintock (1971) for required shoulder thickness and width of such test specimens required to assure plane strain.

Another test of interest would be unequally grooved specimens under pure bending. Slip line fields are known only for two extreme cases: i) single-face-cracked specimens ($2\phi = 180^o$) and ii) double-face-cracked specimens ($2\phi = 0^o$). The slip line field for single-face-cracked specimens under pure bending (Green and Hundy, 1958) gives

$$\frac{M^{LUB}}{0.5kb^2} = 1.261; \quad \theta_s^{LUB} = 72^o; \quad \left(\frac{\sigma_s}{k}\right)_{\theta_s}^{LUB} = 3.08. \tag{3.11}$$

On the other hand, the slip line field for double-face-cracked specimens under pure bending consists of just two circular arcs intersecting at the tips of the groove and

gives (McClintock, 1971; Green and Hundy, 1956):

$$\frac{M^{FIM}}{0.5kb^2} = 1.380; \quad \theta_s = 67^o; \quad \left(\frac{\sigma_s}{k}\right)_{\theta_s} = 2.33. \tag{3.12}$$

Therefore, intermediate back angles, i.e., $0^o < 2\phi < 180^o$, do affect the slip line fields which will be studied next.

Slip line fields for unequally grooved specimens under pure bending

Slip line fields for unequally grooved specimens in tension (Fig. 3.4) and for deep, single-face-cracked specimens under combined bending and tension (Fig. 3.6) suggest the possible slip line field as shown in Fig. 3.15. In the field, the arc AB and the line BC are the α-line, and the arc BD and the line DE are the β-line. The five unknowns, R, α, β, ψ, and d, are shown in Fig. 3.15. Geometry gives

$$\psi = \frac{3}{4}\pi - \phi - \beta, \tag{3.13}$$

$$R(\sin\alpha + \sin\beta) + d\cos\beta = b, \tag{3.14}$$

$$R(\cos\beta - \cos\alpha) = d\sin\beta. \tag{3.15}$$

The other two unknowns can be determined from two force equilibrium conditions. Note that the Hencky equilibrium equation for the β-line gives

$$\sigma_B = \sigma_D - 2k\xi = -2k(\psi + 1), \tag{3.16}$$

and the Hencky equilibrium equation for the α-line gives $\sigma(\theta)$ in the arc AB:

$$\sigma(\theta) = \sigma_B + 2k(\theta + \beta) = 2k\left(\theta + \beta - \psi - \frac{1}{2}\right). \tag{3.17}$$

Force equilibrium in the x-direction gives

$$0 = \Sigma F_x = \int_{-\beta}^{\alpha} [-\sigma(\theta)\sin\theta + k\cos\theta] R d\theta + (k\cos\beta + \sigma_B \sin\beta) d. \tag{3.18}$$

Substituting $\sigma(\theta)$, R, and d by using (3.14), (3.15), and (3.16) into (3.18) gives a nonlinear equation in terms of two angular unknowns α and β:

$$2\sin\beta[-(\sin\alpha + \sin\beta) + \beta(\cos\alpha - \cos\beta) + (\alpha\cos\alpha + \beta\cos\beta)]$$

$$+1 - \cos(\alpha + \beta) = 0. \tag{3.19}$$

Force equilibrium in the y-direction gives

$$0 = \Sigma F_y = \int_{-\beta}^{\alpha} [\sigma(\theta)\cos\theta + k\sin\theta] R d\theta + (\sigma_B \cos\beta - k\sin\beta) d. \tag{3.20}$$

Substituting again $\sigma(\theta)$, R, and d by using (3.14), (3.15), and (3.17) into (3.20) gives another nonlinear equation in terms of two angular unknowns α and β:

$$\sin\beta[(\cos\alpha - \cos\beta) + \beta(\sin\alpha + \sin\beta) + (\alpha\sin\alpha - \beta\sin\beta)]$$

$$+\left(\phi + \beta - \frac{1}{2} - \frac{3}{4}\pi\right)[1 - \cos(\alpha + \beta)] = 0. \tag{3.21}$$

Note the explicit dependence on ϕ in (3.21). For a given back angle ϕ ($0^o < \phi < 90^o$), two angular unknowns α and β can be found from (3.19) and (3.21), and the other variables R, d, and ψ from (3.14), (3.15), and (3.17). The resulting values of α, R/b and ψ are shown in terms of ϕ with the dotted line in Fig. 3.17. Note that for $0^o \leq \phi \leq 30^o$ the field remain unchanged and thus the field variables remain constant.

From geometry, the slip angle θ_s is

$$\theta_s = \alpha. \tag{3.22}$$

The crack tip triaxiality $\sigma_s/(2k)$ is

$$\left(\frac{\sigma_s}{2k}\right)_{\theta_s} = \frac{\sigma_B}{2k} + (\alpha+\beta) = \left(\phi - \frac{1}{2} - \frac{3}{4}\pi\right) + \alpha + 2\beta. \tag{3.23}$$

The resulting values of $\sigma_s/(2k)$ are shown with the dotted line in Fig. 3.18. The bound for the moment M^{SLF} can be determined from the moment equilibrium:

$$\frac{M^{SLF}}{0.5kb^2} = 2\left(\frac{R}{b}\right)^2(\alpha+\beta) + \left(\frac{R}{b}\right)\left(\frac{d}{b}\right) - \left(\phi+\beta-\frac{1}{2}-\frac{3}{4}\pi\right)\left(\frac{d}{b}\right)^2. \tag{3.24}$$

The resulting limit moment are shown with the dotted line in Fig. 3.19. As shown in Fig. 3.17-3.19, the values match with the (existing) slip line field solutions at $\phi = 0^o$, but not at $\phi = 90^o$. Careful examination of the proposed field in Fig. 3.15 shows that the field can not recover the Green and Hundy field at $\phi = 90^o$ and the proposed field gives only upper bounds as ϕ approaches to 90^o. The Green and Hundy slip line field for $\phi = 90^o$ suggest another slip line field which is discussed next.

Figure 3.20 depicts a possible slip line field when ϕ app. aches to 90^o, where four unknowns R, α, d_1 and d_2 should be determined. Similarly as before, from geometry,

$$R\left(\sin\alpha + \sin\frac{\pi}{4}\right) + \frac{1}{\sqrt{2}}(d_1+d_2) = b. \tag{3.25}$$

$$R\left(\cos\frac{\pi}{4} - \cos\alpha\right) - \frac{1}{\sqrt{2}}(d_1-d_2) = 0. \tag{3.26}$$

Two force equilibrium conditions with the Hencky equilibrium equations,

$$\sigma_B = \sigma_C = \sigma_D - 2k\psi = -2k\left(\frac{1+\pi}{2} + \phi\right) \qquad \text{and} \tag{3.27}$$

$$\sigma(\theta) = \sigma_B + 2k\left(\theta + \frac{\pi}{4}\right), \tag{3.28}$$

give two nonlinear equations for two unknowns $\hat{R}(= R/b)$ and α:

$$\hat{R}\left[\left(\frac{\pi}{2} - \frac{1}{2} - \phi\right)\sin\alpha + \left(\alpha - \frac{\pi}{4} - \frac{1}{2} + \phi\right)\cos\alpha + \sqrt{2}\left(\frac{\pi}{2} - \phi\right)\right]$$

$$+\left(\phi-\frac{\pi}{2}\right)=0. \tag{3.29}$$

$$\hat{R}\left[\frac{1}{2}\cos\alpha+\left(\alpha+\frac{\pi}{4}+\frac{1}{2}\right)\sin\alpha\right]$$

$$-1+\left(\phi-\frac{\pi}{2}\right)=0. \tag{3.30}$$

Resulting values of α, R/b, and ψ are shown with the solid line in Fig. 3.17. The crack tip triaxiality $\sigma_s/(2k)$ is

$$\left(\frac{\sigma_s}{2k}\right)_{\theta_s}=\frac{\sigma_B}{2k}+\left(\alpha+\frac{\pi}{4}\right)=\left(\phi-\frac{1}{2}-\frac{1}{4}\pi\right)+\alpha. \tag{3.31}$$

The resulting values of $\sigma_s/(2k)$ are shown with the solid line in Fig. 3.18. The bound for the moment M^{SLF} also can be determined from the moment equilibrium:

$$\frac{M^{SLF}}{0.5kb^2}=2\left(\frac{R}{b}\right)^2\left(\alpha+\frac{\pi}{4}\right)+2\left(\frac{R}{b}\right)\left(\frac{d_1-d_2}{b}\right)-\left(\frac{\sigma_B}{2k}\right)\left(\frac{d_1-d_2}{b}\right)^2$$

$$+\sqrt{2}\left(\frac{R}{b}\right)\left(\frac{d_2}{b}\right)\left(\frac{\sigma_B}{2k}+1\right)\cos\alpha-\left(\frac{R}{b}+\frac{d_1}{b}\right)\left(\frac{d_2}{b}\right)\left(\frac{\sigma_B}{2k}-1\right). \tag{3.32}$$

The resulting limit moment are shown with the solid line in Fig. 3.19.

The results of Fig. 3.17-1.19 give the following observations:

1. The critical half back angle ϕ_c is 75.6°. Therefore, for $\phi \le \phi_c(=75.6^o)$, the field shown in Fig. 3.15 applies and for $\phi \ge \phi_c(=75.6^o)$, the field shown in Fig. 3.20 applies.

2. The normalized limit moment M^{LIM} varies gradually with ϕ, i.e., $M^{LIM}_{max}/(0.5kb^2) = 1.380$ at $0^o \le \phi \le 30^o$ and $M^{LIM}_{min}/(0.5kb^2) = 1.261$ at $\phi = 90^o$, as shown in Fig. 3.19. The slip line angle θ_s also varies gradually with ϕ, i.e., $(\theta_s)_{max} = 72^o$ at $\phi = 90^o$ and 75.6°, and $(\theta_s)_{min} = 66.8^o$ at $0^o \le \phi \le 30^o$, as shown in Fig. 3.17.

3. The crack tip triaxiality $\sigma_s/(2k)$ varies gradually with ϕ when $0^o \leq \phi \leq 70^o$ but varies rapidly when $70^o \leq \phi \leq 90^o$, as shown in Fig. 3.18. This makes pure bending test of unequally grooved specimens very attractive. By varying ϕ, we can change $\sigma_s/(2k)$ quite a lot without changing M^{LIM} and θ_s a lot.

4. CONCLUSIONS

This analysis predicts fully-plastic, plane strain, quasi-steady crack growth for crack tip fields approximated by a pair of slip lines.

At the macro-mechanical scale, a number of growing crack tip fields consist of a pair of slip lines for stationary cracks, along with a decohering zone. These include the fields for extension of unequally grooved specimens and combined bending and tension of deep, single-face-cracked specimens. In those cases the decohering zone is shown to have rigid flanks. The proposed slip line fields relate far-field geometries, loadings, and their increments to near-tip fields characterized by the slip angle θ_s and the normal stress and displacement increment across the slip line, σ_s and δu_s:

$$\left\{ \begin{array}{c} \theta_s \\ \sigma_s \\ \delta u_s \end{array} \right\} = \left\{ \ f \ \right\} \text{(far-field geometry, loadings and their increments).} \qquad (4.1)$$

Note the three-parameter characterization of near tip fields in fully plastic fracture mechanics, in contrast to the one-parameter characterization (K) in elastic fracture mechanics or two-parameter characterization (K or J and T or Q) in non-linear elastic fracture mechanics.

The rigid flanks of the decohering zone imply no direct effect of the decohering zone on the crack tip opening angle ($CTOA$). Thus, the controlling micromechanisms of fracture consist only of hole nucleation, growth, and localization. These micromechanisms are in turn controlled by near-tip plasticity parameters such as σ_s, θ_s, and δu_s. To estimate the dependence of these micromechanisms on near-tip plasticity parameters, a sliding off and shear-cracking model at the meso-mechanical scale is proposed for a growing crack. Together with the hole growth equations, an explicit form of $CTOA$ is developed in terms of crack tip parameters (σ_s/k, θ_s), hardening (n), and material properties:

$$\tan(\frac{CTOA}{2}) = \frac{1}{[2/(\gamma_f \sin 2\theta_s) - 1]} \tan\theta_s, \tag{4.2}$$

$$\text{where} \quad \gamma_f = \frac{(1-n)A}{\sinh[(1-n)\sigma_s/k]} + B(\sigma_s).$$

The term $(1-n)A/\sinh[(1-n)\sigma_s/k]$ is related to the strain for hole growth and the term $B(\sigma_s)$ to that for hole nucleation. The parameters A and B reflect material properties and should be determined from fully plastic crack growth experiments, as suggested in Sec. 3.2. The estimated $CTOA$ in case of no nucleation strain (B=0) exhibits inverse exponential dependence on σ_s/k and nearly higher order parabolic dependence on θ_s, as shown in Figs. 13 and 14. Limited experimental data from the literature are consistent with the dependence of the estimated $CTOA$ on σ_s/k.

From geometry at the crack tip, the crack opening displacement increment δu_t is related to δu_s and θ_s by

$$\delta u_t = \delta u_s \sin\theta_s. \tag{4.3}$$

Also from geometry, the crack growth per unit flank-to-flank crack tip displacement,

$\delta a/\delta u_t$, is related to the $CTOA$ through the tangent of its half angle:

$$\delta a/\delta u_t = 1/(2\tan(CTOA/2)). \tag{4.4}$$

Combining the above ideas provides the crack growth increment δa in terms of far-field geometries, loadings, their increments, and material properties, needed by the structural engineer:

$$\delta a = \widehat{\delta a}(\text{ far field geometry, loadings and their increments, and material properties}). \tag{4.5}$$

REFERENCES

Argon, A.S., Im, J. and Safoglu, R., 1975, "Distribution of Plastic Strain and Negative Pressure in Necked Steel and Copper Bars", *Metallurgical Transaction*, **6A**, pp. 815-838.

Betegón, C. and Hancock, J.W., 1991, "Two Parameter Characterization of Elastic-Plastic Crack Tip Fields", *Journal of Applied Mechanics*, **58**, pp. 104-110.

Budiansky, B., Hutchinson, J.W. and Slutsky, S.. 1982, in *Mechanics of Solids, The Rodney Hill 60th Anniversary Volume*, H.G. Hopkins and M.J. Sewell (eds.), Pergamon Press, Oxford, pp. 13-45.

Carson, J.W., 1970, "A Study of Plane Strain Ductile Fracture", Ph.D. Thesis, Department of Mechanical Engineering, Massachusetts Institute of Technology.

Chen, X.Y. and Drugan, W.J., 1991, "Plane-Strain, Elastic-Ideally Plastic Crack Fields For Mode I Quasistatic Crack Growth at Large-Scale Yielding - II. Global Analytical Solutions for Finite Geometries", *Journal of the Mechanics and Physics of Solids*, **39**, pp. 895-925.

Cox, T.B. and Low, J.R., 1974, "An Investigation of the Plastic Fracture of AISI 4340 and 18 Nickel-200 Grade Maraging Steels", *Metallurgical Transactions*, **5**, pp. 1457-1470.

Dodd, B. and Bai, Y., 1987, *Ductile Fracture and Ductility*, Academic Press, NY.

Drucker, D.C. 1960, "Plasticity" in *Structural Mechanics*, E.H. Lee and P.S. Symmonds, (eds.), Pergamon Press, London, pp. 407-456.

Drugan, W.J. and Chen, X.Y., 1989, "Plane Strain Elastic-Ideally Plastic Crack Fields For Mode I Quasistatic Growth at Large-Scale Yielding - I. A New Family of Analytical Solutions", *Journal of the Mechanics and Physics of Solids*, **37**, pp. 1-26.

Drugan, W.J., Rice, J.R. and Sham, T.L., 1982, "Asymptotic Analysis of Growing Plane Strain Tensile Cracks in Elastic-Ideally Plastic Solids", *Journal of the Mechanics and Physics of Solids*, **30**, pp. 447-473.

Ewing, D.J.F. and Hill, R., 1967, "The Plastic Constraint of V-Notched Tension Bars", *Journal of the Mechanics and Physics of Solids*, **15**, pp. 115-124.

Gao, Y.C. and Hwang, K.C., 1981, "Elastic-Plastic Fields in Steady Crack Growth", in *Three-Dimensional Constitutive Relations and Ductile Fracture*, S. Nemat-Nasser (ed.), North-Holland Publishing Company (1981), pp. 417-434.

Green, A.P. and Hundy, B.B., 1956, "Initial Plastic Yielding in Notch Bend Tests", *Journal of the Mechanics and Physics of Solids*, **4**, pp. 128-144.

Gudmundson, P., 1989, "Validity of Asymptotic Crack Tip Solutions for Plastic Materials", in *Advances in Fracture Research: Proceedings of the 7th International Con-*

ference on Fracture Vol. 1, Pergamon, Oxford, pp. 315-322.

Hancock, J.W., Reuter, W.G. and Parks, D.M., 1991, "Constraint and Toughness Parameterized by T", to appear in *ASTM STP on Constraint Effects in Fracture, Proceedings of ASTM Symposium*, Indianapolis, IN.

Herman, L. and Rice, J.R., 1980, "Comparison of the Theory and Experiment for Elastic-Plastic Plane-Strain Crack Growth", *Metal Science*, August-September, pp. 285-291.

Huang, Y., Hutchinson, J.W., and Tvergaard, V., 1991, "Cavitation Instabilities in Elastic-Plastic Solids", *Journal of the Mechanics and Physics of Solids*, **39**, pp. 223-241.

Huff, H.W., Joyce, J.A. and McClintock, F.A., 1969, "Fully Plastic Crack Growth under Monotonic and Repeated Bending", in *Fracture: Proceedings of the 2nd International Conference on Fracture*, Chapman and Hall, London, pp. 83-94.

Kardomateas, G.A., 1985, "Mixed Mode I and II Fully Plastic Crack Growth From Simulated Weld Defects", Ph.D. Thesis, Department of Mechanical Engineering, Massachusetts Institute of Technology.

Kardomateas, G.A. and McClintock, F.A., 1989, "Shear Band Characterization of Mixed Mode I and II Fully Plastic Fracture", *International Journal of Fracture*, **40**, pp. 1-12.

Kim, Y.J., McClintock, F.A. and Parks, D.M., 1993a, "Yield Locus in Deep, Single-Face-Cracked Specimens Under Combined Bending and Tension", submitted as Brief Note to *Journal of Applied Mechanics.* See also Chapter 4 in this volume.

Kim, Y.J., McClintock, F.A. and Parks, D.M., 1993b, "Global Equilibrium of Least Upper Bound Circular Arcs and its Application to Fracture Mechanics", submitted to *Journal of the Mechanics and Physics of Solids.* See also Chapter 2 in this volume.

Koplik, J. and Needleman, A., 1988, "Void Growth and Coalescence in Porous Plastic Solids", *International Journal of Solids and Structures*, **24**, pp. 835-853.

Lee, H. and Parks, D.M., 1993, "Fully Plastic Analyses of Plane Strain Single Edge Cracked Specimens Subject to Combined Tension and Bending", submitted to *International Journal of Fracture.*

McClintock, F.A., 1990, "Reduced Crack Growth Ductility due to Asymmetric Configurations", *International Journal of Fracture*, **42**, pp. 357-370.

McClintock, F.A. , 1971, "Plasticity Aspects of Fracture", in *Fracture Vol. 3*, H. Liebowitz (ed.), Academic Press, New York, pp. 47-225.

McClintock, F.A., 1969, "Crack Growth in Fully Plastic Grooved Tensile Specimens", in *Physics of Strength and Plasticity: Orowan Anniversary Volume*, A.S. Argon (ed.), M.I.T. Press, Cambridge, pp. 307-326.

McClintock, F.A., 1968a, "On the Mechanics of Fracture from Inclusions", in *Ductility*, American Society of Metals, Metals Park, Ohio, pp. 255-277.

McClintock, F.A., 1968b, "A Criterion for Ductile Fracture by the Growth of Holes", *Journal of Applied Mechanics*, **35**, pp. 363-371.

McClintock, F.A., 1958, "Ductile Fracture Instability in Shear", *Journal of Applied Mechanics*, **25**, pp. 581-588.

McClintock, F.A., Kaplan, S.M. and Berg, C.A., 1966, "Ductile Fracture by Hole Growth in Shear Bands", *International Journal of Fracture Mechanics*, **17**, pp. 201-217.

McClintock, F.A. and Wineman, S.J., 1987, "A Wedge Test for Quantifying Fully Plastic Fracture", *International Journal of Fracture*, **33**, pp. 285-295.

Miyamoto, H., Kikuchi, M. and Kawazoe, T., 1990, "A Study on the Ductile Fracture of Al-Alloys 7075 and 2017", *International Journal of Fracture*, **52**, pp. 389-404.

Nagpal, V., McClintock, F.A., Berg, C.A. and Subudhi, M., 1972, "Traction Displacement Boundary Conditions for Plastic Fracture by Hole Growth", in *International Symposium on the Foundations of Plasticity*, Noordhoff, Neyden, pp. 365-385.

Nilsson, F. and Stahle, P., 1988, "Crack Growth Criteria and Crack Tip Models",

Solid Mechanics Archives, **13**, pp. 193-238.

O'Dowd, N.P. and Shih, C.F., 1992, "Family of Crack-Tip Fields Characterized by A Triaxiality Parameter - II. Fracture Application", *Journal of the Mechanics and Physics of Solids*, **40**, pp. 939-963.

Parks, D.M., 1991, "Advances in Characterization of Elastic-Plastic Crack-Tip Fields", in *Topics in Fracture and Fatigue*, (McClintock Festschrift), Springer-Verlag, pp. 59-98.

Ponte Castañeda, P., 1987, "Asymptotic Fields in Steady Crack Growth with Linear Strain-Hardening", *Journal of the Mechanics and Physics of Solids*, **35**, pp. 227-268.

Rice, J.R., 1972, "The Line-Spring Model for Surface Flaws", in *The Surface Crack: Physical Problems and Computational Solutions*, J.L. Sweldow (ed.), American Society of Mechanical Engineers, New York, pp. 171-185.

Rice, J.R. and Sorensen, E.P., 1978, "Continuing Crack-Tip Deformation and Fracture for Plane-Strain Crack Growth in Elastic-Plastic Solids", *Journal of the Mechanics and Physics of Solids*, **26**, pp. 163-186.

Rice, J.R. and Tracey, D.M., 1969, "On the Ductile Enlargement of Voids in Triaxial Stress Fields", *Journal of the Mechanics and Physics of Solids*, **17**, pp. 201-217.

Shiratori, M. and Dodd, B., 1980, "Effect of Deep Wedge-Shaped Notches of Small

Flank Angle on Plastic Failure", *International Journal of Mechanical Science*, **22**, pp. 127-131.

Thomason, P.F., 1990, *Ductile Fracture of Metals*, Pergamon, Oxford.

Tvergaard, V., 1988, "3-D Analysis of Localization Failure in a Ductile Material Containing Two Size-Scales of Spherical Voids", *Engineering Fracture Mechanics*, **31**, pp. 421-436.

Tvergaard, V., 1982, "Ductile Fracture by Cavity Nucleation between Larger Voids", *Journal of the Mechanics and Physics of Solids*, **30**, pp. 265-286.

Tvergaard, V. and Hutchinson, J.W., 1992, "On the Relation between Crack Growth Resistance and Fracture Process Parameters in Elastic-Plastic Solids", *Journal of the Mechanics and Physics of Solids*, **40**, pp. 1377-1397.

Tvergaard, V. and Needleman, A., 1992, "Effect of Crack Meandering on Dynamic, Ductile Fracture", *Journal of the Mechanics and Physics of Solids*, **40**, 447-471.

Varias, A.G. and Shih, C.F., 1993, "Quasi-Static Crack Advance Under a Range of Constraint - Steady-State Fields Based on a Characteristic Length", *Journal of the Mechanics and Physics of Solids*, **41**, pp. 835-862.

White, C.S., Ritchie, R.O. and Parks, D.M., 1983, "Ductile Growth of Part-Through Surface Cracks: Experiment and Analysis", in *Elastic-Plastic Fracture: Second Sym-*

posium, Volume I-Inelastic Crack Analysis, ASTM STP 803, C.F. Shih and J.P. Gudas (eds.), American Society of Testing Materials, Philadelphia, pp. 384-409.

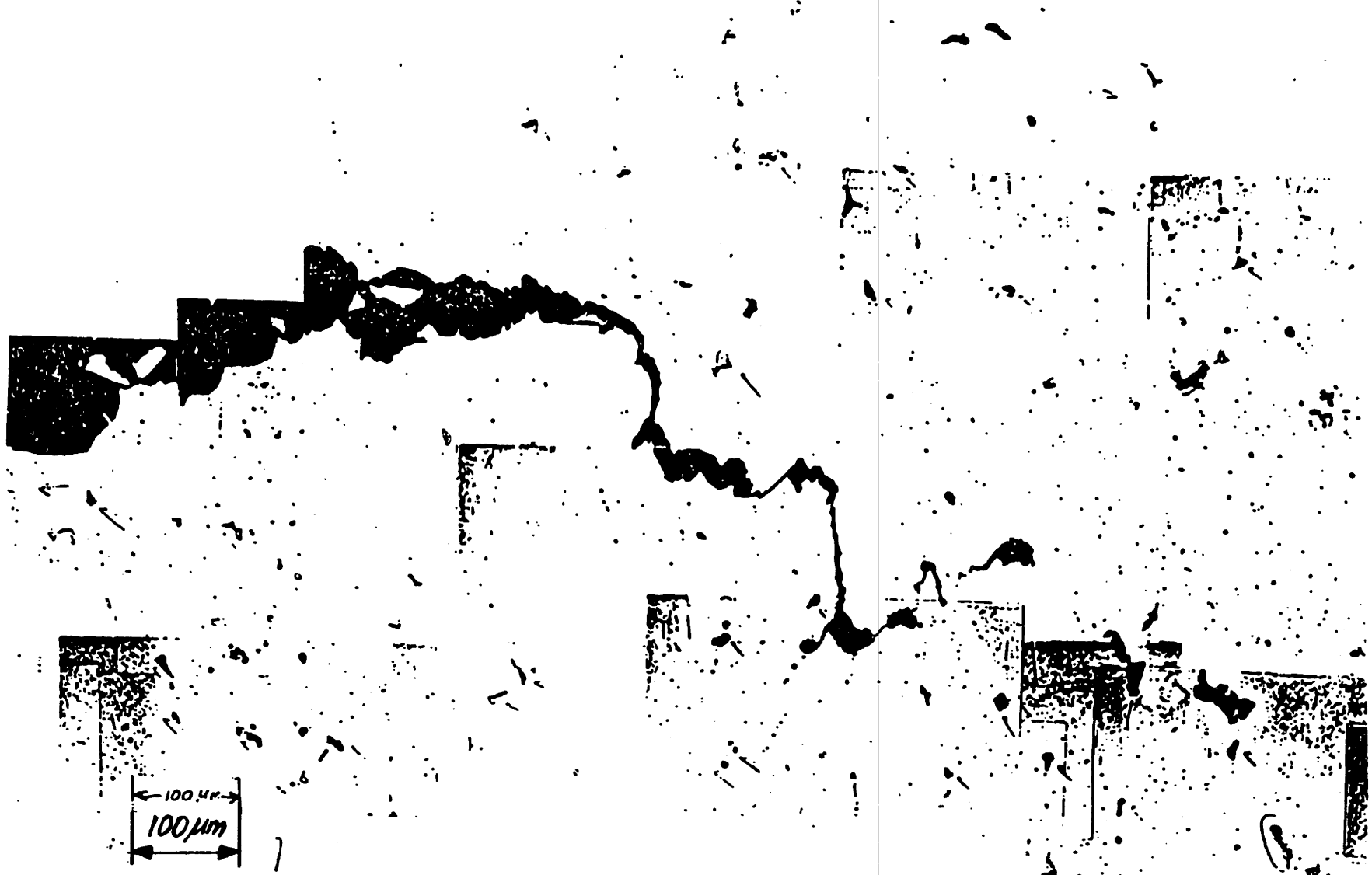

Fig. 3.1. Cross-section of a crack growing in 2024-T4 aluminum

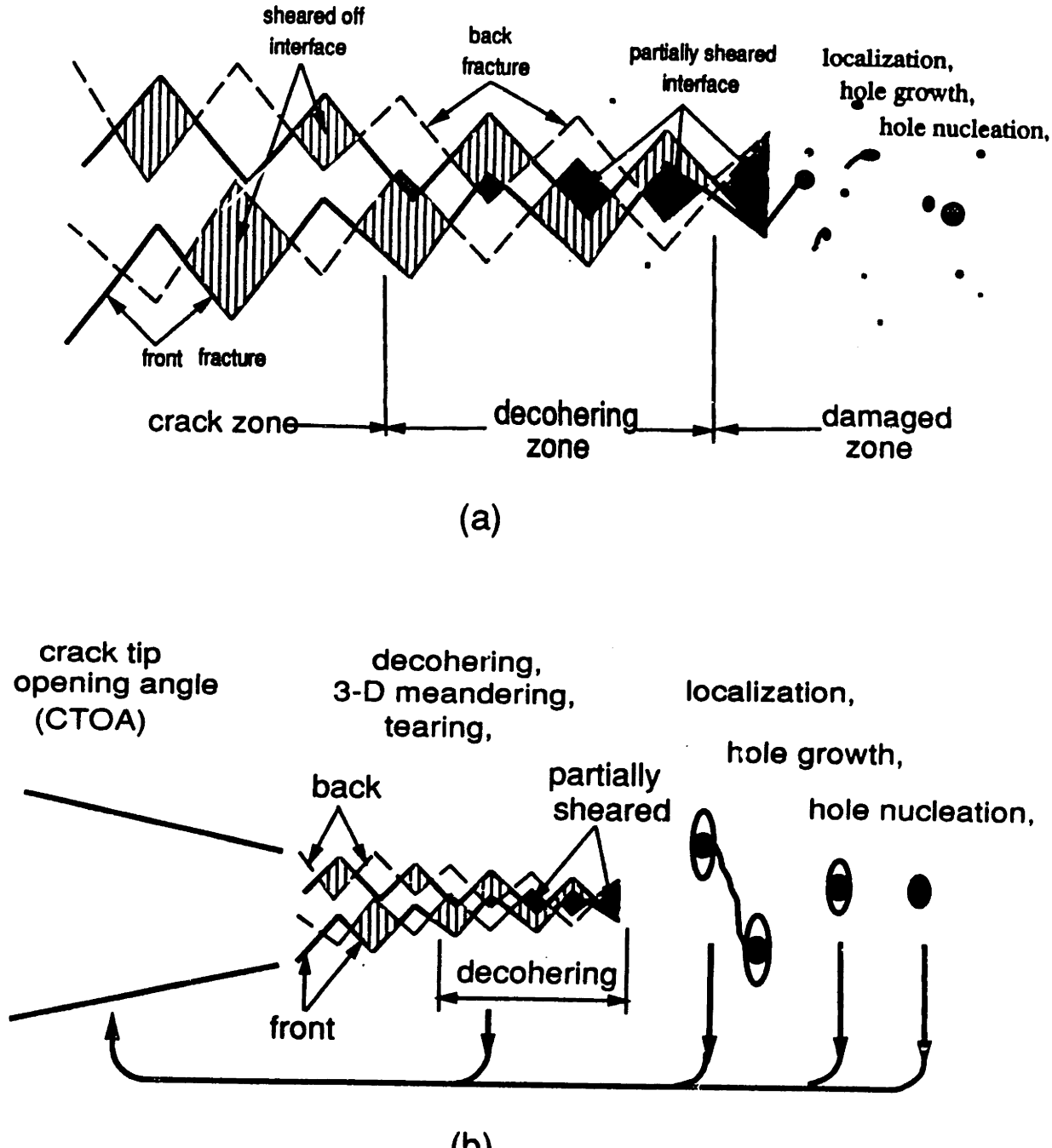

Fig. 3.2. (a) Idealization of a growing crack as in Fig. 1, (b) CTOA from micro-mechanisms of crack growth as in Fig. 1.

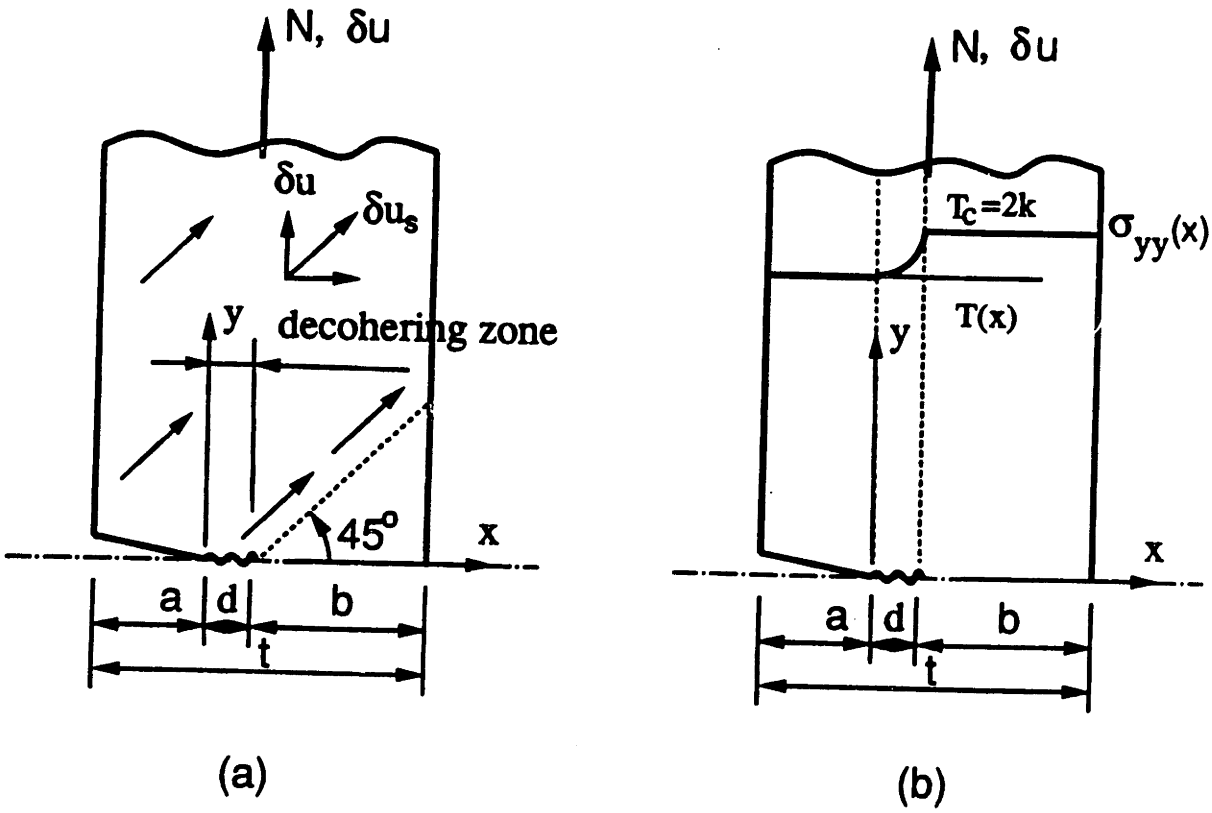

Fig. 3.3. Geometries and loadings for fully plastic ligaments in singly grooved specimen in tension with a decohering zone
(a) assumed displacement field for an upper bound,
(b) assumed stress field for a lower bound.

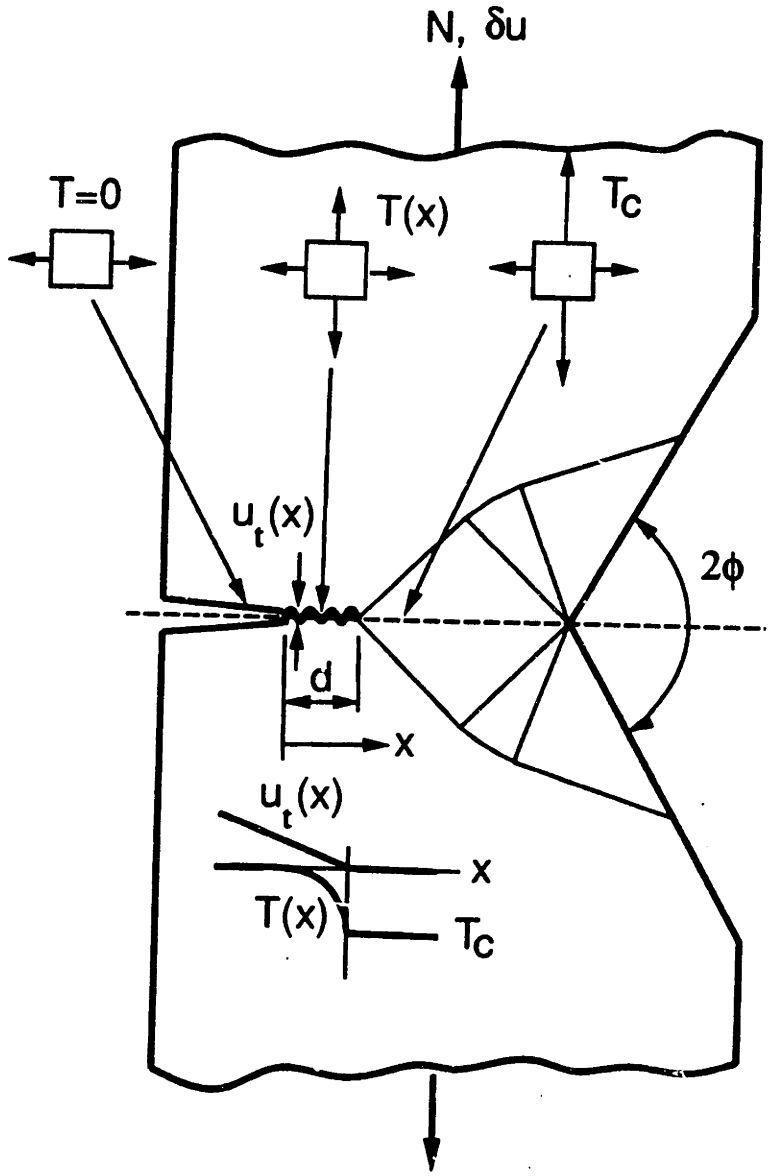

Fig. 3.4. Slip line field with a decohering zone for unequally grooved specimens in tension. Stress component σ_{yy} need not be continuous along crack plane.

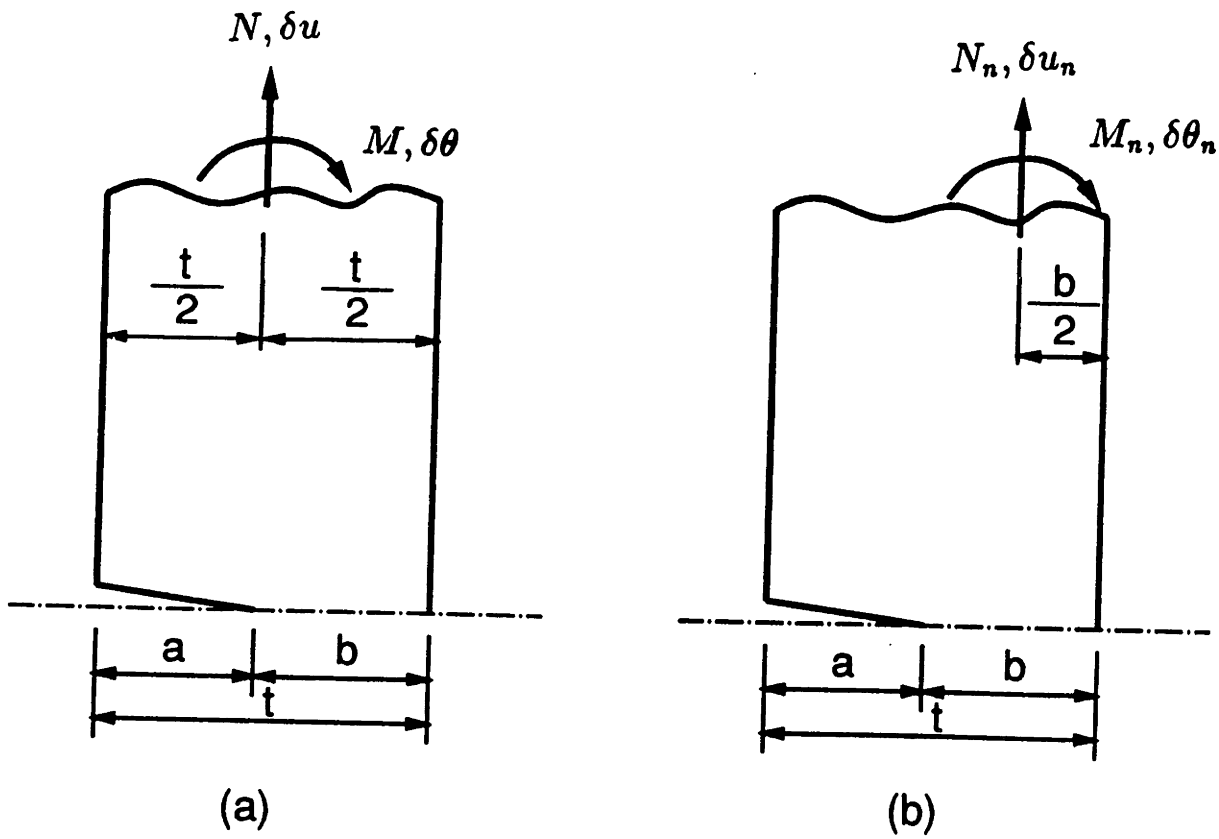

Fig. 3.5. Loadings for fully plastic ligaments in deep, single-face-cracked specimens under combined bending and tension
(a) variables based on a gross section,
(b) variables based on a net section.

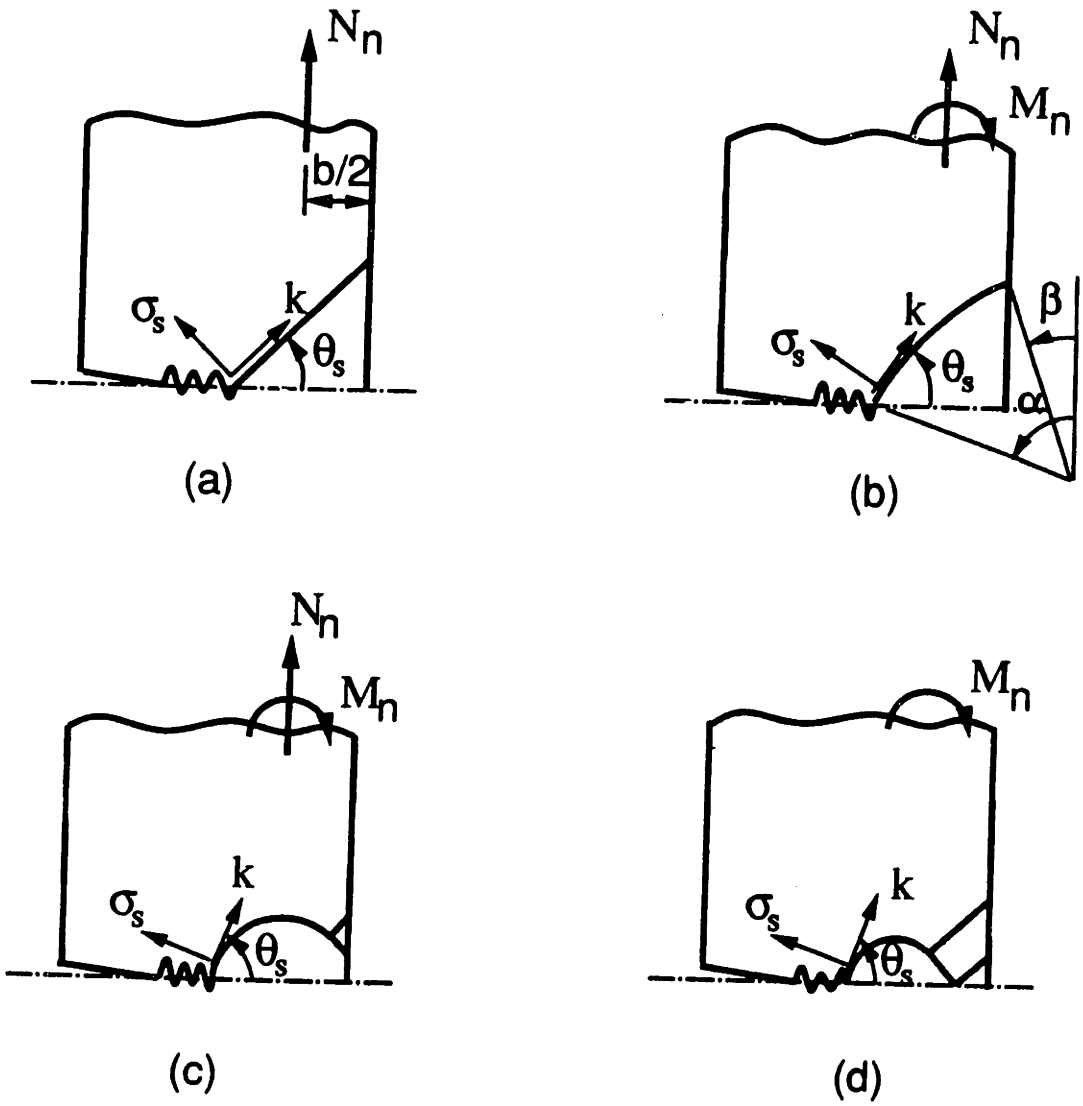

Fig. 3.6. Slip line fields with a decohering zone for deep, single-face-cracked specimens under combined bending and tension
(a) pure extension ($\sigma_s/2k = 0.5$; $\theta_s = 45°$),
(b) bending with large tension,
(c) bending with small tension ($\sigma_s/2k \doteq 1.54$; $\theta_s \doteq 72°$),
(d) pure bending ($\sigma_s/2k \doteq 1.54$; $\theta_s \doteq 72°$).

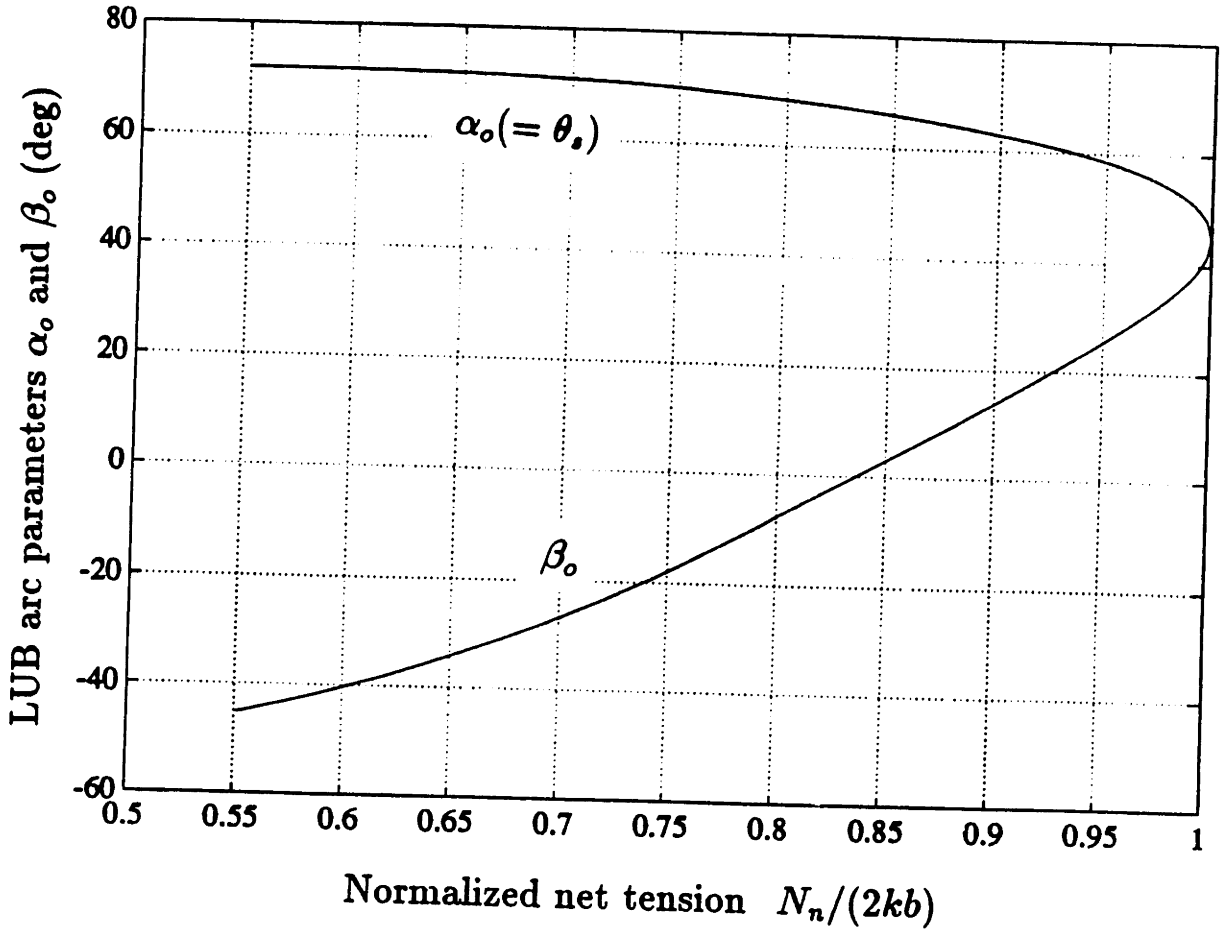

Fig. 3.7. The LUB arc parameters for deep, single-face-cracked specimens under combined bending and tension.

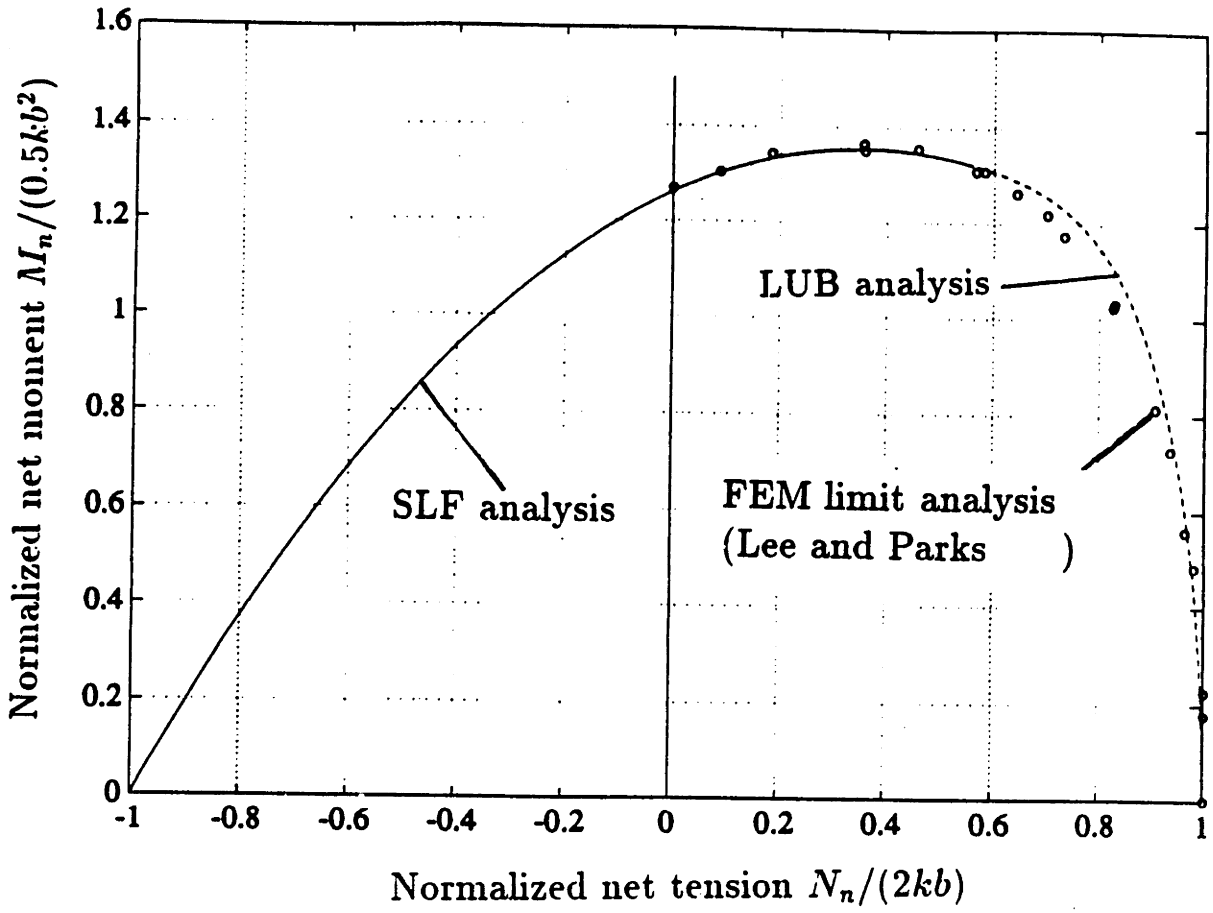

Fig. 3.8. Yield locus for deep, single-face-cracked specimens under combined bending and tension.

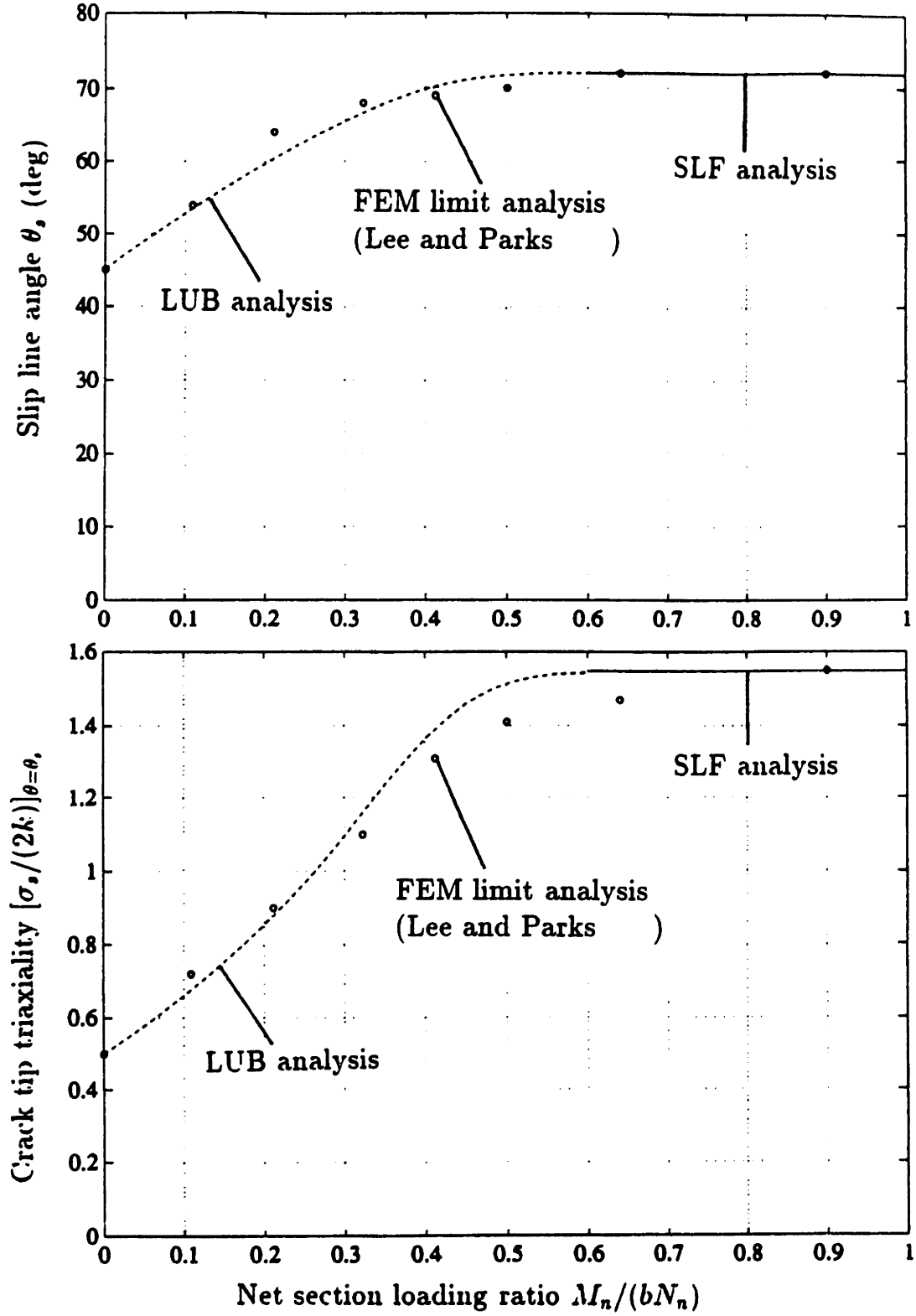

Fig. 3.9. Near-tip slip plane angle and normal stress in deep, single-face-cracked specimens under combined bending and tension.

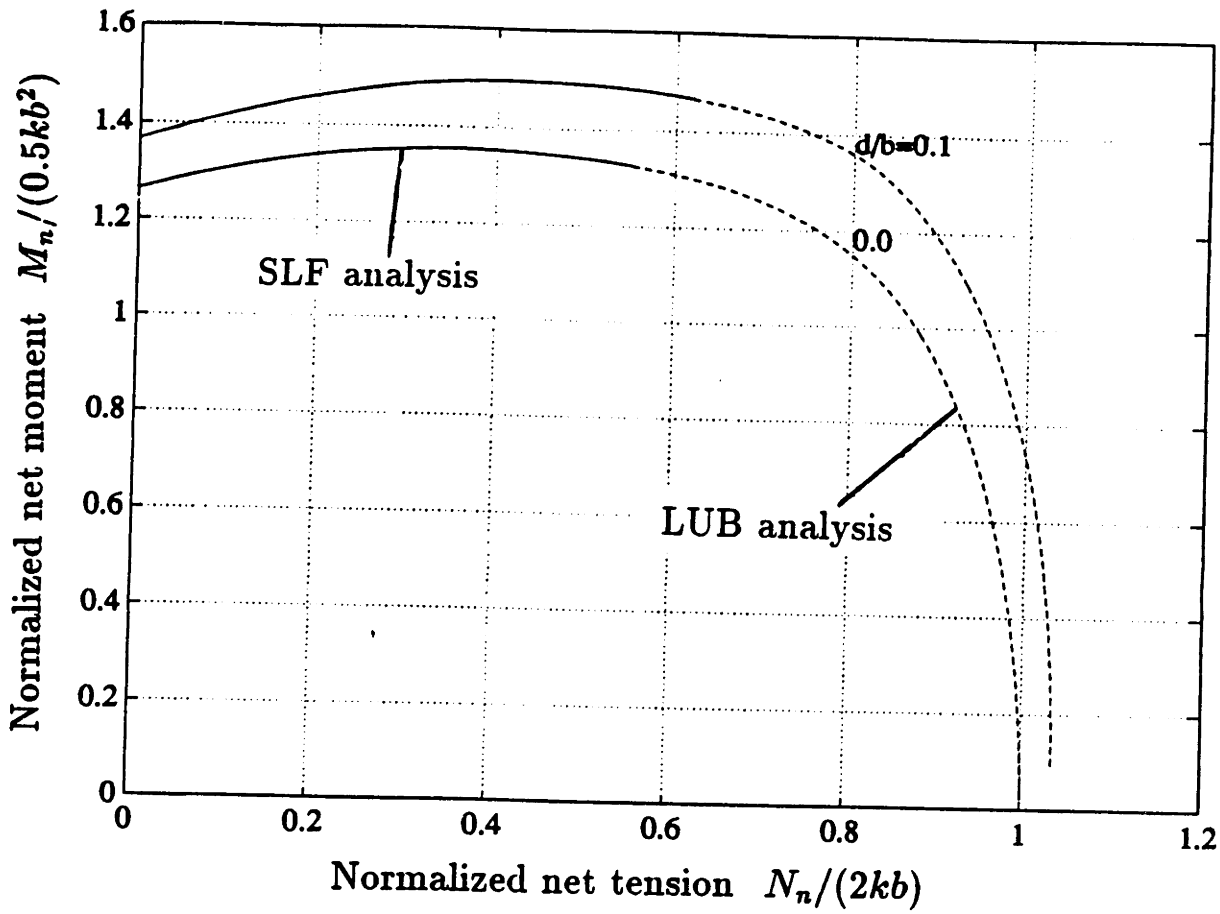

Fig. 3.10. Effects of the decohering zone on the yield surface of deep, single -face-cracked specimens under combined bending and tension.

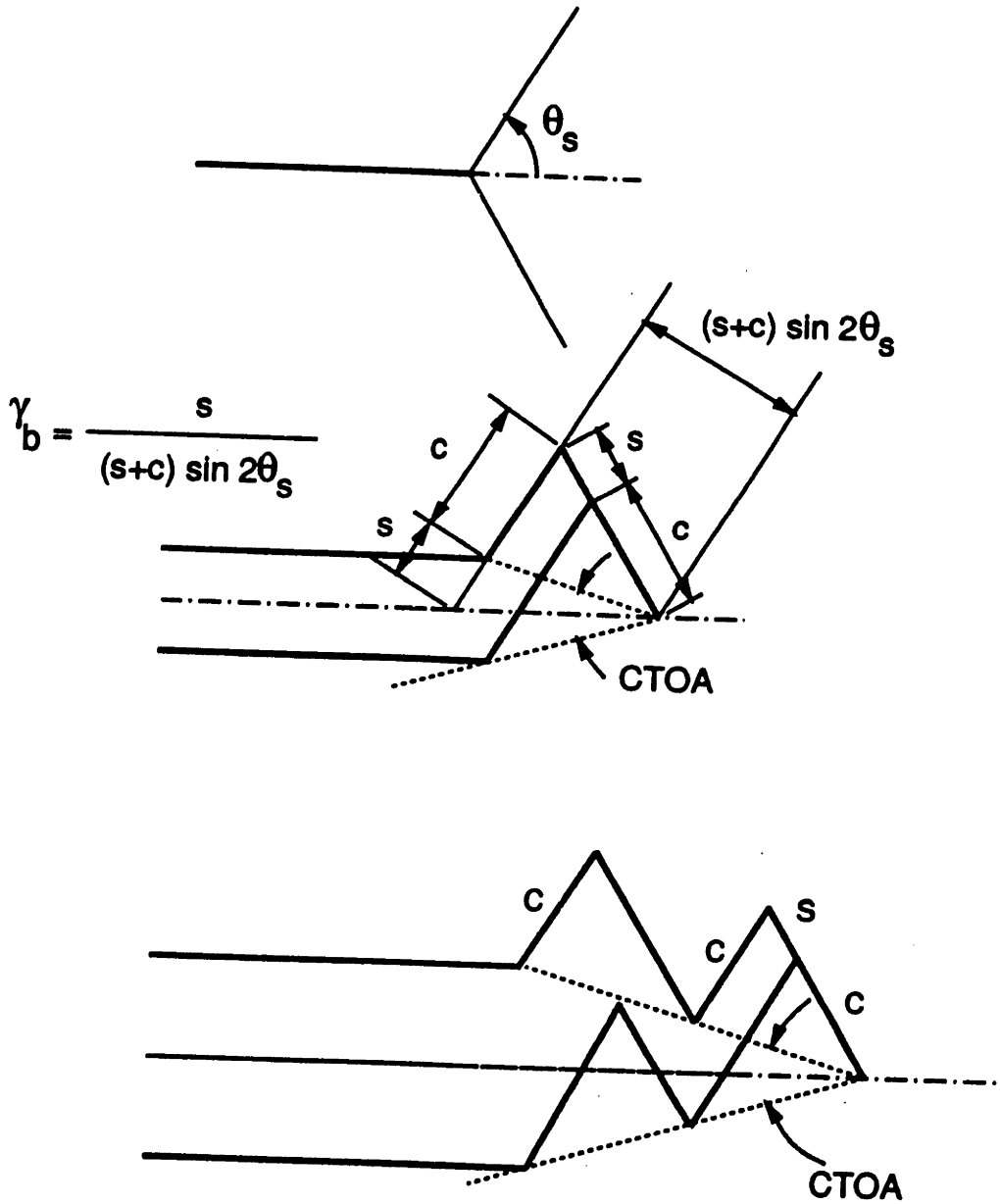

Fig. 3.11. Sliding off and shear cracking model for a growing crack.

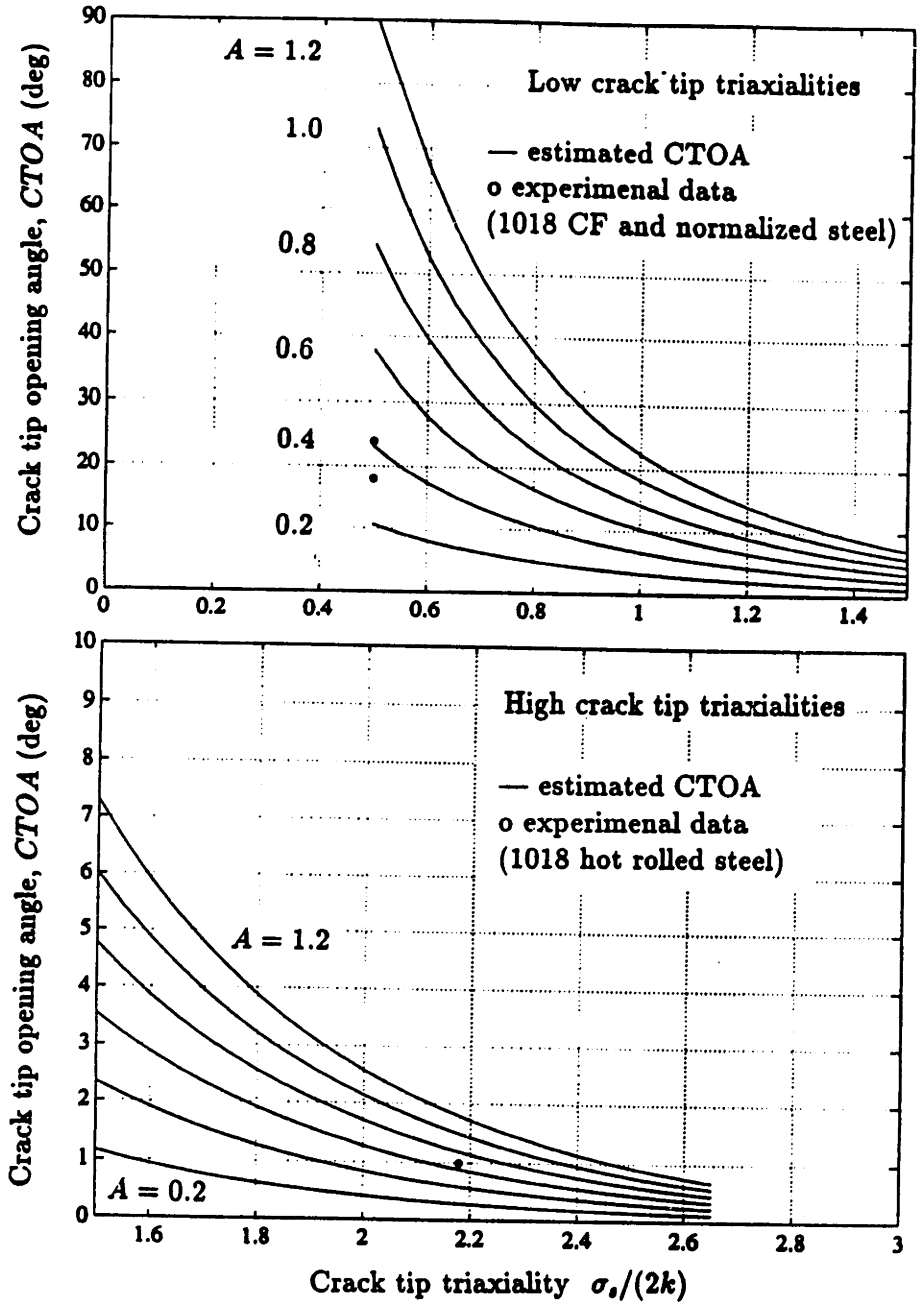

Fig. 3.12. Dependence of the estimated $CTOA$ on $\sigma_e/2k$.
Equations (3.5) and (3.8) with $\theta_e = 45°$, $n = 0$, and $B = 0$.

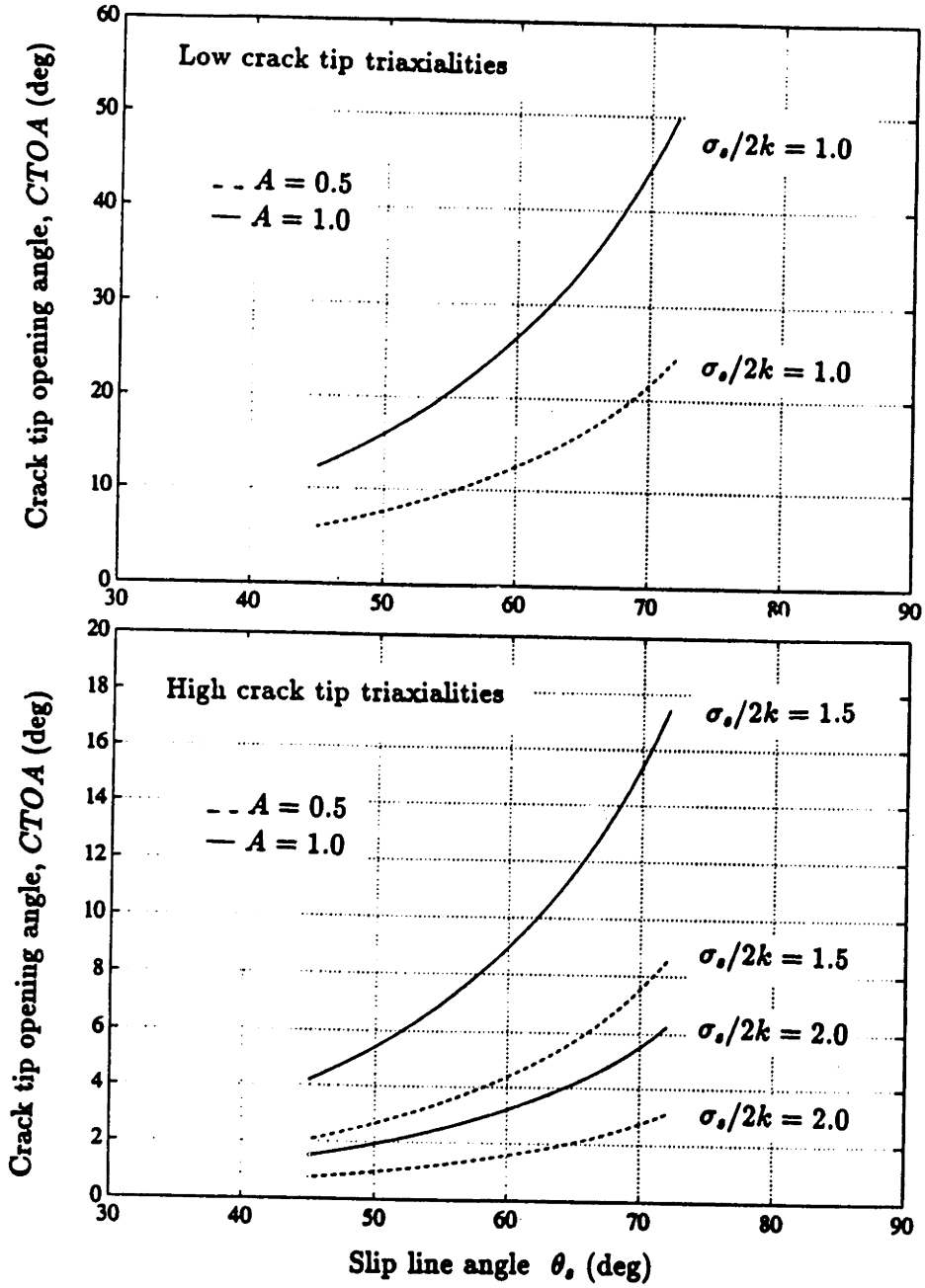

Fig. 3.13. Dependence of the estimated $CTOA$ on the slip angle. Equations (3.5) and (3.8) with $n = 0$ and $B = 0$.

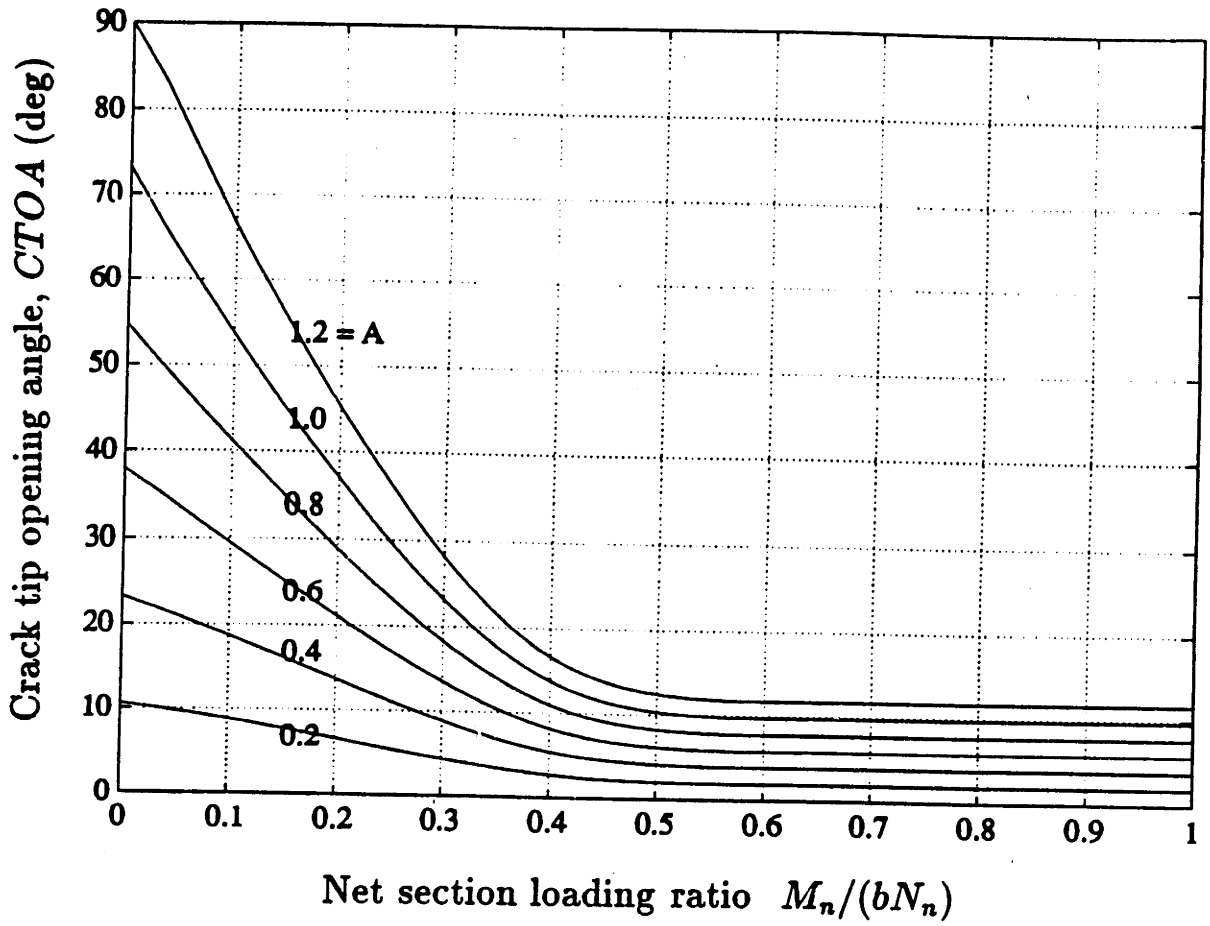

Fig. 3.14. Dependence of the $CTOA$ on net section loading ratio in deep, single-face-cracked specimens under combined bending and tension, Eq. (3.9) with $n = 0$ and $B = 0$.

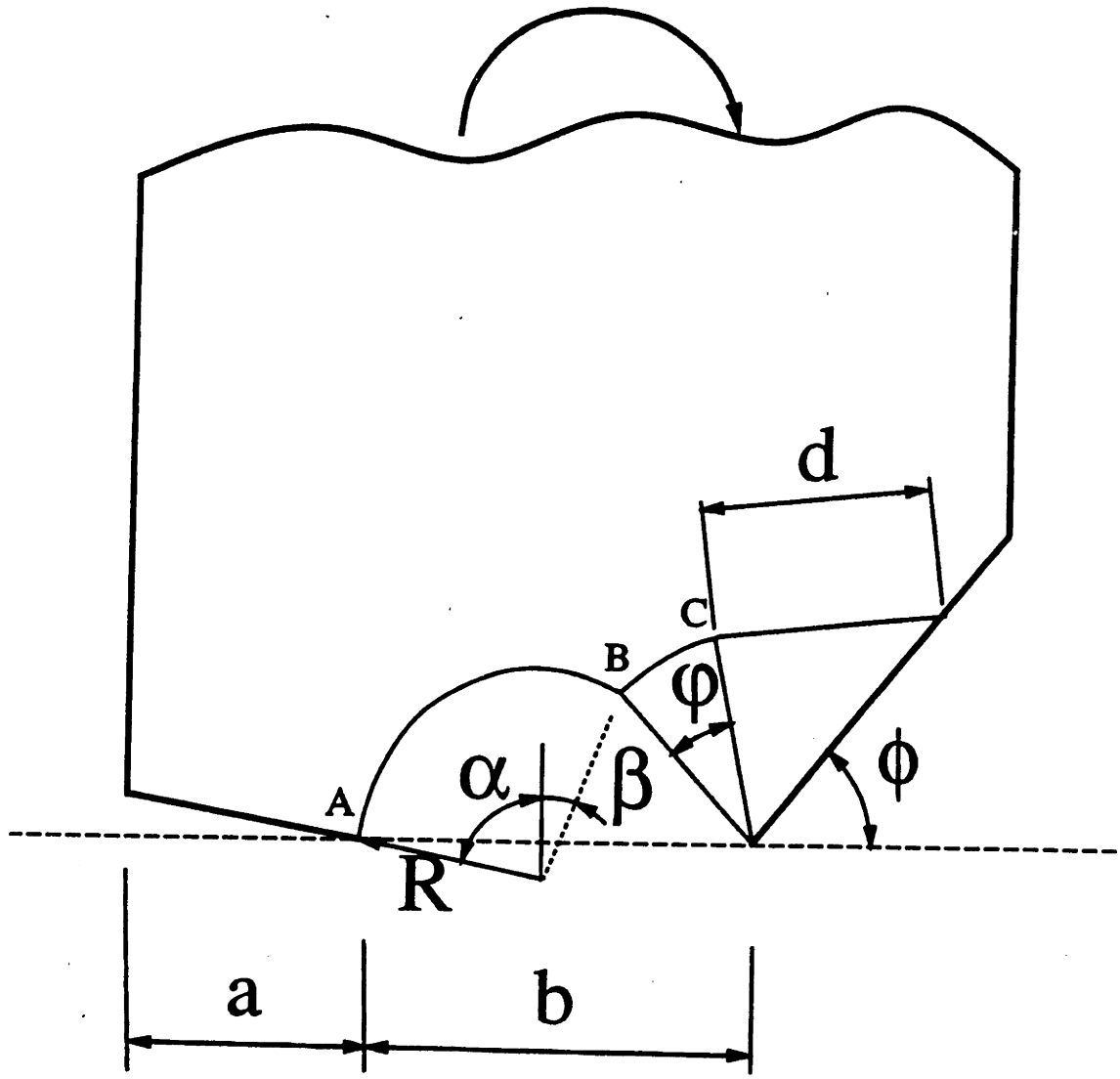

Fig. 3.15. Proposed slip line field for unequally grooved specimens under pure bending.

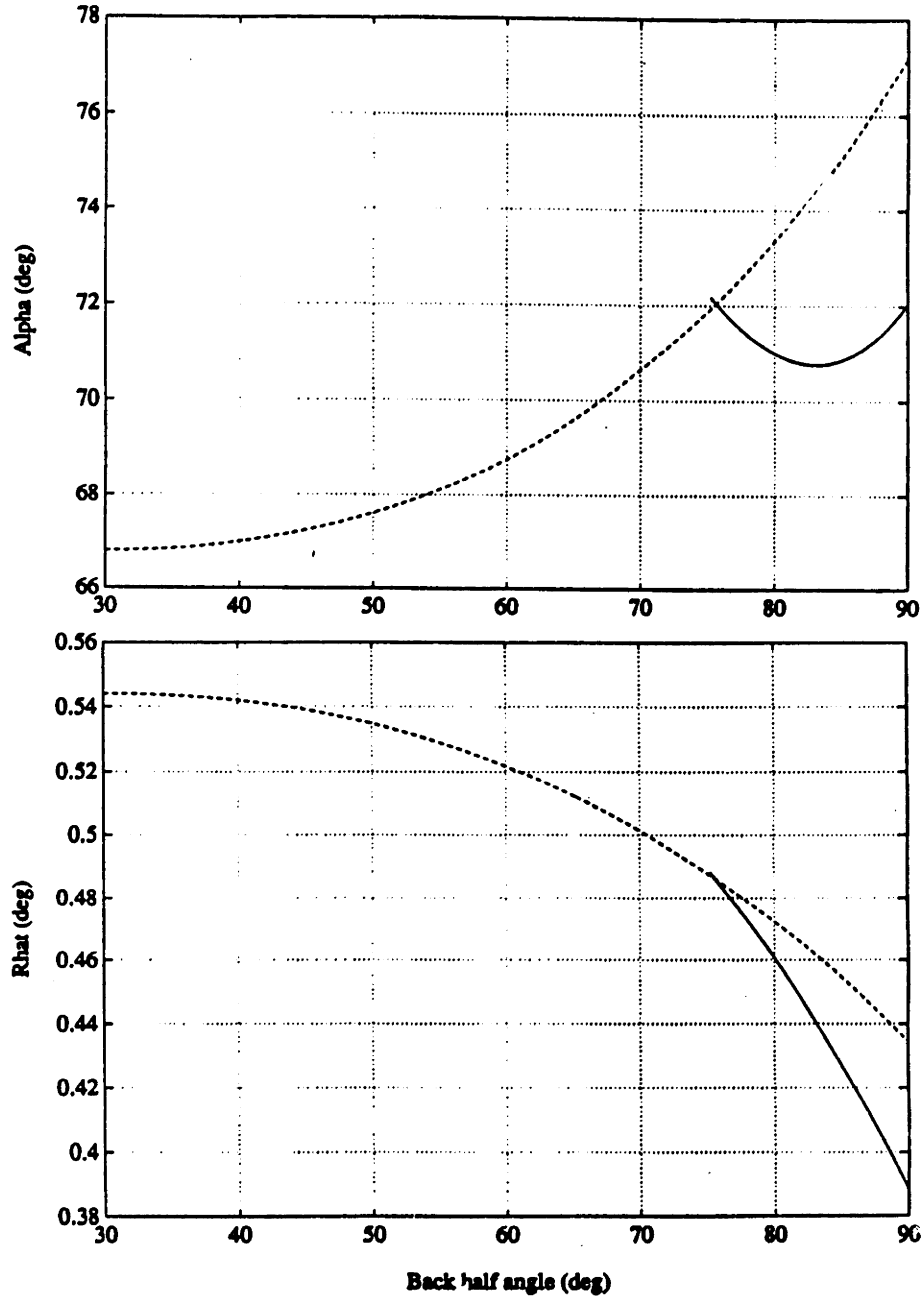

Fig. 3.16. Field parameters in slip line fields for unequally grooved specimens under pure bending: the slip line angle α, the arc radius R and the fan angle ψ.

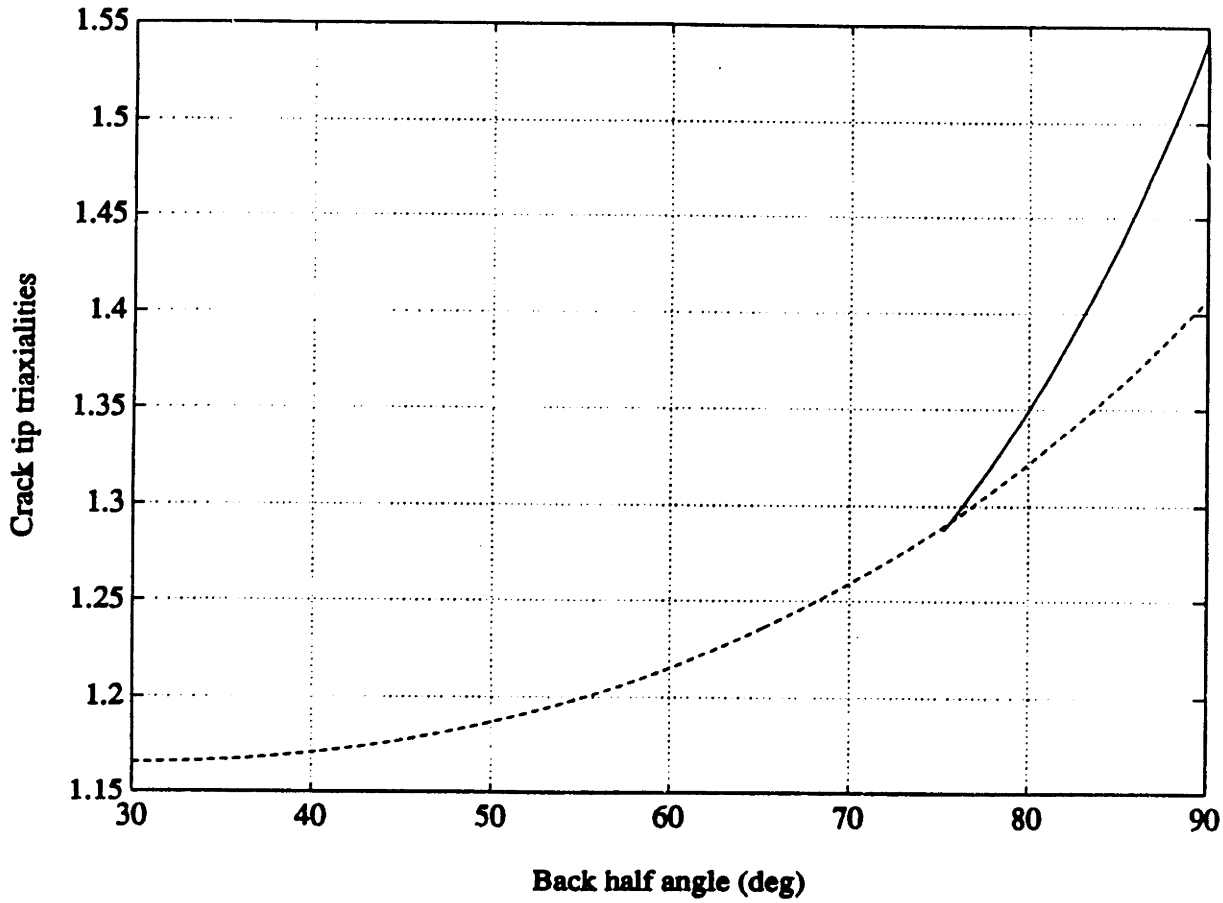

Fig. 3.17. Crack tip triaxiality $\sigma_s/(2k)$ for unequally grooved specimens under pure bending.

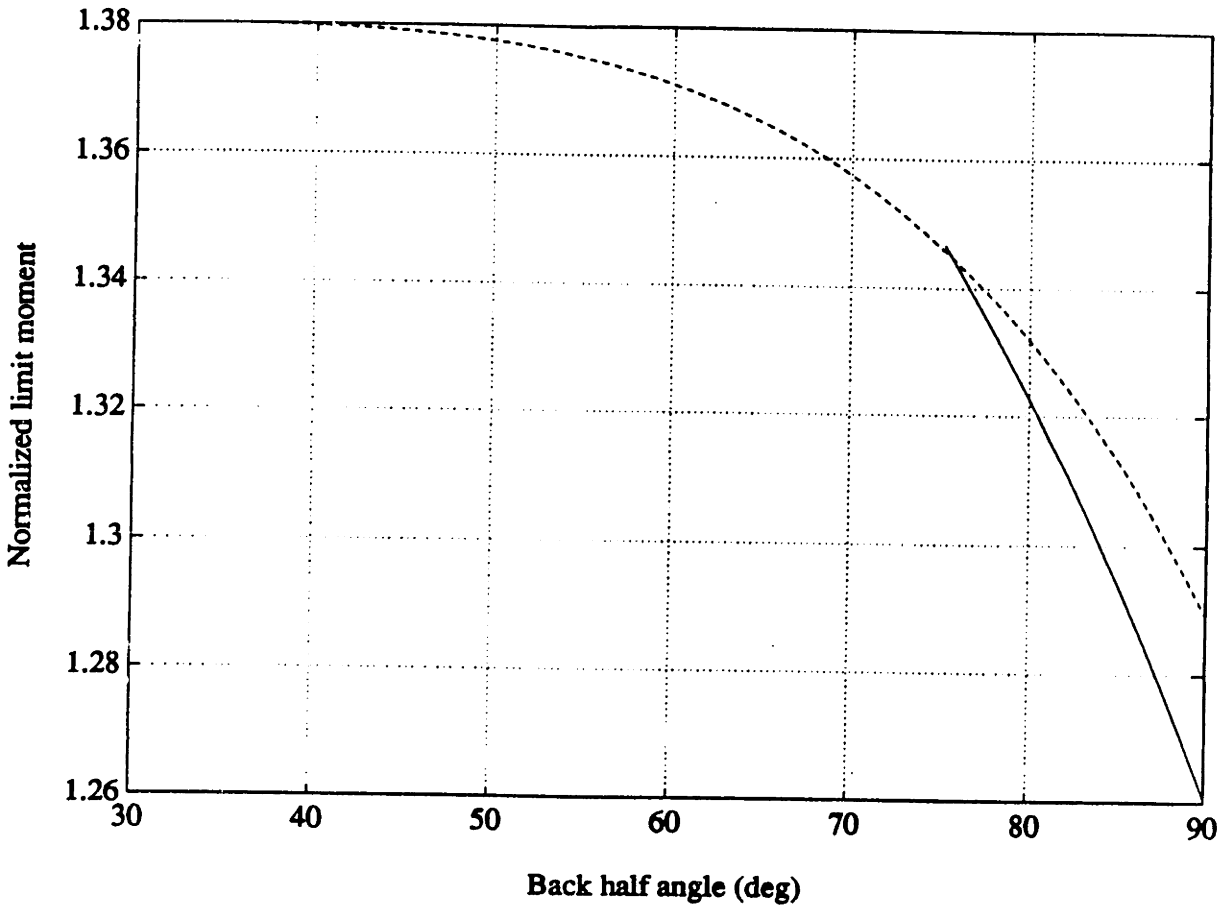

Fig. 3.18. Limit moment M^{LIM} for unequally grooved specimens under pure bending.

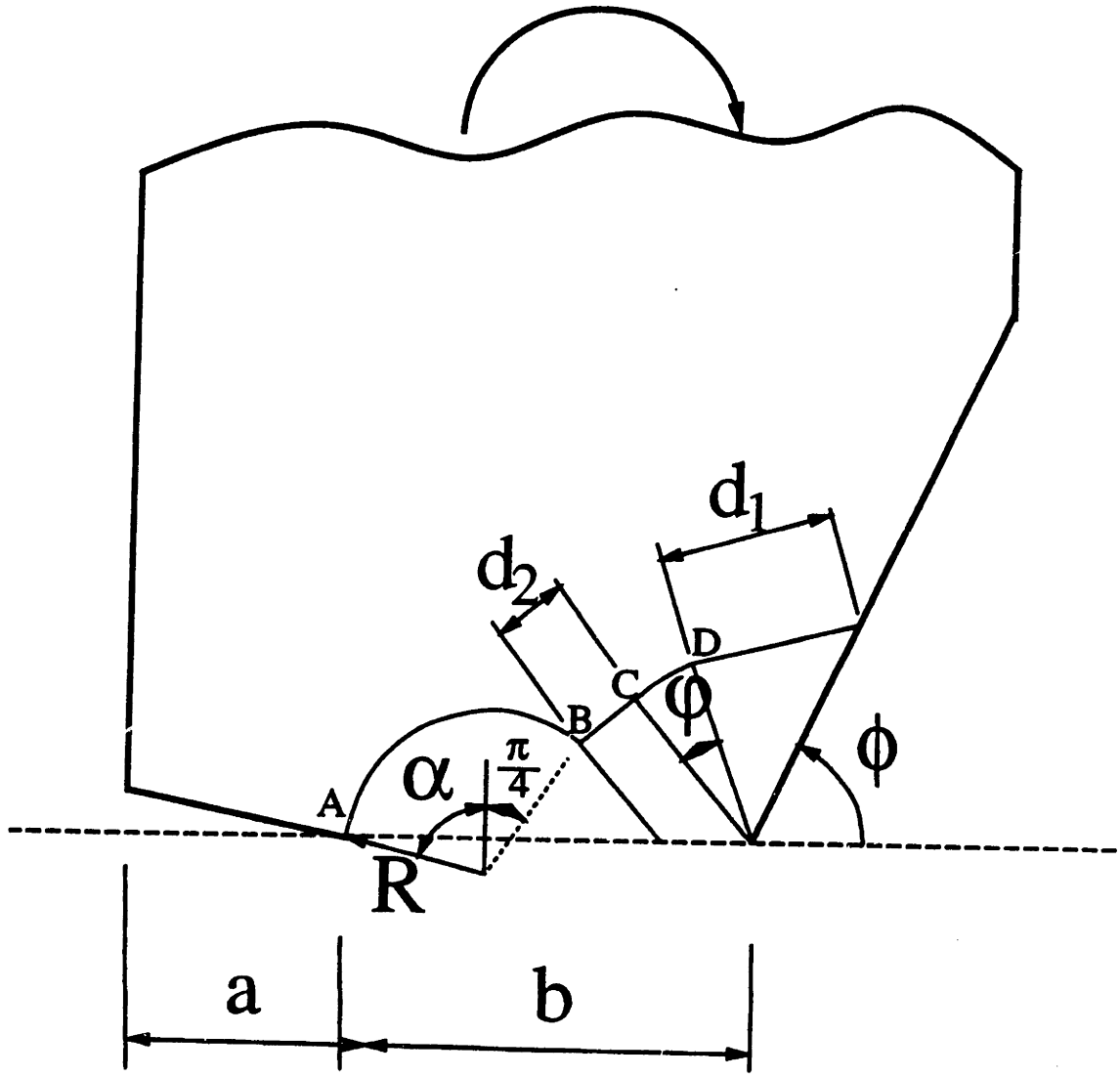

Fig. 3.19. Proposed slip line field for unequally grooved specimens with large back angle under pure bending.

CHAPTER 4

YIELD LOCUS IN DEEP, SINGLE-FACE-CRACKED SPECIMENS UNDER COMBINED BENDING AND TENSION

1. INTRODUCTION

For plates with deep, single face cracks, slip line fields are known under pure tension and under opening bending with compression or small tension (Shiratori and Miyoshi, 1980; Shiratori and Dodd, 1980). For such plates under opening bending and large tension, Rice (1972) gave an analytical-graphical formulation for sliding along the circular arc giving the least upper bound to the limit load. He also proposed an approximate elliptical yield locus for *all* ranges of positive tensions and net-section moments, which has been widely used (e.g., Hu and Albrecht, 1991).

This chapter briefly reviews existing slip line and upper bound fields. We provide a complete analytical formulation for Rice's least upper bound. Then we propose an improved approximate elliptical yield locus and compare it with finite element limit analyses of Lee and Parks (1993). For compact notation, net-section tension N_n and net-section moment M_n are normalized with respect to unnotched plane strain limit loads using the shear strength k and remaining ligament b:

$$\hat{N}_n = N_n/(2kb) \qquad \text{and} \qquad \hat{M}_n = M_n/(0.5kb^2). \tag{1}$$

2. FLOW FIELD

2.1. Opening Bending with Compression or Small Tension

For pure opening bending, Green and Hundy (1956) found the slip line field shown in Fig. 1. For sufficiently small tensile forces, slip line fields can be obtained by "shaving off" some of the constant stress region (for example, up to section A-A in Fig. 4.1). When the constant stress sector just vanishes, force and moment equilibrium lead to

$$\hat{N}_n = 0.5512 \qquad \text{and} \qquad \hat{M}_n = 1.3232. \tag{2}$$

Note that the limiting field of (2) is likely to be only an upper bound: in complete solutions for shallow cracks in pure bending, Ewing (1968) found constant-state triangles at the ends of curved slip lines approaching a free surface. Note also that slip line fields for $\hat{N}_n \leq 0$ with $\hat{M}_n \geq 0$ can be obtained by reducing the circular hinge radius and increasing the constant stress regions. The resulting yield locus from these slip line fields is

$$\Phi_S = \hat{M}_n + 0.7394\hat{N}_n^2 - 0.5212\hat{N}_n - 1.2606 = 0 \qquad \text{for} \qquad -1 \leq \hat{N}_n < 0.5512, \tag{3}$$

as shown by the upper solid line in Fig. 4.4, with the point ($\hat{N}_n = 0.5512$, $\hat{M}_n = 1.3232$) denoted by "X". See Shiratori and Miyoshi (1980), and Shiratori and Dodd (1980) for closed-form analytical expressions for the numerical coefficients in (2) and (3).

2.2. Opening Bending with Large Tension

Slip line fields are not known for large tension ($0.5512 \leq \hat{N}_n < 1$). A possible slip line field, motivated by the field for transverse shear of grooved plates (Mode II) (McClintock and Clerico 1980), is suggested in Fig. 4.2. They showed that the bound to the limit load in shear is only two percent higher if their slip line field, with fan, arc, and constant stress sectors, is replaced by a single straight line. In Fig. 4.3, the suggested slip line field is replaced by a single arc of radius R and angular extent $(\alpha - \beta)$, as proposed by Rice (1972). As L and R tend to ∞, both α and β approach $\pi/4$, and the field approaches that for pure tension.

From relative sliding along the circular arc, the principle of virtual work gives

$$\hat{M}_n = 2(\frac{R}{b})^2(\alpha - \beta) - 4\hat{N}_n(\frac{L}{b} + \frac{1}{2}). \tag{4}$$

For a given $\hat{N}_n$, the least upper bound for $\hat{M}_n$ can be determined by minimizing the right hand side of (4), subject to the two geometric relations from Fig. 4.3:

$$\frac{L}{b} = \frac{R}{b}\sin\beta, \qquad \frac{L}{b} + 1 = \frac{R}{b}\sin\alpha. \tag{5}$$

Eliminating L/b and R/b from (4) using (5) and minimizing the right hand side of (4) with respect to α and β results in two equations in the two unknowns, α and β:

$$(\alpha - \beta)\cos\alpha - (\sin\alpha - \sin\beta)(\frac{1}{2} + \hat{N}_n \sin\beta\cos\alpha) = 0. \tag{6}$$

$$(\alpha - \beta)\cos\beta - (\sin\alpha - \sin\beta)(\frac{1}{2} + \hat{N}_n \sin\alpha\cos\beta) = 0. \tag{7}$$

For a given $\hat{N}_n$, α and β can be determined numerically from (6) and (7). Then $\hat{M}_n$ is determined from (4) with (5) for R/b and L/b. The resulting upper bound to the yield locus is shown in Fig. 4.4.

Rice (1972) assumed that L is given and minimized the right hand side of (4) with respect to β, which leads to

$$2(\alpha - \beta) = \tan\alpha - \tan\beta. \tag{8}$$

(Note that eliminating $\hat{N}_n$ from (6) and (7) also gives (8).) With (8) he performed a graphical minimization of $\hat{M}_n$ to obtain the same least upper bound as from (6) and (7).

3. APPROXIMATE ELLIPTICAL YIELD LOCI

For the full range of positive tension ($0 \leq \hat{N}_n \leq 1$), Rice (1972) approximated the yield locus with an ellipse matched to the slip line solution for pure tension:

$$\Phi_R = \frac{1}{0.49}(\hat{N}_n - 0.3)^2 + \frac{9}{16}\hat{M}_n^2 - 1 = 0 \qquad \text{for} \qquad 0 \leq \hat{N}_n \leq 1. \tag{9}$$

As shown in Fig. 4.4, this approximate locus falls within the least upper bound locus by up to 9% radially.

We here propose a better elliptical yield locus than (9), for $0.5512 \leq \hat{N}_n \leq 1$:

$$\Phi_A = A(\hat{M}_n - B)^2 + C(\hat{N}_n - D)^2 - 1 = 0 \qquad \text{for} \qquad 0.5512 \leq \hat{N}_n \leq 1. \tag{10}$$

The four unknown coefficients A, B, C, and D are determined such that the ellipse smoothly matches the yield loci of the adjacent slip line solutions at the respective end points:

$$\hat{M}_n = 0 \qquad \text{and} \qquad \frac{\partial \hat{N}_n}{\partial \hat{M}_n} = 0 \qquad \text{at} \qquad \hat{N}_n = 1. \tag{11}$$

$$\hat{M}_n = 1.3232 \qquad \text{and} \qquad \frac{\partial \hat{N}_n}{\partial \hat{M}_n} = \frac{-1}{0.2939} \qquad \text{at} \qquad \hat{N}_n = 0.5512. \tag{12}$$

The resulting approximate yield locus, shown in Fig. 4.4, is

$$\Phi_A = 0.5641\hat{M}_n^2 + 3.9258(\hat{N}_n - 0.4953)^2 - 1 = 0 \qquad \text{for} \qquad 0.5512 \leq \hat{N}_n \leq 1. \tag{13}$$

The locus (13) lies within that of the least upper bound analysis by at most 4%. No appreciably better fit could be found with a rotated ellipse satisfying the same end conditions.

Lee and Parks (1993) studied yield loci for various crack depths using finite elements. For a given crack depth and tension-to-bending ratio, they found the limit tension and the limit moment. By comparing yield loci for various crack depths, they suggest that relative crack depths of a/t greater than about 0.35 would be "deep enough" to prevent shoulder deformation for all tension-to-bending ratios. (For pure extension, any crack depth is sufficient.) As shown with circles in Fig. 4.4, their results for relative crack depths of a/t=0.5 and 0.6 are consistent with the modified Green and Hundy solutions. Their results suggest that, for $0.6 \leq \hat{N}_n \leq 0.9$, the least upper bound locus overestimates by up to 3%, and the Rice ellipse underestimates by up to 6%. Surprisingly, the ellipse (13) fits the finite element results within 1%, as shown in Fig. 4.4. For $\hat{N}_n > 0.9$, the agreement is still within 2%, the order of the self-consistency of the FEM calculations.

Therefore for opening bending and compression or tension (3) and (13) provide complete plane strain general yield loci for plates with deep enough cracks and small flank angles.

REFERENCES

Ewing, D.J.F., 1968, "Calculations on the Bending of Rigid/Plastic Notched Bars", *Journal of the Mechanics and Physics of Solids* **16**, pp. 205-213.

Green, A.P. and Hundy, B.B., 1956, "Initial Plastic Yielding in Notch Bend Tests", *Journal of the Mechanics and Physics of Solids* **4**, pp. 128-144.

Hu, J.M. and Albrecht, P., 1991, "Limit Load Solution and Loading Behavior of C(T) fracture specimen", *International Journal of Fracture* **52**, pp. 619-645.

Lee, H. and Parks, D.M., 1993, "Fully Plastic Analyses of Plane Strain Single Edge Cracked Specimens Subject to Combined Tension and Bending", submitted to *International Journal of Fracture.*

McClintock, F.A., 1971, "Plasticity Aspects of Fracture", *Fracture*, Vol. 3, Liebowitz, H. (ed.), Academic Press, New York, pp. 47-225. See pp. 155-162.

McClintock, F.A. and Clerico, M., 1980, "The Transverse Shearing of Singly-Grooved Specimens", *Journal of the Mechanics and Physics of Solids* **28**, pp. 1-16.

Rice, J.R., 1972, "The Line Spring Model for Surface Flaws", *The Surface Crack: Physical Problems and Computational Solutions*, Swedlow, J.L. (ed.), American Society of Mechanical Engineers, New York, pp. 171-185.

Shiratori, M. and Dodd, B., 1980, "Effect of Deep Wedge-Shaped Notches of Small

Flank Angle on Plastic Failure", *International Journal of Mechanical Science* **22**, pp. 127-131.

Shiratori, M. and Miyoshi, T., 1980, "Evaluation of Constraint Factor and J-integral for Single-Edge Notched Specimen", *Proceedings of the Third International Conference on Mechanical Behavior of Materials* **3**, Miller, K.J. and Smith, R.F. (eds.), Pergamon Press, pp. 425-434.

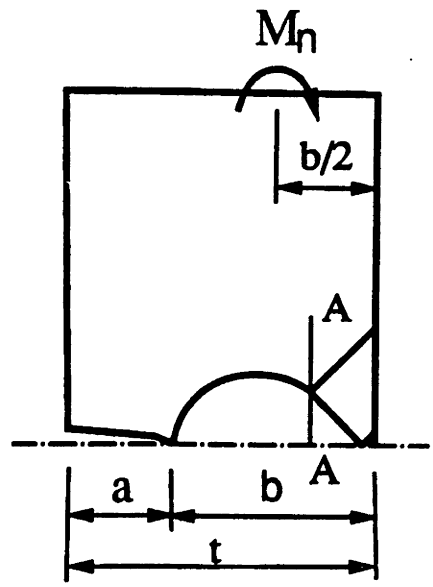

Fig. 4.1. Green and Hundy field for pure bending.

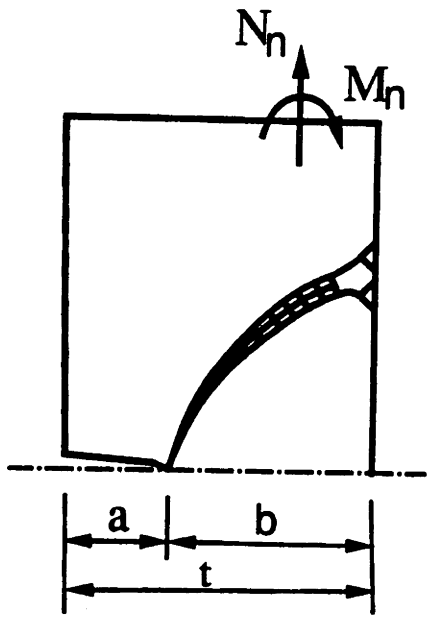

Fig. 4.2. Possible slip line field for combined bending with large tension.

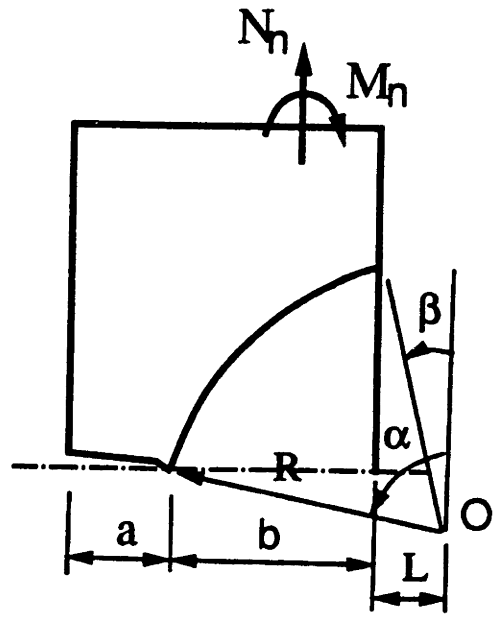

Fig. 4.3. Kinematically admissible upper bound fields.

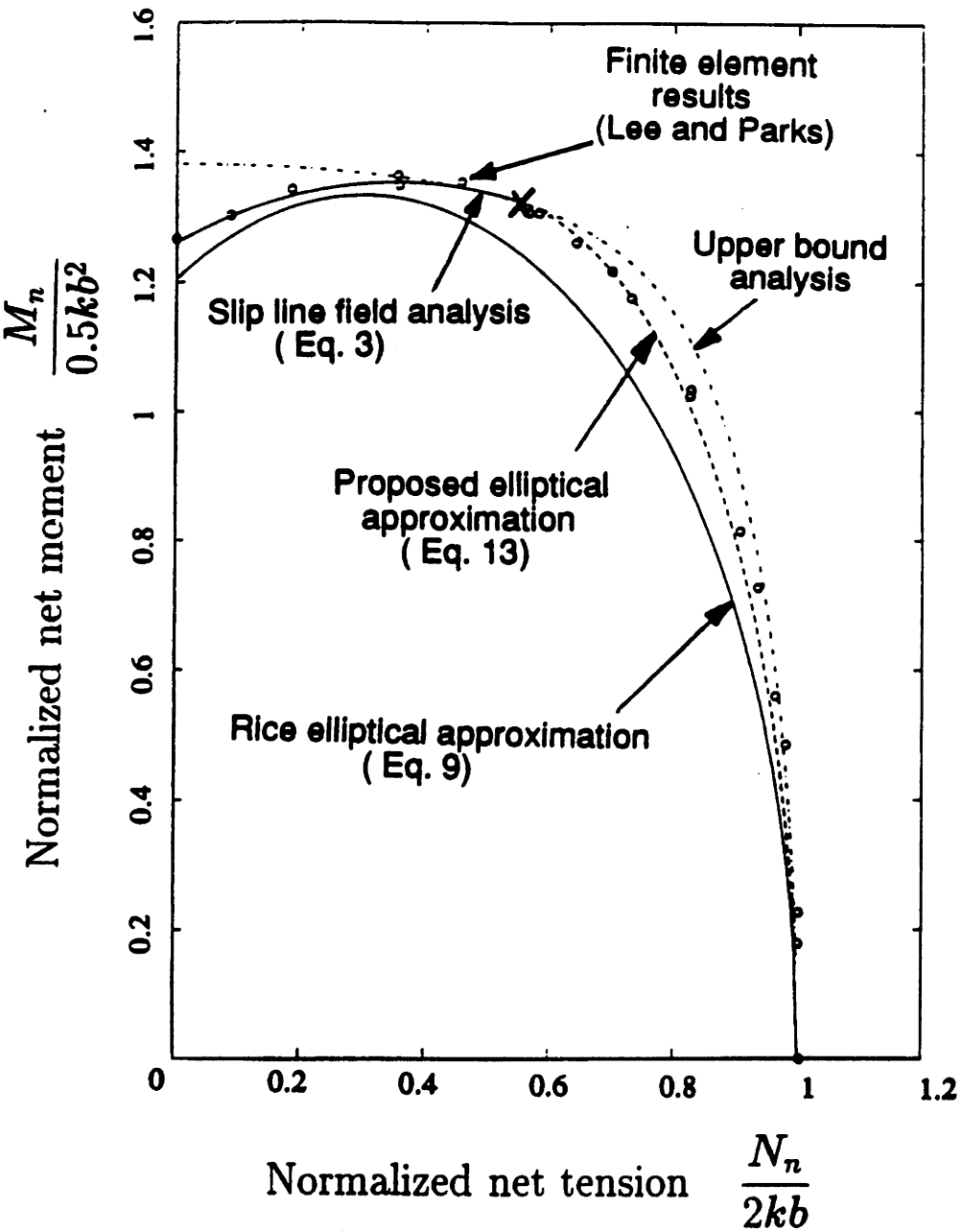

Fig. 4.4. Yield locus for deep, single-face-cracked specimens under combined bending and tension.

CHAPTER 5

LINE-SPRING MODEL FOR FULLY PLASTIC, PLANE STRAIN CRACK GROWTH IN PLATES AND SHELLS

ABSTRACT

A line-spring model is developed for fully plastic, plane strain crack growth in plates and shells. Based on rigid-plastic, non-hardening plasticity, a simple form of incremental compliance of the line-spring, developed from a single-face-cracked specimen under combined bending and tension, is expressed in terms of yield loci and its derivatives, and the crack tip opening angle ($CTOA$) for a growing crack. Then the line-spring is embedded in elastic plates and shells to predict fully plastic crack growth of two kinds of part-through cracks: across plates with pinned or fixed-grip boundary conditions, complete circumferential cracks in long shells under axial tension. The analysis includes the bulging effect of the cracked part. The following effects are reported: boundary conditions, plate lengths L/t, material ductility, initial crack depths in plates, and curvature (R/t, radius-to-thickness ratios) in shells. For plates, the far-field tensile deformation for fracture u_f^∞ increases as L/t increases in pinned conditions, whereas as L/t decreases in fixed-grip conditions. u_f^∞ also decreases for less ductile materials, and for deeper initial crack depths for both conditions. For shells, the effect of curvature (varying R/t) is equivalent to varying L/t under the

fixed-grip conditions, and thus u_f^{∞} increases as R/t decreases.

1. Introduction

1.1. The Line-Spring Model for a Stationary Crack

The line-spring model (LSM) was introduced as a simplified method for analyzing surface cracks in plates and shells-type geometries (Rice and Levy, 1972; Levy and Rice, 1972). The simplicity of the method lies in that a 3-D crack analysis problem is effectively reduced to a quasi 2-D, shell-theory problem, which is much easier and cheaper to analyze than a full 3-D problem. The concept has been embbeded within structural models of either shell theory or shell-type finite elements by Parks and co-workers (Parks, 1981; Parks and White, 1982; White, et al., 1983). In the linear elastic case, it has been found that the model generally provides K_I distribution along essentially all of the surface crack front which is within a few percent of those from detailed numerical analysis (Raju and Newman, 1979).

However, the materials commonly employed in pressure vessels are tough and ductile, and experience extensive plastic deformation and crack tip blunting prior to the initiation of crack growth. Following the basic outline for nonlinear line-spring analysis by Rice (1972), Parks and co-workers extended the LSM to elastic, nonhardening plastic (Parks, 1981) and elastic, hardening plastic response (White, et

al., 1983).

1.2. The Line-Spring Model for a Growing Crack

The line-spring model is even more attractive for crack growth since numerical (e.g., finite element) crack growth analysis is almost impossible due to enormous storage and computing time. For the line-spring model to be capable of crack growth, a fracture criterion should be embedded in the model. Some works have been reported based on J-integral (Miyoshi, et al., 1986), but the J-based criterion can not be applied to low strength alloys (McClintock, et al., 1993).

1.3. Present work

In this chapter, we present a line-spring model for fully plastic, plane strain crack growth in plates and shells. We first develop the line-spring element for a growing crack in the limiting case of rigid-plastic, non-hardening materials in Sec. 2. Elements are embedded in plates to study part-through crack growth in plates under pinned or fixed-grip boundary conditions in Sec. 3. The growth of complete circumferential cracks in pipes under axial tension is studied in Sec. 4.

2. LINE-SPRING ELEMENTS (LSE) FOR FULLY PLASTIC CRACK GROWTH

Consider a single-face-cracked plate of thickness t with a part-through crack of depth a, subject to combined bending and tension (Fig. 5.1). The axial force N and

bending moment M are defined as those for unit thickness. Also all the variables N, M, u, and θ are defined based on the mid-width of the plate near the crack, as shown in Fig. 5.1. To predict crack growth, we have to determine the increments of five unknowns, δN, δM, δu, $\delta\theta$, and δa from given far-field deformation boundary conditions in the surrounding structures which will be discussed in Sec. 3 and 4. For simplicity, consider the limiting case of rigid-plastic, non-hardening materials.

Normalize the length variables using the plate thickness t and the load variables with respect to their unnotched plane strain limit loads using the shear strength k and t::

$$\hat{u} = u/t \ ; \ \hat{\theta} = \theta \ ; \ \hat{a} = a/t. \tag{2.1}$$

$$\hat{N} = N/(2kt) \ ; \ \hat{M} = M/(0.5kt^2). \tag{2.2}$$

2.1. Incremental Compliance of the LSE

For fully plastic and crack extension response, we need a tangent incremental compliance matrix $C_{ij}(i, j = 1, 2)$ connecting the increments $(\delta\hat{N}, \delta\hat{M})$ and $(\delta\hat{u}, \delta\hat{\theta})$:

$$\begin{bmatrix} \delta\hat{u} \\ \delta\hat{\theta} \end{bmatrix} = \begin{bmatrix} C_{11} & C_{12} \\ C_{21} & C_{22} \end{bmatrix} \begin{bmatrix} \delta\hat{N} \\ \delta\hat{M} \end{bmatrix}. \tag{2.3}$$

The incremental compliance C_{ij} can be obtained from plasticity conditions (the normality rule and the yield condition) along with a crack growth criterion, which will be discussed below.

Following the standard plasticity theory, introduce the convex yield surface

$$\Phi(N, M, a) = \Phi(\hat{N}, \hat{M}, \hat{a}) = 0,$$

which will be discussed in detail in Sec. 2.2. It is understood that $\Phi_{,N}$ (or $\Phi_{,\hat{N}}$) denote the partial derivative of Φ with respect to N (or $\hat{N}$). In rigid-plastic material, any deformation requires active plastic loading. Thus the geneneralized displacement increments should obey the normality rule.

$$\delta\hat{u} = \delta\Lambda\Phi_{,\hat{N}} \qquad ; \qquad \delta\hat{\theta} = 4\delta\Lambda\Phi_{,\hat{M}} \,. \tag{2.4}$$

In nonhardening materials, however, the magnitude of the displacement increments $\delta\Lambda$, for a given load increment, can not be determined. Eliminating $\delta\Lambda$ from (2.4) and normalizing variables based on (2.1) and (2.2) gives

$$4\Phi_{,\hat{M}}\,\delta\hat{u} - \Phi_{,\hat{N}}\,\delta\hat{\theta} = 0. \tag{2.5}$$

At the new crack tip position the generalized forces $\hat{N}$ and $\hat{M}$ should remain on the yield surface:

$$\begin{aligned} 0 &= \Phi(\hat{N} + \delta\hat{N}, \hat{M} + \delta\hat{M}, \hat{a} + \delta\hat{a}) \\ &\approx \Phi_{,\hat{N}}\,\delta\hat{N} + \Phi_{,\hat{M}}\,\delta\hat{M} + \Phi_{,\hat{a}}\,\delta\hat{a}. \end{aligned} \tag{2.6}$$

For crack tip fields approximated by a pair of slip lines, McClintock, et al. (1993) proposed a crack growth criterion for a growing crack in a fully plastic material. It gives the crack growth increment $\delta\hat{a}$ in terms of the crack tip opening displacement increment $\delta\hat{u}_t (= \delta u_t/t)$ and $CTOA$:

$$\delta\hat{a} = \frac{\delta\hat{u}_t}{\tan(CTOA/2)}. \tag{2.7}$$

Both SLF and LUB analysis provide $\delta\hat{u}_t$ in terms of $\delta\hat{u}$ and $\delta\hat{\theta}$:

$$\delta\hat{u}_t = \delta\hat{u} + \left(\frac{1}{2} - \hat{a}\right)\delta\hat{\theta}. \tag{2.8}$$

Substituting (2.7) and (2.8) into (2.6) gives

$$\Phi_{,\hat{N}}\,\delta\hat{N}+\Phi_{,\hat{M}}\,\delta\hat{M}+\frac{1}{\tan(CTOA/2)}\Phi_{,\hat{a}}\,\delta\hat{u}+\frac{1}{\tan(CTOA/2)}\Phi_{,\hat{a}}\left(\frac{1}{2}-\hat{a}\right)\delta\hat{\theta}=0. \quad (2.9)$$

Recasting (2.5) and (2.9) into the form of (2.3) gives

$$D=-\frac{\tan(CTOA/2)}{\Phi_{,\hat{a}}\left[\Phi_{\hat{N}}+4(1/2-\hat{a})\Phi_{,\hat{M}}\right]} \quad ; \quad C_{11}=\frac{\Phi_{,\hat{N}}^{2}}{D} \quad ;$$

$$C_{12}=\frac{\Phi_{,\hat{N}}\,\Phi_{,\hat{M}}}{D} \quad ; \quad C_{21}=4\frac{\Phi_{,\hat{N}}\,\Phi_{,\hat{M}}}{D} \quad ; \quad C_{22}=4\frac{\Phi_{,\hat{M}}^{2}}{D}. \quad (2.10)$$

2.2. Yield surface and its derivatives

Consider a single-face-cracked specimen under combined bending and tension with a crack deep enough to prevent shoulder deformation, and sharp enough to prevent flank deformation. From slip line and finite element (FE) limit load analysis, Lee and Parks (1993) find that the relative crack depth of a/t to prevent shoulder deformation ranges from 0 for pure tension through 0.35 for combined bending and tension to 0.3 for pure bending.

For a single-face-cracked specimen under opening bending with small tension or under compression, the modified Green and Hundy slip line fields give the yield locus in terms of normalized loading based on a net-section loading variables N_n and M_n, $\hat{N}_n(=N_n/(2kt))$ and $\hat{M}_n(=M_n/(0.5kt^2))$, and a normalized remaining ligament, $\hat{b}(=b/t=1-\hat{a})$ as (Shiratori and Dodd, 1980)

$$\Phi(\hat{N}_n,\hat{M}_n,\hat{a})=\frac{\hat{M}_n}{\hat{b}^2}+0.7394\frac{\hat{N}_n^2}{\hat{b}^2}-0.5212\frac{\hat{N}_n}{\hat{b}}-1.2606=0$$

$$\text{for} \qquad -\hat{b} \leq \hat{N}_n \leq 0.5512\hat{b}. \tag{2.11}$$

Under bending with large tension, Kim et al. (1993) proposed an approximate yield locus which is within 2% of finite element results (Lee and Parks, 1993):

$$\Phi(\hat{N}_n, \hat{M}_n, \hat{a}) = 0.5641(\frac{\hat{M}_n}{\hat{b}^2})^2 + 3.9258(\frac{\hat{N}_n}{\hat{b}} - 0.4953)^2 - 1 = 0$$

$$\text{for} \qquad 0.5512\hat{b} \leq \hat{N}_n \leq \hat{b}, \tag{2.12}$$

where the constants (0.5641;3.9258;-0.4953) were obtained by matching the slopes and values of the elliptical yield locus at $\hat{N}_n = 0.5512\hat{b}$ and $\hat{N}_n = \hat{b}$ with those of the known SLF solutions (Fig. 5.2). For opening bending and compression or tension, (2.14) and (2.15) provide complete plane strain general yield loci for plates with deep enough cracks and small flank angles.

The complete loci (2.11) and (2.12) expressed in terms gross section variables N and M, $\hat{N}(= N/(2kt))$ and $\hat{M}(= M/(0.5kt^2))$, using

$$\hat{N}_n = \hat{N} \qquad ; \qquad \hat{M}_n = \hat{M} + 2\hat{N}\hat{a}, \tag{2.13}$$

give the resulting yield loci Φ and their derivatives, $\Phi_{,\hat{N}}$, $\Phi_{,\hat{M}}$, and $\Phi_{,\hat{a}}$:

For $-\hat{b} \leq \hat{N} \leq 0.5512\hat{b}$,

$$\Phi(\hat{N}, \hat{M}, \hat{a}) = \frac{\hat{M} + 2\hat{N}\hat{a}}{\hat{b}^2} + 0.7394(\frac{\hat{N}}{\hat{b}})^2 - 0.5212(\frac{\hat{N}}{\hat{b}}) - 1.2606 = 0. \tag{2.14}$$

$$\Phi_{,\hat{N}} = \frac{1}{\hat{b}}\left[2(\frac{\hat{a}}{\hat{b}}) + 1.4788(\frac{\hat{N}}{\hat{b}}) - 0.5212\right]. \tag{2.15}$$

$$\Phi_{,\hat{M}} = \frac{1}{\hat{b}^2}. \tag{2.16}$$

$$\Phi_{,\hat{a}} = \frac{1}{\hat{b}}\left[2(\frac{\hat{M} + 2\hat{N}\hat{a}}{\hat{b}^2}) + 1.4788(\frac{\hat{N}}{\hat{b}}) + 1.4788(\frac{\hat{N}}{\hat{b}})^2\right]. \tag{2.17}$$

For $0.5512\hat{b} \leq \hat{N} \leq \hat{b}$,

$$\Phi(\hat{N}, \hat{M}, \hat{a}) = 0.5641(\frac{\hat{M} + 2\hat{N}\hat{a}}{\hat{b}^2})^2 + 3.9258(\frac{\hat{N}}{\hat{b}} - 0.4953)^2 - 1 = 0. \tag{2.18}$$

$$\Phi_{,\hat{N}} = \frac{1}{\hat{b}}\left[2.2564(\frac{\hat{M} + 2\hat{N}\hat{a}}{\hat{b}^2})(\frac{\hat{a}}{\hat{b}}) + 7.8516(\frac{\hat{N}}{\hat{b}} - 0.4953)\right]. \tag{2.19}$$

$$\Phi_{,\hat{M}} = \frac{1}{\hat{b}^2}\left[1.1282(\frac{\hat{M} + 2\hat{N}\hat{a}}{\hat{b}^2})\right]. \tag{2.20}$$

$$\Phi_{,\hat{a}} = \frac{1}{\hat{b}}\left[2.2564(\frac{\hat{M} + 2\hat{N}\hat{a}}{\hat{b}^2})(\frac{\hat{N}}{\hat{b}} + \frac{\hat{M} + 2\hat{N}\hat{a}}{\hat{b}^2}) + 7.8516(\frac{\hat{N}}{\hat{b}} - 0.4953)(\frac{\hat{N}}{\hat{b}})\right]. \tag{2.21}$$

3. Part-Through Crack Growth in Plates

3.1. Analysis of Elastic Plates

Consider a plate of thickness t, half-length L, a modulus of elasticity E, and a part-through crack of depth a. Due to the part-through crack, the plate bulges (Fig. 5.3). This causes the line of action of the applied load to shift relative to the plate centerline and produces a (negative) bending moment that tends to limit crack tip opening.

Differential equation for elastic plates

The deflection of the elastic plate can be obtained from the tensile analogue of the equation for an eccentrically loaded column [ ]. Let N denote the tensile force present in the plate (Fig. 5.4), and neglect second order terms. The differential equation for the plate deflection $v(x)$ can be given in terms of inverse of wave number,

$\alpha(=\sqrt{12N/Et^3})$, so that αL is the normalized length of the plate:

$$\frac{d^4v(x)}{dx^4} - \alpha^2\frac{d^2v(x)}{dx^2} = 0 \qquad \text{for} \qquad 0 < x < L. \tag{3.1}$$

The solution to (3.1) is

$$v(x) = a_1 + a_2x + a_3\exp(\alpha x) + a_4\exp(-\alpha x). \tag{3.2}$$

Boundary conditions

Consider two limiting types of boundary conditions. The first type is "fixed-grip" conditions where a (negative) bending moment M^∞ is applied to maintain zero slope ($\theta^\infty = 0$) (Fig. 5.3a). The other type is "pinned" condition where no bending moment ($M^\infty = 0$) is applied such that there is nonzero slope ($\theta^\infty \neq 0$) (Fig. 5.3b). From moment equilibrium (Fig. 5.3), the net-section of the cracked part (LSE) is subject to more negative bending moment under the fixed grip condition than under the pinned condition. This means that, under the pinned condition, a crack will be subject to more crack tip bending constraints and thus grow faster. Explicit mathematical forms of the two boundary conditions in terms of $v(x)$ and its derivatives are shown in the Appendix I.

Incremental compliance of elastic plates

We need the local response of elastic plates in terms of local loadings and given far-field deformation increment $\delta\hat{u}^\infty(=\delta u^\infty/t)$:

$$\begin{bmatrix} \delta\hat{u} \\ \delta\hat{\theta} \end{bmatrix} = \begin{bmatrix} E_{11} & E_{12} \\ E_{21} & E_{22} \end{bmatrix} \begin{bmatrix} \delta\hat{N} \\ \delta\hat{M} \end{bmatrix} + \begin{bmatrix} b_1 \\ b_2 \end{bmatrix} \delta\hat{u}^\infty. \tag{3.3}$$

Introducing (pinned or fixed-grip) boundary conditions to (3.2) gives the deflection $v(x)$, $v = \hat{v}(x; N, M)$. By using $\theta = (dv/dx)_{x=0}$, we can obtain the incremental relation between θ and M, $\theta = \hat{\theta}(N, M)$, and thus $f = \hat{f}(\delta N, \delta M, \delta\theta)$ as shown in Appendix I. In terms of normalized variables, the results are

$$\left[\left(\frac{\hat{F}_1}{2\sqrt{\hat{N}}} + \sqrt{\hat{N}}\frac{d\hat{F}_1}{d\hat{N}}\right)\hat{\theta} + \frac{1}{4}\frac{\hat{M}}{\sqrt{\hat{E}/12}}\frac{d\hat{F}_2}{d\hat{N}}\right]\delta\hat{N} + \frac{1}{4}\frac{\hat{F}_2}{\sqrt{\hat{E}/12}}\delta\hat{M} + \sqrt{\hat{N}}\hat{F}_1\delta\hat{\theta} = 0, \quad (3.4)$$

where $\hat{E} = E/(2k)$. Explicit forms of $\hat{F}_1(\hat{N}), \hat{F}_2(\hat{N}), d\hat{F}_1/d\hat{N}$ and $d\hat{F}_2/d\hat{N}$ for pinned and fixed-grip conditions are given in the Appendix I.

The axial force-deflection relation in elastic plates provides the relation between $\delta\hat{u}$ and $\delta\hat{u}^{\infty}$ in terms of $\hat{L}(= L/t)$ and $\delta\hat{N}$:

$$\delta\hat{u} = -\frac{\hat{L}}{\hat{E}}\delta\hat{N} + \delta\hat{u}^{\infty}. \quad (3.5)$$

Combining (3.4) and (3.5) with matrix manipulations gives the form of (3.3) with

$$\hat{E}_{11} = -\frac{\hat{L}}{\hat{E}} \quad ; \quad \hat{E}_{12} = 0$$

$$\hat{E}_{21} = \left(\frac{1}{2\hat{N}} + \frac{1}{\hat{F}_1}\frac{d\hat{F}_1}{d\hat{N}}\right)\hat{\theta} + \frac{\hat{M}}{4\sqrt{\hat{N}\hat{E}/12}}\frac{1}{\hat{F}_1}\frac{d\hat{F}_2}{d\hat{N}} \; ; \; \hat{E}_{22} = \frac{1}{4\sqrt{\hat{N}\hat{E}/12}}\frac{\hat{F}_2}{\hat{F}_1}$$

$$b_1 = 1 \quad ; \quad b_2 = 0. \quad (3.6)$$

Combining the incremental compliance for elastic plates, (3.6), with that for the plastic LSE, (2.3) gives

$$\begin{bmatrix} C_{11} - E_{11} & C_{12} - E_{12} \\ C_{21} - E_{21} & C_{22} - E_{22} \end{bmatrix}\begin{bmatrix} \delta\hat{N} \\ \delta\hat{M} \end{bmatrix} = \begin{bmatrix} 1 \\ 0 \end{bmatrix}\delta\hat{u}^{\infty}, \quad (3.7)$$

3.3. Calculations and Results

In this section, fully plastic crack growth of the part-through crack in a plate is numerically simulated for given initial crack depths $\hat{a}_0(= a_0/t)$, plate lengths $\hat{L}(= L/t)$ and a normalized Young's modulus $\hat{E}(= E/(2k)$ as follows:

- Initial elastic deformation:

  Determine an initial tensile force $\hat{N}_0$ to cause the plastic LSE to fully yield. Note that $\hat{N}_0$ can be determined from the yield condition (2.14) or (2.18) with $\hat{M} = 0$, depending on $\hat{a}_0$. Up to this point the plastic LSE remains rigid ($\delta\hat{u} = \delta\hat{\theta} = 0$) due to the rigid-plastic assumption. The corresponding initial far-field deformation $\delta\hat{u}_0^{\infty}$ can be determined from (3.5):

$$\delta u^{\infty} = \frac{\hat{L}}{\hat{E}}\hat{N}_0. \tag{3.8}$$

- Plastic deformation with crack growth

  1. Determine the corresponding $CTOA(\hat{M}/\hat{N})$ and the compliance matrices, $C_{ij}(\hat{N}, \hat{M}, \hat{a}, CTOA)$ $(i, j = 1, 2)$ from (2.10) and $E_{ij}(\hat{N}, \hat{M}, \hat{a}, CTOA)$ from (3.6). Note that the $CTOA$ should depend on the tension-to-bending ratio and materials. By combining a sliding off and shear cracking model with the equations from micromechanisms of crack growth, McClintock, et al. (1993) proposed the $CTOA$ in terms of an effective slip direction θ_s, the normal stress across that direction, σ_s, and the material. For a material with the strain hardening exponent n in $k = k_o\gamma^n$ with k_o=constant, the result is

$$\tan\left(\frac{CTOA}{2}\right) = \frac{1}{[2/(\gamma_f \sin 2\theta_s) - 1]} \tan\theta_s,$$

$$\text{where} \quad \gamma_f(\sigma_s, \text{material}) = \frac{(1-n)A}{\sinh[(1-n)\sigma_s/k]} + B(\sigma_s). \tag{3.9}$$

The term $(1-n)A/\sinh[(1-n)\sigma_s/k]$ is related to the strain for hole growth and the term $B(\sigma_s)$ to that for hole nucleation. The parameters A and $B(\sigma_s)$ reflect material properties and should be determined from fully plastic crack growth experiments. The parameter A is related to the strain for hole growth ratio up to localization, (R_l/R_o): $A = 2\ln(R_f/R_o)$. The parameter $B(\sigma_s)$ is related to the strain for hole nucleation. The parameters θ_s and σ_s/k have been determined in terms of the tension-to-bending ratio either from slip line field (SLF) analysis (McClintock, et al., 1993) or from the least upper bound (LUB) analysis based on a circular arc (Kim, et al., 1993b). Figure 5.4 shows the dependence of θ_s and $\sigma_s/(2k)$ on the net-section bending ratio $\mu_n(= M_n/(bN_n)$, where $b = t - a)$.

2. For the given far-field deformation $\delta\hat{u}^\infty$, determine increments of the generalized forces, $\delta\hat{N}$ and $\delta\hat{M}$, from (3.7). Once $\delta\hat{N}$ and $\delta\hat{M}$ are determined, we can determine other variables such as $\delta\hat{u}$ and $\delta\hat{\theta}$ from either (2.3) or (3.6), and $\delta\hat{a}$ from (2.7) and (2.8). Note that the new loading variables $\hat{N}(= \hat{N} + \delta\hat{N})$ and $\hat{M}(= \hat{M} + \delta\hat{M})$, and the new crack tip position $\hat{a}(= \hat{a} + \delta\hat{a})$ do not satisfy the yield condition.

3. Correct $\delta\hat{N}$ and $\delta\hat{M}$ radially such that they satisfy the yield condition for the new crack tip position, and determine corresponding corrections for $\delta\hat{u}$, $\delta\hat{\theta}$ and $\delta\hat{a}$. This correction is done a few times iteratively.

4. Update variables (e.g., $\hat{N} = \hat{N} + \delta\hat{N}$, $\hat{u} = \hat{u} + \delta\hat{u}$, etc.) and go to Step 1.

Effect of plate lengths

Figure 5.5 shows fully plastic crack growth results under pinned and fixed-grip conditions for five different plate lengths of $L/t = 1, 2.5, 5, 10$, and 20. The initial crack depth $\hat{a}_0 (= a_0/t)$ is set to be 0.4 which is deep enough to prevent shoulder deformation for all tension-to-bending ratios (Lee and Parks, 1993). Material parameters are assumed as follows:

$$\hat{E} = \frac{\sqrt{3}}{2}500 \ ; \ A = 1.175 \ ; \ B(\sigma_s) = 0.$$

Note that $\hat{E}$ is related to the yield strain ϵ_y:

$$\hat{E} = E/2k = (\sqrt{3}/2)(E/\sqrt{3}k) = (\sqrt{3}/2)(1/\epsilon_y). \tag{3.10}$$

Thus the above value corresponds to typical yield strain for common low strength alloys, $\epsilon_y = 0.002$. The assumed values for $A = 1.175$ and $B(\sigma_s) = 0$ correspond to hole growth ratio of $(R_f/R_o) = 1.8$ with the negligible nucleation strain, and to a fracture shear strain of unity, $\gamma_f = 1$, under crack tip triaxiality of $\sigma_s/(2k) = 0.5$.

In Figs. 5.5, results for pinned conditions are drawn with solid lines and those for the fixed grip condition drawn in dotted lines. Note that all the variables are re-normalized using the initial remaining ligament $\hat{b}_0 (= 1 - \hat{a}_0)$ instead of the plate thickness t, such that $(a - a_0)/b_0$ and $N/(2kb_0)$ vary from 0 to 1 during entire crack growth.

For pinned conditions, as the far-field deformation $\hat{u}^\infty$ is increased, the cracked part continuously bulges out and the effect is more pronounce for longer plates (Fig.

5.5j). Due to the bulging effect the net section for longer plate is aligned quickly with the load line and thus is subject to less bending moment (or crack tip constraint) (Fig. 5.5c) and therefore the crack growth behavior is similar to that under pure extension. In Fig. 5.5, the characteristic behaviors of the LSE are also included, such as pure extension and pure tension. Resulting tension force N is shown in terms of crack growth and of the far-field deformation $\hat{u}^{\infty}$ in Fig. 5.5b and 5.5a, respectively. For a short plate such as $L/t = 1$, the response is expected to be similar to that for pure extension (Fig. 5.5b). On the other hand, for a long plate such as $L/t = 20$, the bulging effect makes the net-section aligned quickly with the load line and thus the response is expected to be similar to that for pure extension, as shown in Fig. 5.5b. Note the difference in slope $d\hat{N}/d\hat{u}^{\infty}$ of two plate lengths $L/t = 1$ and 20. This can be related to stability of crack growth. One interesting point is that, for small amount of crack growth in longer plate (e.g., $L/t = 5, 10$ and 20), the load N may increase as the crack grows due to the load adjustment. The net-section load histories are shown in Fig. 5.5e. Again we can see that the loading history for $L/t = 1$ is similar to that for pure tension. The variation of $CTOA$ during crack growth is shown in Fig. 5.5g. For a long plate such as L/t =5-20, the $CTOA$ quickly changes to that for pure extension (here $CTOA = 90^{o}$). For L/t=2.5, the $CTOA$ is gradually increasing to 90°. For L/t=1, the $CTOA$ keeps on decreasing until the crack is deep enough for the modified Green and Hundy field to apply, where the near tip fields such as σ_s and θ_s remain constant so that the $CTOA$ remains constant. Figure 5.5e suggests that various loading histories (or tension-to-bending ratios) can be obtained by varying plate lengths. Histories for generalized displacements $\hat{u}$ and $\hat{\theta}$ are shown in Fig. 5.5h and 5.5i. Note that for very short plate such as $L/t = 1$ our elastic analysis does not apply when rotation θ becomes too large where elastic assumptions are no longer

valid. (The results for $L/t = 1$ shown in Fig. 5.5 are up to the point where $\theta \leq 10^o$.)

For the fixed grip condition, as the far-field deformation $\hat{u}^\infty$ is increased, the cracked part is initially bulging (but by smaller amount compared to those for the pinned condition) and later is closing as shown in Fig. 5.5j). For longer plates, the bulging effect is pronounce as in the pinned case. In the pinned condition, the bulging effect was the main reason for pure extension behavior. In the fixed grip condition, the bulging effect is less important but the large (negative) moment M^∞ should be applied to maintain zero slope in the far-field (Fig. 5.5f). Note that from moment equilibrium in Fig. 5.4,

$$M^\infty = M - Nv(0). \tag{3.9}$$

For shorter plates, more (negative) M^∞ should be applied to maintain zero slope $\theta^\infty = 0$ (Fig. 5.5f) and thus, from moment equilibrium (3.9), the net-section is subject to less bending moment (Fig. 5.5c). This makes physically sense because, for a short plate such as $L/t = 1$, we expect that the response should be similar to that for pure extension. For a long plate such as $L/t = 20$, the response should be similar to that in the pinned condition, because in the limiting case of infinitely long plate, both conditions should give the same results, as will be discussed later. Therefore, for the grip condition with varying L/t, all the responses are similar to that for pure extension, as shown in Fig. 5.5a-5.5i. However, for different material ductility, the response can be quite different from these figures, which will be shown in the next section.

For a limiting case of infinitely long plate, the effect of the loads N and M due to the crack dies out and thus the deflection $v(x)$ and its derivatives are zero at $x = L$,

and thus both boundary conditions should give same results. This condition holds for a plate with finite length which is represented as a characteristic length L_c. The L_c is approximately proportional to

$$\frac{L_c}{t} \propto \sqrt{\frac{\hat{E}}{\hat{N}}}. \tag{3.10}$$

As the crack grows, the load $\hat{N}$ is eventually getting smaller and thus L_c is increasing. As shown in Fig. 5.5a to 5.5h, the responses of $L/t = 20$ for both boundary conditions are almost identical. However, the responses of θ and $v(0)$ are initially similar but later very different.

Effect of material ductility

In this section, two materials with different ductilities are considered. The material parameters used for two materials are as follows: For the material I (same as before),

$$\hat{E} = \frac{\sqrt{3}}{2}500 \ ; \ A = 1.175 \ ; \ B(\sigma_s) = 0,$$

and for the material II,

$$\hat{E} = \frac{\sqrt{3}}{2}250 \ ; \ A = 1.3 \ ; \ B(\sigma_s) = 0.$$

Figure 5.6 shows the effect of material ductility under the pinned condition for two plate lengths ($L/t = 2.5$ and 10). The change in slope of N vs. u^∞ and u vs. δa can be observed in Fig. 5.6a and 5.6g, respectively. From other responses, we can conclude that the response of the less ductile plate is similar to that for more ductile plate of shorter length. For example, the response of the material II with $L/t = 10$ is similar to that of the material I with $L/t = 5$, and the response of the material II with $L/t = 2.5$ to that of the material I with $L/t = 1$.

Figure 5.7 shows the effect of material ductility under the fixed grip condition for two plate lengths ($L/t = 2.5$ and 10). Here we can also observe the change in slope of N vs. u^{∞} and u vs. δa from Fig. 5.6a and 5.6h, respectively. In the fixed grip case, the response of the less ductile plate of a short length is similar to that for more ductile plate of longer length. For example, the response of the material II with $L/t = 2.5$ is similar to that of the material I with $L/t = 10$. However, the response of the less ductile plate of a long length initially is similar to that for more ductile plate of shorter length *under the pinned condition.* For example, the response of the material II with $L/t = 10$ is similar to that of the material I with $L/t = 2.5$.

Effect of initial crack depth

In this section, two different initial crack depths $a_0/t = 0.4$ and 0.6 are considered. The same material parameters are used as before, namely,

$$\hat{E} = \frac{\sqrt{3}}{2}500 \ ; \ A = 1.175 \ ; \ B(\sigma_s) = 0.$$

Figure 5.8 show the effect of a_0/t under the pinned condition for two plate lengths ($L/t = 2.5$ and 10), and Fig. 5.9 shows the effect under the fixed grip condition. The results show that the initial crack depth does not affect response except u^{∞} and u which are scaled based on approximately the ratio of a_0/t.

4. Complete Circumferential Crack Growth in Sufficiently Long Shells

Fully plastic growth of radial and circumferential cracks in pipes has been studied by Zahoor and Kanninen (1981) for pipes under bending, and Zahoor and Norris (1984) for pipes under tension. They assessed the stability of crack growth using the J-integral-based Tearing Modulus approach.

4.1. Analysis of Elastic Shells

Consider a complete circumferential crack in shells, subject to axial tension, with a shell thickness t, a radius $R(\gg t)$, a length L and a Young's modulus E with a complete circumferential crack of depth a, as shown in Fig. 5.10.

Differential equation for elastic shells

By considering additional moment due to deflection caused by load shifting, we can obtain the following differential equations for elastic shells:

$$D\frac{d^4v}{dx^4} - N\frac{d^2v}{dx^2} + \frac{Et}{R^2}v = 0 \quad \text{for } 0 < x < L, \tag{4.1}$$

where $D(= Et^3/[12(1-\nu^2)])$ is the flexural rigidity of the shell. Note that the axial force N in (4.1) is the force per unit width of the shell. In the extreme when there is no tension force $N = 0$, the (4.1) recovers the well-known shell equation (Timoshenko and Woinowsky-Krieger, 1970). In the other extreme when the shell radius R is sufficiently large ($R \gg t$), (4.1) recovers that for plates with the part-through crack. (Note the factor $(1-\nu^2)$ comes from the assumption of a very wide plate. For the condition of the width of the plate, refer to McClintock and Argon (1965).) Introducing two parameters α and β which are related to characteristic

lengths: one for plates, αL, and the other for shells, βL.

$$\alpha^2 \equiv \frac{N}{D} = \frac{12N(1-\nu^2)}{Et^3} \;\; ; \;\; 4\beta^4 \equiv \frac{Et}{R^2 D} = \frac{12(1-\nu^2)}{R^2 t^2}, \tag{4.2}$$

then (4.1) becomes

$$\frac{d^4 v}{dx^4} - \alpha^2 \frac{d^2 v}{dx^2} + 4\beta^4 v = 0 \quad \text{for } 0 < x < L. \tag{4.2}$$

Boundary conditions

For simplicity, consider sufficiently long shells, i.e., $\beta L \gg 1$. Timoshenko and Woinowsky-Krieger (1970) showed that shells can be assumed to be sufficiently long if $\beta L \geq 5$. Note that this condition corresponds to

$$\left(\frac{L}{t}\right)^2 \geq 15.3\left(\frac{R}{t}\right) \quad \text{or} \quad \left(\frac{L}{t}\right) \geq 3.9\sqrt{\frac{R}{t}}. \tag{4.3}$$

In such case, the boundary conditions at $x = L$ do not affect the solution since the solution and its derivatives vanish at $x = L$. Under this assumption, only two boundary conditions are needed, namely, (i) the given bending moment at $x = 0$, $(M_x)_{x=0} = M$, and (ii) no shear force at $x = 0$, $(Q_x)_{x=0} = 0$. Introducing these two boundary conditions into (4.3), we can obtain the relation between θ and M. The details are shown in the Appendix II and the only final result are given here in terms of normalized variables:

$$\left[\frac{\hat{F}_1}{d\hat{N}} - \frac{3(1-\nu^2)}{\hat{E}}\frac{\hat{F}_2}{d\hat{N}}\hat{M}\right]\delta\hat{N} - \frac{3(1-\nu^2)}{\hat{E}}\hat{F}_2\delta\hat{M} + \hat{F}_1\delta\hat{\theta} = 0. \tag{4.4}$$

Explicit forms of $\hat{F}_1(\hat{N}), \hat{F}_2(\hat{N}), d\hat{F}_1/d\hat{N}$ and $d\hat{F}_2/d\hat{N}$ are also given in the Appendix II.

The axial force-deflection relation in elastic shells provides the relation between $\delta\hat{u}$ and $\delta\hat{u}^\infty$ in terms of $\hat{L}(= L/t)$ and $\delta\hat{N}$:

$$\delta\hat{u} = -\frac{\hat{L}}{\hat{E}}\delta\hat{N} + \delta\hat{u}^\infty. \tag{4.5}$$

Combining (4.4) and (4.5) with matrix manipulations gives the form of (3.3) with

$$\hat{E}_{11} = -\frac{\hat{L}}{\hat{E}} \quad ; \quad \hat{E}_{12} = 0$$

$$\hat{E}_{21} = -\frac{1}{\hat{F}_1}\frac{d\hat{F}_1}{d\hat{N}} + \frac{3(1-\nu^2)}{\hat{E}}\frac{\hat{M}}{\hat{F}_1}\frac{d\hat{F}_2}{d\hat{N}} \; ; \; \hat{E}_{22} = \frac{3(1-\nu^2)}{\hat{E}}\frac{\hat{F}_2}{\hat{F}_1}$$

$$b_1 = 1 \; ; \; b_2 = 0. \tag{4.6}$$

4.3. Calculations and Results

Figure 5.11 show crack growth results for various shell radius-to-thickness ratio R/t=1, 10, 100 and 1000. The length of the shell, L/t, is assumed to be 40. Note that for $L/t = 40$ the required R/t for condition of sufficiently long shell is, from (4.6), $R/t \leq 105$. (Even though the case of $R/t = 1000$ does not meet this condition, we include that result to see the trend.) Other parameters are assumed as before in the plate case, i.e.,

$$\frac{a_0}{t} = 0.4 \; ; \; \hat{E} = \frac{\sqrt{3}}{2}500 \; ; \; A = 1.175 \; ; \; B(\sigma_s) = 0.$$

In Fig. 5.11, the corresponding response of part-through cracks in plates are also included. (Note that when $L/t = 40$, both the pinned and fixed grip boundary condition in plates give the almost same result, which verifies that the plate with $L/t = 40$ is indeed sufficiently long.) As $R/t \to \infty$, we expect that the shell solution should approach to the plate solution, which can be clearly seen in Fig. 5.11.

One interesting result is that the effect of curvature (varying R/t) is very similar to the effect of the plate length L/t under the fixed grip condition. See Fig. 5.5 for

comparison. Increasing R/t in shell is equivalent to increase L/t in plate under the fixed grip condition. This result would be extremely useful since the effect of other parameters can be deduced from the parametric study of the plate.

5. CONCLUSION

A line-spring model is developed for fully plastic, plane strain crack growth in plates and shells. Based on rigid-plastic, non-hardening plasticity, a simple form of incremental compliance of the line-spring, developed from a single-face-cracked specimen under combined bending and tension, is expressed in terms of yield loci and its derivatives, and the crack tip opening angle ($CTOA$).

Then the line-spring is embedded in elastic plates and shells to predict fully plastic crack growth of two kinds of part-through cracks: across plates with pinned or fixed-grip boundary conditions, complete circumferential cracks in long shells under axial tension. The analysis includes the bulging effect of the cracked part. Parametric studies show:

For growth of a part-through crack in the plate:

1. Under pinned conditions, the bulging effect is important. Due to bulging, for longer plates, the net-section is subject to less bending moment. Thus the far-field deformation for fracture u_f^∞ increases as L/t increases.

2. Under fixed-grip conditions, the bulging effect is less important. However, shorter plates require larger negative moments applied in the far-field to maintain zero slope there. Therefore, for shorter plates, the net-section is subject to less bending moment. Thus u_f^∞ increases as L/t decreases.

3. For less ductile plates under the pinned condition, responses of longer plates are similar to those of shorter but more ductile plates. For less ductile plates under the fixed grip condition, responses of shorter plates are similar to those of longer but more ductile plates. Therefore, u_f^∞ decreases for less ductile materials regardless of the type of the boundary conditions.

4. Deeper initial crack depths reduces u_f^∞.

For crack growth of the complete circumferential crack in the shell, the effect of curvature (varying R/t) is equivalent to the effect of the plate length (varying L/t) under the fixed grip condition. Therefore, u_f^∞ increases as R/t decreases.

REFERENCES

Kim, Y.J., McClintock, F.A. and Parks, D.M., 1993a, "Yield Locus in Deep, Single-Face-Cracked Specimens Under Combined Bending and Tension", submitted as Brief Note to *Journal of Applied Mechanics.*

Kim, Y.J., McClintock, F.A. and Parks, D.M., 1993b, "Global Equilibrium of Least Upper Bound Circular Arcs and its Application to Fracture Mechanics", submitted to *Journal of the Mechanics and Physics of Solids.*

Levy, N, and Rice, J.R., 1972, "Surface Cracks in an Elastic Plates and Shells", unpublished manuscript.

McClintock, F.A. and Argon, A.S., 1966, *Mechanical Behavior of Materials*, Addison Wesley.

McClintock, F.A., Kim, Y.J., and Parks, D.M., 1993, "Criteria for Fully Plastic, Plane Strain, Quasi-Steady Crack Growth", submitted to *International Journal of Fracture.*

Miyoshi, T., Shiratori, M. and Yoshida, Y., 1986, "Analysis of J-integral and Crack Growth for Surface Cracks by Line-Spring Method", ASME *Journal of Pressure Vessel Technology*", **108**, 305-311.

Parks, D.M., 1981, "The Inelastic Line-Spring: Estimates of Elastic-Plastic Fracture Mechanics Parameters for Surface-Cracked Plates and Shells", ASME *Journal*

of Pressure Vessel Technology", **103**, 246-254.

Parks, D.M. and White, C.S., 1982, "Elasic-Plastic Line-Spring Finite Elements for Surface-Cracked Plates and Shells", ASME *Journal of Pressure Vessel Technology*", **104**, 287-292.

Raju, I.S. and Newman, J.C., Jr., 1979, "Stress Intensity Factors for a Wide Range of Semi-Elliptical Surface Cracks in Finite-Thickness Plates", *Engineering Fracture Mechanics*, **11**, 817-829.

Rice, J.R., 1972, "The Line-Spring Model for Surface Flaws", *The Surface Crcak: Physical Problems and Computational Solutions*, ed. J.L. Sweldow, American Society of Mechanical Engineers, New York, 171-185.

Rice, J.R. and Levy, N, 1972. "The Part-Through Surface Crack in an Elastic Plates", ASME *Journal of Applied Mechanics*", **39**, 185-194.

Timoshenko, S.P. and Woinowsky-Krieger, S., 1970, *Theory of Plates and Shells*, McGraw-Hill.

White, C.S., Ritchie, R.O. and Parks, D.M., 1983, "Ductile Growth of Part-Through Surface Cracks: Experiments and Analysis", *Elastic-Plastic Fracture: Second Symposium. Volume I - Inelastic Crack Analysis*, ASTM STP 803, C.F. Shih and J.P. Gudas, Eds., American Society for Testing and Materials, I-384-I-409.

Yagawa, G., Takahashi, Y., Kashima, K., Hasegawa, K., Saito, M., Umemoto, T., and Sasaki, N., 1984, "Stable Growth and Instability of Circumferential Cracks in Type 304 Stainless Steel Pipes Under Tensile Load", *Journal of Pressure Vessel Technology*, Vol. 106, pp. 405-411.

Zahoor, A. and Kanninen, M.F., 1981, "A Plastic Fracture Instability Analysis of Wall Breakthrough in a Circumferentially Cracked Pipe Subject to Bending Loads," *Journal of Engineering Materials and Technology*, Vol. 103, pp. 194-200.

Zahoor, A. and Norris, P.M., 1984, "Ductile Fracture of Circumferentially Cracked Type-304 Stainless Steel Pipes in Tension", *Journal of Pressure Vessel Technology*, Vol. 106, pp. 399-404.

APPENDICES

I. Analysis of Plates with a Part-Through Crack

The differential equation for the deflection of the plate, $v(x)$, in terms of $\alpha = \sqrt{12N/Et^3}$ is

$$\frac{d^4v(x)}{dx^4} - \alpha^2\frac{d^2v(x)}{dx^2} = 0 \qquad \text{for} \qquad 0 < x < L. \tag{A.1}$$

The general solution to (A.1) is

$$v(x) = a_1 + a_2x + a_3\exp(\alpha x) + a_4\exp(-\alpha x). \tag{A.2}$$

The four coefficients $a_i (i = 1, 2, 3, 4)$ should be determined from boundary conditions. We consider two types of boundary conditions at $x = L$: pinned and fixed-grip conditions.

Boundary Condition I: Pinned Conditions

For pinned conditions, the boundary conditions are as follows:

i) For zero deflection at $x = L$

$$v(x = L) = 0. \tag{A.3}$$

ii) For zero moment at $x = L$

$$\left[\frac{Et^3}{12}\frac{d^2v}{dx^2}\right]_{x=L} = 0. \tag{A.4}$$

iii) For zero shear force at $x = 0$

$$\left[N\frac{dv}{dx} - \frac{Et^3}{12}\frac{d^3v}{dx^3}\right]_{x=0} = 0. \tag{A.5}$$

iv) For a given moment M at x=0

$$\left[\frac{Et^3}{12}\frac{d^2v}{dx^2}\right]_{x=0} = -M. \tag{A.6}$$

The coefficients $a_i (i = 1, 2, 3, 4)$ can be determined by introducing boundary conditions (A.3)-(A.6) into (A.2). The results are

$$a_2 = 0 \;\; ; \;\; a_1 = -2\exp(\alpha L)a_3 = -\frac{2}{\exp(\alpha L)}a_4 = -\frac{M}{N}\left[\frac{2\exp(\alpha L)}{1+\exp(2\alpha L)}\right]. \tag{A.7}$$

Therefore for pinned conditions,

$$v(x) = -\frac{M}{N}\left[\frac{\exp(\alpha x)}{1+\exp(2\alpha L)}\right][1 - \exp\alpha(L-x)]^2. \tag{A.8}$$

$$v_0 = v(x=0) = -\frac{M}{N}\left[\frac{(1-\exp(\alpha L))^2}{1+\exp(2\alpha L)}\right]. \tag{A.9}$$

$$\theta = \left[\frac{dv}{dx}\right]_{x=0} = -\frac{1}{\sqrt{Et^3/12}}\frac{M}{\sqrt{N}}\left[\frac{1-\exp(2\alpha L)}{1+\exp(2\alpha L)}\right]. \tag{A.10}$$

Boundary Condition II: Fixed-Grip Conditions

For fixed-grip conditions, the boundary conditions are the same as those in pinned conditions except (A.4), zero moment at $x = L$ instead of zero slope at $x = L$:

$$\left[\frac{dv}{dx}\right]_{x=L} = 0. \tag{A.11}$$

Similarly as before,

$$a_1 = a_2 = 0 \;\; ; \;\; a_3 = -\frac{a_4}{\exp(2\alpha L)} = -\frac{M}{N}\left[\frac{1}{1-\exp(2\alpha L)}\right]. \qquad (A.12)$$

$$v(x) = -\frac{M}{N}\left[\frac{\exp(\alpha x)}{1-\exp(2\alpha L)}\right][1+\exp 2\alpha(L-x)]. \qquad (A.13)$$

The deflection v_0 and slope θ of the cracked section ($x = 0$) can be determined from (A.13):

$$v_0 = v(x=0) = -\frac{M}{N}\left[\frac{1+\exp(2\alpha L_J}{1-\exp(2\alpha L)}\right]. \qquad (A.14)$$

$$\theta = \left[\frac{dv}{dx}\right]_{x=0} = -\frac{1}{\sqrt{Et^3/12}}\frac{M}{\sqrt{N}}\left[\frac{1+\exp(2\alpha L)}{1-\exp(2\alpha L)}\right]. \qquad (A.15)$$

Incremental Compliance of Elastic Plates

For both pinned and fixed-grip conditions, the relation between θ and M, (A.10) and (A.15), can be expressed as

$$\sqrt{N}F_1(N)\theta + \frac{F_2(N)}{\sqrt{Et^3/12}}M = 0, \qquad (A.16)$$

where for pinned conditions,

$$F_1(N) = 1-\exp(2\alpha L) \;\; ; \;\; F_2(N) = 1+\exp(2\alpha L), \qquad (A.17)$$

and for fixed-grip conditions,

$$F_1(N) = 1+\exp(2\alpha L) \;\; ; \;\; F_2(N) = 1-\exp(2\alpha L). \qquad (A.18)$$

The incremental form of (A.16) is obtained by differentiating with respect to N. Noting that F_1 and F_2 are fuctions of N, the result is

$$\left[\left(\frac{F_1}{2\sqrt{N}} + \sqrt{N}\frac{dF_1}{dN}\right)\theta + \frac{M}{\sqrt{Et^3/12}}\frac{dF_2}{dN}\right]\delta N + \frac{F_2}{\sqrt{Et^3/12}}\delta M + \sqrt{N}F_1\delta\theta = 0, \qquad (A.19)$$

where for pinned conditions,

$$\frac{dF_1}{dN} = -\frac{dF_2}{dN} = -\frac{L}{\sqrt{Et^3/12}}\frac{1}{\sqrt{N}}\exp(2\alpha L), \tag{A.20}$$

and for fixed-grip conditions,

$$\frac{dF_1}{dN} = -\frac{dF_2}{dN} = \frac{L}{\sqrt{Et^3/12}}\frac{1}{\sqrt{N}}\exp(2\alpha L). \tag{A.21}$$

Normalize the variables in addition to (2.1) and (2.2)

$$\hat{L} = \frac{L}{t} \;\; ; \;\; \hat{E} = \frac{E}{2k} \;\; ; \;\; \hat{\alpha} = \alpha L = \sqrt{\frac{\hat{N}}{12\hat{E}}}\hat{L}. \tag{A.22}$$

Then (A.19) in terms of normalized variables is

$$\left[\left(\frac{\hat{F}_1}{2\sqrt{\hat{N}}} + \sqrt{\hat{N}}\frac{d\hat{F}_1}{d\hat{N}}\right)\hat{\theta} + \frac{1}{4}\frac{\hat{M}}{\sqrt{\hat{E}/12}}\frac{d\hat{F}_2}{d\hat{N}}\right]\delta\hat{N} + \frac{1}{4}\frac{\hat{F}_2}{\sqrt{\hat{E}/12}}\delta\hat{M} + \sqrt{\hat{N}}\hat{F}_1\delta\hat{\theta} = 0, \tag{A.23}$$

where for pinned conditions,

$$\hat{F}_1(N) = 1 - \exp(2\hat{\alpha}) \;\; ; \;\; \hat{F}_2(N) = 1 + \exp(2\hat{\alpha}) \;\; ;$$

$$\frac{d\hat{F}_1}{d\hat{N}} = -\frac{d\hat{F}_2}{d\hat{N}} = -\frac{\hat{L}}{\sqrt{\hat{E}/12}}\frac{1}{\sqrt{\hat{N}}}\exp(2\hat{\alpha}), \tag{A.24}$$

and for fixed-grip conditions,

$$\hat{F}_1(N) = 1 + \exp(2\hat{\alpha}) \;\; ; \;\; \hat{F}_2(N) = 1 - \exp(2\hat{\alpha}) \;\; ;$$

$$\frac{d\hat{F}_1}{d\hat{N}} = -\frac{d\hat{F}_2}{d\hat{N}} = \frac{\hat{L}}{\sqrt{\hat{E}/12}}\frac{1}{\sqrt{\hat{N}}}\exp(2\hat{\alpha}). \tag{A.25}$$

Sufficiently Long Plates

For sufficiently long plates (i.e., $\hat{\alpha} = \alpha L \gg 1$), the effect of the applied moment M at $x = 0$ die out so that the deflection $v(x)$ and its derivatives vanishes at $x = L$.

In such case, both pinned and fixed-grip conditions give the same result:

$$\sqrt{N}\theta - \frac{1}{\sqrt{Et^3/12}}M = 0. \tag{A.26}$$

The incremental form of (A.26) is

$$\left(\frac{1}{2\sqrt{N}}\theta\right)\delta N - \frac{1}{\sqrt{Et^3/12}}\delta M + \sqrt{N}\delta\theta = 0. \tag{A.27}$$

In terms of normalized variables,

$$\left(\frac{1}{2\sqrt{\hat{N}}}\hat{\theta}\right)\delta\hat{N} - \frac{1}{4}\frac{1}{\sqrt{\hat{E}/12}}\delta\hat{M} + \sqrt{\hat{N}}\delta\hat{\theta} = 0. \tag{A.28}$$

II. Analysis of Sufficiently Long Shells with a Complete Circumeferential Crack

The differential equation for the deflection of the shell, $v(x)$, is

$$\frac{d^4v}{dx^4} - \alpha^2\frac{d^2v}{dx^2} + 4\beta^4 v = 0 \quad \text{for } 0 < x < L, \tag{A.29}$$

where

$$D \equiv \frac{Et^3}{12(1-\nu^2)} \;\; ; \;\; \alpha^2 \equiv \frac{N}{D} = \frac{12N(1-\nu^2)}{Et^3} \;\; ; \;\; 4\beta^4 \equiv \frac{Et}{R^2D} = \frac{12(1-\nu^2)}{R^2t^2}. \tag{A.30}$$

Assuming the solution to (A.29) of the form

$$v(x) = \Sigma a_i \exp(\lambda_i x) \tag{A.31}$$

leads to the following characteristic equation:

$$\lambda^4 - \alpha^2\lambda^2 + 4\beta^4 = 0. \tag{A.32}$$

The solution to (A.32) is

$$\lambda^2 = \frac{\alpha^2}{2} \pm \frac{1}{2}\sqrt{\alpha^4 - 16\beta^4} = \frac{\alpha^2}{2} \pm \frac{1}{2}\sqrt{(\alpha^2 + 4\beta^2)(\alpha^2 - 4\beta^2)}. \tag{A.33}$$

Depending on the sign of $(\alpha^2 - 4\beta^2)$, two cases should be considered.

Boundary Conditions for Sufficiently long shell

For sufficiently long shells, the solution $v(x)$ and its derivatives should vanish at $x = L$. Therefore, the boundary conditions are as follows:

(i) for the solution $v(x)$ and its derivatives at $x = L$

$$v(x=L) = \left[\frac{dv}{dx}\right]_{x=L} = \left[\frac{d^2v}{dx^2}\right]_{x=L} = \left[\frac{d^3v}{dx^3}\right]_{x=L} = 0. \tag{A.34}$$

(*ii*) the given moment M at $x = 0$

$$(M_x)_{x=0} = -\frac{Et^3}{12(1-\nu^2)}\left[\frac{d^2v}{dx^2}\right]_{x=0} = -M. \tag{A.35}$$

(*iii*) zero shear force at $x = 0$

$$(Q_x)_{x=0} = -\frac{Et^3}{12(1-\nu^2)}\left[\frac{d^3v}{dx^3}\right]_{x=0} + N\left[\frac{dv}{dx}\right]_{x=0} = 0. \tag{A.36}$$

I. Case of $(\alpha^2 - 4\beta^2) > 0$

In this case, the characteristic equation (A.32) has four distinct real (two positive and two negative) roots:

$$\lambda_{1,2} = -\sqrt{\frac{\alpha^2}{2} \pm \frac{1}{2}\sqrt{\alpha^4 - 16\beta^4}}\,(> 0)\,. \tag{A.37}$$

$$\lambda_{3,4} = \sqrt{\frac{\alpha^2}{2} \pm \frac{1}{2}\sqrt{\alpha^4 - 16\beta^4}}\,(< 0)\,. \tag{A.38}$$

From the boundary condition (A.34), the positive terms must vanish. Hence $a_3 = a_4 = 0$, and thus from (A.31)

$$v(x) = a_1 \exp(\lambda_1) + a_2 \exp(\lambda_2). \tag{A.39}$$

Introducing the boundary conditions (A.35) and (A.36) into (A.39) gives

$$a_1 = -\frac{\lambda_1}{\lambda_2}a_2 = -\frac{12(1-\nu^2)M}{Et^3}\left[\frac{\lambda_1}{(\lambda_1^3 - \lambda_2^3)}\right]. \tag{A.40}$$

Therefore, at $x = 0$, the deflection v_0 and slope θ are

$$v_0 = v(x=0) = a_1 + a_2 = \frac{12(1-\nu^2)M}{Et^3}\left[\frac{1}{(\alpha^2 + 2\beta^2)}\right]. \tag{A.41}$$

$$\theta = \left[\frac{dv}{dx}\right]_{x=0} = a_1\lambda_1 + a_2\lambda_2 = \frac{12(1-\nu^2)M}{Et^3}\left[\frac{(\lambda_1 + \lambda_2)}{(\alpha^2 + 2\beta^2)}\right]. \tag{A.42}$$

Note that when the shell radius R is very large (i.e., $R \gg t$), then $\beta \to 0$, and (A.42) with $\alpha^2 = 12N/(Et^3)$ recovers that for sufficiently long plates, (A.26), differed by a factor of $(1 - \nu^2)$.

II. Case of $(\alpha^2 - 4\beta^2) < 0$

In this case, we have four distinct complex solutions:

$$\lambda^2 = \frac{\alpha^2}{2} \pm \frac{1}{2}\sqrt{(16\beta^4 - \alpha^4)}j. \tag{A.43}$$

The solutions to (A.43) are two complex conjugates:

$$\lambda_{1,2} = -a \pm bj \;\; ; \;\; \lambda_{3,4} = a \pm bj, \tag{A.44}$$

where

$$a = \sqrt{\frac{\alpha^2}{4} + \beta^2} \;\; ; \;\; b = \sqrt{\beta^2 - \frac{\alpha^2}{4}}. \tag{A.45}$$

Then the deflection $v(x)$ is

$$v(x) = e^{-ax}[a_1 \cos(bx) + a_2 \sin(bx)] + e^{ax}[a_3 \cos(bx) + a_4 \sin(bx)]. \tag{A.46}$$

From the boundary condition (A.34), the positive terms must vanish. Hence $a_3 = a_4 = 0$, and we obtain

$$v(x) = e^{-ax}[a_1 \cos(bx) + a_2 \sin(bx)]. \tag{A.47}$$

Introducing the boundary conditions (A.35) and (A.36) into (A.47) gives

$$a_1 = \frac{b}{a}a_2 = M\frac{12(1-\nu^2)}{Et^3}\left[\frac{1}{\alpha^2 + 2\beta^2}\right]. \tag{A.48}$$

Therefore, at the cracked section ($x = 0$), the deflection v_o and slope θ are

$$v_0 = v(x=0) = M\frac{12(1-\nu^2)}{Et^3}\left[\frac{1}{(\alpha^2 + 2\beta^2)}\right]. \tag{A.49}$$

$$\theta = \left[\frac{dv}{dx}\right]_{x=0} = \frac{12(1-\nu^2)M}{Et^3}\left[\frac{2a}{\alpha^2+2\beta^2}\right]. \qquad (A.50)$$

Incremental Compliance of Elastic Shells

The relation between θ and M, (A.42) and (A.50), can be written as

$$F_1(N)\theta - \frac{12(1-\nu^2)}{Et^3}F_2(N)M = 0, \qquad (A.51)$$

where

$$F_1(N) = \alpha^2 + 2\beta^2 \qquad \text{and} \qquad (A.52)$$

$$F_2(N) = \lambda_1 + \lambda_2 \text{ for } (\alpha^2 - 4\beta^2) \geq 0 \;;\; F_2(N) = a \text{ for } (\alpha^2 - 4\beta^2) < 0, \qquad (A.53)$$

In (A.52) and (A.53), λ_1, λ_2 and a are from (A.37) and (A.45). The incremental form of (A.53) can be obtained by differentiating with respect to N. Noting that F_1 and F_2 are fuctions of N, the result is

$$\left(\frac{dF_1}{dN} - \frac{12(1-\nu^2)}{Et^3}\frac{dF_2}{dN}M\right)\delta N - \frac{12(1-\nu^2)}{Et^3}F_2\delta M + F_1\delta\theta = 0, \qquad (A.54)$$

where

$$\frac{dF_1}{dN} = \frac{12(1-\nu^2)}{Et^3} \qquad \text{and}$$

$$\frac{dF_2}{dN} = \frac{3(1-\nu^2)}{2Et^3}\left[\frac{1}{\lambda_1}\left(1 + \frac{\alpha^2}{\sqrt{\alpha^4 - 16\beta^4}}\right) + \frac{1}{\lambda_2}\left(1 - \frac{\alpha^2}{\sqrt{\alpha^4 - 16\beta^4}}\right)\right] \text{ for } (\alpha^2 - 4\beta^2) \geq 0$$

$$\frac{dF_2}{dN} = \frac{3(1-\nu^2)}{2Et^3}\frac{1}{\sqrt{\alpha^2/4 + \beta^2}} \text{ for } (\alpha^2 - 4\beta^2) < 0. \qquad (A.55)$$

Normalize the variables in addition to (2.1) and (2.2) as

$$\hat{R} = \frac{R}{t} \;;\; \hat{E} = \frac{E}{2k} \;;\; \hat{\alpha} = \alpha t = \sqrt{\frac{12(1-\nu^2)}{\hat{E}\hat{N}}} \;;\; \hat{\beta} = \beta t = \sqrt{\frac{3(1-\nu^2)}{\hat{R}^2}}. \qquad (A.56)$$

In addition to (A.56), the normalized auxiliary variables are

$$\hat{\lambda_1} = \sqrt{\frac{\hat{\alpha}^2}{2} + \frac{1}{2}\sqrt{\hat{\alpha}^4 - 16\hat{\beta}^4}} \;;\; \hat{\lambda_2} = \sqrt{\frac{\hat{\alpha}^2}{2} - \frac{1}{2}\sqrt{\hat{\alpha}^4 - 16\hat{\beta}^4}} \;;\; \hat{a} = \sqrt{\frac{\hat{\alpha}^2}{4} + \hat{\beta}^2}. \qquad (A.57)$$

In terms of normalized variables, (A.54) is expressed as

$$\left(\frac{\hat{F}_1}{d\hat{N}} - \frac{3(1-\nu^2)}{\hat{E}}\frac{\hat{F}_2}{d\hat{N}}\hat{M}\right)\delta\hat{N} - \frac{3(1-\nu^2)}{\hat{E}}\hat{F}_2\delta\hat{M} + \hat{F}_1\delta\hat{\theta} = 0. \qquad (A.58)$$

In (A.58),

$$\hat{F}_1(\hat{N}) = \hat{\alpha}^2 + 2\hat{\beta}^2 \;;\; \frac{d\hat{F}_1}{d\hat{N}} = \frac{12(1-\nu^2)}{\hat{E}}. \qquad (A.59)$$

For $\hat{N} > \hat{E}/\hat{R}\sqrt{3(1-\nu^2)}$,

$$\hat{F}_2 = \hat{\lambda}_1 + \hat{\lambda}_2 \;;\; \frac{d\hat{F}_2}{d\hat{N}} = \frac{3(1-\nu^2)}{2\hat{E}}\left[\frac{1}{\hat{\lambda}_1}\left(1 + \frac{\hat{\alpha}^2}{\sqrt{\hat{\alpha}^4 - 16\hat{\beta}^4}}\right) + \frac{1}{\hat{\lambda}_2}\left(1 - \frac{\hat{\alpha}^2}{\sqrt{\hat{\alpha}^4 - 16\hat{\beta}^4}}\right)\right]. \qquad (A.60)$$

For $\hat{N} < \hat{E}/\hat{R}\sqrt{3(1-\nu^2)}$,

$$\hat{F}_2 = \hat{a} \;;\; \frac{d\hat{F}_2}{d\hat{N}} = \frac{3(1-\nu^2)}{2\hat{E}}\frac{1}{\sqrt{\hat{\alpha}^2/4 + \hat{\beta}^2}}. \qquad (A.61)$$

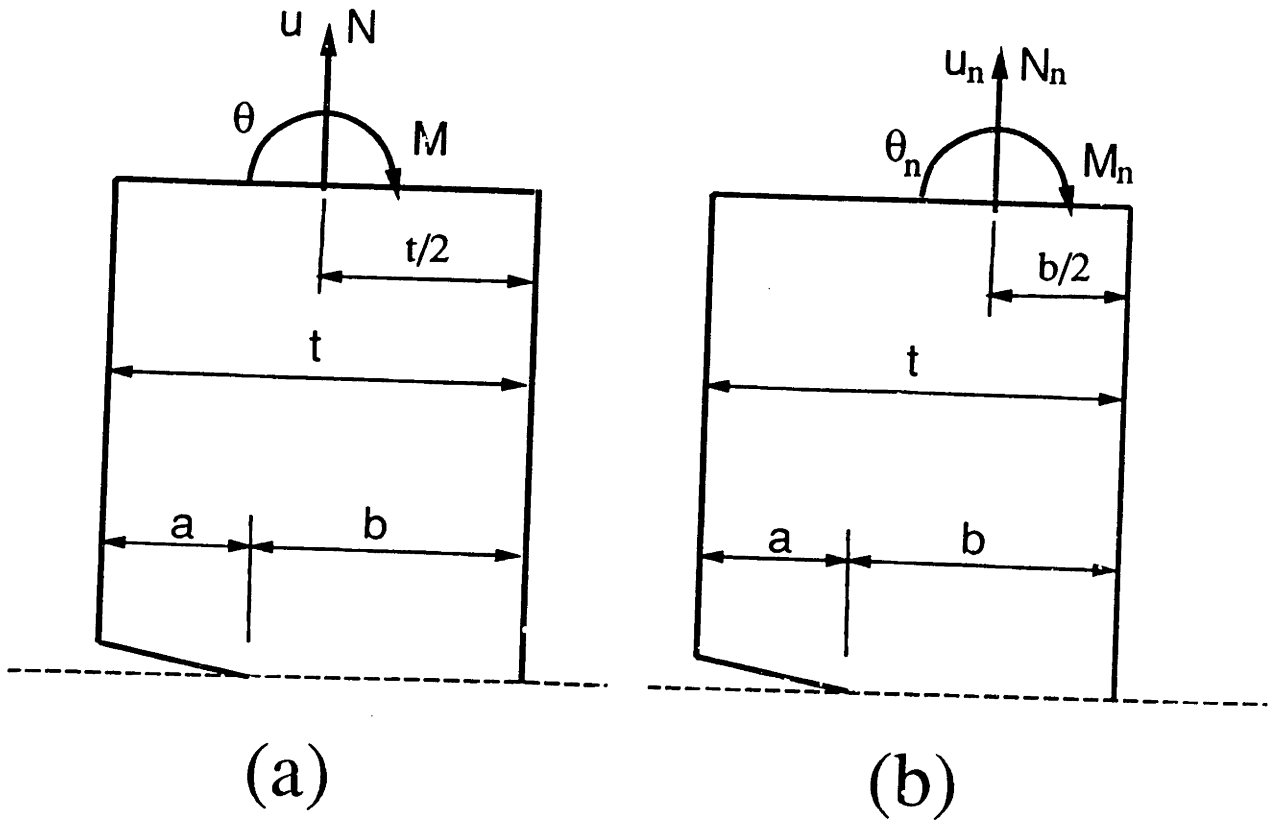

Fig. 5.1. Deep, single-face-cracked plates under combined bending and tension. Variables based (a) on a gross-section, and (b) on a net-section.

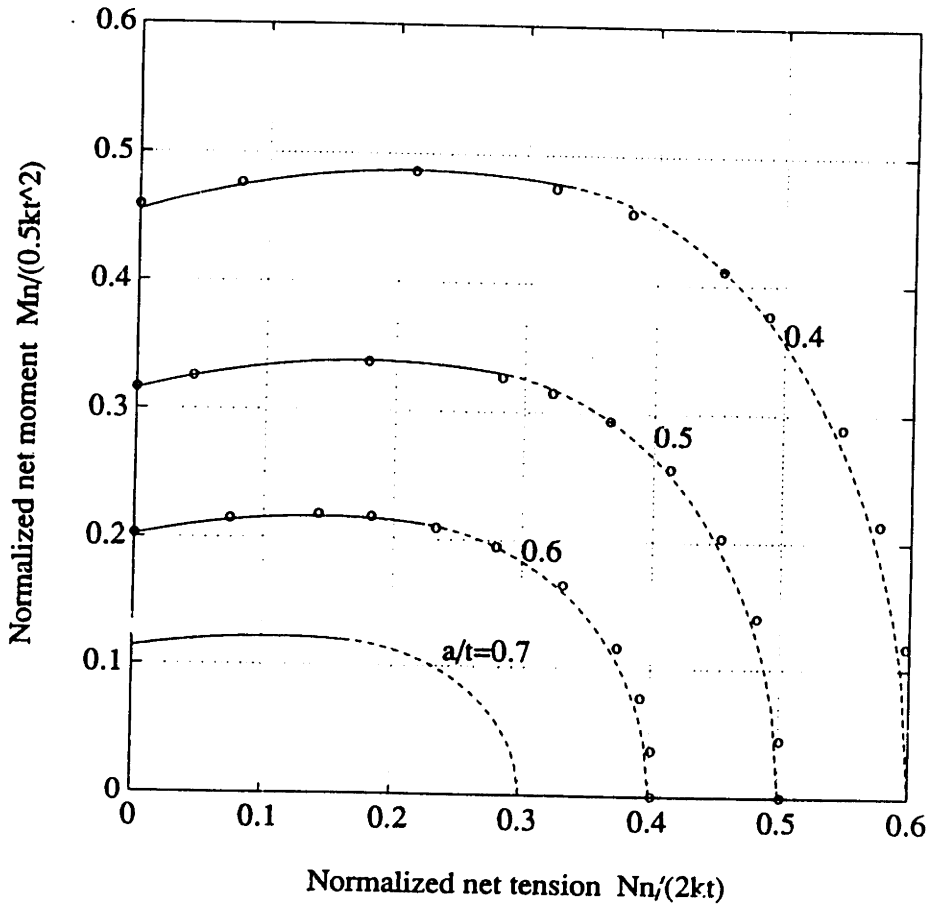

Fig. 5.2. Yield loci for various crack depths a/t of deep, single-face-cracked plates under combined bending and tension.

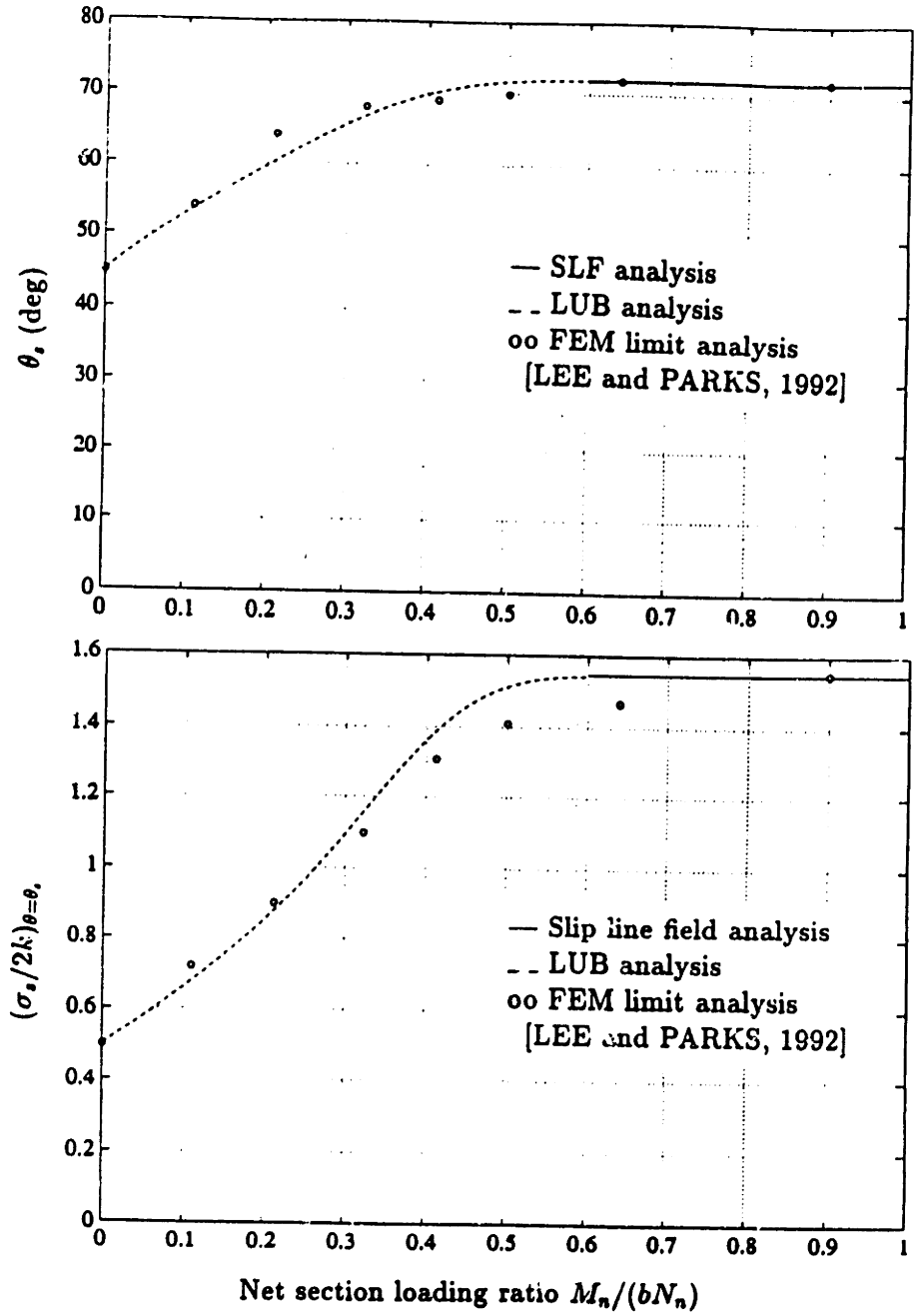

Fig. 5.2. Near tip slip angle θ_s and normal stress σ_s for deep, single-face-cracked plates under combined bending and tension.

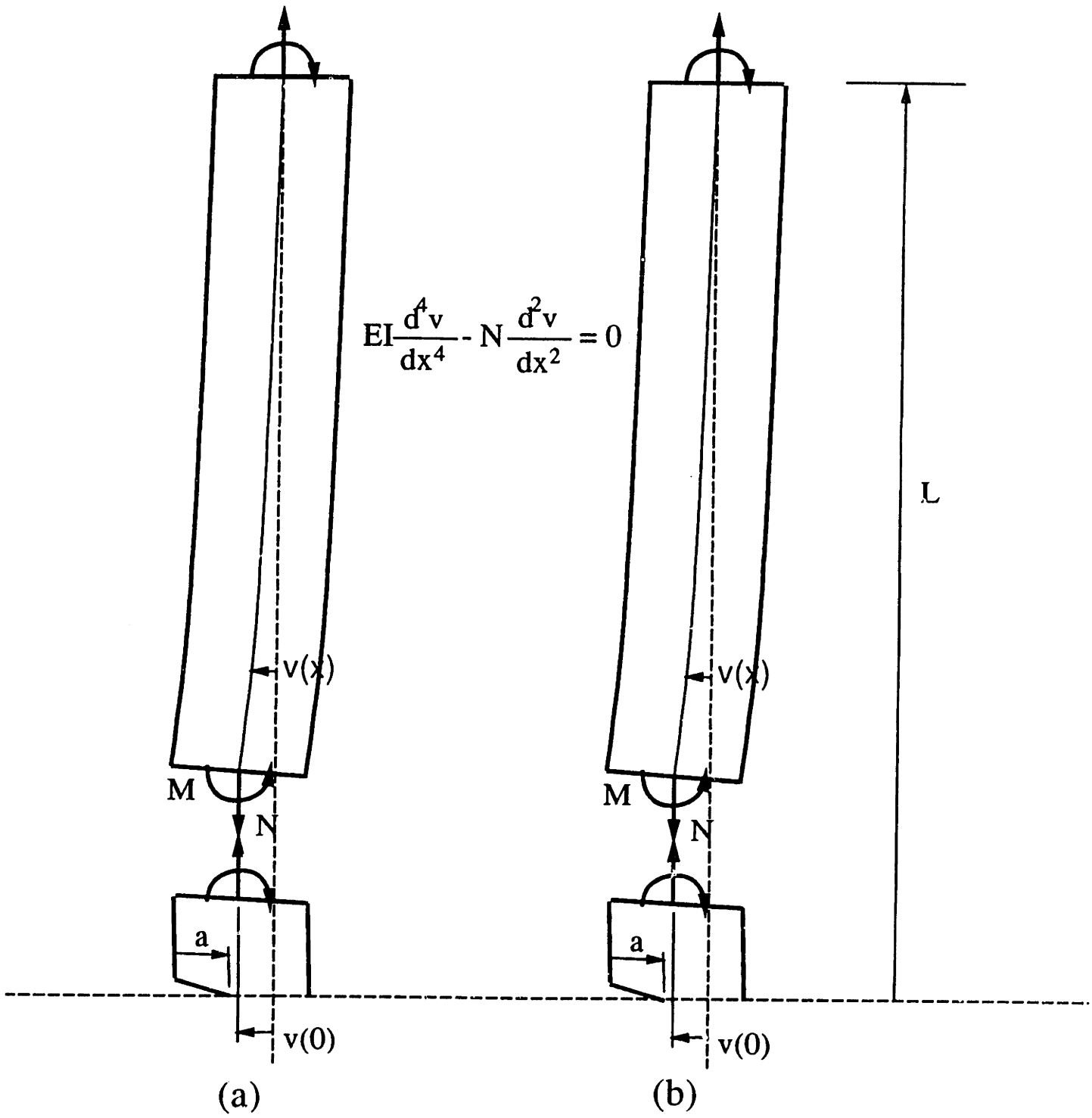

Fig. 5.5. Free body diagram (FBD) of the plate with a part-through crack subject (a) to a pin condition, and (b) to a fixed grip condition.

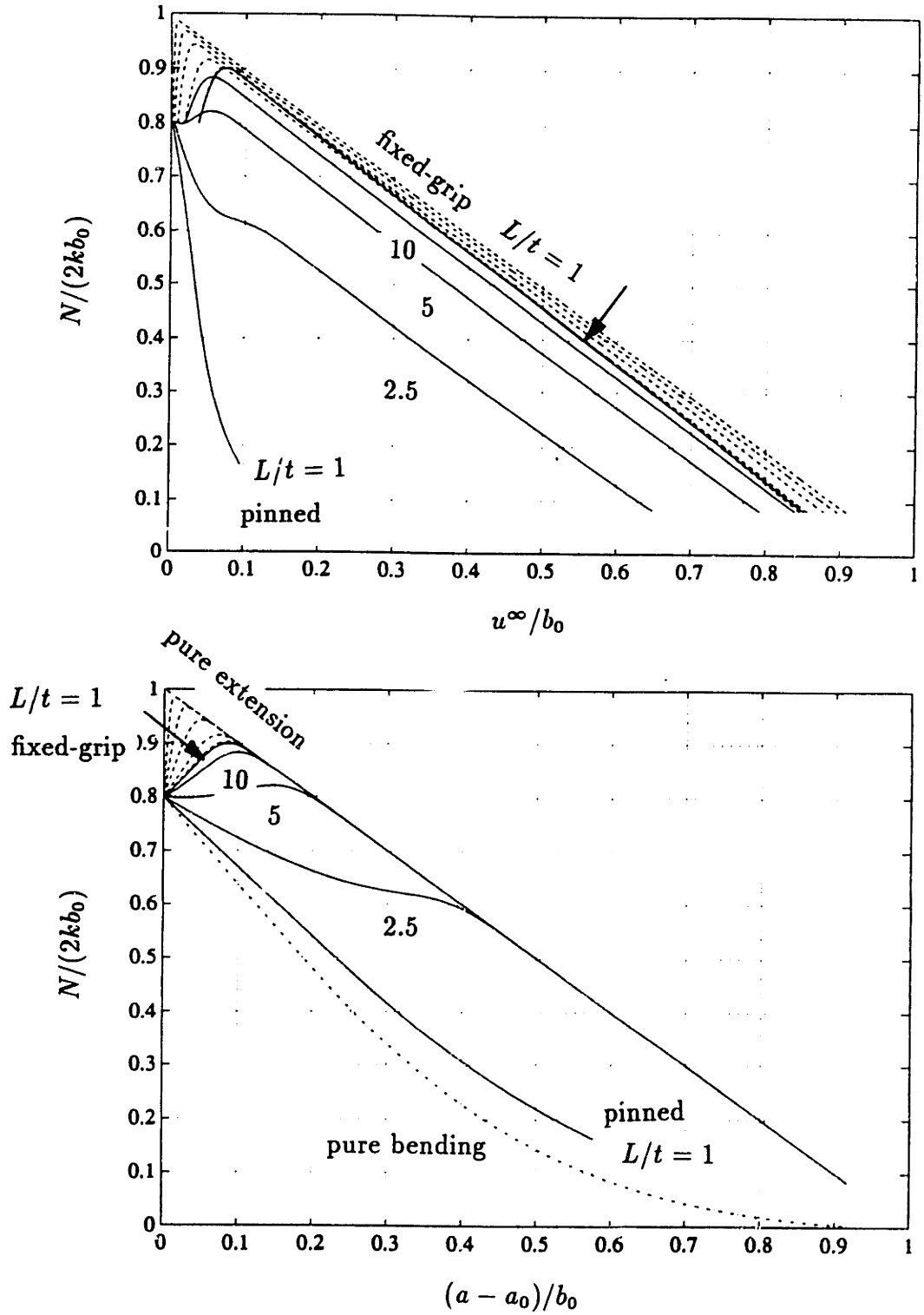

Fig. 5.5. Effect of boundary conditions and plate lengths L/t on part-through crack growth in plates.
($a_0/t = 0.4; \epsilon_y = 0.002; A = 1.175; B(\sigma_,) = 0; n = 0; L/t = 1, 2.5, 5, 10, 20$)
(a) Tensile force $N/(2kb_0)$ vs. Far-field displacement u^∞/b_0.
(b) Tensile force $N/(2kb_0)$ vs. Crack growth amount $(a - a_0)/b_0$.

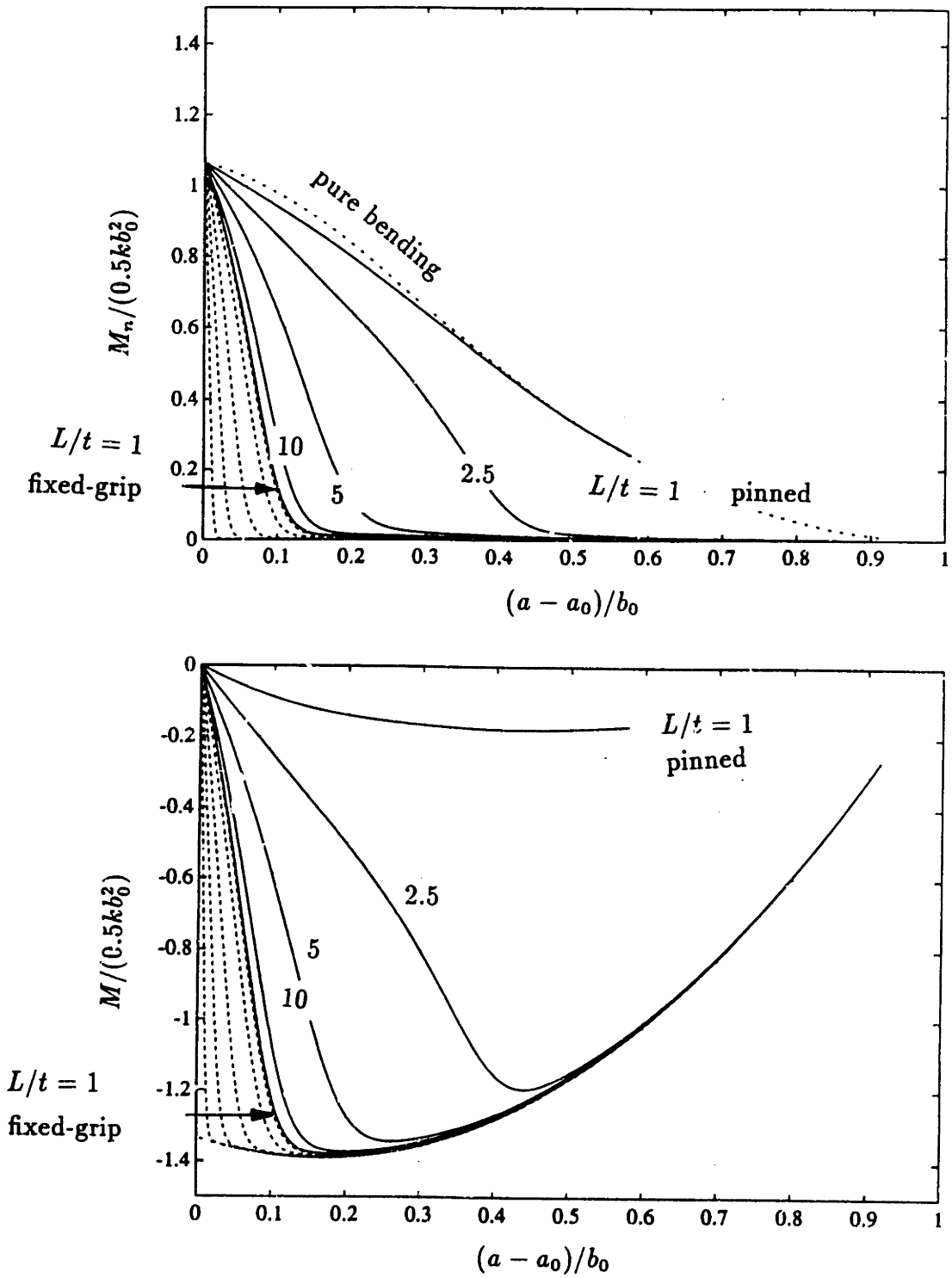

Fig. 5.5. Effect of boundary conditions and plate lengths L/t on part-through crack growth in plates.
($a_0/t = 0.4; \epsilon_y = 0.002; A = 1.175; B(\sigma_s) = 0; n = 0; L/t = 1, 2.5, 5, 10, 20$)
(c) Net moment $M_n/(0.5kb_0^2)$ vs. Crack growth amount $(a - a_0)/b_0$.
(d) Gross moment $M/(0.5kb_0^2)$ vs. Crack growth amount $(a - a_0)/b_0$.

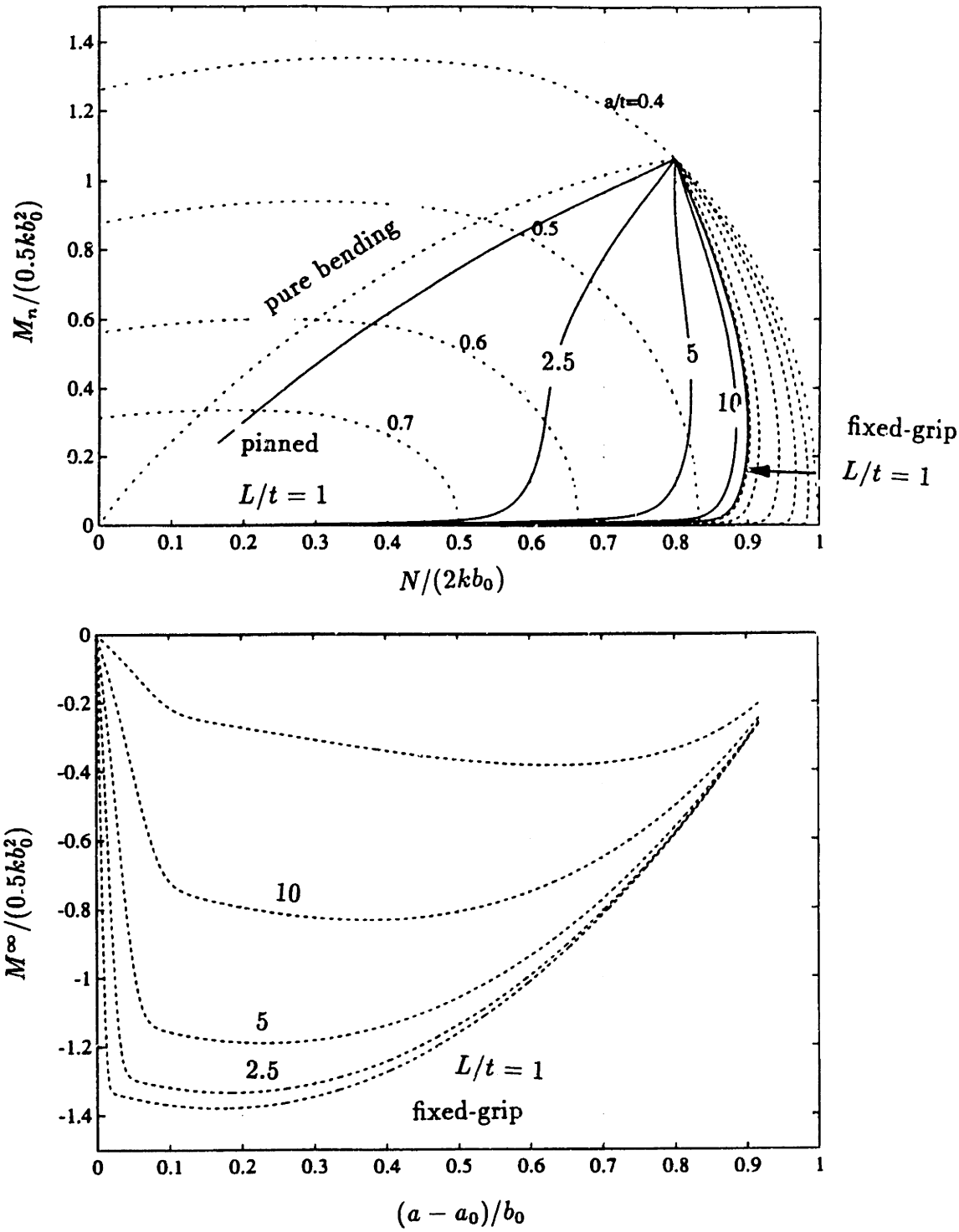

Fig. 5.5. Effect of boundary conditions and plate lengths L/t on part-through crack growth in plates.
($a_0/t = 0.4; \epsilon_y = 0.002; A = 1.175; B(\sigma_s) = 0; n = 0; L/t = 1, 2.5, 5, 10, 20$)
(e) Gross moment $M/(0.5kb_0^2)$ vs. Tensile force $N/(2kb_0)$.
(f) Far-field moment $M^\infty/(0.5kb_0^2)$ vs. Crack growth amount $(a - a_0)/b_0$.

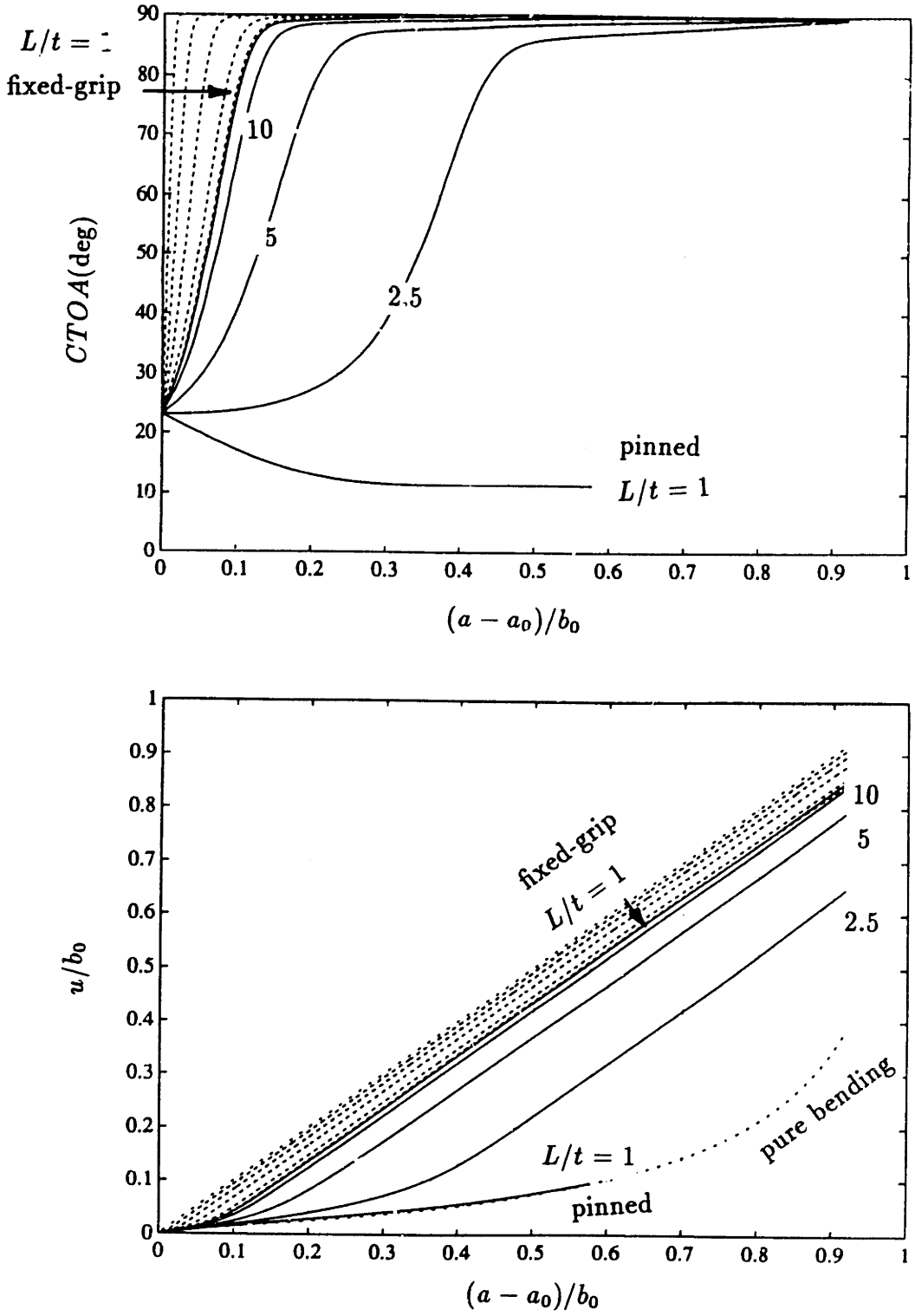

Fig. 5.5. Effect of boundary conditions and plate lengths L/t on part-through crack growth in plates.
($a_0/t = 0.4; \epsilon_y = 0.002; A = 1.175; B(\sigma_s) = 0; n = 0; L/t = 1, 2.5, 5, 10, 20$)
(g) Crack tip opening angle $CTOA$ (deg) vs. Crack growth amount $(a - a_0)/b_0$.
(h) Displacement u/b_0 vs. Crack growth amount $(a - a_0)/b_0$.

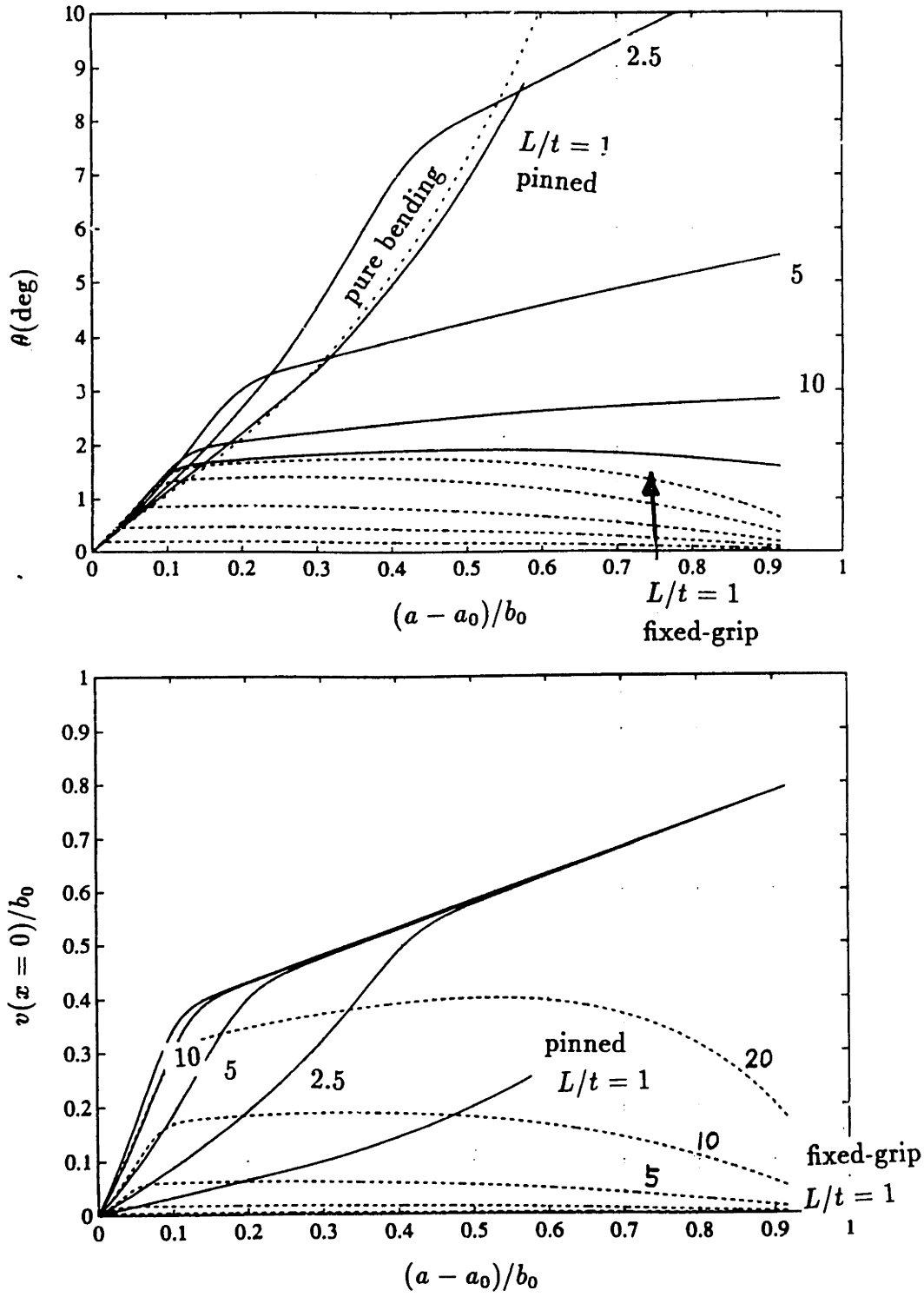

Fig. 5.5. Effect of boundary conditions and plate lengths L/t on part-through crack growth in plates.
($a_0/t = 0.4; \epsilon_y = 0.002; A = 1.175; B(\sigma_s) = 0; n = 0; L/t = 1, 2.5, 5, 10, 20$)
(i) Rotation θ (deg) vs. Crack growth amount $(a - a_0)/b_0$.
(j) Cracked part deflection $v(x = 0)/b_0$ vs. Crack growth amount $(a - a_0)/b_0$.

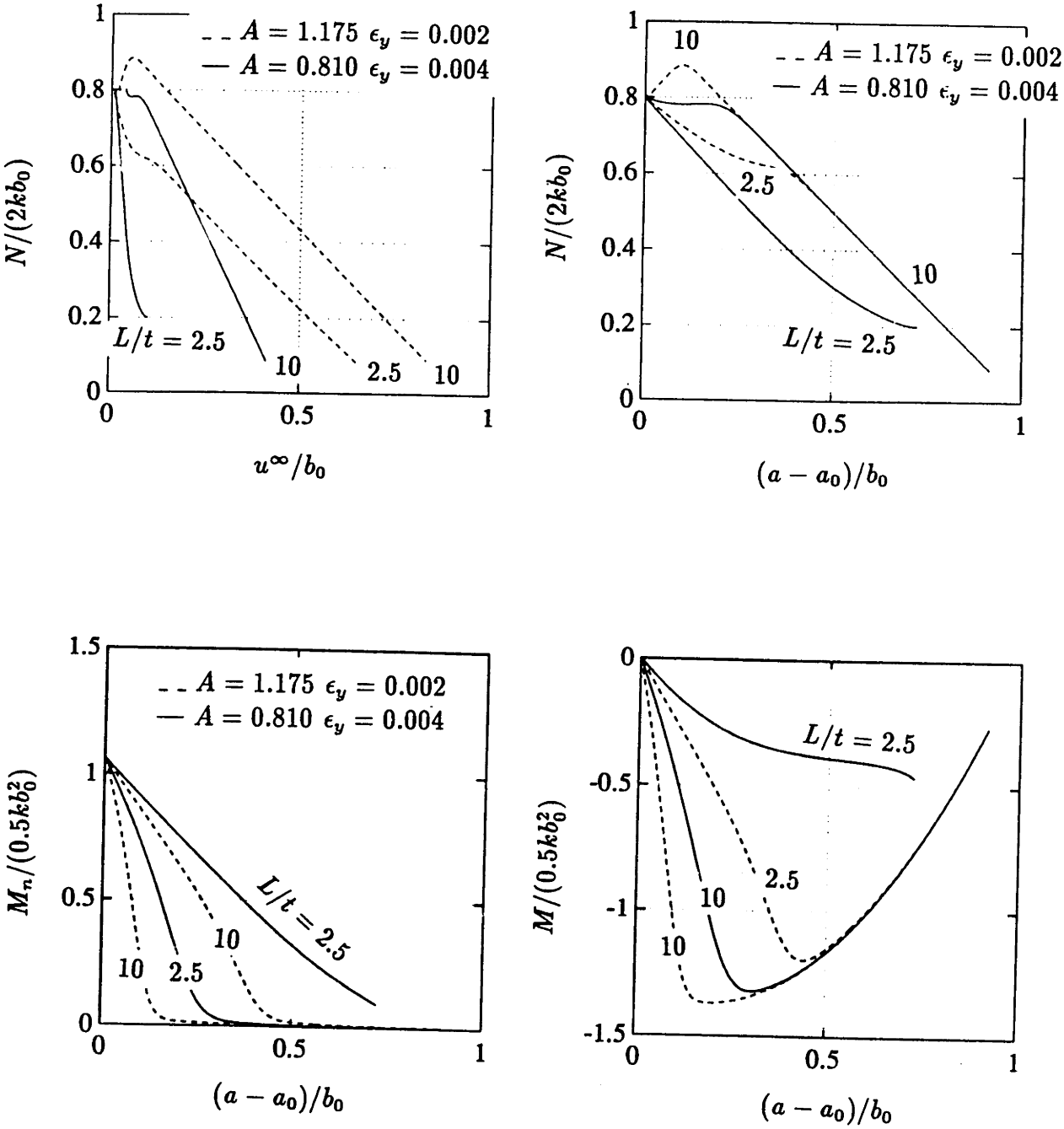

Fig. 5.6. Effect of material ductility on part-through crack growth in plates under pinned conditions ($a_0/t = 0.4; B(\sigma_s) = 0; n = 0$).
(a) Tensile force $N/(2kb_0)$ vs. Far-field displacement u^∞/b_0.
(b) Tensile force $N/(2kb_0)$ vs. Crack growth amount $(a - a_0)/b_0$.
(c) Net moment $M_n/(0.5kb_0^2)$ vs. Crack growth amount $(a - a_0)/b_0$.
(d) Gross moment $M/(0.5kb_0^2)$ vs. Crack growth amount $(a - a_0)/b_0$.

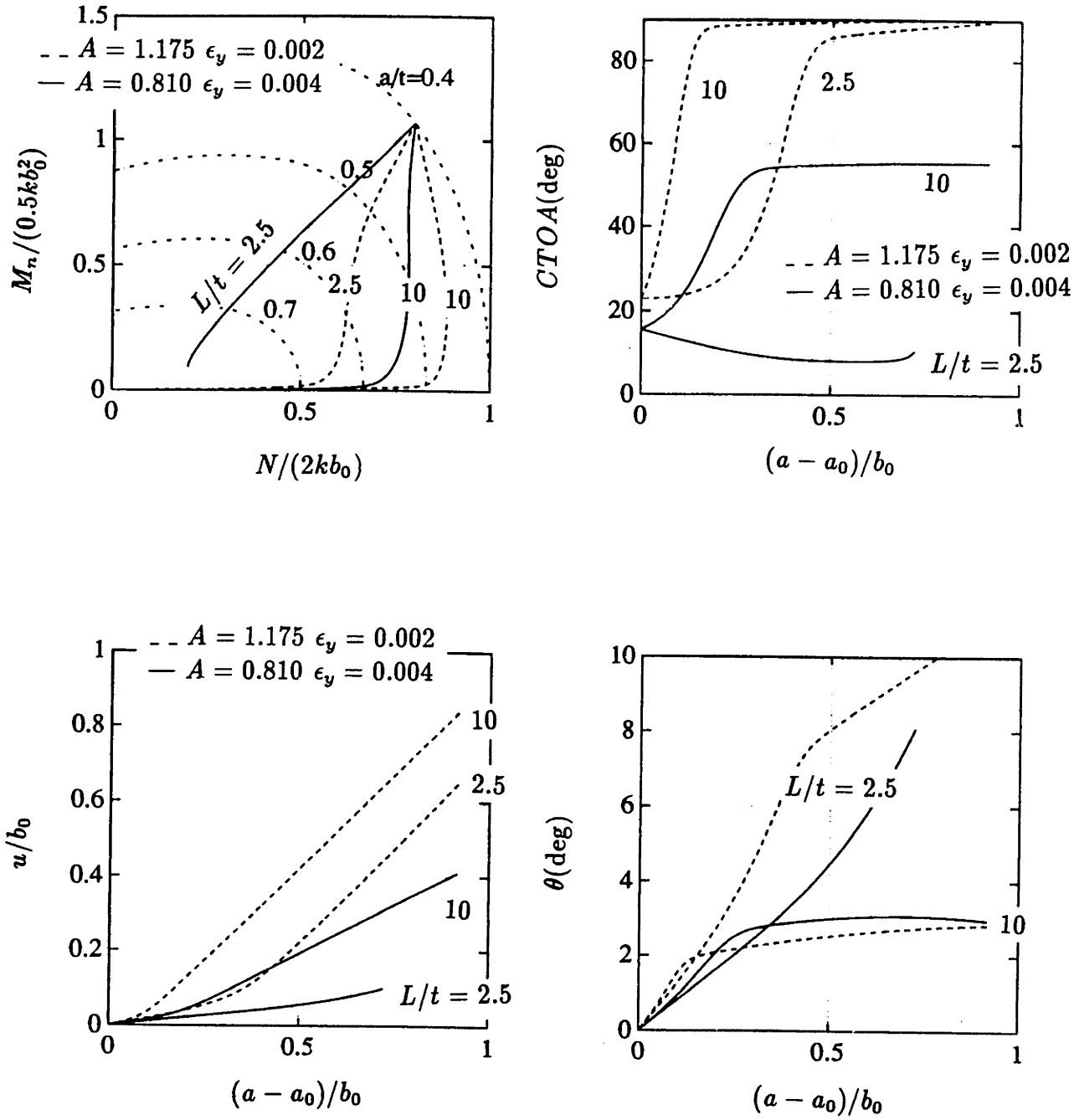

Fig. 5.6. Effect of material ductility on part-through crack growth in plates. under pinned conditions ($a_0/t = 0.4; B(\sigma_s) = 0; n = 0$).
(e) Gross moment $M/(0.5kb_0^2)$ vs. Tensile force $N/(2kb_0)$.
(f) Crack tip opening angle $CTOA$ (deg) vs. Crack growth amount $(a - a_0)/b_0$.
(g) Displacement u/b_0 vs. Crack growth amount $(a - a_0)/b_0$.
(h) Rotation θ (deg) vs. Crack growth amount $(a - a_0)/b_0$.

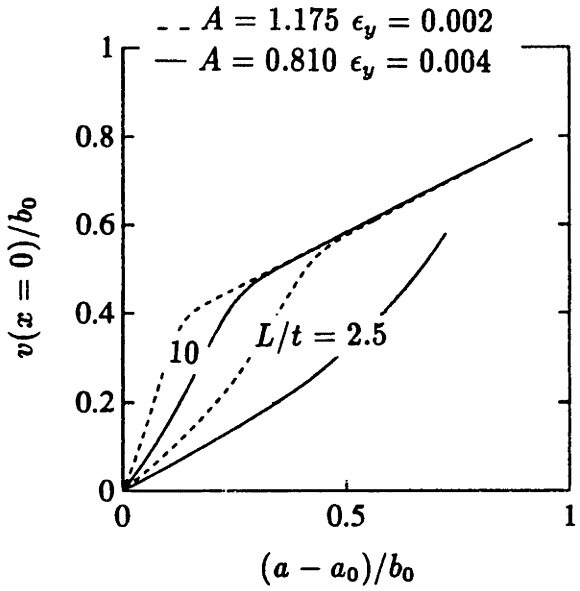

Fig. 5.6. Effect of material ductility on part-through crack growth in plates. under pinned conditions ($a_0/t = 0.4; B(\sigma_s) = 0; n = 0$).
(i) Cracked part deflection $v(x=0)/b_0$ vs. Crack growth amount $(a-a_0)/b_0$.

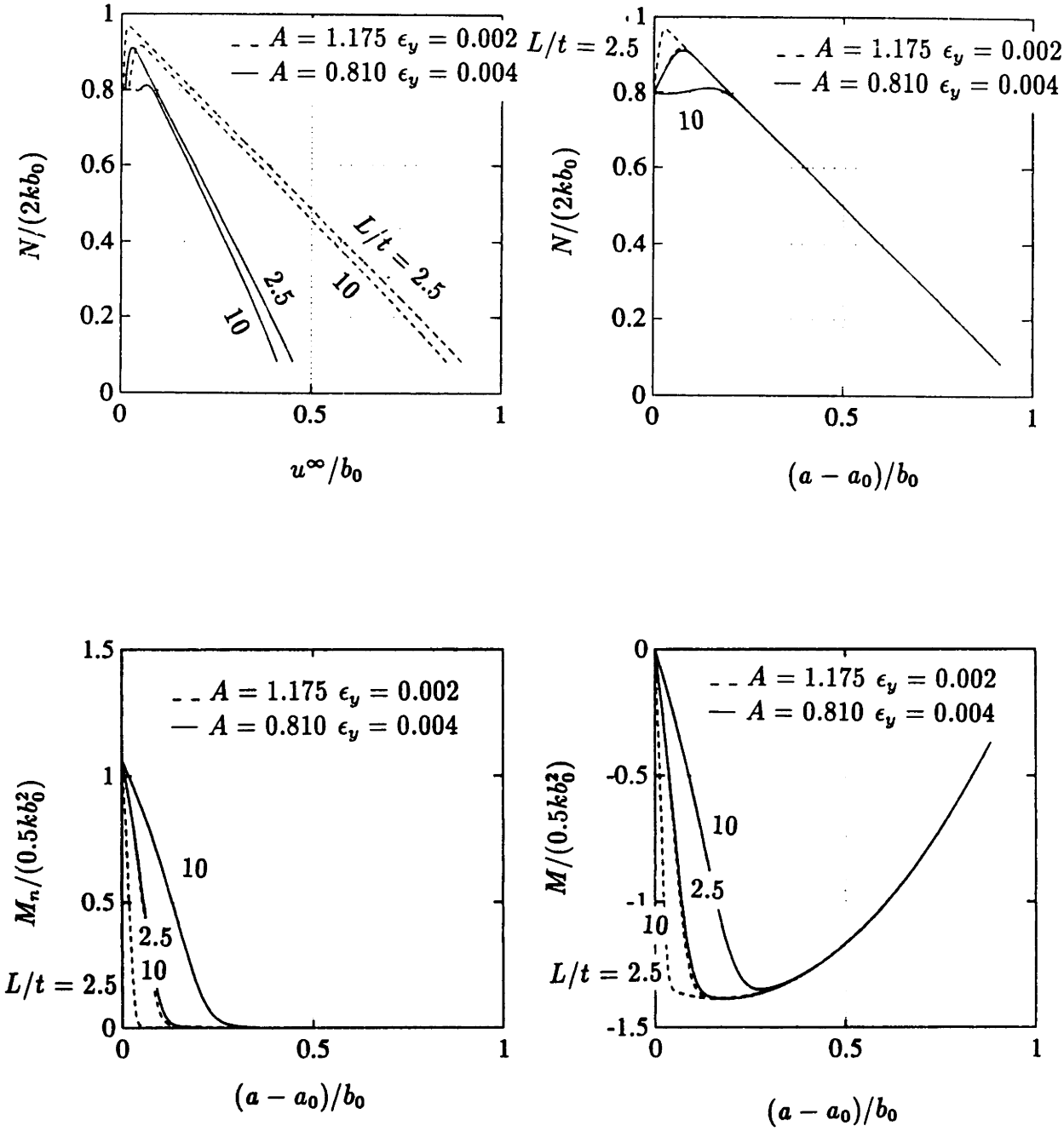

Fig. 5.7. Effect of material ductility on part-through crack growth in plates under fixed-grip conditions ($a_0/t = 0.4$; $B(\sigma_s) = 0; n = 0$).
(a) Tensile force $N/(2kb_0)$ vs. Far-field displacement u^∞/b_0.
(b) Tensile force $N/(2kb_0)$ vs. Crack growth amount $(a - a_0)/b_0$.
(c) Net moment $M_n/(0.5kb_0^2)$ vs. Crack growth amount $(a - a_0)/b_0$.
(d) Gross moment $M/(0.5kb_0^2)$ vs. Crack growth amount $(a - a_0)/b_0$.

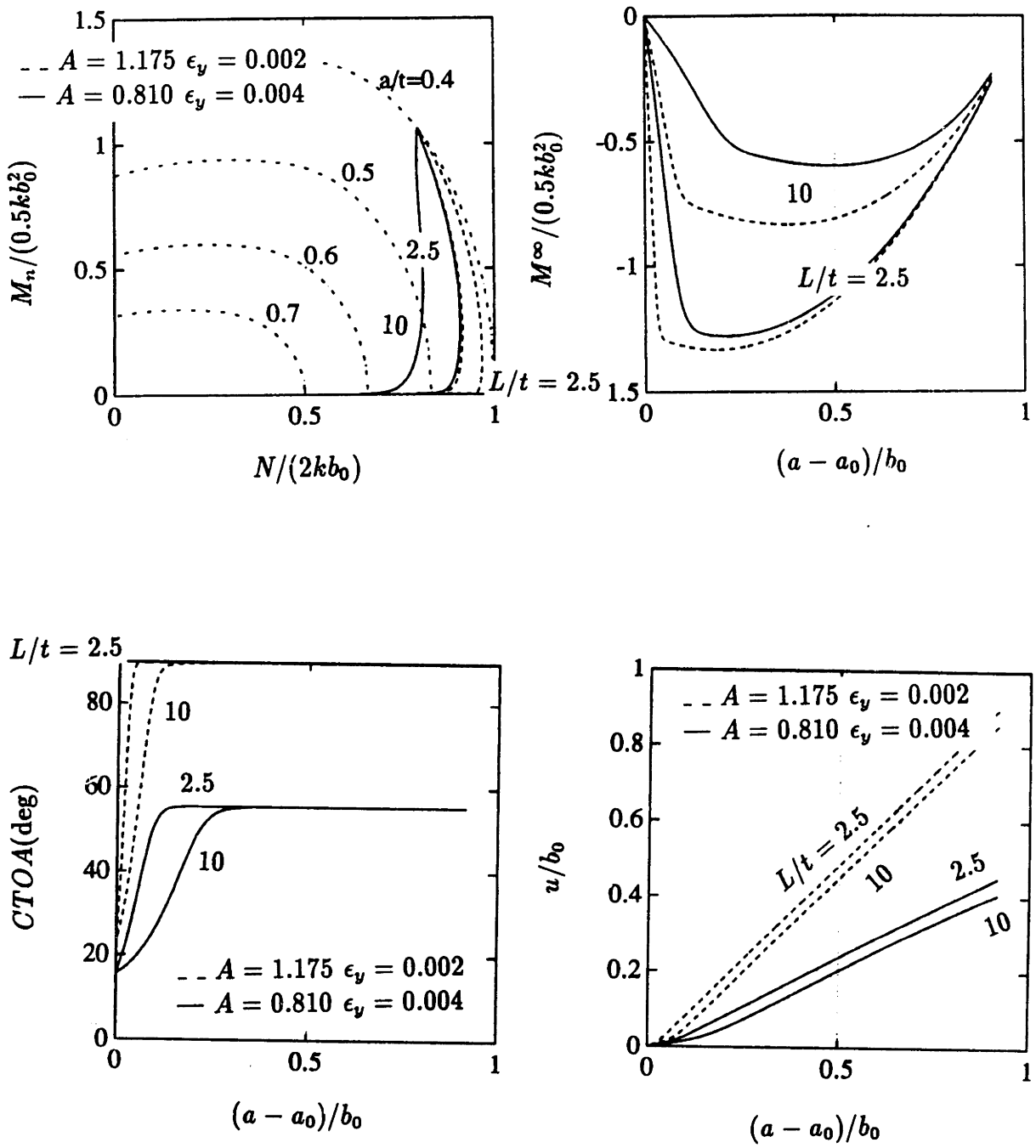

Fig. 5.7. Effect of material ductility on part-through crack growth in plates. under fixed-grip conditions ($a_0/t = 0.4; B(\sigma_s) = 0; n = 0$).
(e) Gross moment $M/(0.5kb_0^2)$ vs. Tensile force $N/(2kb_0)$.
(f) Far-field moment $M^\infty/(0.5kb_0^2)$ vs. Crack growth amount $(a - a_0)/b_0$.
(g) Crack tip opening angle $CTOA$ (deg) vs. Crack growth amount $(a - a_0)/b_0$.
(h) Displacement u/b_0 vs. Crack growth amount $(a - a_0)/b_0$.

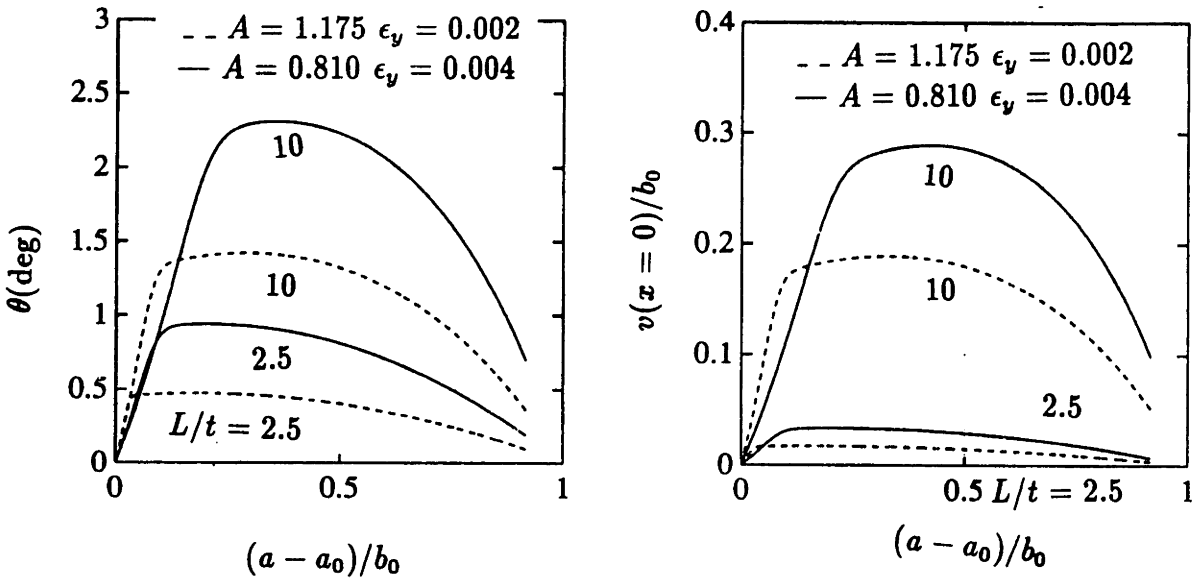

Fig. 5.7. Effect of material ductility on part-through crack growth in plates.
under fixed-grip conditions ($a_0/t = 0.4; B(\sigma_s) = 0; n = 0$).
(i) Rotation θ (deg) vs. Crack growth amount $(a - a_0)/b_0$.
(j) Cracked part deflection $v(x = 0)/b_0$ vs. Crack growth amount $(a - a_0)/b_0$.

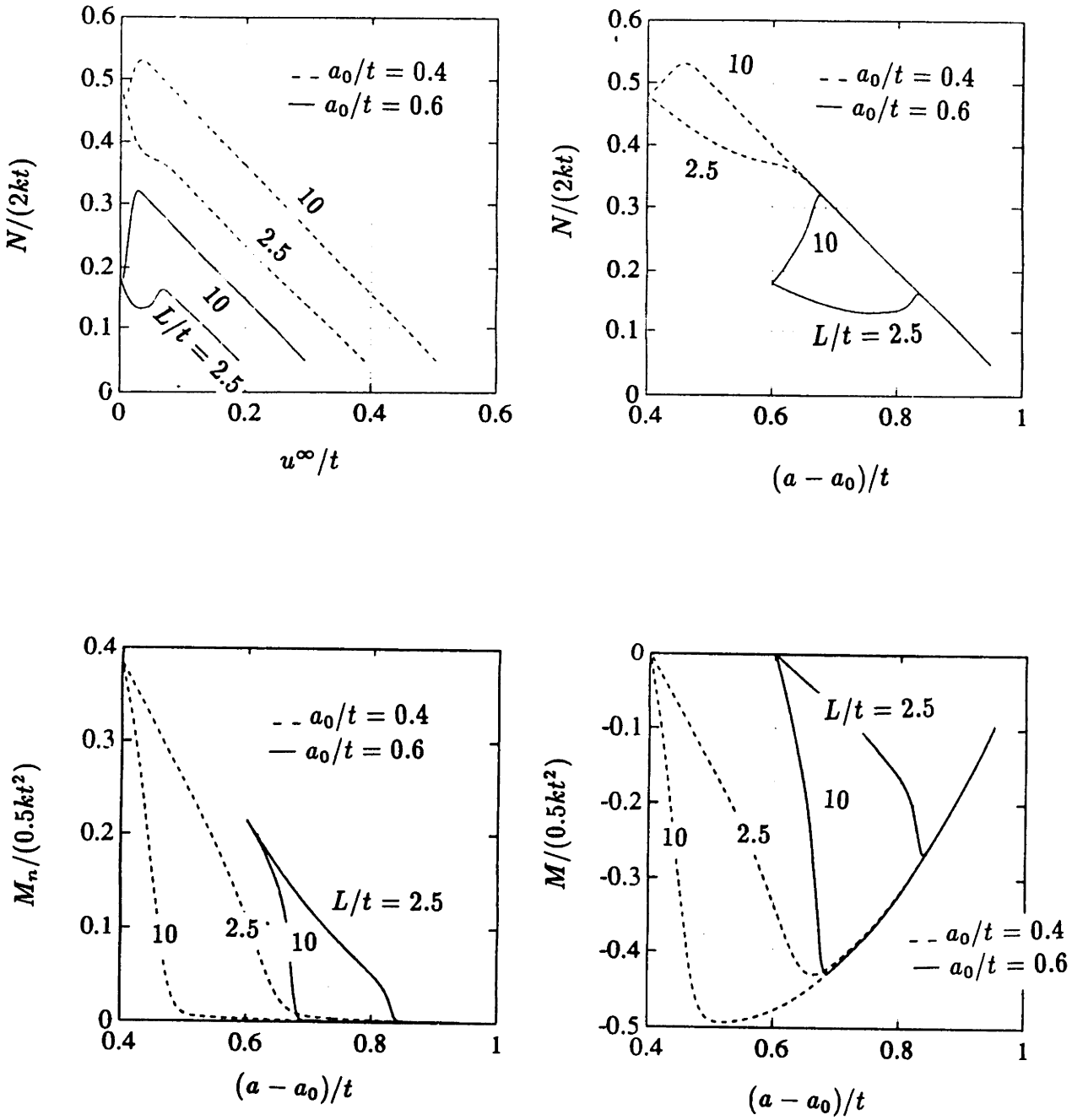

Fig. 5.8. Effect of initial crack depths a_0/t on part-through crack growth in plates under pinned conditions ($\epsilon_y = 0.002; A = 1.175; B(\sigma_s) = 0; n = 0$).
(a) Tensile force $N/(2kt)$ vs. Far-field displacement u^∞/t.
(b) Tensile force $N/(2kt)$ vs. Crack growth amount a/t.
(c) Net moment $M_n/(0.5kt^2)$ vs. Crack growth amount a/t.
(d) Gross moment $M/(0.5kt^2)$ vs. Crack growth amount a/t.

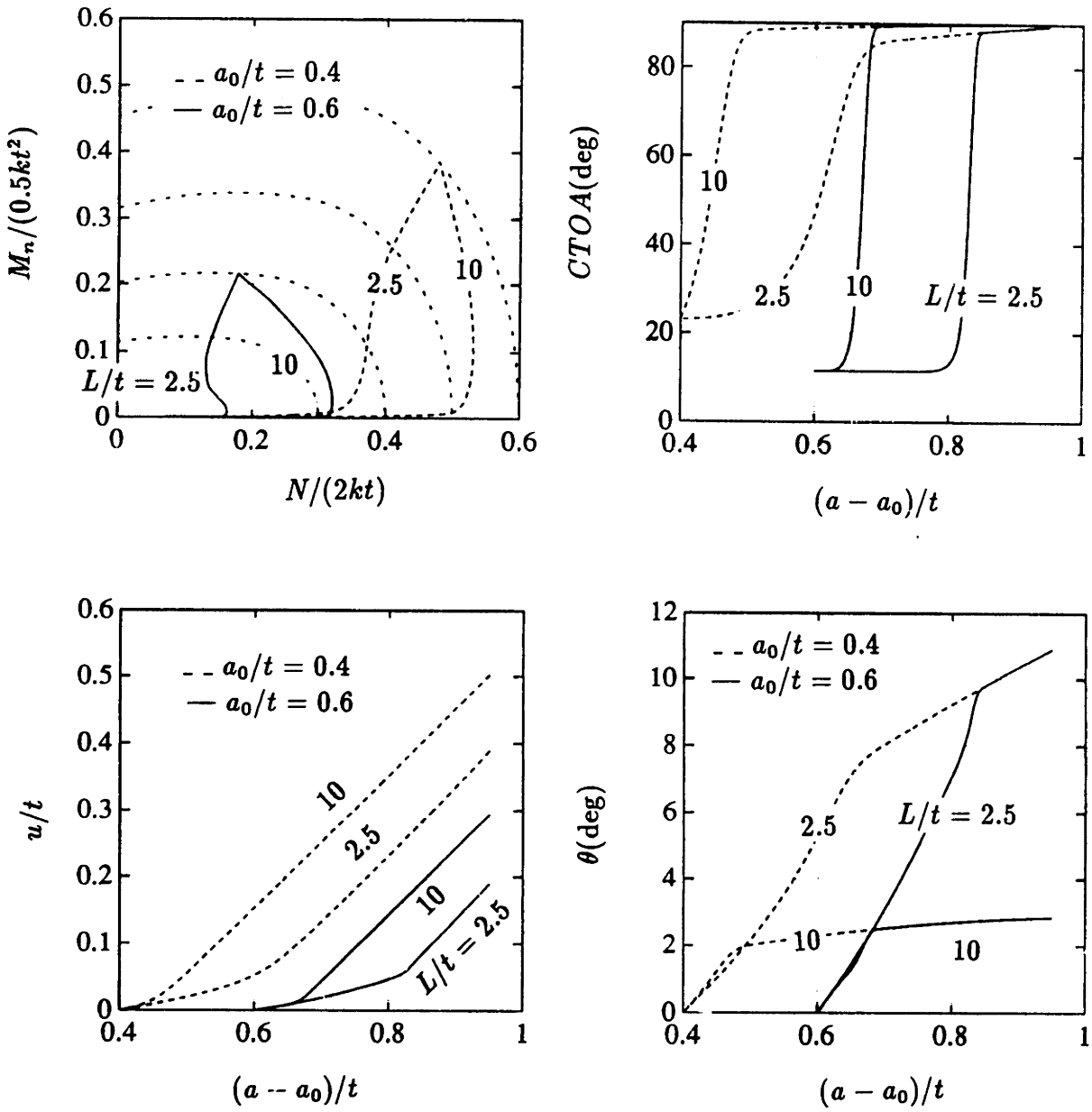

Fig. 5.8. Effect of initial crack depths a_0/t on part-through crack growth in plates under pinned conditions ($\epsilon_y = 0.002$; $A = 1.175$; $B(\sigma_s) = 0$; $n = 0$).
(e) Gross moment $M/(0.5kt^2)$ vs. Tensile force $N/(2kt)$.
(f) Crack tip opening angle $CTOA$ (deg) vs. Crack growth amount a/t.
(g) Displacement u/t vs. Crack growth amount a/t.
(h) Rotation θ (deg) vs. Crack growth amount a/t.

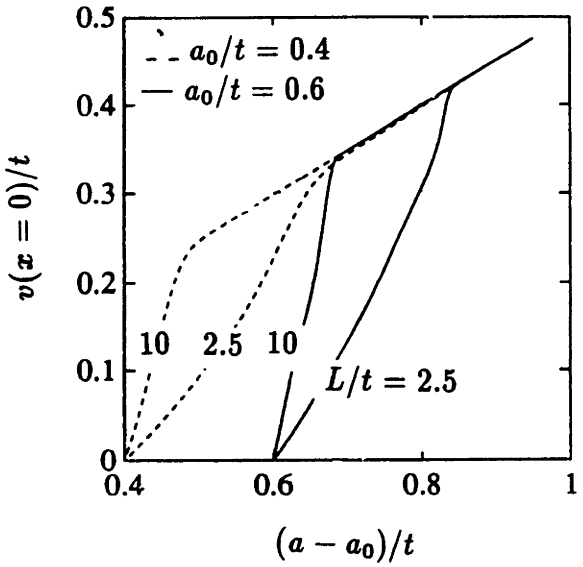

Fig. 5.8. Effect of initial crack depths a_0/t on part-through crack growth in plates under pinned conditions ($\epsilon_y = 0.002; A = 1.175; B(\sigma_s) = 0; n = 0$).
(i) Cracked part deflection $v(x=0)/t$ vs. Crack growth amount a/t.

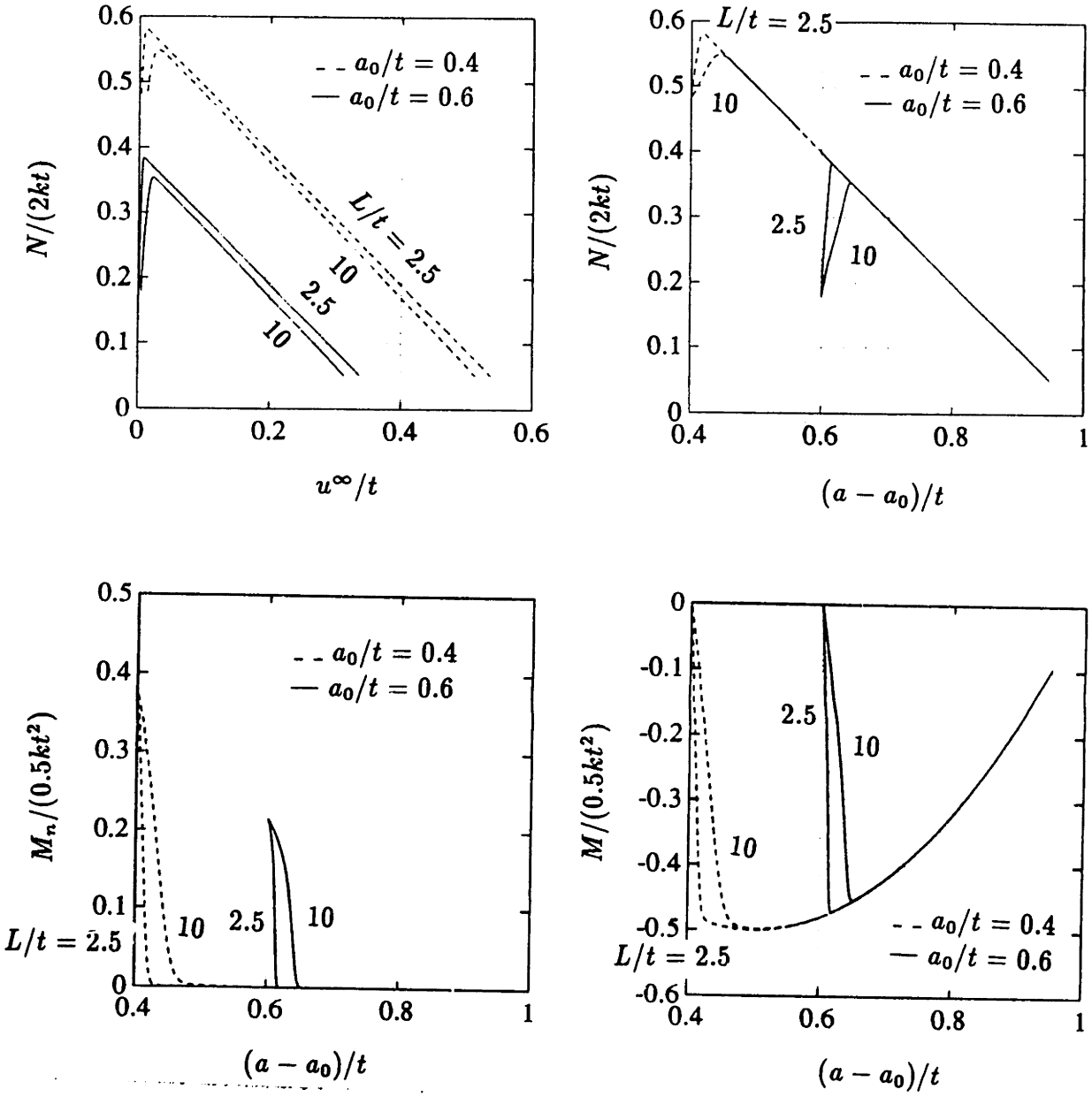

Fig. 5.9. Effect of initial crack depths a_0/t on part-through crack growth in plates under fixed-grip conditions ($\epsilon_y = 0.002; A = 1.175; B(\sigma_s) = 0; n = 0$).
(a) Tensile force $N/(2kt)$ vs. Far-field displacement u^∞/t.
(b) Tensile force vs. Crack growth amount a/t.
(c) Net moment $M_n/(0.5kt^2)$ vs. Crack growth amount a/t.
(d) Gross moment $M/(0.5kt^2)$ vs. Crack growth amount a/t.

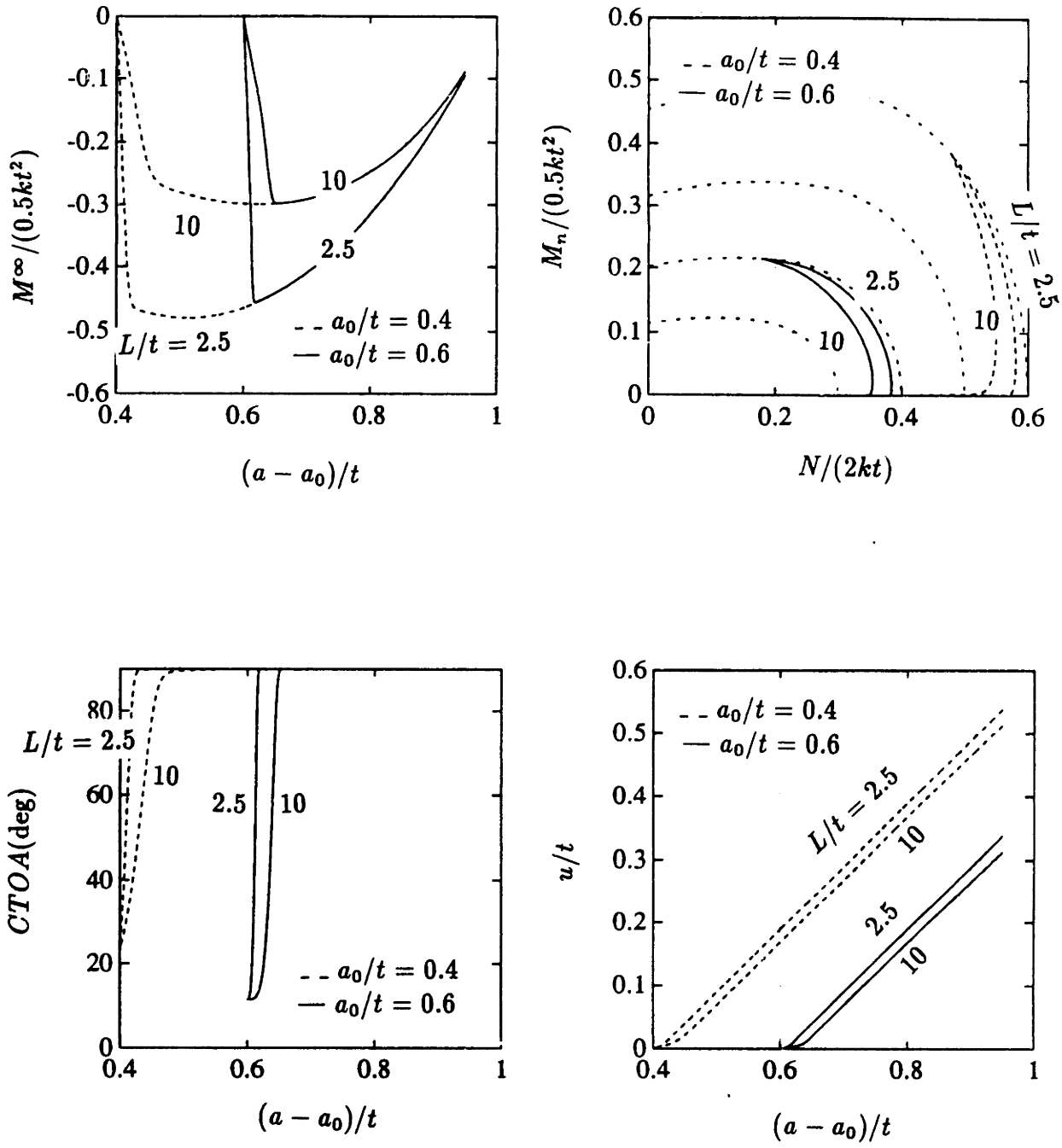

Fig. 5.9. Effect of initial crack depths a_0/t on part-through crack growth in plates. under fixed-grip conditions ($\epsilon_y = 0.002; A = 1.175; B(\sigma_s) = 0; n = 0$).
(e) Gross moment $M/(0.5kt^2)$ vs. Tensile force $N/(2kt)$.
(f) Far-field moment $M^\infty/(0.5kt^2)$ vs. Crack growth amount a/t.
(g) Crack tip opening angle $CTOA$ (deg) vs. Crack growth amount a/t.
(h) Displacement u/t vs. Crack growth amount a/t.

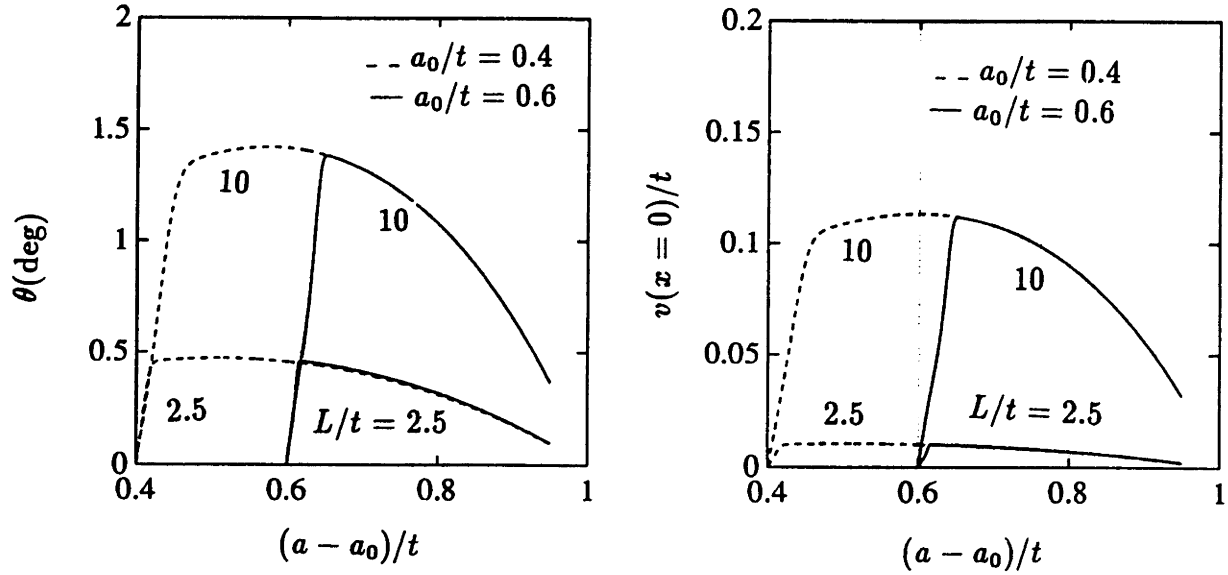

Fig. 5.9. Effect of initial crack depths a_0/t on part-through crack growth in plates. under fixed-grip conditions ($\epsilon_y = 0.002; A = 1.175; B(\sigma_s) = 0; n = 0$).
(i) Rotation θ (deg) vs. Crack growth amount a/t.
(j) Cracked part deflection $v(x = 0)/t$ vs. Crack growth amount a/t.

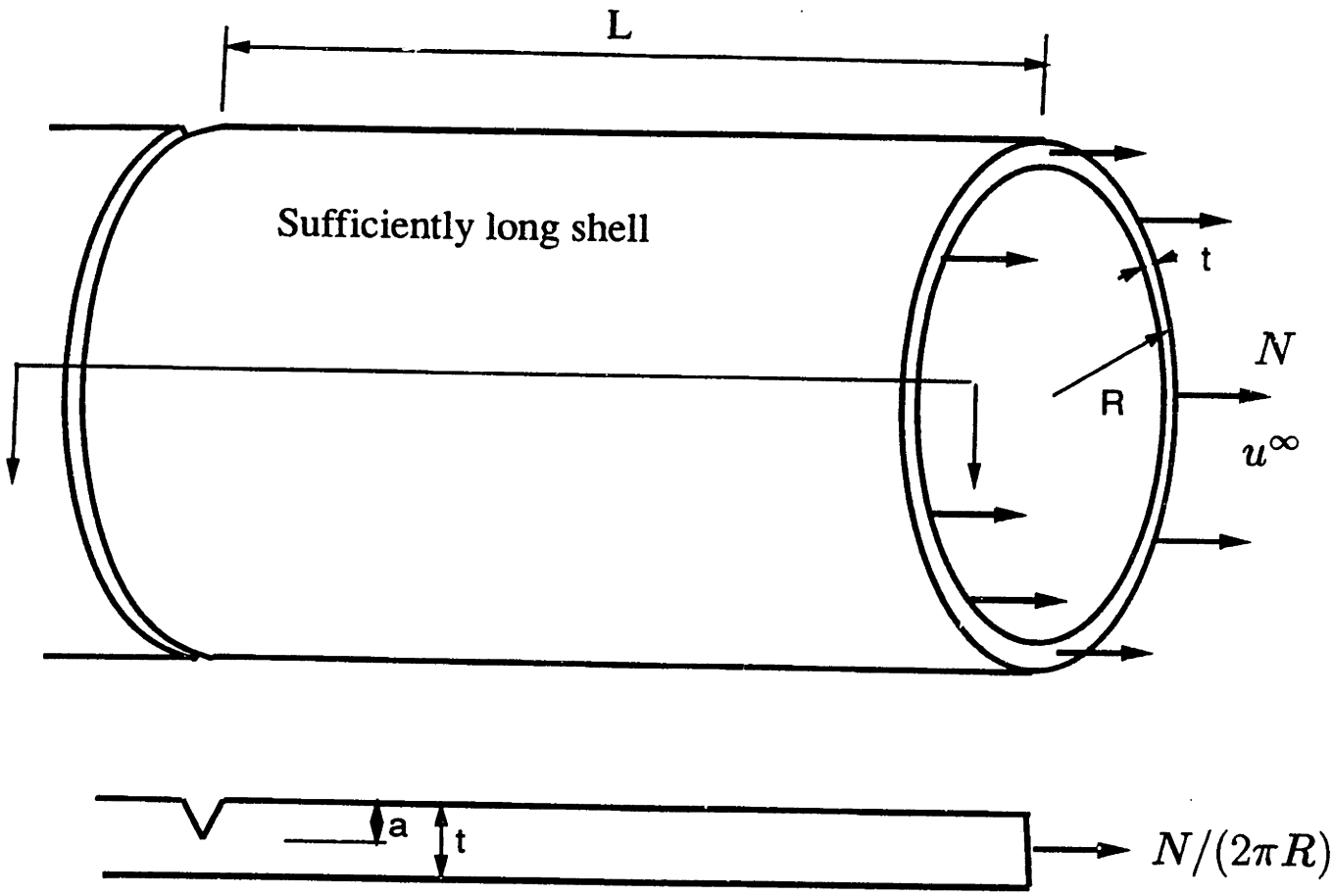

Fig. 5.10. Shell with a completely circumferential crack; subject to axial Tensile force.

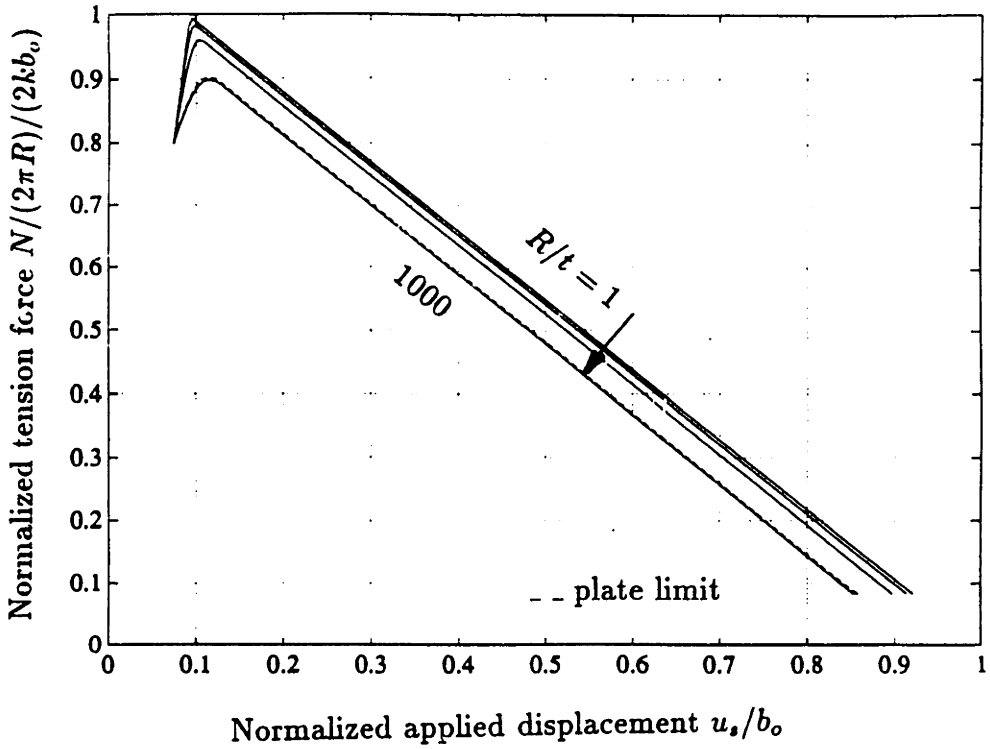

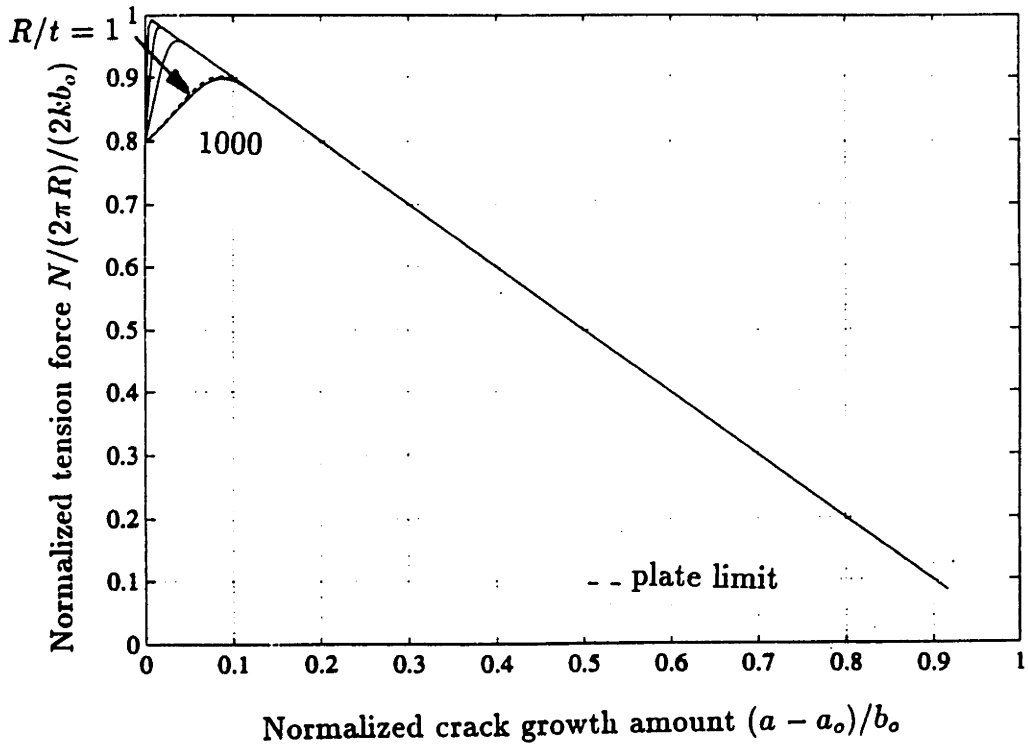

Fig. 5.11. Effect of shell radius R/t on crack growth of completely circumferential cracks in sufficiently long shells.
$(L/t = 40; a_0/t = 0.4; \epsilon_y = 0.002; A = 1.175; B(\sigma_s) = 0; n = 0; R/t = 1, 10, 100, 1000)$
(a) Tensile force $N/(2\pi R)/(2kb_0)$ vs. Far-field displacement u^∞/b_0.
(b) Tensile force $N/(2\pi R)/(2kb_0)$ vs. Crack growth amount $(a - a_0)/b_0$.

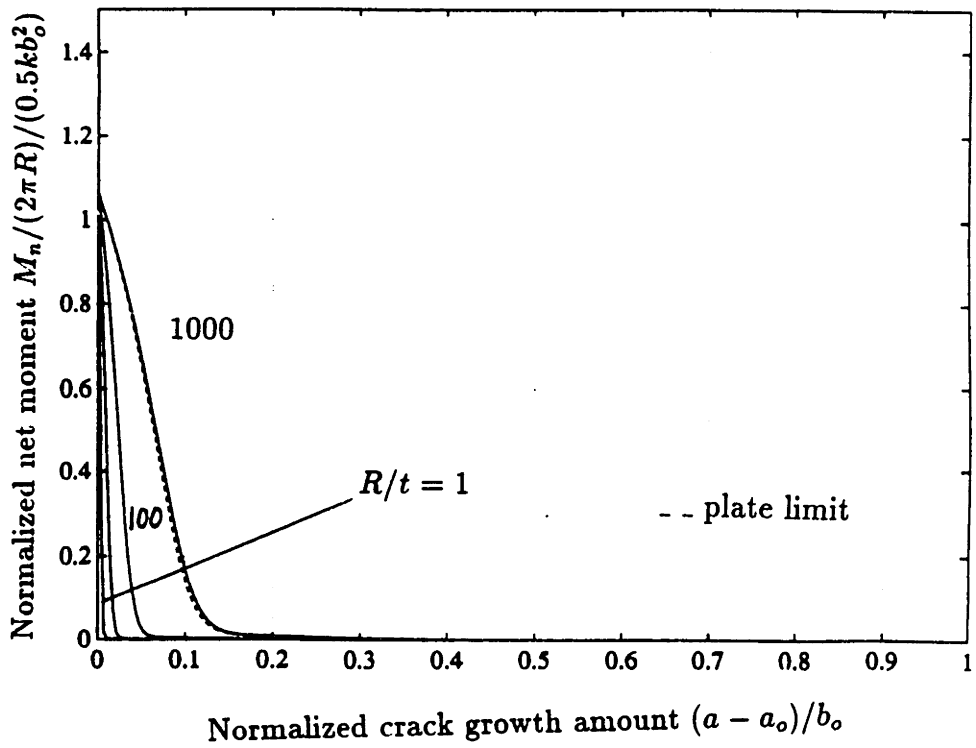

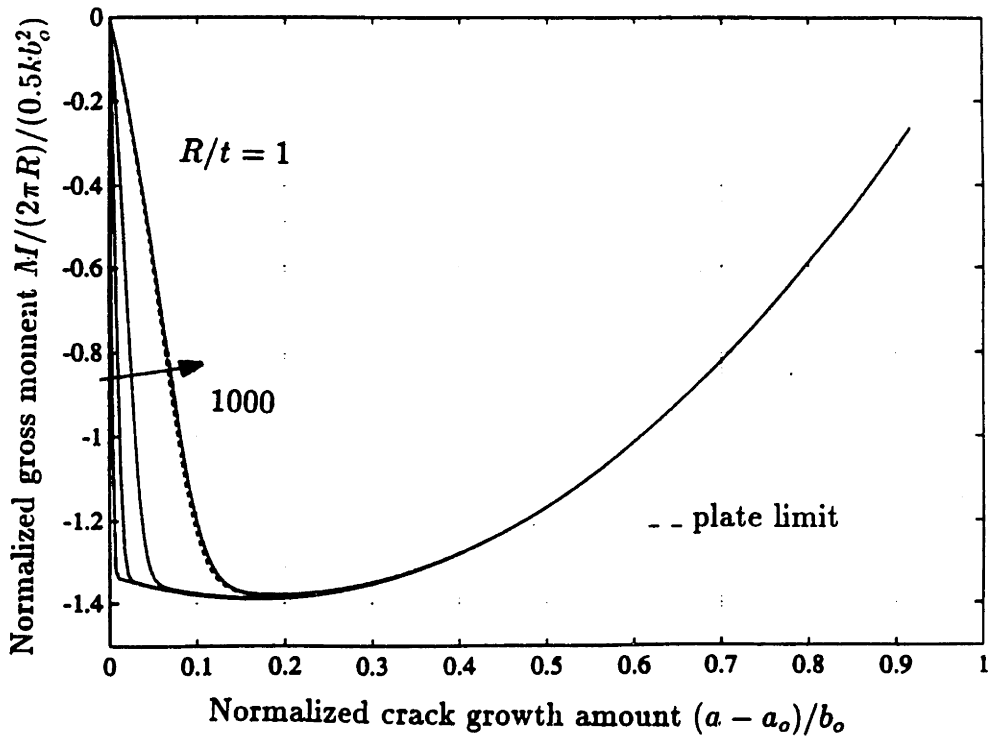

Fig. 5.11. Effect of shell radius R/t on crack growth of completely circumferential cracks in sufficiently long shells.
$(L/t = 40; a_0/t = 0.4; \epsilon_y = 0.002; A = 1.175; B(\sigma_s) = 0; n = 0; R/t = 1, 10, 100, 1000)$
(c) Net moment $M_n/(2\pi R)/(0.5kb_0^2)$ vs. Crack growth amount $(a - a_0)/b_0$.
(d) Gross moment $M/(2\pi R)/(0.5kb_0^2)$ vs. Crack growth amount $(a - a_0)/b_0$.

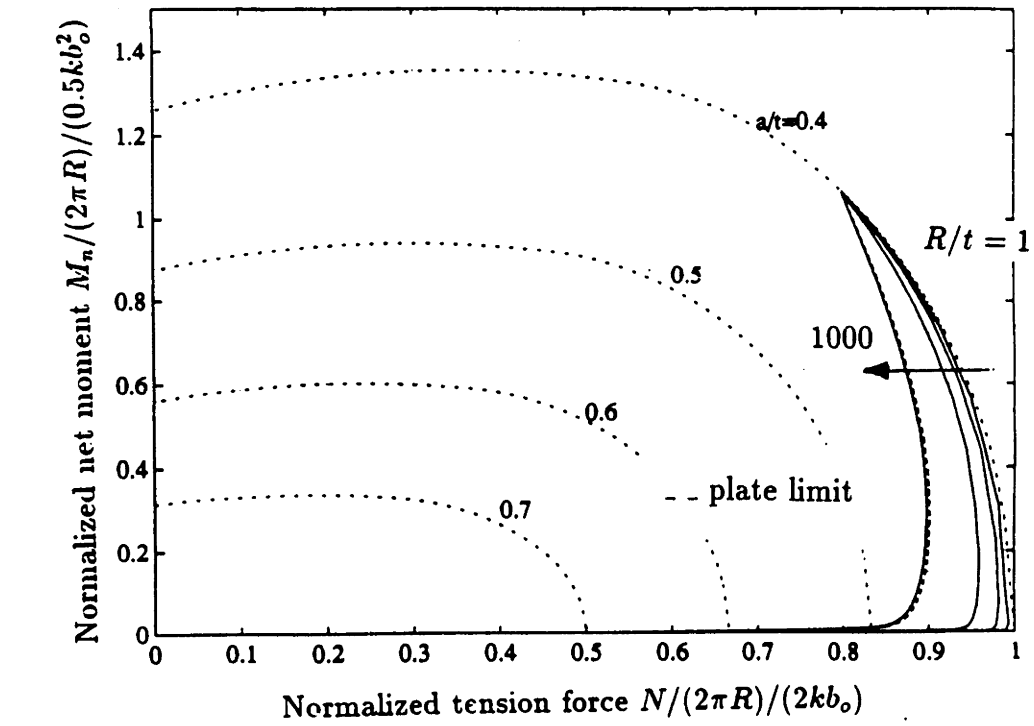

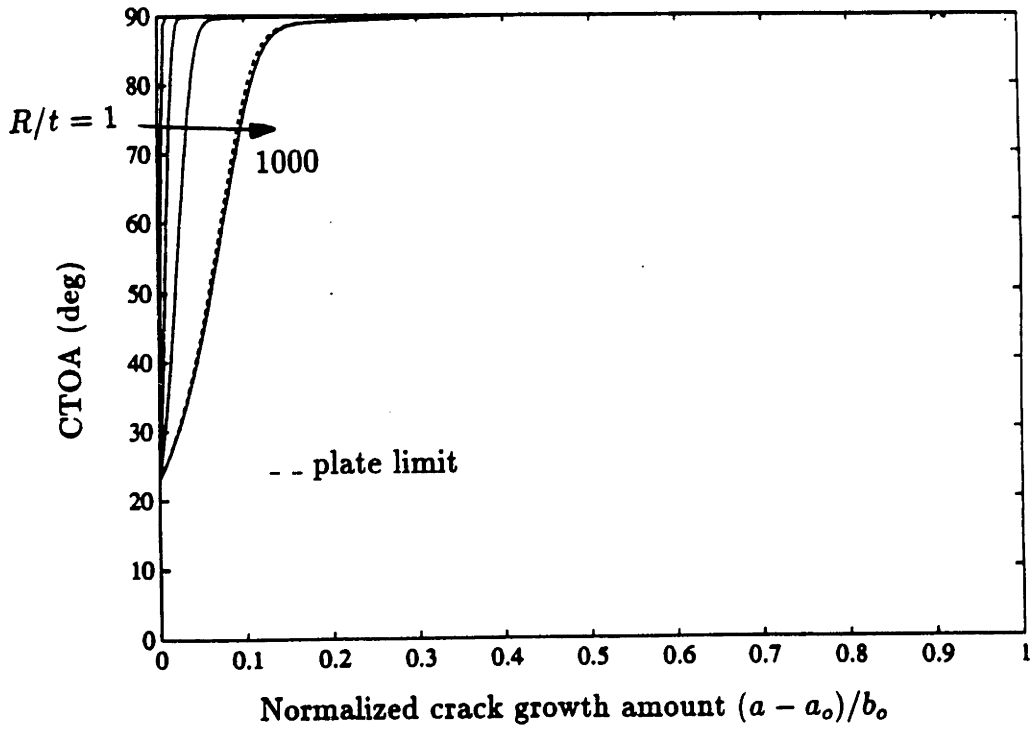

Fig. 5.11. Effect of shell radius R/t on crack growth of completely circumferential cracks in sufficiently long shells.
$(L/t = 40; a_0/t = 0.4; \epsilon_y = 0.002; A = 1.175; B(\sigma_s) = 0; n = 0; R/t = 1, 10, 100, 1000)$
(e) Net moment $M_n/(2\pi R)/(0.5kb_0^2)$ vs. Tensile force $N/(2\pi R)/(2kb_0)$.
(f) Crack tip opening angle $CTOA$ (deg) vs. Crack growth amount $(a - a_0)/b_0$.

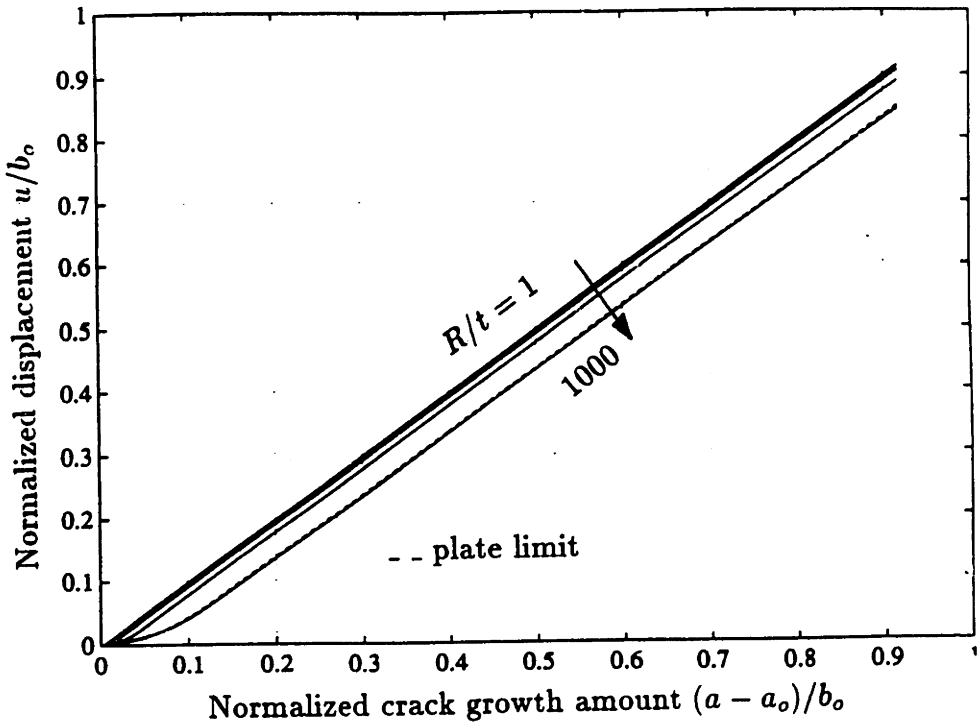

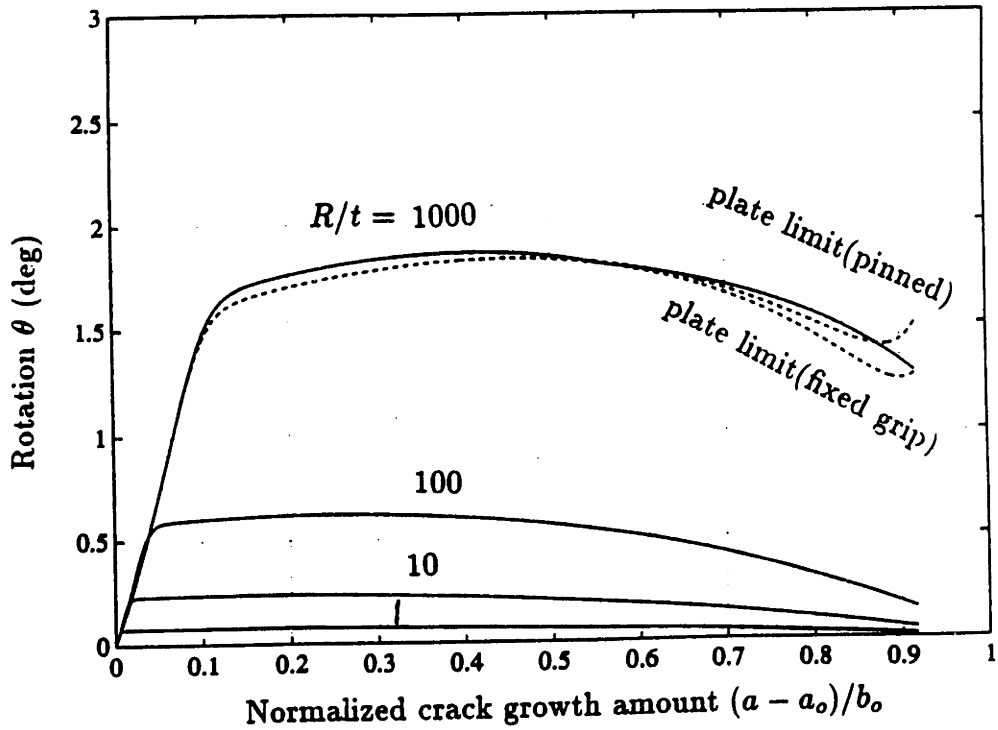

Fig. 5.11. Effect of shell radius R/t on crack growth of completely circumferential cracks in sufficiently long shells.
($L/t = 40; a_0/t = 0.4; \epsilon_y = 0.002; A = 1.175; B(\sigma_s) = 0; n = 0; R/t = 1, 10, 100, 1000$)
(g) Displacement u/b_0 vs. Crack growth amount $(a - a_0)/b_0$.
(h) Rotation θ (deg) vs. Crack growth amount $(a - a_0)/b_0$.

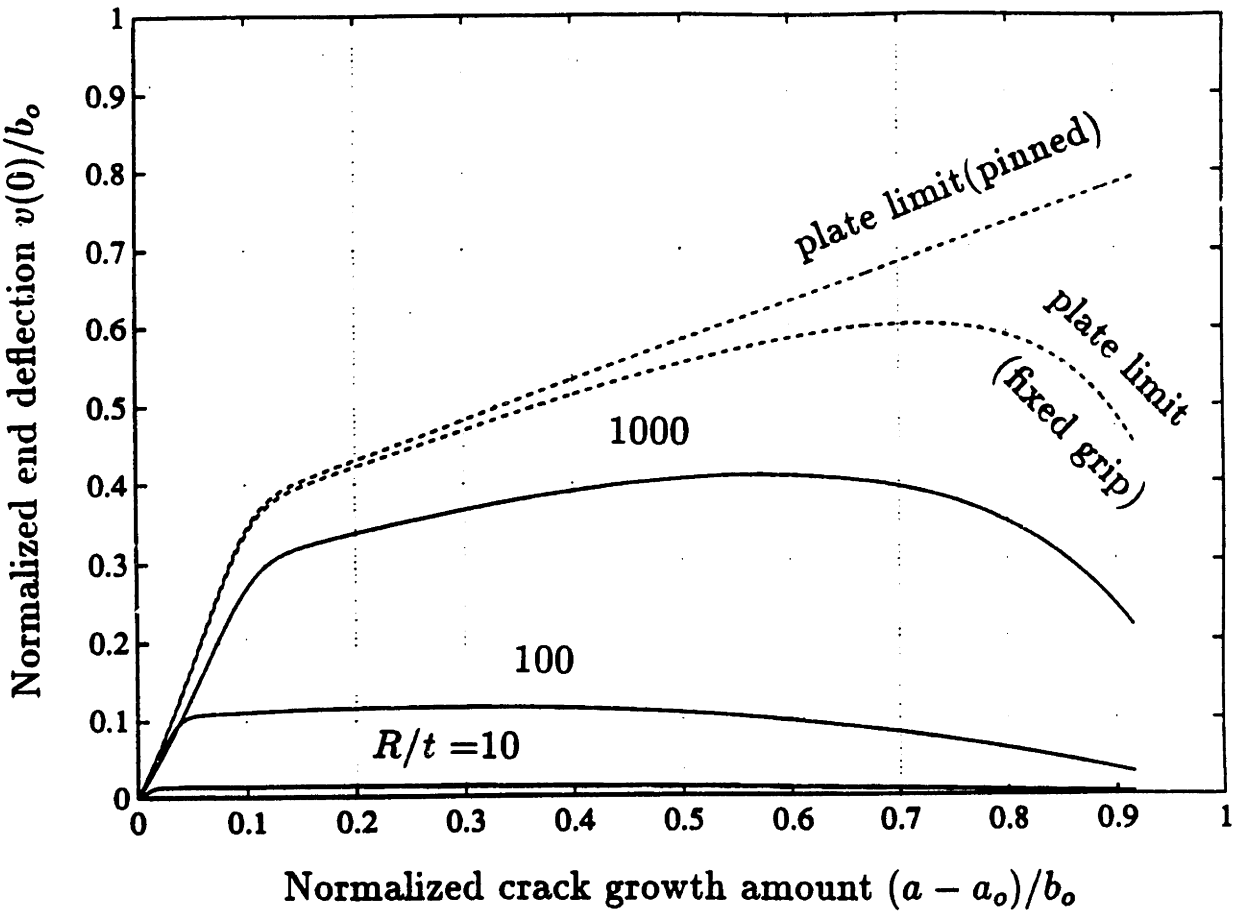

Fig. 5.11. Effect of shell radius R/t on crack growth of completely circumferential cracks in sufficiently long shells.
$(L/t = 40; a_0/t = 0.4; \epsilon_y = 0.002; A = 1.175; B(\sigma_s) = 0; n = 0; R/t = 1, 10, 100, 1000)$
(i) Cracked part deflection $v(x = 0)/b_0$ vs. Crack growth amount $(a - a_0)/b_0$.

CHAPTER 6

CONCLUSIONS

The thesis explores a new area in fracture mechanics, namely, *fully plastic crack growth mechanics* (FPCG) for low strength alloys. For high strength alloys, there have been a number of works in *elastic-plastic crack growth mechanics* (EPCG) from well-contained yielding to general yielding conditions. In contrast, problems of FPCG has not been drawn much attention in spite of its importance. The typical applications of FPCG are, for instance, design of possibly cracked structures that must remain ductile under accidental overloads such as earthquakes, tank car accidents, collisions and ship groundings. For such problems, the thesis presents a theory for fully plastic, plane strain crack growth. The results are summarized below.

1. NEAR-TIP FIELD CHARACTERIZATION FOR A GROWING CRACK IN FULLY PLASTIC, PLANE STRAIN CONDITIONS

1.1. Slip Line Field Analysis

Plane strain slip line fields of stress and displacement increments for cracked structures of rigid-plastic, non-hardening materials have been found for a variety of geometries and loadings (see McClintock, 1971). At the crack tip, most of these fields

consist simply of a pair of slip lines surrounded by rigid regions, e.g., deep, single-face-cracked plates in pure bending (Fig. 6.1a). Other fields consist of a pair of deforming fans surrounded by regions with less concentrated plastic flow, e.g., doubly-grooved specimens under tension (Fig. 6.1b). To simplify such problem, regard the deformation in the fan at the crack tip as being concentrated on a single slip line which is surrounded by rigid regions.

For symmetric geometry and loading, the near tip fields are characterized by just three parameters: the slip line angle θ_s and the normal stress σ_s and shear displacement δu_s across the slip line. If pairs of slip lines are available for the problem at the hand, they describe a local field as a function of loading and geometry:

$$\left\{ \begin{array}{c} \theta_s \\ \sigma_s \\ \delta u_s \end{array} \right\} = \left\{ f \right\} \text{(far-field geometry, loadings and their increments).} \qquad (6.1)$$

This three-parameter characterization of near tip fields in fully plastic fracture crack growth mechanics presents a contrast to the one-parameter (K) in elastic fracture mechanics, the two-parameter (K or J and T or Q) characterization in elastic-plastic fracture mechanics for crack initiation (Parks, 1991; O'Dowd and Shih, 1992), or the one-parameter characterization in elastic-plastic fracture mechanics for crack growth (Varias and Shih, 1993).

Next we consider forms of (6.1) for cases in which the slip line fields are not available or are more complicated than pair of slip lines.

1.2. Least Upper Bound Analysis based on a Circular Arc

1.2.1. Finding an approximate θ_s and δu_s

The least upper bound (LUB) field based on a circular arc provides a estimate not only of the limit load, but also of the slip plane angle θ_s and displacement δu_s, all in terms of far-field geometry and loadings. For example, consider a single-face-cracked plate subject to combined bending and large tension. Comparing limit loads with existing finite element (FE) results (Lee and Parks, 1993), the yield locus from the LUB analysis is no more than 2% above the FE results.

1.2.2. Finding an approximate σ_s

It is very difficult to glean information on the local stress from lower bound stress fields satisfying equilibrium, the yield condition, and traction boundary conditions. A new simple/efficient method is proposed to approximate σ_s from the least upper bound based on a circular arc.

Consider rigid-body rotation across a circular arc extending from a crack tip across a ligament in a plate, subject to general loading with three components: V, N, and M. Suppose that two loading components are specified and that the circular arc for the LUB to the unspecified loading component has been found. Then, it is proven that the one-parameter description of traction across the arc which is consistent with the Hencky equilibrium equation can be chosen such that the tractions on the LUB arc satisfy all three in-plane components of global equilibrium. Therefore the LUB arc provides an approximation to the stress and deformation fields at a crack tip, consistent with global equilibrium.

To test accuracy with an example, consider again the single-face-cracked plate under combined bending and large tension, for which exact slip line field solutions are not known but finite element results are available (Lee and Parks, 1993). For bending with large tension, the LUB values of θ_s and $\sigma_s/2k$ appear accurate within 5%. The accuracy of the third parameter, δu_s, is not available from the FEM results. (For pure tension and for limiting case of the modified Green and Hundy field, δu_s from the LUB is exactly that from the SLF. This agreement is somewhat coincidental, because for pure bending δu_s from the LUB is 1.4 times that from the SLF.)

The accuracy of the LUB analysis has also been considered for three cases with known SLF. For a single-face-cracked plate in pure shear, θ_s from the LUB analysis is zero compared to $\pm 8.2^o$ from the SLF analysis; $\sigma_s/2k$ is zero compared to ± 0.14, and δu_s is exact. For a three-point bend plate with a total length to ligament ratio of 6, θ_s from the LUB analysis is 56^o compared to 68^o; $\sigma_s/2k$ is 1.06 compared to 1.22, and δu_s is 2.4 times the SLF value for the same end displacements. As here, the agreement is worst with fields involving constant state regions or fans. For the classical double-face-cracked plate in tension, the fan runs from 45^o to 135^o with $\sigma_s/2k$ falling from 2.1 to 0.5; θ_s from the LUB analysis comes in at a reasonable $\theta_s = 68^o$, but $\sigma_s/2k$ is high at 2.54, δu_s is low by a factor of 0.5 to 0.67, depending on whether the Prandtl, Hill (Hill, 1950), or Neimark (Neimark, 1968) displacement field is used for comparison. In this case, improved agreement would require more parameters in the fracture criterion. In other cases, values from the LUB analysis might be improved by extending the LUB fields to include constant deformation fields, as well as arcs.

2. FULLY PLASTIC CRACK GROWTH CRITERION

With the local field characterized by three parameters such as θ_s, σ_s, and δu_s, the crack growth increment δa in terms of those parameters can be expressed through the crack tip opening angle $CTOA$:

$$\delta a(\theta_s, \sigma_s, \delta u_s) = \frac{\delta u_s \sin\theta_s}{\tan(CTOA/2)}, \quad \text{where } CTOA(\theta_s, \sigma_s, \text{material}). \tag{6.2}$$

The functional form of $CTOA$ should ultimately be determined by experiment. Such experiments are outlined below, but for insight, we consider a micromechanical model.

2.1. A Sliding Off and Shear-Cracking Model for a Growing Crack

We propose a sliding off and shear cracking model where a crack grows in zig-zag fashion, sliding off by s and cracking by c along a shear band before changing direction. The model gives the form of $CTOA$ in terms of θ_s and the fracture shear strain in the band, γ_f:

$$\tan\left(\frac{CTOA}{2}\right) = \frac{1}{[2/(\gamma_f \sin 2\theta_s) - 1]} \tan\theta_s. \tag{6.3}$$

The fracture strain γ_f will depend on the mean normal stress in the shear band, σ_s, and on material properties such as hardening and an initial volume fraction of holes, which will be discussed next.

2.2. Fracture Strain in the Shear Band

Accounting for micromechanisms for crack growth such as hole nucleation, hole growth, and linkage by localization or fine cracking, we propose

$$\gamma_f = \frac{(1-n)A}{\sinh[(1-n)\sigma_s/k]} + B(\sigma_s), \tag{6.4}$$

where A is the parameter, and n is the strain hardening exponent in $k = k_o\gamma^n$ with k_o=constant. The first term on the RHS of (6.4) can be viewed as a strain for hole growth to linkage by localization or by fine cracking (McClintock, et al., 1968). The second term, $B(\sigma_s)$, can be viewed as a strain for hole nucleation, which is generally a function of mean normal stress (e.g., Argon, et al., 1976). For preliminary insight, assume non-hardening flow ($n = 0$) and the nucleation strain is negligible ($B(\sigma_s) = 0$). Then the estimated $CTOA$ function has an inverse exponential dependence on σ_s/k and a higher order parabolic dependence on θ_s ($45^o \leq \theta_s \leq 72^o$).

The parameters A and the function $B(\sigma_s)$ in (6.4) reflect material properties and should be found from fully plastic crack growth experiments, as follows.

2.3. Suggested Experimental Determination of $CTOA$ function

The functional dependence of $CTOA(\theta_s, \sigma_s)$ on the parameters A and the function $B(\sigma_s)$ of the fracture criterion of (6.3) with (6.4) can be found by fully plastic crack growth tests. For example, at $\theta_s = 45^o$, $\sigma_s/2k$ can be increased from 0.5 to 1.547 in the unequally grooved specimens of Fig. 6.2a by decreasing the back-angle 2ϕ from 180^o to 60^o (McClintock, 1971). Solving (6.3) with (6.4) from the experimental data would allow fitting the constants A and B. For higher values of θ_s, consider 4-point bending specimens of Fig. 6.2b. According to the SLF analysis proposed in Chapter 3, decreasing the back-angle 2ϕ from 180^o to 90^o would decrease $\sigma_s/2k$ from 1.543 to 1.177 with θ_s nearly constant in the range from 67^o to 72^o.

3. LINE-SPRING MODEL FOR FULLY PLASTIC CRACK GROWTH IN PLATES AND SHELLS

A line-spring model is developed for fully plastic, plane strain crack growth in plates and shells. Based on rigid-plastic, non-hardening plasticity, a simple form of incremental compliance of the line-spring, developed from a single-face-cracked specimen under combined bending and tension, is expressed in terms of yield loci and its derivatives, and the crack tip opening angle ($CTOA$).

Then the line-spring is embedded in elastic plates and shells to predict fully plastic crack growth of two kinds of part-through cracks: across plates with pinned or fixed-grip boundary conditions, complete circumferential cracks in long shells under axial tension. The analysis includes the bulging effect of the cracked part. Parametric studies show:

For growth of a part-through crack in the plate:

1. Under pinned conditions, the bulging effect is important. Due to bulging, for longer plates, the net-section is subject to less bending moment. Thus the far-field deformation for fracture u_f^∞ increases as L/t increases.

2. Under fixed-grip conditions, the bulging effect is less important. However, shorter plates require larger negative moments applied in the far-field to maintain zero slope there. Therefore, for shorter plates, the net-section is subject to less bending moment. Thus u_f^∞ increases as L/t decreases.

3. For less ductile plates under the pinned condition, responses of longer plates are similar to those of shorter but more ductile plates. For less ductile plates

under the fixed grip condition, responses of shorter plates are similar to those of longer but more ductile plates. Therefore, u_f^∞ decreases for less ductile materials regardless of the type of the boundary conditions.

4. Deeper initial crack depths reduces u_f^∞.

For crack growth of the complete circumferential crack in the shell, the effect of curvature (varying R/t) is equivalent to the effect of the plate length (varying L/t) under the fixed grip condition. Therefore, u_f^∞ increases as R/t decreases.

REFERENCES

Argon, A.S., Im, J. and Safoglu, R., 1975, "Distributuion of Plastic Strain and Negative Pressure in Necked Steel and Copper Bars", *Metallurgical Transcations*, 6A 815.

Lee, H. and Parks, D.M., 1993, "Fully Plastic Analyses of Plane Strain Single Edge Cracked Specimens Subject to Combined Tension And Bending", *International Journal of Fracture* (submitted for publication).

McClintock, F.A., 1971, "Plasticity Aspects of Fracture", in *Fracture Vol. 3*, Academic Press, New York 47.

McClintock, F.A., Kaplan, S.M. and Berg, C.A., 1966, "Ductile Fracture by Hole Growth in Shear Bands", *International Journal of Fracture Mechanics* 17, 201.

Hancock, J.W., Reuter, W.G. and Parks, D.M., 1991, "Constraint and Toughness Parameterized by T", to appear in *ASTM STP on Constraint Effects in Fracture,*

Proceedings of ASTM Symposium, Indianapolis, IN.

Rice, J.R., 1972, "The Line-Spring Model for Surface Flaws", in *The Surface Crack: Physical Problems and Computational Solutions*, J.L. Sweldow (ed.), American Society of Mechanical Engineers, New York, pp. 171-185.

Tvergaard, V. and Hutchinson, J.W., 1992, "On the Relation between Crack Growth Resistance and Fracture Process Parameters in Elastic-Plastic Solids", *Journal of the Mechanics and Physics of Solids*, **40**, pp. 1377-1397.

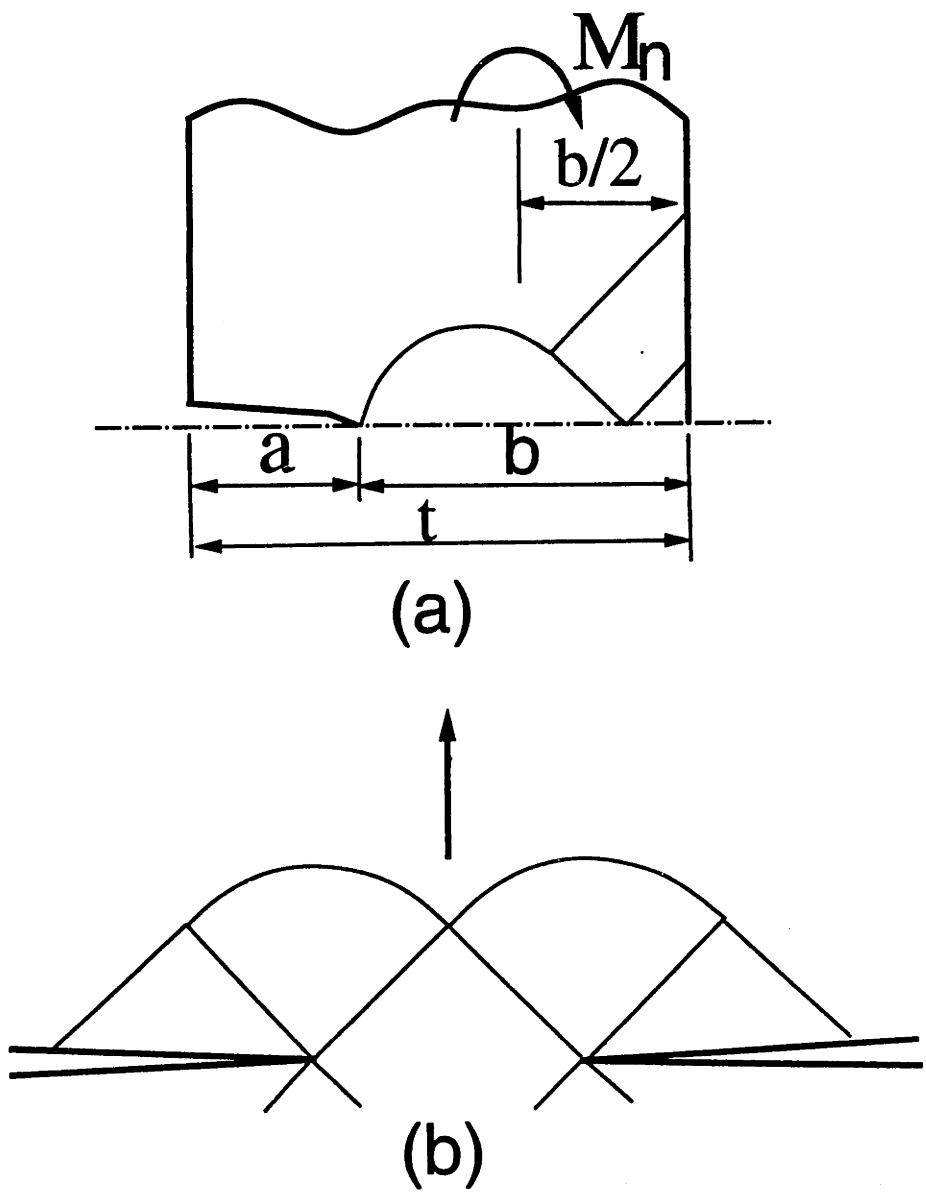

Fig. 6.1. Slip line fields (a) for a deep, single-face-cracked plate under pure bending, and (b) a symmetric doubly-cracked plate in tension. (The dotted line in Fig. 6.1b represents the field approximated by a pair of slip line.)

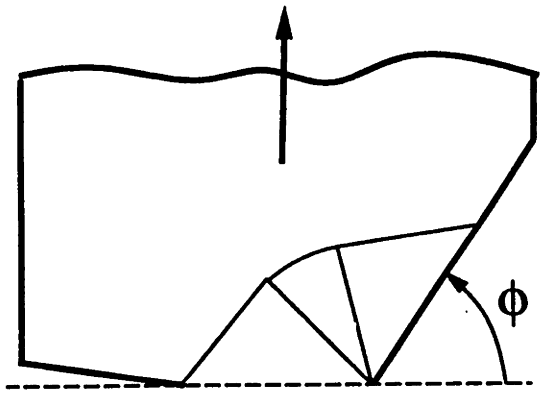

(a)

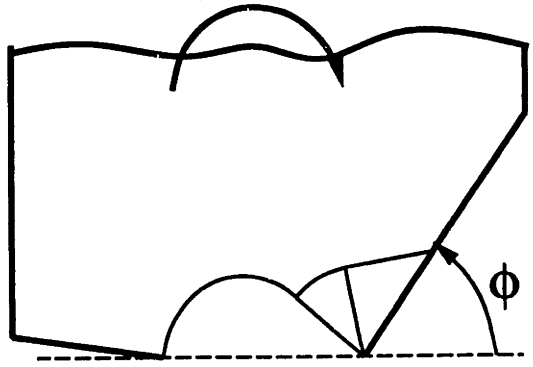

(b)

Fig. 6.2. Slip line fields for unequally grooved specimens (a) under pure extension, and (b) under pure bending.